"Towards improving subgrid surface flow hydrograph estimation using the relative surface connection function as a connectivity indicator"

Penuela Fernandez, Andres

Abstract

A major challenge in present-day hydrological sciences is to enhance the performance of existing distributed hydrological models through a better description of subgrid processes, in particular the subgrid connectivity of flow paths. The relative surface connection function (RSCf) was proposed by Antoine et al. (2009) as a functional indicator of overland flow connectivity. This function performs better compared to previous connectivity indicators and it can be potentially integrated in hillslope or watershed models as a descriptive function of subgrid overland flow dynamics. Nevertheless, several issues remained to be addressed, which was the subject of the present research. First, it was as yet unknown how changes in scale affect the RSCf and whether it can be extrapolated to other scales. We found that both scale effects and border effects affect the RSCf at the plot scale and a minimal scale to study overland flow connectivity was identified. The RSCf showed a great potential to ...

Document type : *Thèse (Dissertation)*

Towards improving subgrid surface flow hydrograph estimation using the relative surface connection function as a connectivity indicator

Andrés Peñuela-Fernández

Thèse présentée en vue de l'obtention du titre de docteur en sciences agronomiques et ingénierie biologique

Septembre 2015

Université catholique de Louvain
Earth and Life Institute/ Environmental Sciences
Louvain-la-Neuve
Belgique

THESIS EXAMINING BOARD

SUPERVISORS	Prof. C.L. Bielders	(UCL, Belgium)
	Prof. M. Javaux	(UCL, Belgium)
JURY PRESIDENT	Prof. M. Vanclooster	(UCL, Belgium)
JURY MEMBERS	Prof. A. Cerdà	(UV, Spain)
	Prof. F. Darboux	(INRA, France)
	Prof. E. Hanert	(UCL, Belgium)
	Prof. J. Wainwright	(DU, England)

Acknowledgments

Hay muchas personas que han pasado por mi vida en estos cinco años, personas que han pasado dejando su huella, personas que se han quedado en mi vida y también personas que se han ido. A todas ellas agradecerles todo lo que me han aportado, gracias. Y a las que se han ido, solo decir que no os olvido, papá y abuela.

Nunca pensé hacer un doctorado, ni siquiera lo tenía claro cuando llegué por primera vez a Bélgica para encontrarme con Charles y Mathieu. Pero ya me veis, he aguantado cinco años en la lluviosa Bélgica y creo que gran parte de culpa de ello y de que me guste tanto la investigación la tienen mis promotores. Todo este tiempo ha sido un placer trabajar con vosotros, Mathieu y Charles. Creo que tenido mucha suerte y no podría imaginar mejores promotores de tésis. Ademéas de grandes personas, he apreciado mucho vuestros sabios consejos, vuestro interés y liderazgo. Cuando oigo a gente decir que hacer un doctorado es demasiado duro, no lo llego a entender, para mi ha sido un placer.

Je dois également remercier Frédéric pour ton aide, tes commentaires, nos discussions et pour ton intérêt. Ce fut un plaisir et un privilège de travailler avec toi.

I would like to thank the jury members of my thesis and reviewers for your commentaries. You all have helped me improve this document.

Je tiens à ce propos à remercier l'UCL et le FNRS pour son financement.

Esta experiencia no habría sido nada de lo que ha sido, sin mis amigos y colegas del GERU. En este aspecto también he tenido mucha suerte, he conocido mucha gente en Bélgica, la mayoría grandes personas con las que he pasado muy buenos momentos, que me han aportado mucho y que me han apoyado. Gracias.

Por último, recordar y dedicar esta tesis a mi familia, gracias mamá, gracias Tati, no puede haber mejor madre y hermana en el mundo.

Y para despedirme, mandar un beso muy fuerte a mi sobrina Sara y a mi peque, me habéis alegrado aún más la vida.

Summary

A major challenge in present-day hydrological sciences is to enhance the performance of existing distributed hydrological models through a better description of subgrid processes, in particular the subgrid connectivity of flow paths. The relative surface connection function (RSCf) was proposed by Antoine et al. (2009) as a functional indicator of overland flow connectivity. This function performs better compared to previous connectivity indicators and it can be potentially integrated in hillslope or watershed models as a descriptive function of subgrid overland flow dynamics. Nevertheless, several issues remained to be addressed, which was the subject of the present research.

First, it was as yet unknown how changes in scale affect the RSCf and whether it can be extrapolated to other scales. We found that both scale effects and border effects affect the RSCf at the plot scale and a minimal scale to study overland flow connectivity was identified. The RSCf showed a great potential to be extrapolated to larger scales.

Secondly, it was also unknown how the RSCf is affected by surface roughness and slope and whether these effects can be predicted. Results showed that the characteristic parameters of the RSCf are greatly influenced by surface roughness and slope. Based on a simple rectangular conceptualization of surface roughness, predictive equations relating the RSCf in function of slope and roughness were established.

Finally, it was still unknown how the RSCf evolves after erosion processes and to what extent changes in the RSCf reflect changes in overland flow generation. The RSCf showed important changes in terms of both maximum depression storage and shape. These changes were found to be highly correlated to the delay and the rate of increase of the hydrograph, flow velocities continuity and erosion energy.

Table of contents

Table of contents

List of figures

List of figures

List of tables

List of tables

Acronyms and abbreviations

Abbreviation	Meaning
A	Area occupied by stored water [mm^2]
α	Slope angle of the profile [rad]
β	Angle given by arctan(σ/2R) [rad]
C	Ratio of surface connected to the outlet to the total surface of the plot [m^2/m^2]
C_0	Ratio of initially connected surface to the outlet to the total surface of the plot [m^2/m^2]
C_{CT}	Ratio of surface connected to the outlet at the connectivity threshold to the total surface of the plot [m^2/m^2]
c_j	Column (j) median of the grid elevations [mm]
DS	Depression storage [mm]
DS_{max}	Maximum depression storage [mm]
DS_{CT}	Depression storage at the connectivity threshold [mm]
$\gamma(l)$	Variogram [mm^2]
L	length of the longitudinal profile [mm]
l	Lag distance between two points [mm]
m	Sum of the overall median of the grid elevations [mm]
NRMSE	Normalized root-mean-square error
NSE	Nash–Sutcliffe model efficiency coefficient
ξ	Connectivity length [mm]
R	Range of the variogram [mm]
RDS	Relative depression storage [mm/mm]
RDS_{CT}	Relative depression storage at the connectivity threshold [mm/mm]
RE	Rainfall erosivity [MJ ha^{-1} mm h^{-1}]
r_i	Transect (i) median of the grid elevations [mm]
R_{ij}	Residual term at the grid (i, j) [mm]
σ	Sill of the variogram expresses as the standard deviation [mm]
Y_{ij}	Elevation at the grid (i, j) [mm]

$z(x)$	Elevation of the point x [mm]

CHAPTER 1

1 Introduction

1.1 Overland flow

Overland flow generation is a discontinuous process that needs the presence of water on the surface to initiate. During a rainfall event, water appears on the surface when the soil gets saturated, either from above, when the rainfall intensity exceeds the infiltration capacity of the soil, or from below, when the groundwater table or when the sub-surface flow reaches the soil surface. Surface runoff is generated by these two mechanisms, the first one being known as infiltration excess or Hortonian surface runoff (Horton, 1933) and the second one as saturation-excess runoff (Dunne and Black, 1970). Traditional research on runoff processes has focused on the identification and differentiation of runoff mechanisms. The Hortonian mechanism is usually considered as characteristic of arid or semi-arid regions, but it can also be present in temperate regions on crusted soils, and only from certain areas in the watershed (Partial area theory; Betson, 1964). However, it is also the dominant process on sealed (crusted) soils, which are common in many regions including agricultural land in temperate regions. On the other hand, the saturation excess mechanism is considered as characteristic of humid regions, at scales of tenths of metres, becoming dominant as the scale of study increases (Blöschl and Sivaplan, 1995). Because the saturated areas vary in extent during rainfall events and from one rainfall event to another, saturation excess runoff is associated with variable source areas (VSA; Hewlett and Hibbert, 1967). Typically, saturation-excess runoff initially spreads up low-order tributaries, then up unchanneled swales and gentle footslopes (Dunne et al., 1975). The position and expansion of the saturated areas is related to geology, topography, soil type, rainfall characteristics and vegetation (Dunne and Black, 1970).

The relative importance of the different runoff mechanisms depends on specific thresholds that are conditioned by rainfall and soil

characteristics. During a low-intensity rainfall event, it is assumed that runoff can only be generated by saturation excess. For high intensity rainfalls, runoff can also be produced at non-saturated areas when the rainfall rate is higher than the infiltration capacity of the soil. Therefore, for moderate and high intensity rainfalls, runoff can be produced by a combination of both mechanisms. Moreover, infiltration capacity of the soil is variable in time and space due to soil degradation processes such as compaction and surface sealing (Deasy et al., 2009). Saturation levels are also variable due to groundwater fluctuations in time and space (Heathwaite et al., 2005), and precipitation dynamics are also heterogeneous in time and space. Due to these sources of heterogeneity, runoff thresholds and hence runoff mechanisms are variable in space and time, in terms of extent, volume, rate and timing. This temporal and spatial heterogeneity creates variable sources areas which are heterogeneously distributed over the surface.

1.2 Hydrological connectivity

Regardless of the runoff mechanism, in a catchment one can identify "active" and "contributing" source areas. The former generate runoff and the latter also generate runoff but they are necessarily spatially connected to the channel network and hence contribute to the outlet output and to the hydrological response of the system (Ambroise, 2004). Therefore, in order to better understand and to predict the hydrological response of a system, we need to move forward from the traditional view, which focuses on identifying the different runoff mechanisms and sources areas, and to determine whether and how source areas get connected and contribute to the hydrological response of the system. While this connection process could be explicitly treated by hydrological models, it would strongly increase the input data and the computation time requirements. Therefore, new concepts able to provide hydrological models with relevant information about this connection process without critically increasing input data and computation time requirements must be defined. A new concept,

increasingly applied in a diverse range of disciplines (Figure 1-1), is connectivity. The concept of connectivity aims at characterizing the behaviour of heterogeneous systems according to the intrinsic organization of the heterogeneities. In geomorphology and hydrology we can distinguish three general types of connectivity: (a) *landscape connectivity*, defined as the degree to which the landforms facilitate or impede movement between resource patches (Taylor et al., 1993), (b) *hydrological connectivity*, which refers to the movement of water from one part of the system to another; and (c) *sedimentological connectivity*, which refers to the movement of sediments and attached pollutants through the system (Bracken and Croke, 2007). In hydrology, connectivity is used across a wide variety of scales (catchment, hillslope, plot) and processes (surface and subsurface flow), and for different purposes (develop a better understanding of hydrological processes, improvement of the prediction of hydrological processes, flood risk management, characterization of hydrological systems).

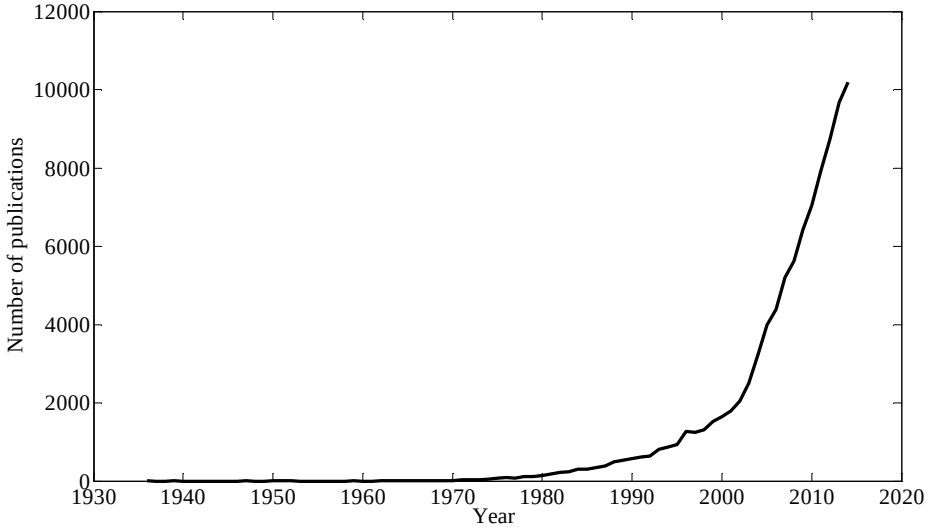

Figure 1-1 Number of publications containing the word "connectivity" in title, abstract or keywords.

By analogy to landscape connectivity, hydrological connectivity can be conceptualized into ‘structural’ and ‘functional’ connectivity

(Tischendorf and Fahring, 2000; Turnbull et al., 2008). Structural connectivity refers to spatial patterns in the landscape and the spatial adjacency and continuity of landscape elements. Structural connectivity is not necessarily static since these patterns can change over time under the influence of the hydrological processes taking place. Functional connectivity refers to the influence of the landscape patterns on hydrological processes such as the dynamics of overland flow (Larsen et al., 2012). This process-based nature of functional connectivity makes it dependent on the initial and boundary conditions of the system and hence more difficult to measure and quantify than structural connectivity (Bracken and Croke, 2007; Lexartza-Artza and Wainwright, 2009). Moreover, the lack of measureable key parameters characterizing functional connectivity limits its practical application (Bracken et al., 2013).

In a catchment one can identify “active” and “contributing” hydrological areas. The former generate runoff and the latter also generate runoff but they are necessarily spatially connected to the channel network and hence contribute to the outlet output (Ambroise, 2004). Similarly, connectivity has also been assessed by partitioning the catchment into “wet” and “dry” areas according to their soil moisture (Ali and Roy, 2010a). This has led to new ways of conceptualizing hydrological processes, such as the “fill” and “spill” concept (Tromp-Van Meerveld and McDonnell, 2006b) and the use of percolation theory (Darboux et al., 2002a; Lehmann et al., 2007). This conceptualization divides the system into different units with varying characteristics and thresholds that need to be exceeded before these units get activated. The spatial-temporal pattern of these activated units reflects the hydrological connectivity and determines the hydrological response of the system. It has been applied to sub-surface flow at the watershed scale (James and Roulet, 2007; Ali et al., 2011), sub-surface flow at the hillslope scale (Tromp-van-Meerveld and McDonnell, 2006a; 2006b; Lehman et al., 2007; Hopp and McDonnell, 2009), surface flow at the watershed scale (Spence, 2007,2010; Shaw et al., 2012) and surface flow at the plot scale

(Darboux et al., 2002a; Antoine et al., 2009; Frei et al., 2010; Peñuela et al., 2013; Yang and Chu, 2013).

Before an area becomes activated and hence starts generating runoff, infiltration and surface storage thresholds must be reached. During a rainfall event an area starts to store water on the surface when either the topsoil becomes saturated or when the rainfall rate exceeds the infiltration capacity of the soil. When this stored water at the surface reaches a certain depth or threshold the water surplus overflows and the area becomes activated, i.e. generates runoff. Thus these thresholds, and hence whether an area becomes activated, depend on structural characteristics such as soil type, soil moisture, land use and topography. These thresholds can also evolve in time under the influence of natural processes or under the human influence. Natural processes such as surface sealing or erosion can facilitate the activation of areas by reducing the infiltration capacity or reducing soil roughness, respectively. Land use changes or land management practices can also produce major effects on the thresholds, e.g. impervious urban surfaces such as roads (Hairsine et al., 2002) or increased soil roughness in freshly tilled agricultural fields (Takken et al., 2001a, b). However, whether an area becomes a contributing area depends not only on the interaction of these thresholds and the rainfall characteristics but also on the spatial pattern and interaction between contributing areas (Cammeraat, 2002). Cammeraat (2002) demonstrated that, whatever the scale, in order to understand these complex interactions it is necessary to apply the concept of connectivity.

Because functional connectivity is not easily measurable, hydrological connectivity has been mainly characterized by the use of structural connectivity indices (Smith et al., 2010; Bracken et al., 2013). Some studies use purely structural approaches, i.e. terrain connectivity, in order to assess the effect produced by agricultural dams and terraces (Callow and Smettem, 2009; Meerkerk et al., 2009) or roads and tracks (Haisine et al, 2002; Heathwaite et al., 2005) on hydrological

connectivity. However, the study of structural connectivity only infers potential runoff sources and connections, i.e. active areas, and hence, only infers potential hydrological connectivity (Bracken et al., 2013). Other studies analyze structural elements of the landscape in order to identify sensitive areas, to characterize qualitatively the effect of structural connectivity on flow patterns or as a means to understand the hydrological response of a system (Kirkby et al., 2002; Lane et al., 2004; Heathwaite et al., 2005; Fryris et al., 2007). Many studies have emphasized the importance of characterizing the soil moisture patterns in order to understand the hydrological response of catchments (Western et al., 2001, Grayson et al., 2002; Ali and Roy, 2010a) and hillslopes (Tromp van Meerveld and McDonnell, 2006a,b; Lehmann et al., 2007). In order to do so, different approaches have been used, from approaches where connectivity areas are characterized by statistical indicators (Western et al., 2001), to approaches where “dry” and “wet” areas are defined by experimental criteria (Ali and Roy, 2010a). Although the study of patterns, such as soil moisture, can develop a better understanding of the hydrological processes, its ability to predict the hydrological response and the nonlinearity of the hydrological system is limited (Zehe and Bloschl, 2004; James and Roulet, 2007).

As argued by Bracken et al. (2013), for effective catchment management a conceptual and process-based rather than an empirical understanding of hydrological connectivity is required in order to predict the functioning of hydrological system and to understand how continuous flow fields develop in the system. At a smaller scale, a conceptual and process-based understanding of overland flow connectivity is necessary to interpret the process of overland flow generation and better predict the hydrological response of a system.

As mentioned previously, hydrological connectivity can also be addressed through the use of functional connectivity, and more precisely through the interaction between structural and functional connectivity. Functional connectivity, by definition, is related to

structural connectivity and this relationship determines the dynamics and nonlinear behaviour of a system, which cannot be explained by the sole study of structural connectivity (Bracken and Croke, 2007; Smith et al., 2010). In other words, whereas the physical adjacency between two points at the soil surface, i.e. structural connectivity, does not automatically imply the occurrence of water fluxes between them, functional connectivity does imply water fluxes and hence the existence of structural connectivity. Therefore, the study of the hydrological response of a system solely by means of structural connectivity is incomplete and a linkage between them to identify process-relevant features is necessary. This linkage is thus the functional or process-based connectivity. Research in process-based connectivity has shown the importance of representing the spatial variability and patterns of single processes such as flow resistance and infiltration both at the catchment (Mueller et al, 2007) and at the hillslope scale (Reaney et al., 2007; Smith et al., 2010) to better understand the hydrological response of the system.

Besides using hydrological connectivity for explaining catchment response, a major challenge in hydrology resides in applying connectivity for predictive purposes and thus to improve the response of hydrological models. From the hillslope to the small watershed scale, distributed hydrological models frequently use “plot size” (1–1000 m^2) elementary cells allowing for an explicit analysis of inter-grid connectivity. However, such hydrological models do not explicitly treat connectivity below the grid cell scale. Yet, the conceptualization of runoff source areas as a dynamic ‘spatial mosaic’ also applies at the subgrid scale. As for the catchment scale, at small scales, a conceptual and process-based understanding of overland flow connectivity, rather than an empirical one, is necessary to better predict the hydrological response of a system (Bracken et al., 2013). At this scale, spatial variability and arrangement of flow resistance, infiltration capacity (Langhans et al., 2011) and depression storage (Darboux et al., 2002a; Chu et al, 2013; Yang and Chu, 2013) are still important and governed by surface roughness (Appels et al., 2011;

Smith et al., 2011) and vegetation pattern (Cerdà, 1998; Ludwig et al., 2005). Regarding roughness, models generally simplify the hydrological representation of the micro-topography using two parameters, the maximum depression storage (i.e. maximum volume of water that the soil is able to store in surface depressions) and the effective friction factor (i.e. resistance to flow) (Singh and Frevert, 2002; Smith et al., 2007). These parameters are estimated from tables or from regressions linking them to easily measured indices characterizing the surface roughness, such as the random roughness (RR), defined as the standard deviation of point elevations (Kamphorst et al., 2000). By using these two factors hydrological models, such as WEPP (Lane and Nearing, 1989; Flanagan and Nearing, 1995), EUROSEM (Morgan et al., 1998) or HEC-HMS (Hydrologic Engineering Center, 1998), consider that overland flow is uniformly distributed within the grid and that overland flow generation only starts after the cumulative excess rainfall becomes equal to the maximum depression storage (bucket model; Figure 1-2; Singh, 1995; Singh and Frevert, 2002). In some cases, surface storage is ignored altogether (no storage model; Figure 1-2). It has been shown, however, that these simplified representations fail to predict satisfactorily overland flow initiation at the grid level as well as the gradual nature of the overland flow generation process (Antoine et al., 2011).

Overland flow is a spatially distributed process of gradual filling and connection of depressions (Onstad, 1984; Darboux et al., 2002b). In order to explicitly take this process into account, it would be necessary to provide hydrological models with subgrid micro-topographical information. The use of high resolution digital elevation models (mm–cm resolution) in hydrological models would strongly increase the input data and the computation time requirements. However, the use of functional connectivity indicators, able to differentiate between different surface morphologies and to link them to their hydrological responses, could potentially improve the prediction of flows without critically increasing computation time and topographical data

requirements of distributed hydrological models (Antoine et al., 2011).

In a general context, Bracken and Croke (2007) proposed the use of the concept of "volume to breakthrough", which means the necessary cumulative runoff volume per unit width at a point before flow appears at the downslope outlet, as a means to quantify functional connectivity. Functional connectivity indicators based on this concept have shown to perform better than other connectivity indicators in both subsurface hydrology (Knudby and Carrera, 2005) and surface hydrology (Antoine et al., 2009). Based on this concept, Antoine et al. (2009) proposed an overland flow functional connectivity indicator called the Relative Surface Connection function (RSCf). This indicator is based on a simplification of the runoff hydrograph (surface detention dynamics are not considered) and expresses the percentage of the surface connected to the bottom outlet of the field plot as a function of the degree of filling of the depression storage. The main advantages of this indicator are: 1) as a simplified representation of the runoff hydrograph it can provide essential information about the distribution of flow paths since it explicitly integrates the flow network at the soil surface, 2) it can be calculated much faster than the full resolution of the St. Venant equations, 3) it has shown good results in capturing runoff-relevant connectivity properties compared to other connectivity indicators (Antoine et al., 2009) and 4) it allows simulated and experimental hydrographs to be mimicked in a simple way by adding surface detention dynamics to the RSCf (Antoine et al., 2011).

The RSCf can be potentially integrated in hillslope or watershed models as a descriptive function of subgrid overland flow dynamics (Antoine et al., 2009, 2011). Yet several issues must be addressed before it can be successfully integrated. Whereas the RSCf showed very promising results at the square meter scale as a functional connectivity indicator, it may be scale-dependent and affected by border effects. However, it is as yet unknown how changes in scale

affect the RSCf and whether and how the RSCf can be extrapolated to other scales. It is also unknown how the RSCf is affected by surface roughness and slope and whether these effects can be predicted. Furthermore, the approach of Antoine et al. (2011) was based on the full knowledge of the RSCf. Obtaining the RSCf requires detailed knowledge of the surface micro-topography. For a generalization of the approach proposed by Antoine et al. (2011), it would be beneficial to parameterize the RSCf, and to investigate whether these characteristic parameters can be estimated from more easily quantifiable indices of surface roughness and from slope. Besides it is still unknown how the RSCf evolves after erosion processes and to what extent these changes in the RSCf reflect changes in the hydrological response.

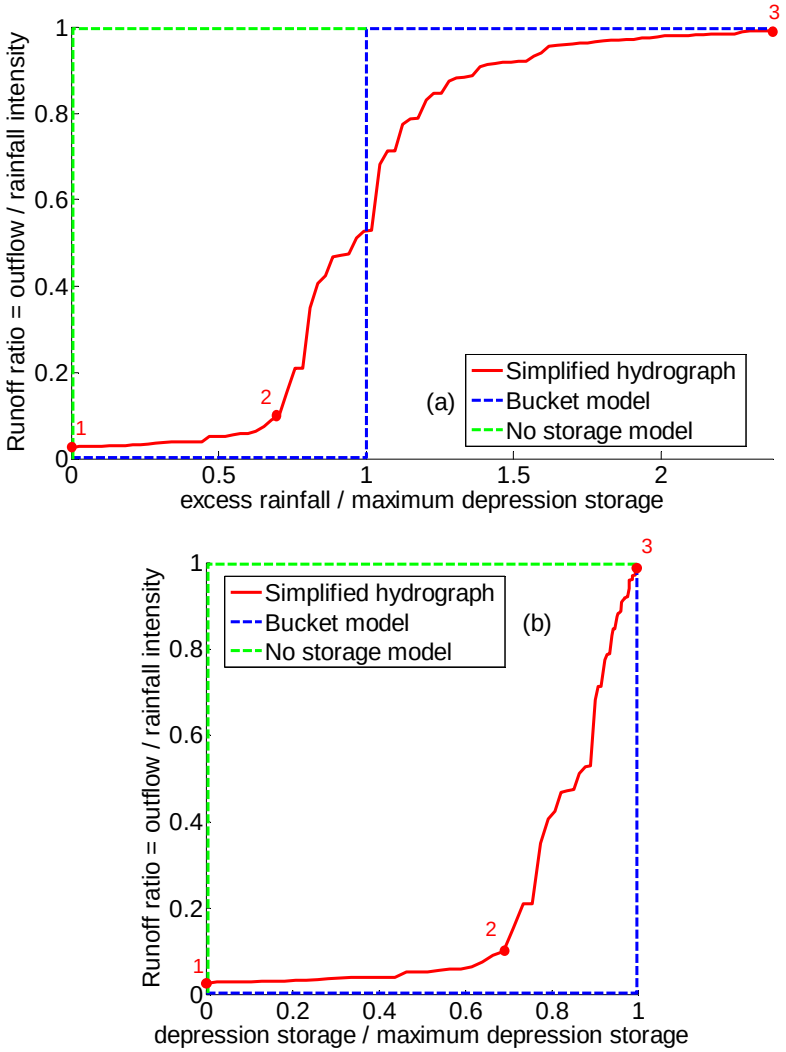

Figure 1-2 Comparisons of different simplified representations of overland flow generation as a function of (a) excess rainfall normalized by maximum depression storage and (b) depression storage normalized by maximum depression storage. The no-storage model assumes zero depression storage. The bucket model assumes that runoff occurs only after all depressions have been filled. The simplified hydrograph is based on the gradual filling of depressions and spilling of water as determined through a conditional walker technique applied to a 3-D representation of the surface micro-topography (Antoine et al., 2009). (1 = runoff from areas initially connected to the outlet; 2 = runoff threshold; 3 = steady state).

1.3 Objectives

The goal of the present research is to develop a better understanding of overland flow connectivity at the subgrid scale in order to enhance the performance of distributed hydrological models in predicting surface flow hydrograms. More specifically, the objectives of the present study are:

Objective 1, to determine the effect of spatial scale on the Relative Surface Connection function (RSCf), including the minimal scale at which to study overland flow connectivity and the potential of the RSCf to be extrapolated to larger scales.

Objective 2, to quantify the effect of soil random roughness and slope on overland flow connectivity, the latter being characterized by the RSCf.

Objective 3, to determine to what extent the RSCf can be predicted on the basis of slope and structural indicators of soil micro-topography.

Objective 4, to determine how temporal changes in micro-topography affect overland flow connectivity.

Objective 5, to evaluate to what extent changes on the RSCf can be linked to the overland flow generation process.

1.4 Outline of the thesis

After this first chapter presenting the general context, the state of the art of the research and the research needs, a second chapter presents the general methodology used to study overland flow connectivity. It includes the description of the structural connectivity indicator used to characterize soil roughness and the RSCf, including its main advantages and the issues remain to be addressed in order to effectively use the RSCf in distributed hydrological models. In chapter

three, the scale effect on the RSCf is studied. Chapter four is dedicated to the study of the effect soil roughness and slope gradient on the RSCf and the prediction of such effect. Finally, in chapter five we look at the temporal evolution of the RSCf and at the link between the RSCf and the overland flow generation. The present study focuses on the hydrological connectivity at the plot scale, considering no interferences from infiltration, i.e. the infiltration capacity of the soil is assumed to be spatially homogeneous, constant over time and lower than the rainfall intensity. These assumptions, which do not take into account the effect of the spatial heterogeneity of the soil hydraulic conductivity on surface runoff (Langhans et al., 2011), facilitate the study of the effects of the surface morphology.

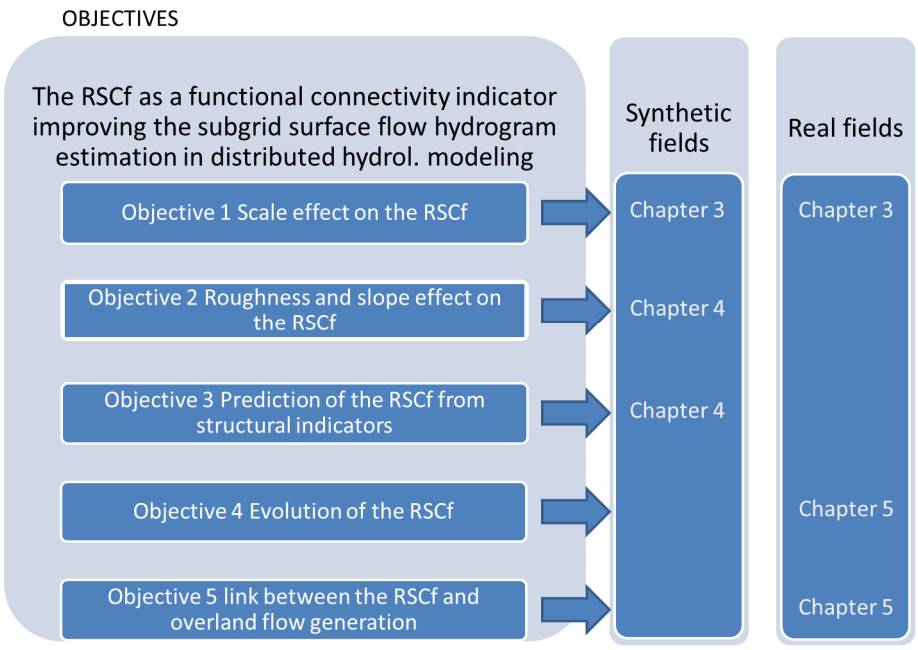

Figure 1-3 Outline of the thesis, showing the correspondence between the objectives and the chapters. The chapters are classified according the type of digital elevation models used (synthetic or real fields).

CHAPTER 2

2 Material and methods

In this chapter the Relative Surface Connection function (RSCf) and the variogram are presented.

2.1 The Relative Surface Connection function

Different theories and concepts, such as the graph theory, the percolation theory, the queuing theory or the volume to breakthrough, are applied to characterize hydrological connectivity and to define connectivity indicators. The graph theory consists of reducing the complexity of a system into understandable elements represented graphically. Sources areas are represented as nodes and flow paths as links which join different pairs of nodes following a number of rules. Indicators based on this theory, such as the directional connectivity index (DCI; Larsen et al., 2012), are suitable to identify source areas or barriers, evaluate their importance and to reveal patterns of interaction between nodes. They are not suitable for predictive purposes, since they are based on inferring processes from measured catchment characteristics (Bracken et al., 2015). Another theory applied in hydrological connectivity is the percolation theory. This theory is based on the probability that certain points within the system are connected and on the percolation phenomenon, defined as “the special property of the system which emerges at the onset of macroscopic connectivity within it” (Berkowitz and Balberg, 1993). This theory has been successfully applied to characterize the transition between spatially random to spatially connected soil moisture patterns (Di Domenico, 2007), to model the critical point at which the system triggers rapid drainage in subsurface fill-and-spill mechanisms (Lehmann et al., 2007) and to describe Hortonian runoff on rough surfaces (Darboux et al., 2002a). However, the applicability of the percolation theory for predictive purposes can be limited if critical features are not considered (Tromp-van Meerveld and Weiler, 2008), such as the topography or the soil depth (Lehmann et al., 2007). A more realistic approach is the directed percolation (Janzen and McDonnell, 2015), in which the movement of flow is based on features such as topography or soil depth. Thus, this approach is able to represent flow paths along

heterogeneous surfaces following not only the general slope gradient but also the local gradients produced by the heterogeneities. Another theory applied on connectivity is the queueing theory. This theory, based on the conceptualization of the reinfiltration process as the customers waiting time in a single server queue (Jones et al, 2013; Harel and Mouche, 2013), provides a theoretical link between the statistical description of soil infiltration heterogeneity, reinfiltration and runoff generation. In order to establish this link, some important simplifying assumptions must be considered: steady-state conditions, rainfall intensity and infiltration capacity exponentially distributed, slope and surface roughness effects not considered, mean rainfall intensity lower than mean infiltration capacity and infinite slope length. While this theory seems to be consistent with runoff observations, these simplifications limit the applicability of this theory to heterogeneous and more realistic areas (Jones et al, 2013). The "volume to breakthrough" is another concept applied in connectivity. This concept is defined as the necessary cumulative runoff volume per unit width at a point before flow appears at the downslope outlet. Therefore, connectivity is a function of the runoff produced, transmission losses due to factors such as infiltration or depression storage, slope length and gradient, and the existence of topographical features that either facilitate connectivity, e.g. rills, or impedes connectivity, e.g. crests and depressions. Thus, connectivity is controlled by both precipitation and soil characteristics. Functional connectivity indicators based on this concept have shown to perform better than other connectivity indicators in both subsurface hydrology (Knudby and Carrera, 2005) and surface hydrology (Antoine et al., 2009) and its use has been proposed as a means to quantify functional connectivity (Bracken and Croke, 2007).

Given the better performance of indicators based on the "volume to breakthrough" concept an overland flow connectivity indicator based on this concept and proposed by Antoine et al. (2009) was used in this present thesis. This indicator is based on a simplification of the runoff hydrograph (surface detention dynamics are not considered) and expresses the percentage of the surface connected to the bottom outlet of the field plot as a function of the degree of filling of the depression storage. The main

advantages of this indicator are: 1) it provided essential information about the distribution of flow paths since it explicitly integrates the flow network at the soil surface, 2) it can be calculated much faster than the full resolution of the St. Venant equations, 3) it has shown good results in capturing runoff-relevant connectivity properties compared to other connectivity indicators (Antoine et al., 2009) and 4) it allows simulated and experimental hydrographs to be mimicked in a simple way by adding surface detention dynamics to the RSCf (Antoine et al., 2011).

The RSCf is calculated by means of a filling algorithm that simulates a simplified process of overland flow generation over the Digital Elevation Model (DEM) of the soil surface assuming infinite surface water velocity. Infiltration is not considered explicitly, which is equivalent to considering excess rainfall for spatially homogeneous and temporally constant infiltration. At every time step, a certain volume of water is applied in every pixel of the DEM. This volume of water "walks" over the DEM to the lowest pixel selected by an 8-neighbour scheme until they reach a depression or the outflow boundary. In a depression, this volume of water is stored as depression storage. Once the depression overflows, any excess of water flows to the next depression or to the outflow boundary. When a drop reaches the outflow boundary it is added to the hydrograph. At any given time, it is thus possible to determine the plot area that is hydraulically connected to the outlet ('contributing area') as a function of the degree of filling of the depression storage (DS). The resulting RSCf can be assimilated to a simplified hydrograph where the vertical axis represents the instantaneous overland flow rate at the bottom outlet normalized by the instantaneous rainfall rate, yielding the ratio of area connected to the bottom outlet (C; $0 \leq C \leq 1$; Figure 2-1). The horizontal axis represents the depression storage depth which can be also normalized by the maximum depression storage value (DS_{max}), yielding the Relative Depression Storage (RDS; $0 \leq RDS \leq 1$).

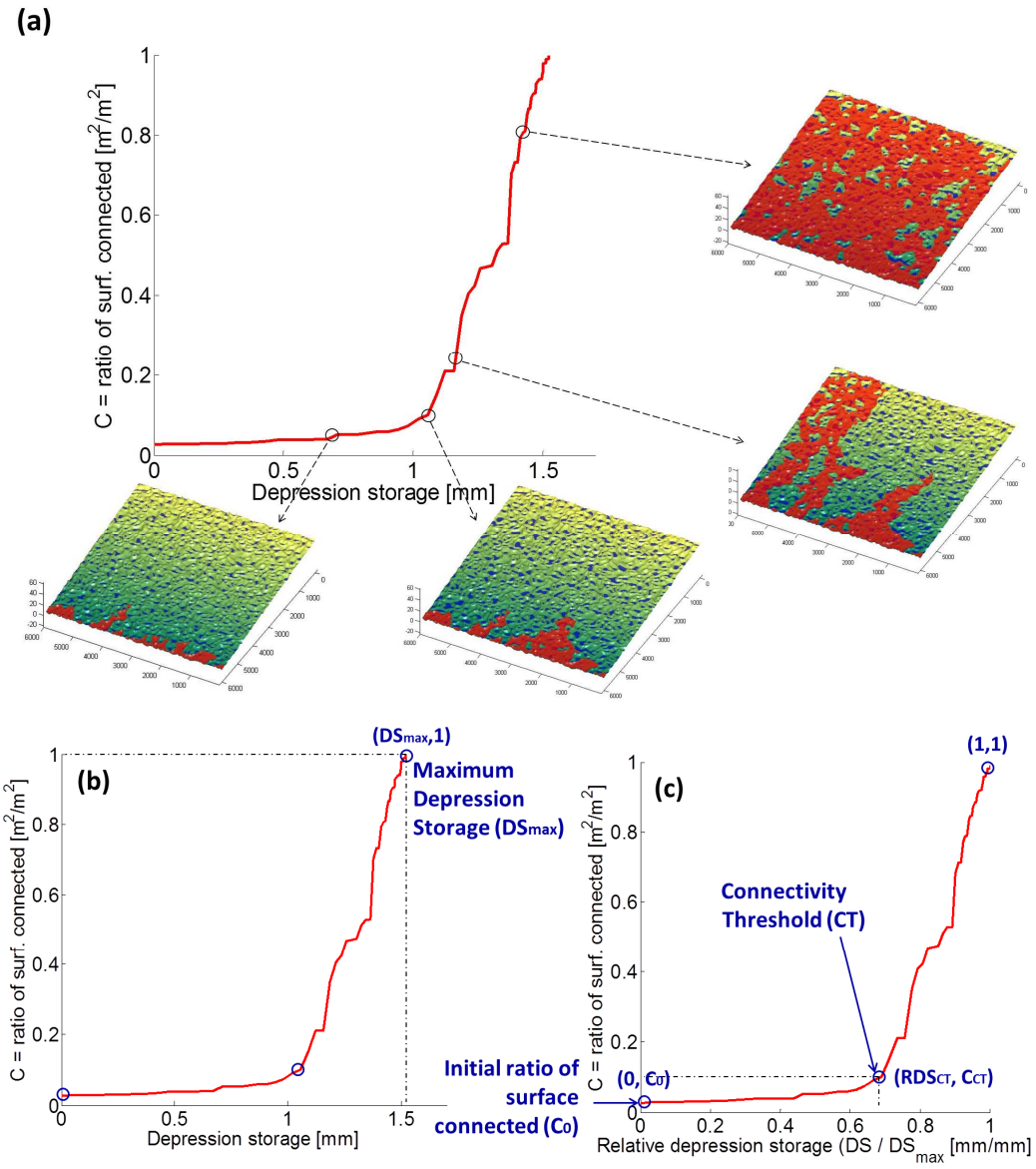

Figure 2-1 (a) Connectivity process and RSCf (area connected to the bottom outlet represented in red) and characteristic points of (b) the RSCf and (c) the normalized RSCf.

In order to quantify the effects of roughness and slope on the RSCf, three characteristic points defining the RSCf were considered (Figure 3-1b and c and Table). First, the ratio of area connected to the outlet when DS is equal to 0 (C_0). This is the plot area already connected to the outlet before any water is added (Darboux et al., 2002a; Yang and Chu, 2013). Second, the connectivity threshold (CT) where *C* increases sharply for a small increase in depression storage. It represents the threshold phenomenon commonly observed in overland flow generation (Darboux et al., 2002a; Yang and Chu, 2013; Chu et al., 2015). In practice, CT was defined as the point where the rate of increase of *C* is equal to the rate of relative filling of depressions, namely, when the slope of the normalized RSCf equals 1. In order to minimize the effect of small local variations of the slope of the RSCf on the identification of CT, we used an interval of calculation of 5% of relative depression storage to calculate the slope of the RSCf. CT is characterized by its two coordinates, the ratio of surface connected and the relative depression storage at the connectivity threshold, C_{CT} and RDS_{CT} respectively. The third characteristic point of the RSCf is the maximum depression storage of the soil micro-topography (Figure 3-1b). At this point all the depressions are completely filled and hence the whole surface is connected to the outlet (C=1). In total four characteristic parameters will thus be used to characterize the RSCf: C_0, C_{CT}, RDS_{CT} and DS_{max} (Table 2-1).

Table 2-1 Coordinates of the characteristic points defining the RSCf.

Characteristic points of the RSCf	Ratio of surface connected (C) [m²/m²]	Depression Storage (DS) [mm]	Relative Depression Storage (RDS) [mm/mm]
Initial ratio of surface connected	C_0	0	0
Connectivity threshold	C_{CT}	DS_{CT}*	RDS_{CT}
Maximum depression storage	1	DS_{max}	1

* This variable was not used in this study since it is highly correlated to DS_{max} (see Section 5.4.6).

In order to calculate the RSCf we considered the following simplifications or assumptions: rainfall and infiltration are uniform in space, rainfall intensity is always higher than the infiltration capacity of the soil, existence, existence of a single and general slope gradient, the lateral and top boundaries of the DEM are closed and hence no runon is considered.

2.2 Variogram

The variogram $\gamma(l)$ was used as a means to characterize surface roughness and as a structural connectivity indicator. In a stationary field, it is defined as:

$$\gamma(l) = ½\ \sigma^2\ [z(x) - z(x + l)]$$

Equation 2-1

where σ^2 is the variance [mm²] of the difference between two elevation points z [mm] separated by l, l is the Euclidean distance between points [mm]. The variogram is characterized by two parameters: the sill and the range. The sill [mm²] is the limit of $\gamma(l)$ when the lag distance tends to infinity. It is indicative of the amplitude of variation (total variance) of the point elevation of the soil surface. In this study, the standard deviation σ [mm] of the point elevation was used instead of the variance. The range [mm] is the minimum lag distance at which a correlation between elevation measurements is no longer observed. It is a measure of the amplitude of the horizontal variability of the soil surface. R and σ convey information about the frequency distribution of the topography and thus on the size and shape of micro-depressions.

Two types of variograms were used in this study, the Gaussian variogram and the exponential variogram. The Gaussian variogram exhibits a stronger continuity at short distances compared to the exponential one. The Gaussian variogram was used to generate synthetic topographical fields (Chapter 3 and 4) following the work of

Antoine et al. (2009). It results in smoother surfaces compared to the exponential variogram. The exponential variogram is characteristic of noisier surfaces, i.e. with higher spatial variability at the micro-scale (mm-cm). It was used for real fields in Chapter 3 and 5. The smoother surface of the synthetic fields facilitates the identification of the main surface roughness elements, i.e. micro-depressions and crests (see Section 3.3.1). However, the lower micro-scale spatial variability present in the synthetic fields may decrease their DS_{max} since the heterogeneities present in real fields may be able to store water. Nevertheless, the connectivity process is not expected to be affected significantly by the differences on the variogram type, since this process is mainly controlled by the vertical and horizontal variability of the meso-scale elements (cm-dm) of the micro-topography (micro-depressions, rills and crests) characterized by the sill and the range of the variogram, respectively.

2.3 Goodness-of-fit statistics

In order to evaluate the goodness-of-fit between observed and predicted values, three statistics were used:

- The root-mean-square error (RMSE):

$$\mathrm{RMSE} = \sqrt{\frac{\sum_{i=1}^{n}(Pi-Oi)}{n}} \qquad \text{Equation 2-2}$$

- The normalized root-mean-square error (NRMSE):

$$\mathrm{NRMSE} = \frac{RMSE}{\bar{O}} \qquad \text{Equation 2-3}$$

- The Nash–Sutcliffe model efficiency coefficient (NSE):

$$\mathrm{NSE} = 1 - \frac{\sum_{i=1}^{n}(Oi-Pi)^2}{\sum_{i=1}^{n}(Oi-\bar{O})^2} \qquad \text{Equation 2-4}$$

where P_i and O_i are the predicted and observed values, respectively, n is the total number of data and $\bar{O}$ is the mean of the observed values.

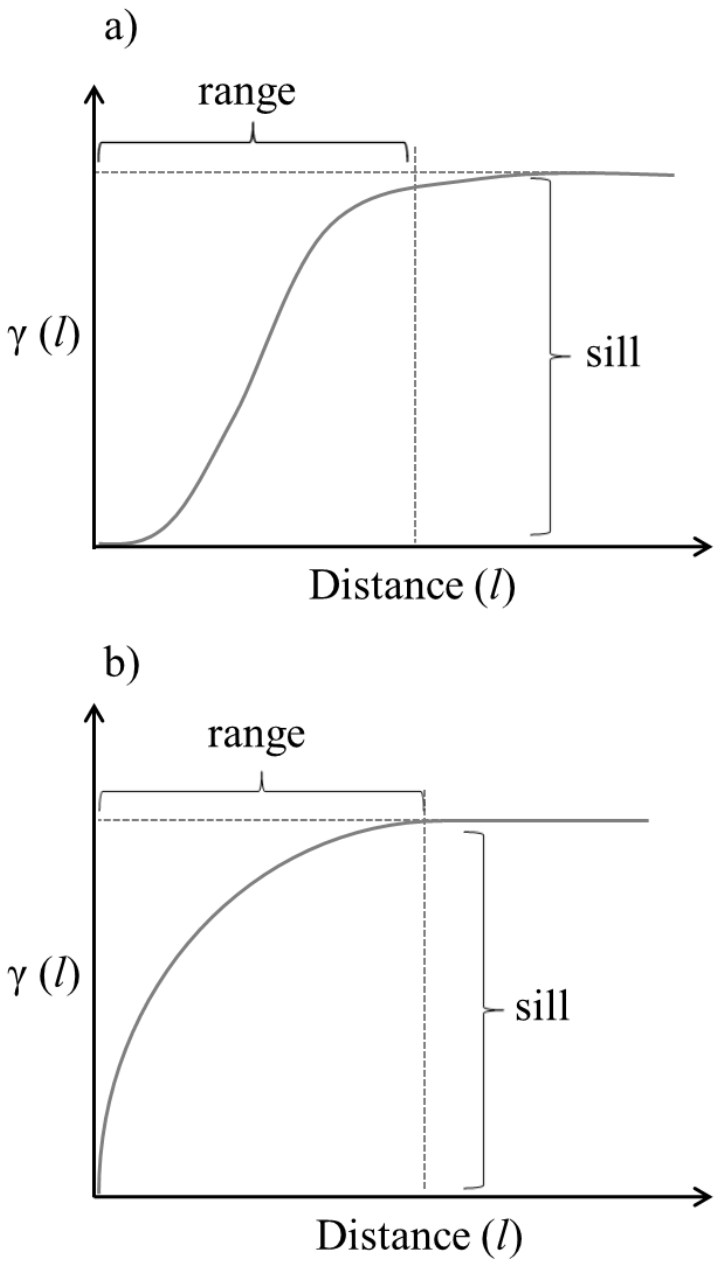

Figure 2-2 (a) Gaussian variogram and (b) exponential variogram.

CHAPTER 3[1]

[1] Based on: *Peñuela, A., Javaux, M., Bielders, C.L., 2013. Scale effect on overland flow connectivity at the plot scale. Hydrol Earth Syst Sci 17, 87–101. doi:10.5194/hess-17-87-2013*

3 Scale Effect on Overland Flow Connectivity at the Plot Scale

3.1 Abstract

A major challenge in present-day hydrological sciences is to enhance the performance of existing distributed hydrological models through a better description of subgrid processes, in particular the subgrid connectivity of flow paths. The Relative Surface Connection function (RSCf) was proposed by Antoine et al. (2009) as a functional indicator of runoff flow connectivity. For a given area, it expresses the percentage of the surface connected to the outflow boundary (*C*) as a function of the degree of filling of the depression storage. This function explicitly integrates the flow network at the soil surface and hence provides essential information regarding the connectivity of flow paths. It has been shown that this function could help improve the modeling of the hydrograph at the square metre scale, yet it is unknown how the scale affects the RSCf, and whether and how it can be extrapolated to other scales. The main objective of this chapter is to study the scale effect on overland flow connectivity (RSCf). For this purpose, digital elevation data of a real field (9×3 m) and three synthetic fields (6×6 m) with contrasting hydrological responses were used, and the RSCf was calculated at different scales by changing the length (*l*) or width (*w*) of the field. To different extents depending on the micro-topography, border effects were observed for the smaller scales when decreasing *l* or *w*, which resulted in a strong decrease or increase of the maximum depression storage, respectively. There was no scale effect on the RSCf when changing *w*, but a remarkable scale effect was observed in the RSCf when changing *l*. In general, for a given degree of filling of the depression storage, *C* decreased as *l* increased, the change in *C* being inversely proportional to the change in *l*. However, this observation applied only up to approx. 50–70 % (depending on the hydrological response of the field) of filling of depression storage, after which no correlation was found between *C*

and *l*. The results of this study help identify the minimal scale for studying overland flow connectivity. At scales larger than the minimal scale, the RSCf showed a great potential to be extrapolated to other scales.

3.2 Introduction

As subgrid functional connectivity is expected to be scale-dependent, special attention must be paid in order to select an appropriate size of the grid cell. Some studies have reported the existence of a representative elementary area (Wood et al., 1988) or length scale (Julien and Moglen, 1990) that could serve to determine the grid cell scale in hydrological models. First, the grid cell must be sufficiently large to be representative of the process of overland flow connectivity at the plot scale, i.e. all the connectivity relevant components and the relationships between them must be represented (Ali and Roy, 2009). Secondly, the size must be selected so as to minimize border effects, i.e. relevant components should neither be missed nor be modified. In addition, slope length has been observed to influence the response of the overland flow, showing a lower runoff coefficient with increasing length (Van de Giessen et al., 2000; Cerdan et al., 2004). It has generally been assumed that this results from the spatial variability of rainfall and infiltration capacity (Yair and Lavee, 1985). Yet this effect has also been observed on homogenous hillslopes, in which case it was attributed to a change in residence time (Stomph et al., 2002). According to the definition of overland flow connectivity (see Section 1.2), connectivity is expected to decrease with increasing slope lengths, since the probability for the water flow to encounter depressions is higher. However, the effect of slope length on overland flow connectivity and the runoff coefficient is still unclear.

The objective of this study is twofold. The first objective is to study the effect of changing scale on the RSCf for scales ranging from 0.18 m^2 to 36 m^2. And the second objective is to investigate the potential of the RSCf to be extrapolated to larger scales. For that purpose, the

RSCf will be calculated and compared at different scales and for different micro-topography types. Comparison of the RSCfs should allow us to find a relationship between scale and overland flow connectivity.

3.3 Materials and methods

3.3.1 Characteristics of the micro-topographies

Two types of DEMs were used, real and synthetic ones. First, we used the DEM from a field located near Fort Collins, Colorado (USA), obtained by laser scanning (courtesy of the USDA-ARS Agricultural Systems Research Unit in Fort Collins). The field had been under grassland but the grass had been killed chemically and left to decay before scanning. The total size of the DEM is 9.5 m × 4.8 m, the spatial *x-y* resolution is 1.5 mm and the vertical resolution is 0.1 mm. The natural slope of the field is 6.6 %. In order to avoid border effects that may have been generated during the process of obtaining the DEM, this study focuses on the central area, with a size of 9 m × 3 m. This was also guided by the need to have three square replicate areas of the largest possible size (in this case, 3 m × 3 m). For computational reasons, the spatial *x-y* resolution of the DEM was reduced to 3 mm. The semi-variograms of the three replicates had a range of approximately 600 mm and a sill of 80–110 mm^2 (Table 3-1).

Secondly, in order to evaluate the scale effect in scenarios with different hydrological characteristics and connectivity patterns, synthetic fields with contrasting micro-topographies were generated using a method developed by Zinn and Harvey (2003) and adapted by Antoine et al. (2009). The synthetic fields present identical statistics in terms of mean elevation, standard deviation and variogram. However, they have different connectivity patterns. In this study a Gaussian variogram model was used (see Section 2.2). This method also allowed us to study the scale effect at larger scales compared to the real field case, though the size of the fields was nevertheless limited

for computational reasons. Three different types of micro-topographies were generated using this method: (a) “river”, (b) “crater” and (c) “random” type (Figure 3-1; Antoine et al., 2009). The “river” type micro-topography presents high areas connected by a system of rills. On the other hand, the “crater” type, which is the reverse of the river type, presents a system of crests that isolate the depressions from each other. The “random” type micro-topography is an intermediate scenario represented by a standard multi-Gaussian synthetic field. The three synthetic fields are characterized by values of sill (100 mm^2) and range (100 mm) of the variogram also observed in real fields (Vidal Vazquez et al., 2005) and experimental plots (Darboux et al., 2002b). A slope equal to the natural slope (6.6 %) of the real field was also added. This slope was considered appropriate to contrast the process overland flow connectivity between the different micro-topographies. Using considerably higher slopes would have dissimulated the effect of micro-topography. At low and moderate slopes, flow connectivity is mainly due to a micro-depressions filling and spilling process. While at high slopes, in which the general slope gradient is higher than local gradients produced by the soil surface elements, such as depressions, the connection mechanism consists in the development of preferential flow paths parallel to the general slope gradient, regardless the micro-topography (Figure 3-2).

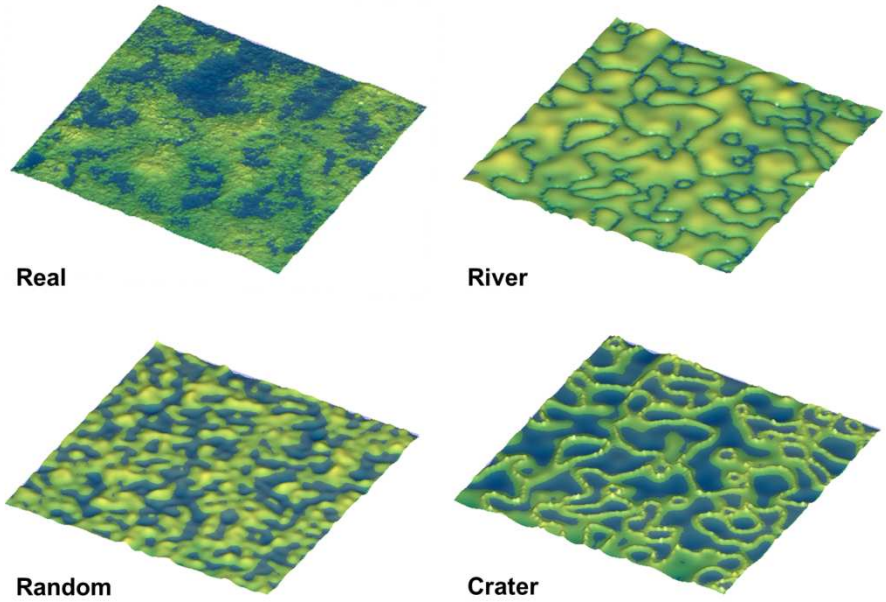

Figure 3-1 Detail of the four micro-topography types (2 m × 2 m) with depressions partially filled with water (in blue) in order to highlight the contrasting connectivities.

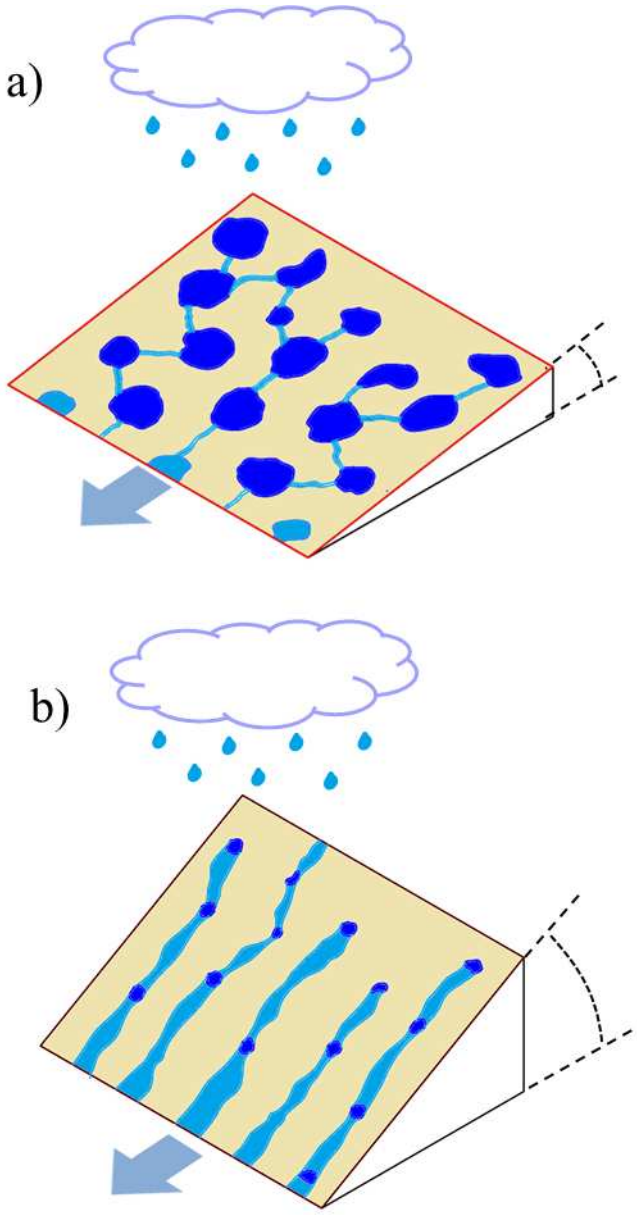

Figure 3-2 Schematic representation of the overland flow connectivity mechanism: (a) predominant filling process for low to moderate slopes and (b) predominant spilling process for high slopes. Stored water in micro-depressions in dark blue. Preferential flow paths and micro-depressions initially connected in light blue.

3.3.2 *Process of fragmentation and calculation of the RSCf*

Two different scale effects were considered, i.e. changing the width of the plot area and changing the length of the plot area. Therefore, the area was first divided into narrower areas (from 1/2 up to 1/32 of the initial width) keeping the initial length constant (Figure 3-3a), and secondly the area was divided into shorter areas (from 1/2 up to 1/32 of the initial length) keeping the initial width constant (Figure 3-3b). The process of fragmentation of the areas and the calculation of the RSCf was exactly the same for all the fields. After the plot areas were divided, the filling algorithm was run in each of these sub-areas in order to obtain their RSCf (Chapter 2.1). Finally, for a given scale, the RSCfs obtained in each sub-area were averaged in order to compare overland flow connectivity at different scales.

Table 3-1 Characteristics of the micro-topographies

		Synthetic Fields		
	Real field	River	Random	Crater
Size [m × m]	3 × 3	6 × 6	6 × 6	6 × 6
Spatial resolution [mm pixel^{-1}]	3	10	10	10
Slope [%]	6.6	6.6	6.6	6.6
Standard deviation of elevation [mm]	1.8	1.3	1.3	1.3
Variogram – sill [mm²]	80–110	100	100	100
Variogram – range [mm]	600	100	100	100
Depression storage [mm]	0.53	0.5	1.275	2.55
Percolation threshold [relative depression storage]	0.66	0.77	0.75	0.73

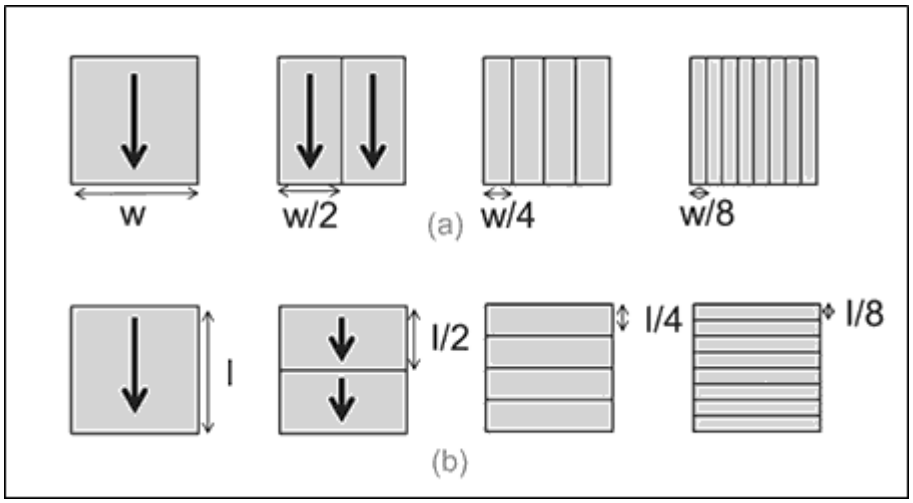

Figure 3-3 Division pattern when changing (a) width and (b) length of the plot

3.3.3 Representative width and length

In order to identify the minimal scale at which overland flow connectivity can be studied, a threshold width and a threshold length must be defined. Since border effects are expected to mainly cause variations in the DS_{max} of the field, the threshold width and length will be defined in function of the observed change in the DS_{max}. These thresholds were arbitrarily set at 10% deviation of the DS_{max} when $w \rightarrow \infty$ and $l \rightarrow \infty$ in the present study. The value of the corresponding width and length will be referred to as the "representative width" and "representative length", and will be used to quantify and compare the scale effects between the four micro-topography types.

3.4 Results

3.4.1 Real field

Scale effect produced by changing only the width

When representing the average RSCf for each width in the same graph (Figure 3-4a), a gradual shift of the RSCf to the left is observed, indicating a gradual decrease of the DS_{max} with increasing width. This decrease in DS_{max} is inversely proportional to the width, tending asymptotically to a constant value (Figure 3-4b). This can be represented adequately by the following expression:

$$\mathrm{DSmax} = \frac{k}{w} + v \qquad \text{Equation 3-1}$$

where DS_{max} is the maximum depression storage [mm] for a given width w [mm] of the plot, k [mm] is a constant (Table 3-2) whose value reflects the magnitude of the asymptotic decrease of the DS_{max} when increasing the width of the plot, and v represents the DS_{max} when w tends to infinity ($DS_{max,w\to\infty}$).

A “representative width” can be defined based on an arbitrary threshold at 10 % deviation from $DS_{max,w\to\infty}$ (Table 3-2). This arbitrary threshold is represented in Figure 3-4b as dashed lines.

In order to compare the shape of the different RSCfs, the depression storage was normalized by the value of the maximum depression storage for each scale (Figure 3-5). This way of representing the RSCf shows that the shape is little affected by width except for the two smallest scales (width = 0.188 m and 0.09 m), which present a strong deviation in the last third of the function (relative depression storage approximately > 2/3). These two curves show a displacement to the right, i.e. for the same value of relative depression storage the

connectivity is lower for the two smallest scales as compared to the larger scales.

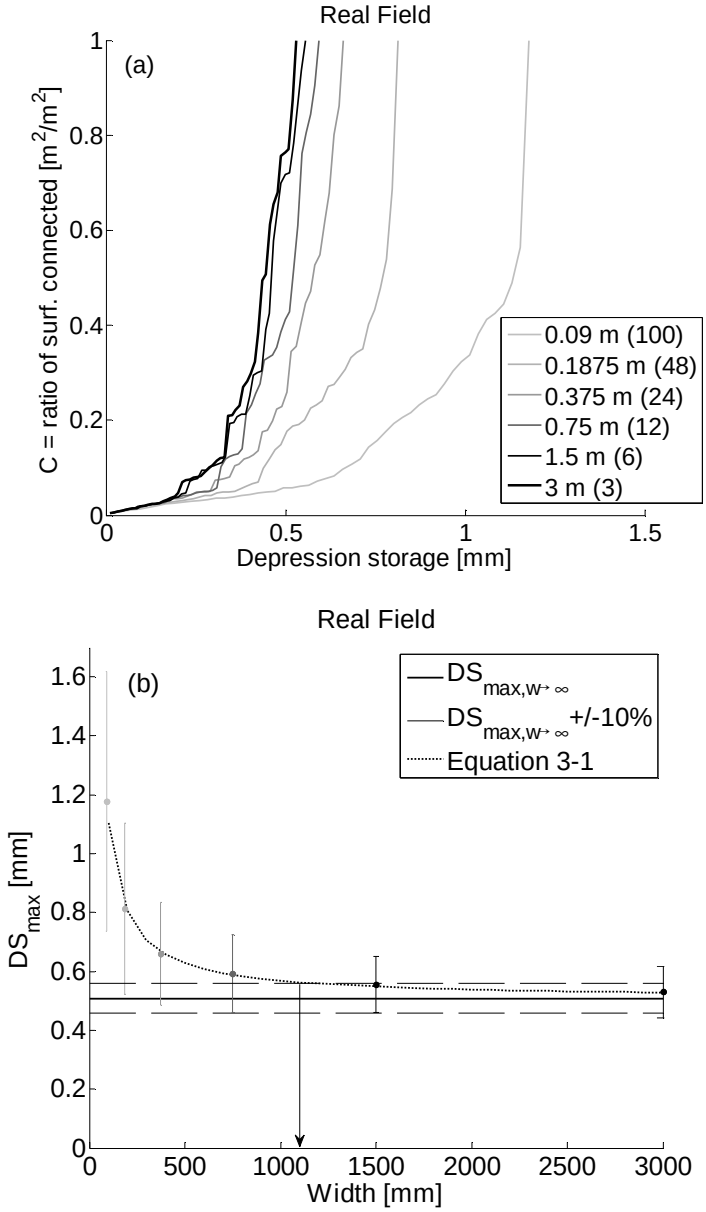

Figure 3-4 Real field – effect of plot width (a) on the RSCf and (b) on the maximum depression storage (DS_{max}). The number in parentheses indicates the number of RSCf used for calculating the average RSCf. Vertical bars = standard deviations. The arrow indicates the representative width. All the plots are 3 m long.

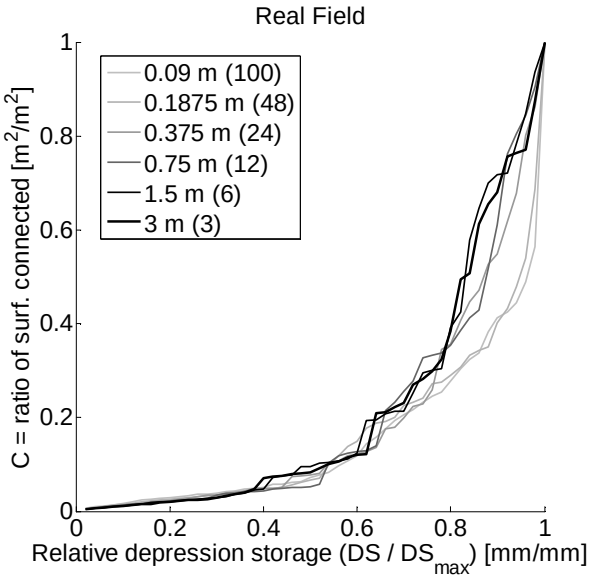

Figure 3-5 Real Field - effect of plot width on the average normalized RSCf (Depression storage (x axis) scaled by the maximum depression storage; all the plots are 3 m long).

Scale effect produced by changing only the length

When changing the length for a constant width of 3 m, the average RSCfs show the opposite trend than was observed when changing the width. The RSCf shows a gradual shift to the right as the plot length increases (Figure 3-6a), i.e. a gradual increase of the DS_{max} with increasing length. This increase in DS_{max} with plot length can also be fitted adequately by Equation 3-1, after replacing w by l and with $k < 0$ (Figure 3-6b). The corresponding parameters are provided in Table 3-3. In this case, v represents the DS_{max} when l tends to infinity ($DS_{max,l\to\infty}$).

A reduction in length not only causes a decrease in DS_{max} but also a change in the shape of the RSCfs. For a given value of the relative depression storage, a decrease in connectivity is observed as the length increases (Figure 3-13). The RSCf tends from a convex shape for the largest plot lengths to a straighter or even concave shape,

especially for the smallest scales (length = 0.375 m and 0.188 m). The change in the shape of the RSCf is least pronounced for the river type and most pronounced for the crater type.

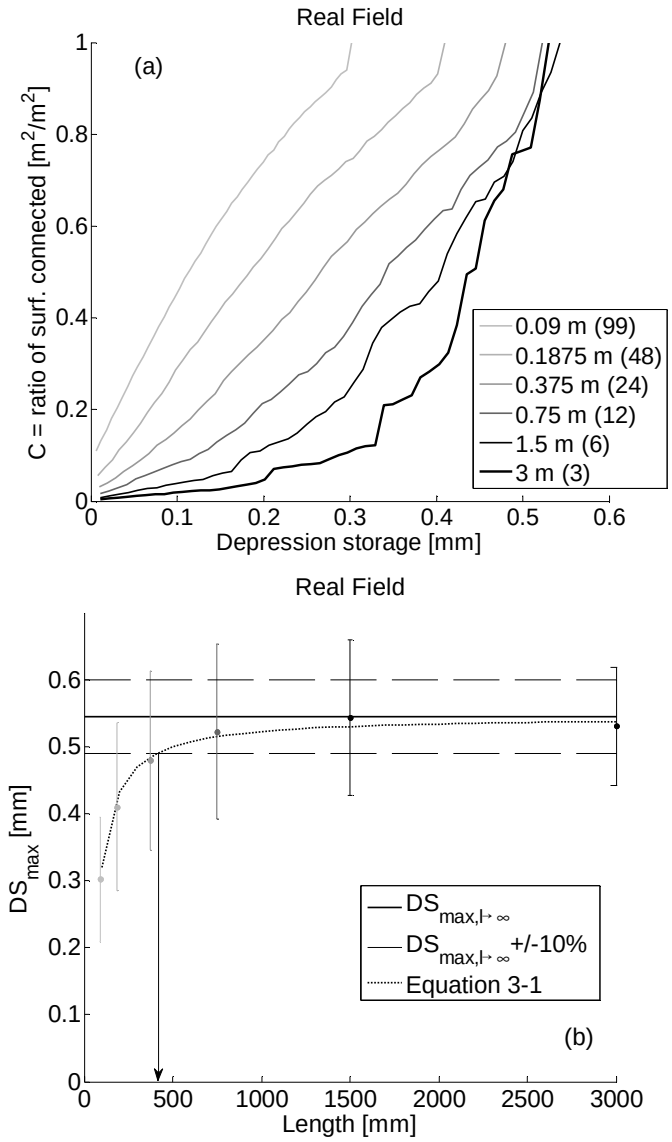

Figure 3-6 Real field – effect of plot length (a) on the RSCf and (b) on the maximum depression storage (DS_{max}). The number in parentheses indicates the number of RSCf used for calculating the average RSCf. Vertical bars = standard deviations. The arrow indicates the representative length. All the plots are 3 m wide.

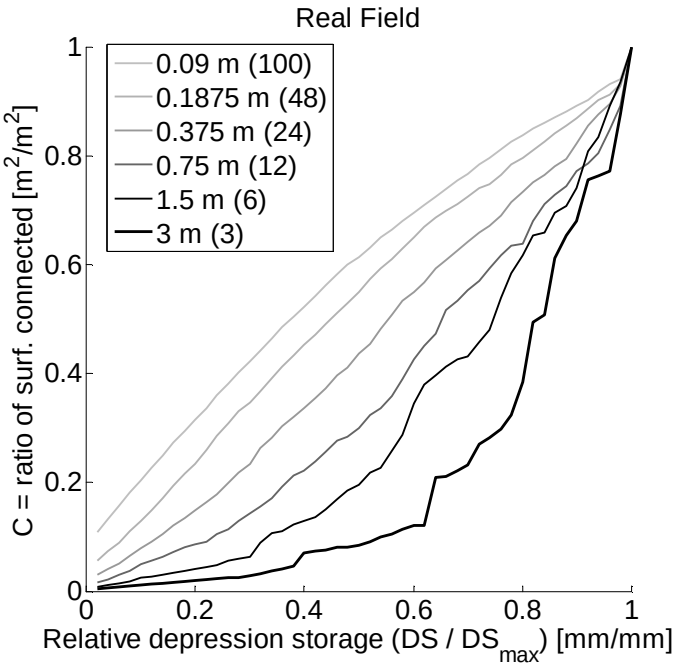

Figure 3-7 Real field – effect of plot length on the average normalized RSCf. Depression storage (x-axis) was scaled by the maximum depression storage. The numbers in parentheses indicate the number of connectivity curves used for calculating the average normalized RSCfs. All the plots are 3 m wide.

3.4.2 Synthetic fields

Scale effect produced by changing only the width

As for the real field, when increasing the plot width, a gradual shift of the RSCf to the left is observed (Figure 3-8), reflecting a gradual decrease of the DS_{max}. DS_{max} decreases asymptotically towards a constant value as the width is increased (Figure 3-9), which can be represented adequately by Equation 3-1. The corresponding parameters are provided in Table 3-2. $DS_{max,w\to\infty}$ increases gradually from the river to the crater topography. As indicated by the k-values, the asymptotic decrease of DSmax with increasing widths is most pronounced for the crater micro-topography. However, as the representative width is determined based on an threshold of 90 % on

the estimation of $DS_{max,w\to\infty}$, the river micro-topography is characterized by a higher representative width (2500 mm) as compared to the random and crater micro-topographies that show smaller yet similar representative widths (1100 mm and 900 mm, respectively).

The shape of the RSCf, as for the real field, is little affected by a change in width, except for the smallest values of width (Figure 3-10). For the random and river types, this deviation is only observable at the two smallest scales (width = 0.375 m and 0.188 m) in the last third of the RSCf. For the crater type, a deviation is also noticeable in the last third of the RSCf for the intermediate widths (width = 0.75 m and 1.5 m).

Scale effect produced by changing only the length

When reducing the length and keeping the initial width (6 m), the average RSCfs show the opposite effect compared to when changing the width, just like the real field. Again, there is a gradual shift of the RSCf to the right with increasing length (Figure 3-11). The DS_{max} increases asymptotically towards a constant value as the length increases (Figure 3-12), which can be fitted by Equation 3-1 after replacing w by l. The corresponding values of k ($k < 0$) and v are given in Table 3-3. As indicated by the k-values, the river micro-topography tends more rapidly to its asymptotic value than the random or crater micro-topographies. The representative length increases from the river (300 mm) to the crater type (950 mm).

As for the real field, a reduction in length not only causes a decrease in DS_{max} but also a change in the shape of the RSCfs. For a given value of the relative depression storage, a decrease in connectivity is observed as the length increases (Figure 3-13). The RSCf tends from a convex shape for the largest plot lengths to a straighter or even concave shape, especially for the smallest scales (length = 0.375 m and 0.188 m). The change in the shape of the RSCf is least pronounced for the river type and most pronounced for the crater type.

Table 3-2 Parameters of Equation 3-1 when changing width (*w*), goodness of fit expressed as the sum of squares (SS) and the pseudo R^2, and representative width for the four micro-topography types

	DS_{max} [mm]	*k* [mm]	*v* [mm²]	Sum of squares [mm]	Pseudo R^2	Rep. width [mm]
Real	0.53	60	0.51	0.00036	0.9986	1200
River	0.5	145	0.47	0.00451	0.96952	2500
Random	1.275	129	1.26	0.00102	0.99131	1100
Crater	2.55	222	2.52	0.00145	0.97064	900

Table 3-3 Parameters of Equation 3-1 when changing length (*l*), goodness of fit expressed as the sum of squares (SS) and the pseudo R^2, and representative length for the four micro-topography types

	DS_{max} [mm]	*k* [mm]	*v* [mm²]	Sum of squares [mm]	Pseudo R^2	Rep. length [mm]
Real	0.53	–23	0.55	0.00059	0.93334	400
River	0.5	–16	0.5	0.00009	0.95344	300
Random	1.275	–71	1.29	0.00026	0.98167	600
Crater	2.55	–237	2.57	0.00385	0.99702	950

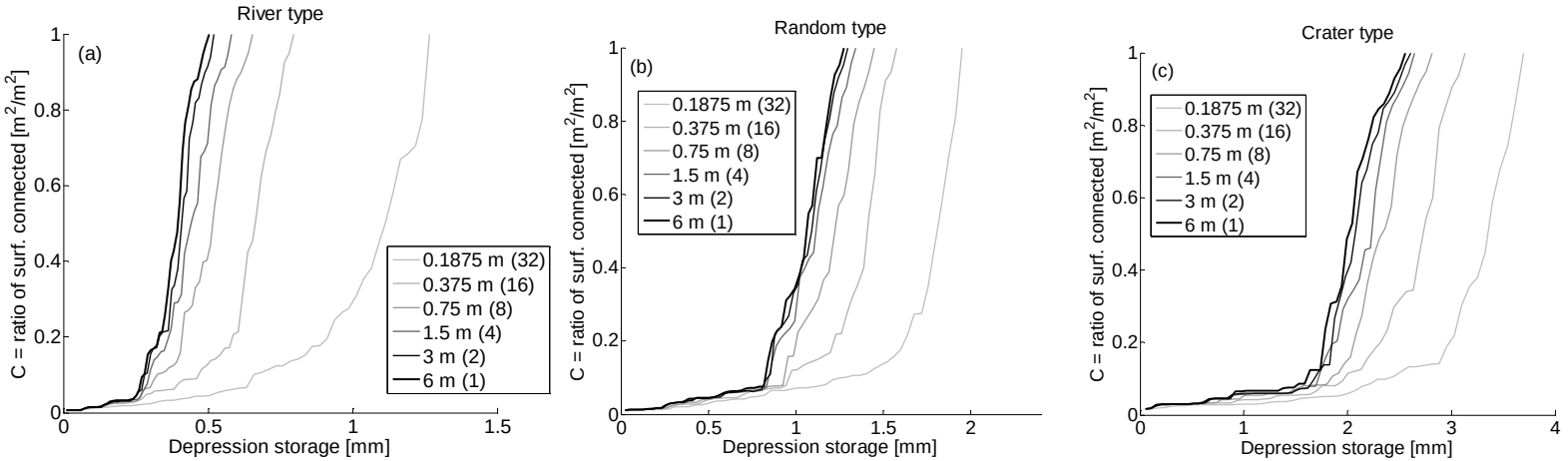

Figure 3-8 Synthetic fields – effect of plot width on the average RSCf for the (a) river, (b) random and (c) crater type micro-topographies. The numbers in parentheses indicate the number of connectivity curves used for calculating the average RSCfs. All plots are 6 m long.

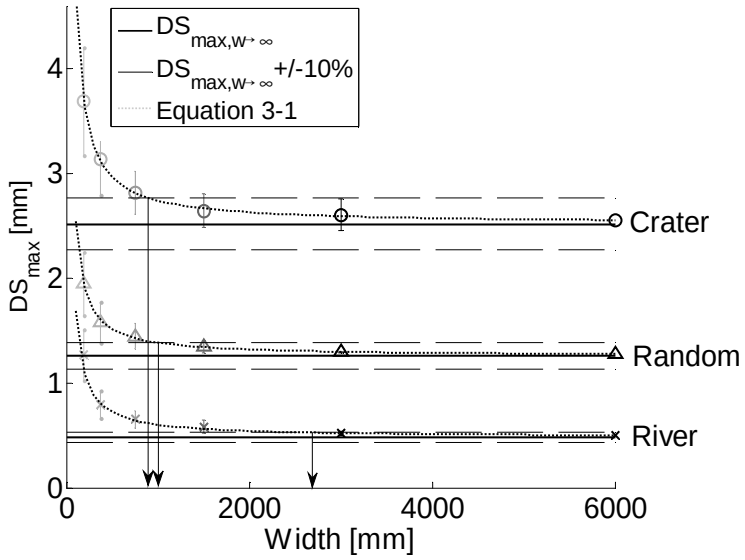

Figure 3-9 Synthetic fields – effect of plot width on the maximum depression storage for the river, random and crater type micro-topographies. Vertical bars = standard deviations. The arrows indicate the representative widths. All the plots are 6 m long.

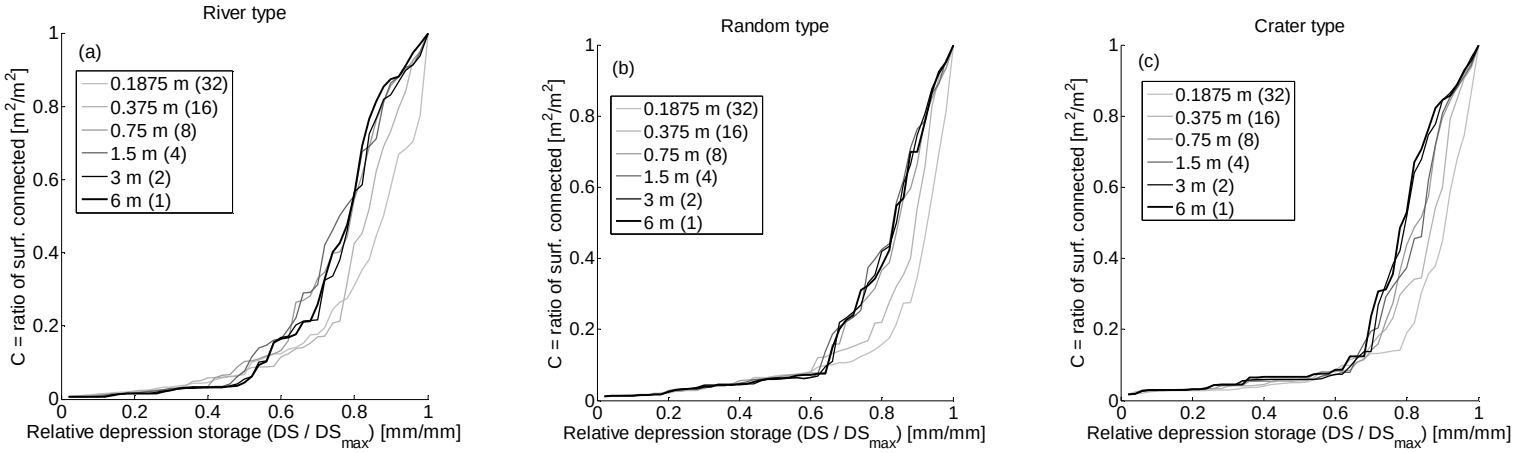

Figure 3-10 Synthetic fields – effect of plot width on the average normalized RSCf for the river, random and crater type micro-topographies. Depression storage (x-axis) was scaled by the maximum depression storage. The numbers in parentheses indicate the number of connectivity curves used for calculating the average normalized RSCfs. All plots are 6 m long.

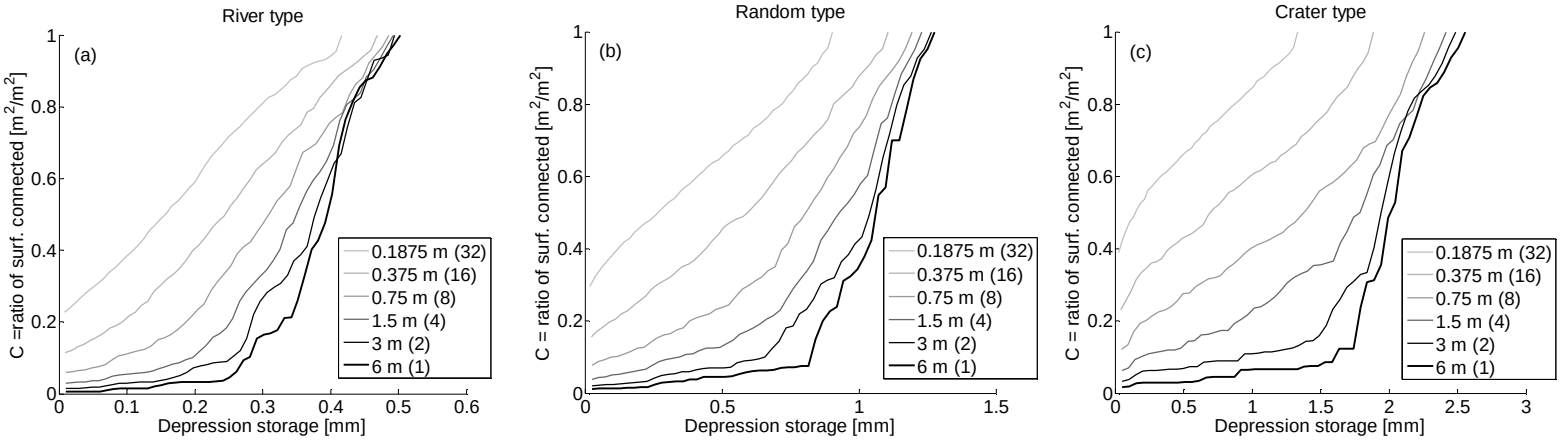

Figure 3-11 Synthetic fields – effect of plot length on the average RSCf for the river, random and crater type micro-topographies. The numbers in parentheses indicate the number of connectivity curves used for calculating the average RSCfs. All plots are 6 m wide.

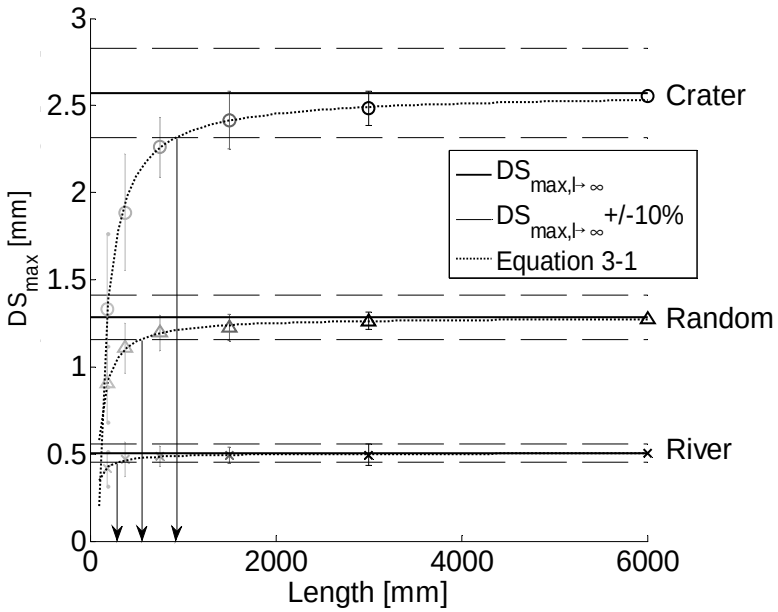

Figure 3-12 Synthetic fields – effect of plot length on the average RSCf for the river, random and crater type micro-topographies. The numbers in parentheses indicate the number of connectivity curves used for calculating the average RSCfs. The arrows indicate the representative lengths. All plots are 6 m wide.

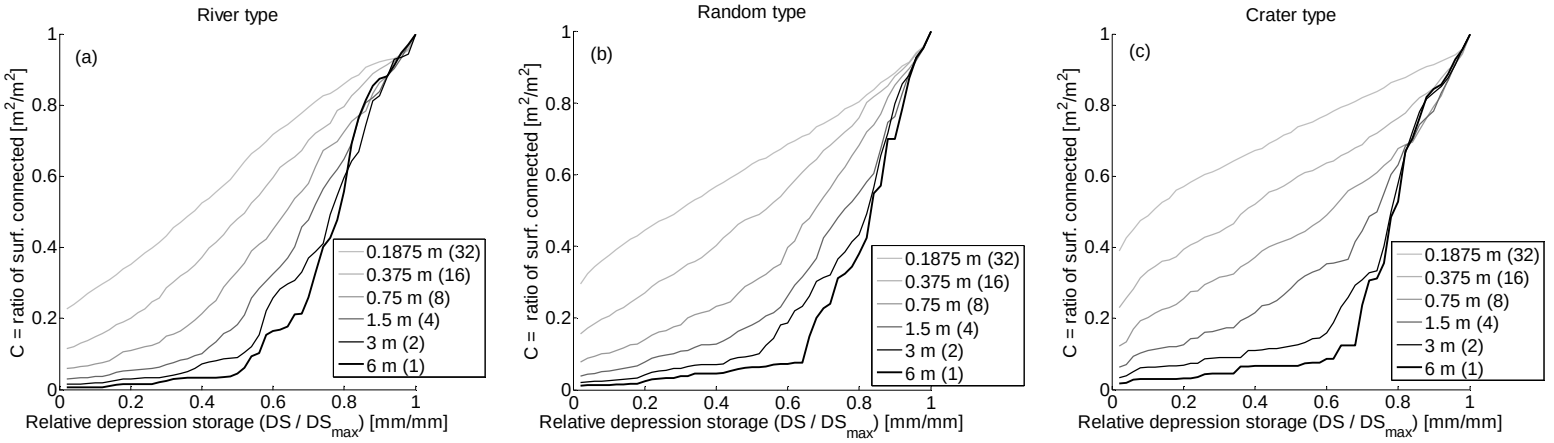

Figure 3-13 Synthetic fields – effect of plot length on the average normalized RSCf for the river, random and crater type micro-topographies. Depression storage (x-axis) was scaled by the maximum depression storage. The numbers in parentheses indicate the number of connectivity curves used for calculating the average normalized RSCfs. All plots are 6 m wide.

3.5 Discussion

3.5.1 Scale effect on the DS_{max}

For all the cases studied, a gradual increase or decrease of the DS_{max} has been observed when decreasing the width or the length, respectively. This can be explained by the increasing influence of the lateral and bottom boundaries when reducing the scale, i.e. by two border effects. On the one hand, the reduction of the width causes the interruption of the connecting paths between depressions (Figure 3-4b, Figure 3-9 and Figure 3-14). Below a certain scale, the deviation of the DS_{max} from the $DS_{max,w\to\infty}$ starts to be considerable. The connections between depressions are not completely included in this area and consequently water has to find new paths to reach the outflow boundary (Figure 3-14). These new paths require higher levels of stored water, i.e. the depth of water needed to overflow the depressions gets higher, and consequently the value of DS_{max} increases. On the other hand, when the plot length is reduced below a certain scale (Figure 3-6b and Figure 3-12), the resulting area becomes less and less representative of all the components that cause the accumulation of water in the depressions (i.e. barriers in the direction of flow). In other words, as the length decreases, a larger proportion of depressions get crossed by the virtual downstream outflow boundary, and hence they get more easily connected to it and do not store water (Figure 3-15).

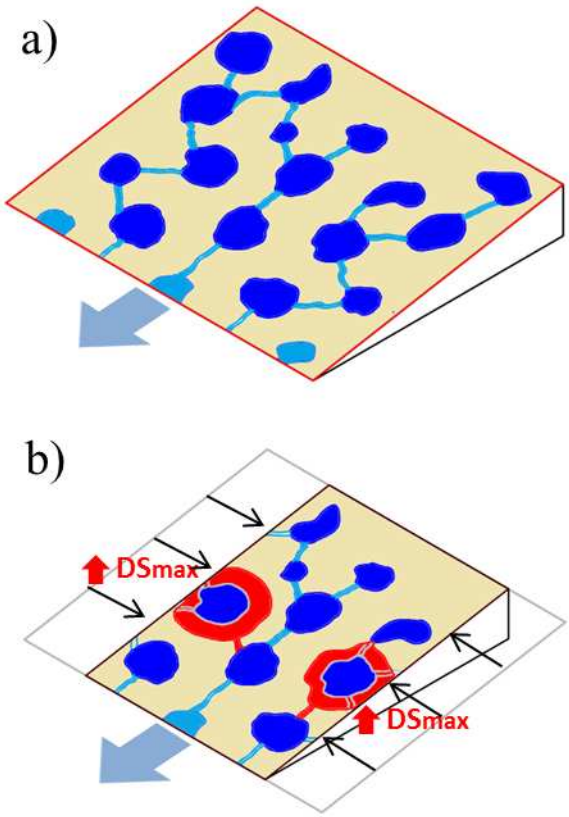

Figure 3-14 Schematic representation of the overland flow pattern for a predominant micro-depressions filling process (a) for the original plot size and (b) after reducing the plot width. Stored water in micro-depressions in dark blue. Preferential flow paths and micro-depressions initially connected in light blue. Increase of micro-depressions area and new preferential flow paths after plot width reduction in red. Original size of micro-depressions and preferential flow paths before reducing the plot length in gray.

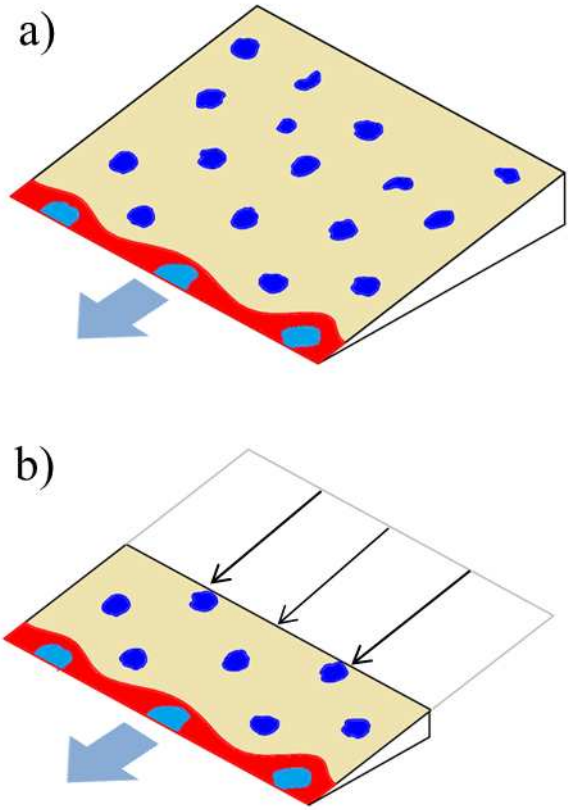

Figure 3-15 Schematic representation of the scale effect on the first stage of the depression filling process produced by changing only the plot length. (a) Original size of the plot and (b) after reducing its length. Stored water in micro-depressions in dark blue. Area connected to the bottom boundary in red. Micro-depressions initially connected and crossed by the bottom boundary in light blue.

These two border effects affect all the micro-topography types similarly in a qualitative way but differently in a quantitative way. In order to quantify and compare these effects between the different micro-topography types, a representative scale was defined based on an acceptable deviation of the DS_{max} by 10 % from its asymptotic value (Figure 3-4b, Figure 3-6b, Figure 3-9, and Figure 3-12). This representative scale represents the width or length below which the border effects start to be considerable, i.e. the plot is neither long enough nor wide enough to be representative of the process of

overland flow connectivity occurring at larger scales. A 10 % deviation from $DS_{max,w\to\infty}$ or $DS_{max,l\to\infty}$ was selected since smaller deviations of the DS_{max} would barely affect results in hydrological modeling. Indeed, in our study, $DS_{max,w\to\infty}$ or $DS_{max,l\to\infty}$ values ranged from 0.5 mm to 2.5 mm, such that a 10 % deviation would lead to an absolute variation comprised between 0.05 mm and 0.25 mm. We believe that having a greater accuracy on the DS_{max} would not be relevant for most practical applications, whereas accepting a higher deviation, especially in fields with high values of DS_{max}, might lead to a substantial bias in hydrograph estimation.

The proposed representative scale provides a measure of the sensitivity of the different micro-topographies to these two border effects. It is calculated using Equation 3-1 (Table 3-2 and Table 3-3). When plotted as a function of $DS_{max,w\to\infty}$ or $DS_{max,l\to\infty}$ (Figure 3-16a and b), the sensitivity of the four micro-topography types to scaling can be compared.

On the one hand, Figure 3-16a shows a decrease of the representative width as the $DS_{max,w\to\infty}$ increases. This decrease seems to follow a linear trend except for the river micro-topography whose representative width is approximately double of the real micro-topography, even though they both have approximately the same value of $DS_{max,w\to\infty}$. This shows a higher sensitivity of the DS_{max} to changes in width for the river micro-topography compared to the other micro-topographies. On the other hand, Figure 3-16b shows an increase of the representative length as the $DS_{max,l\to\infty}$ increases. This increase seems to be approximately linear and, as opposed to the width border effect, the length border effect shows the highest sensitivity to changes in length for the crater micro-topography and a lowest sensitivity for the river one.

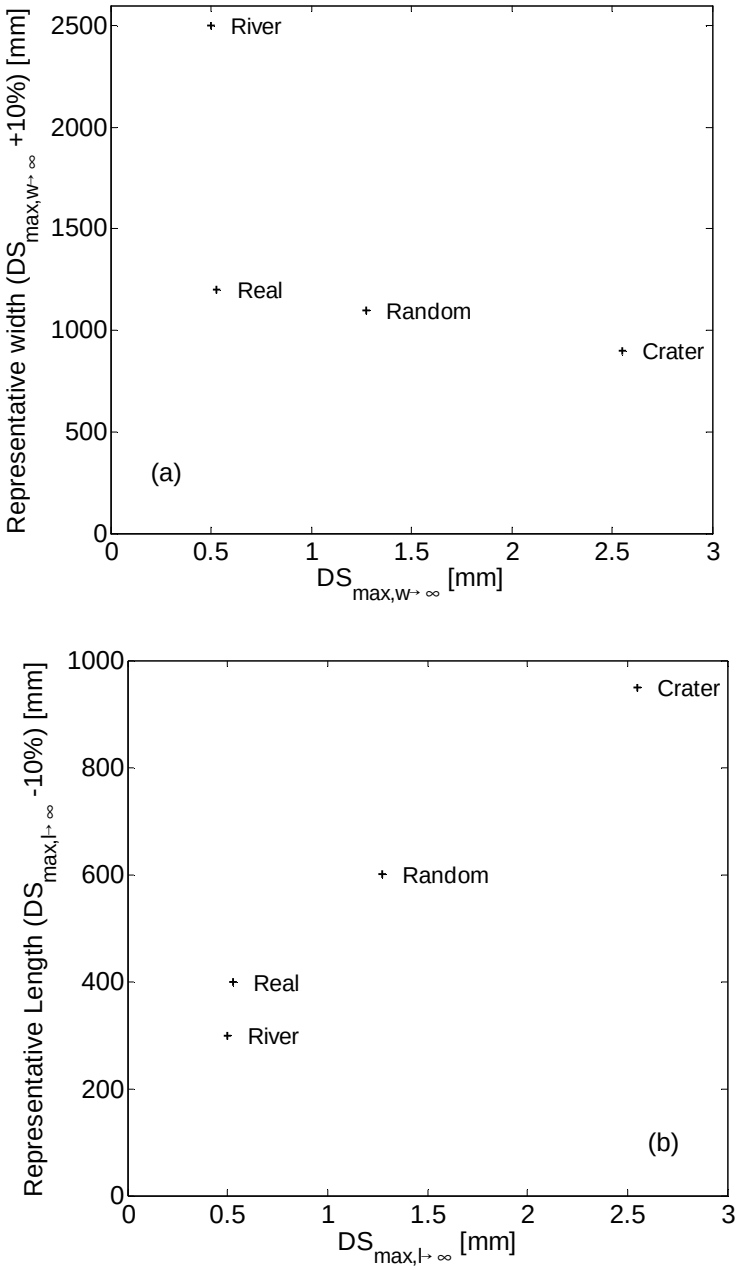

Figure 3-16 (a) Representative width as a function of the DS_{max} value for $w\to\infty$ for the four micro-topography types and (b) representative length as a function of the DS_{max} value for $l\to\infty$ for the four micro-topography types.

These differences between the width and the length border effects and between different micro-topographies can be explained by the preferential directions of flow and the different mechanisms of overland flow connectivity. Since a constant slope of 6.6% was applied to all the micro-topographies, the preferential direction of flow is expected to follow the maximum slope direction, parallel to the lateral boundaries, until the bottom boundary. However, flow paths in the direction perpendicular to the lateral boundaries may also be important for the overland flow connectivity. This is the case of the river micro-topography, which is the most sensitive to the width border effect. The mechanism of overland flow connectivity in this micro-topography type is based on connections by a system of narrow rills which do not follow a preferential direction. When these rills are blocked by the virtual lateral boundaries, water must overflow higher areas of the plot to flow either to other rills or down to the bottom boundary. As a consequence, the overland flow process changes from a connectivity-driven process to an overflow-driven process as width decreases, causing a higher storage of water inside the disconnected areas, i.e. an increase of the DS_{max}. On the contrary, connectivity in the crater micro-topography, which is the least sensitive to the width border effect, is already driven by an overflow mechanism, meaning that water stored in depressions must overflow the system of crests to flow either to other depressions or down to the outflow boundary. In this case, water overflows the crests located at the lower part of the depressions, thus overland flow tends to follow the maximum slope direction, which is parallel to the lateral boundaries. Since water tends to flow parallel to the lateral boundaries, the latter are less likely to block connections between depressions, and as a consequence, reducing the width has a lower impact on the connectivity process and on the DS_{max}.

Conversely to the width border effect, as the length is decreased the mechanism of connectivity becomes less based on the overflow of depressions since a larger proportion of depressions gets crossed by the downstream outflow boundary, and consequently the DS_{max}

gradually decreases. In the crater micro-topography, which is the most sensitive to the length border effect, connectivity is driven by an overflow process for large lengths, as explained above. Nevertheless, depressions located downstream and crossed by the outflow boundary get directly connected since water does not need to overflow the system of crests. On the contrary, in the river micro-topography, which is the least sensitive to the length border effect, overland flow from higher areas is stored in the system of rills. This mechanism of connectivity stores a very low volume of water since most rills are interconnected. Only locally disconnected areas, which need to overflow to get connected, store a significant volume of water. Therefore, the length border effect is considerable only when the downstream outflow boundary crosses a large fraction of these isolated areas, which only occurs when the length of the plots becomes very small (i.e. ≤300 mm for the river micro-topography).

For the two other micro-topography types, real and random, the sensitivity to the two border effects is, as expected, situated between the two extreme cases, river and crater (Figure 3-16). The width border effect affects the real and random types to a slightly higher extent than the crater type but considerably less than the river type. This suggests that the preferential direction of flow is parallel to the lateral boundaries. In addition, the connectivity mechanism for the real and random micro-topographies appears to be intermediate between the overflow of depressions and the connection through rills. However, since the representative length of the real micro-topography is closest to the river type, the connectivity mechanism may be predominately based on rill connections rather than the overflow of depressions.

As shown above, the sensitivity to border effects depends on the preferential direction of flow and the hydrological response of the field. Even micro-topographies with the same statistical properties (Table 3-1) showed different sensitivities to border effects and "representative" scales. This is explained by the fact that these

statistics can be considered as structural indicators whereas the RSCf is a functional indicator. Structural indicators such as the variogram can be useful to describe the spatial heterogeneity (Western et al., 1998), and as a heterogeneity index they can be interpreted as a link between pattern and process (Gustafson, 1998). As opposed to functional indicators, they are, however, not able to adequately account for the complexity of overland flow patterns. In the case of the synthetic fields, spatial statistics such as the variogram are furthermore scale-insensitive. Functional connectivity indicators like the RSCf are needed to study how connectivity is affected by the border effects. Not only do functional connectivity indicators help identify the sensitivity to border effects but they may also help understand the connectivity process and discriminate between different mechanisms of connectivity.

3.5.2 Scale effect on overland flow connectivity produced by changing only the width

Apart from the border effect on the DS_{max} when changing width, the shape of the RSCf does not seem to be considerably affected by a change in width (Figure 3-5 and Figure 3-10). Only when the width of the sub-areas of study is less than a certain scale ($\leq 0.375\,m$) do border effects get more noticeable. In that case, they not only have an effect on the DS_{max} but also a non-negligible impact on the shape of the RSCf. As width increases, this border effect becomes less and less noticeable both on the DS_{max} and on the shape of the RSCf. Therefore, regions of a field wider than the minimal representative width may be considered representative of the functional connectivity of the whole field.

3.5.3 Scale effect on overland flow connectivity produced by changing only the length

When length decreases, it not only produces a decrease in the DS_{max} but also a considerable increase of the connectivity, as can be seen

from a comparison of the normalized RSCfs (Figure 3-7 and Figure 3-12). In order to quantify the change in shape of the normalized RSCf, the connectivity value of the largest field $C(lref)$, taken as a reference, was divided by the connectivity value of the other scales $C(l)$ for each value of relative depression storage (Figure 3-17a and 3-15a). For the first part of the graphs (RDS <0.5–0.7), the connectivity ratios appear to oscillate around a mean value without any clear increasing or decreasing trend. In this interval the separation between two successive curves remains approximately constant, whilst for larger DS_{max} values, the $C(lref)/C(l)$ ratio increases rapidly and the separation between the curves progressively decreases until they all meet when the field is completely connected (relative depression storage $=1$).

Since for a given scale the ratio $C(lref)/C(l)$ appears to oscillate around a mean value as long as RDS <0.5–0.7, the values of $C(lref)/C(l)$ for this part of the function were averaged and compared to the ratio $l/lref$, where $lref$=3 m for the real field (Figure 3-17b) and $lref$=6 m for the synthetic fields (Figure 3-18b). In this interval of RDS, both ratios show a direct correlation, implying that the rate of change of the ratio $C(l)/C(lref)$ is inversely proportional to the rate of change of the length ratio ($l/lref$). Since connectivity is the ratio of area connected to the outflow boundary and it increases at the same rate as the length decreases, the size of the area connected (in absolute units, m^2) must be approximately the same for all the length scales. This is supported by Figure 3-20, and can be explained as follows. For the first part of the RSCf, which represents the first stage of the depression filling process, the depressions that are most likely to be already connected are the ones located closest to the bottom boundary. These depressions, which occupy a specific area (Figure 3-15a), behave independently with regard to the rest of the depressions, further away from the bottom boundary. This connected area keeps the same size independently of the plot length (Figure 3-15) except for plots shorter than this area (Figure 3-20 and Figure 2-1a). Therefore,

the connectivity *C* gets higher when decreasing the plot length since the total area of study decreases.

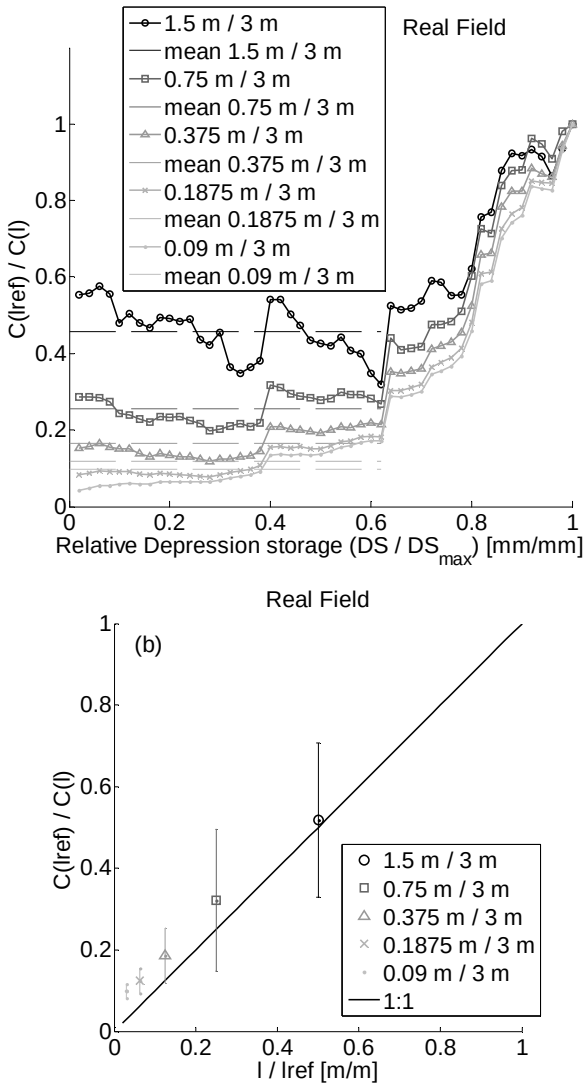

Figure 3-17 Real field – scale effect when changing the length: (a) ratio of connectivities at different scales as a function of the relative depression storage. Horizontal dashed lines correspond to the mean value of the connectivity ratio calculated over the range RDS = 0 to RDS = 0.62. (b) Correlation between the scale ratios and the ratios of connectivities for the first two thirds of the RSCf. Vertical lines = standard deviation. All the plots are 3 m wide.

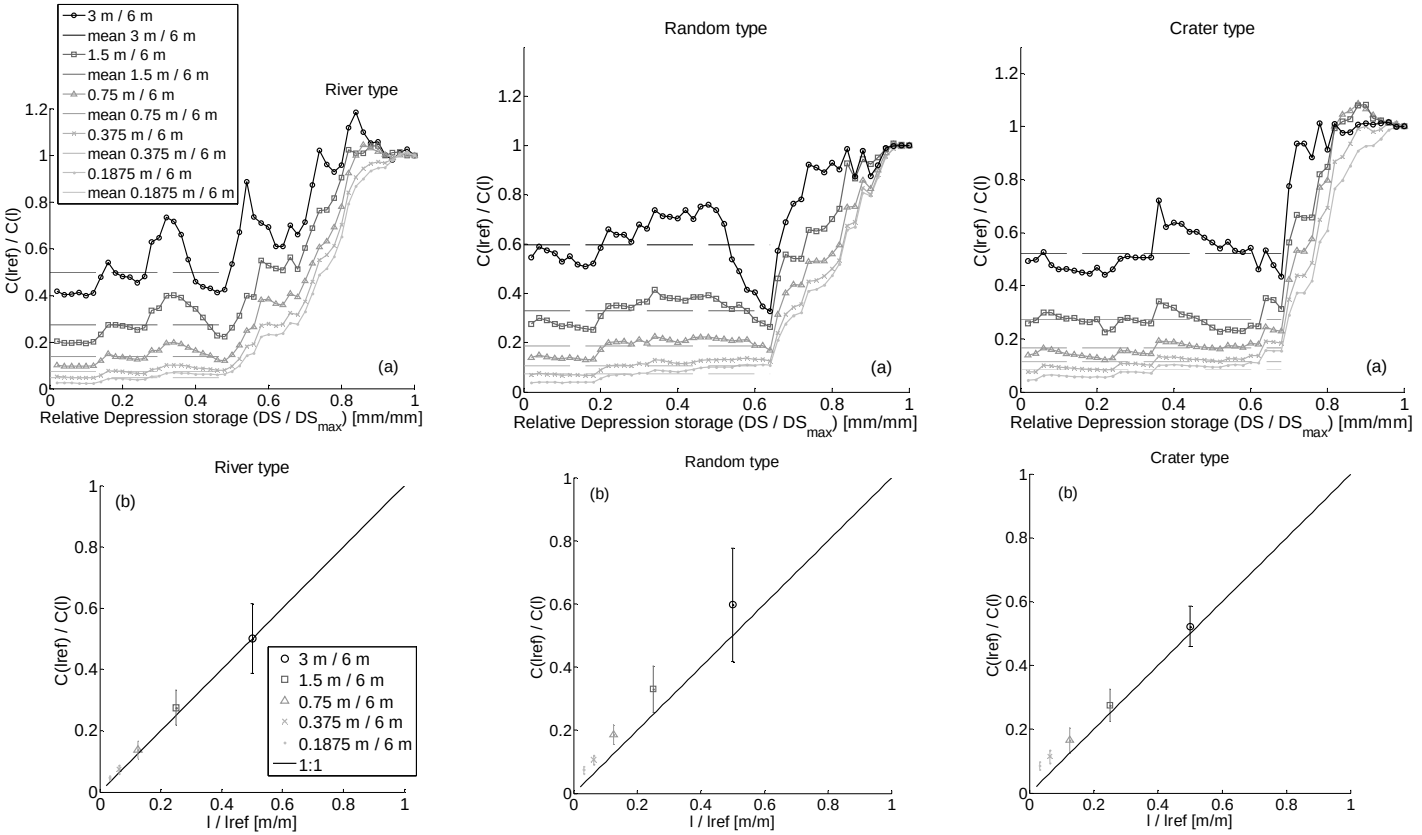

Figure 3-18 Synthetic fields – scale effect when changing the length for the river, random and crater micro-topographies: (a) ratio of connectivities at different scales as a function of the relative depression storage. Horizontal dashed lines correspond to the mean value of the connectivity ratio calculated over the range RDS = 0 to RDS = 0.5–0.7. (b) Correlation between the scale ratios and the ratios of connectivities for the first two thirds of the RSCf. Vertical lines = standard deviation. All the plots are 6 m wide.

After this first stage of the depression filling process (RDS < 0.5–0.7), a quick process of connection of the depressions starts and depressions located further from the outflow boundary get connected. This "jump" or sharp threshold in the RSCf, which has been observed in all four micro-topographies, is more noticeable for the longer plots (> 3 m) (Figure 3-20). This threshold is consistent with percolation theory (Berkowitz and Ewing, 1998), whose applicability on overland flow was demonstrated by Darboux et al. (2002a) and Lehman et al. (2007). It relies on the existence of a threshold relationship between rainfall and overland flow, caused by variations in the storage capacity and connectivity. Below a certain threshold, preferential pathways that go from the top to the bottom boundary are still not connected and the overland flow remains very low. But when this threshold is exceeded, the pathways become connected and a sharp increase in the overland flow occurs. Applying this concept, the percolation threshold can be calculated as the value of relative depression storage needed to connect the bottom boundary with the top boundary (Table 3-1). The values obtained for the four micro-topography types are slightly higher than the threshold observed in the RSCf. This observed threshold can be assumed to represent the initiation of the connection between the bottom and the top boundary of the plot just before the complete percolation threshold is reached.

Assuming that for RDS < 0.5–0.7 only the depressions close to the bottom boundary are connected, it may be possible to relate this stage to specific characteristics of the structural connectivity of the field, such as the average size of the depressions (puddles) or the range and sill of the variogram. It may then be possible to predict this first stage of the RSCf.

For the last part of the RSCf, which represents the last stage of the depression filling process, the depressions that are less likely to be connected are the ones located closest to the top boundary. Since no runon is considered, these depressions barely receive water from the upslope area and the main contributor to the filling process is rainfall.

Therefore, these depressions start to overflow and hence get connected later than the rest of depressions closer to the bottom boundary (Figure 3-19a). Since the rate of filling for the depressions closest to the top boundary is lower than for the rest of the depressions, the connection of the entire plot surface is delayed in time and a higher cumulated rainfall volume is needed. As for the depressions closest to the bottom boundary, the depressions closest to the top boundary, which occupy a specific area (Figure 3-19a), behave independently with regard to the downslope depressions. This unconnected area keeps the same size independently of the plot length (Figure 3-19b) except for plots shorter than this area. For longer areas, this effect does not affect DS_{max}, but in terms of time, the delay caused by the slower filling process of the micro-depressions closest to the top boundary is likely to become relatively more important for the overland flow hydrogram as the length decreases. Since the area of the unconnected area becomes relatively larger compare to the size of the plot, the connection of a relatively larger part of the plot would be delayed.

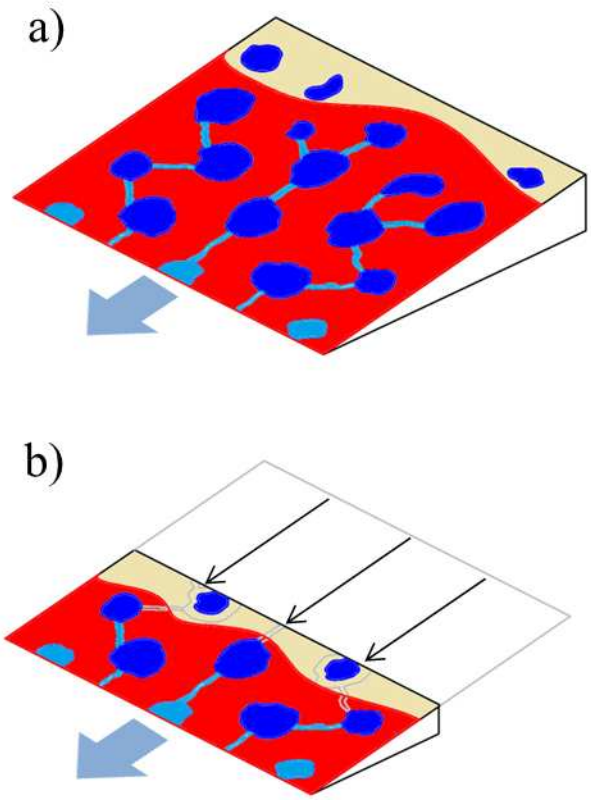

Figure 3-19 Schematic representation of the scale effect on the last stage of the depression filling process produced by changing only the plot length. (a) Original size of the plot and (b) after reducing its length. Stored water in micro-depressions in dark blue. Area connected to the bottom boundary in red. Micro-depressions initially connected and crossed by the bottom boundary and preferential flow paths in light blue. Original size of micro-depressions and preferential flow paths before reducing the plot length in gray.

These results show a great potential for the RSCf to be extrapolated from small scales to larger scales on fields with a constant slope such that a spatial autocorrelation (range) can be observed in the variogram. At scales larger than the minimal representative scale, once the percolation threshold is identified and predicted, we can divide the RSCf in two parts. The first part, before the percolation threshold, can be directly extrapolated by applying the inverse correlation between

length and connectivity. The second part, after the percolation threshold, in which no correlation between scales has been found, may be obtained by assuming a linear relationship between depression storage and connectivity. Given that the DS_{max} converges to a constant value for a given micro-topography and that border effects become negligible beyond the minimum representative length and width (Figure 3-4b, Figure 3-6b, Figure 3-9 and Figure 3-12), it may be possible to apply the present results to scales larger than the ones used in this study. However, the present results may not be applicable in the absence of a spatial autocorrelation in the variogram since connectivity may then be affected by the effect of variable slope or variable random roughness inside the plot. Further research is needed to assess and confirm this.

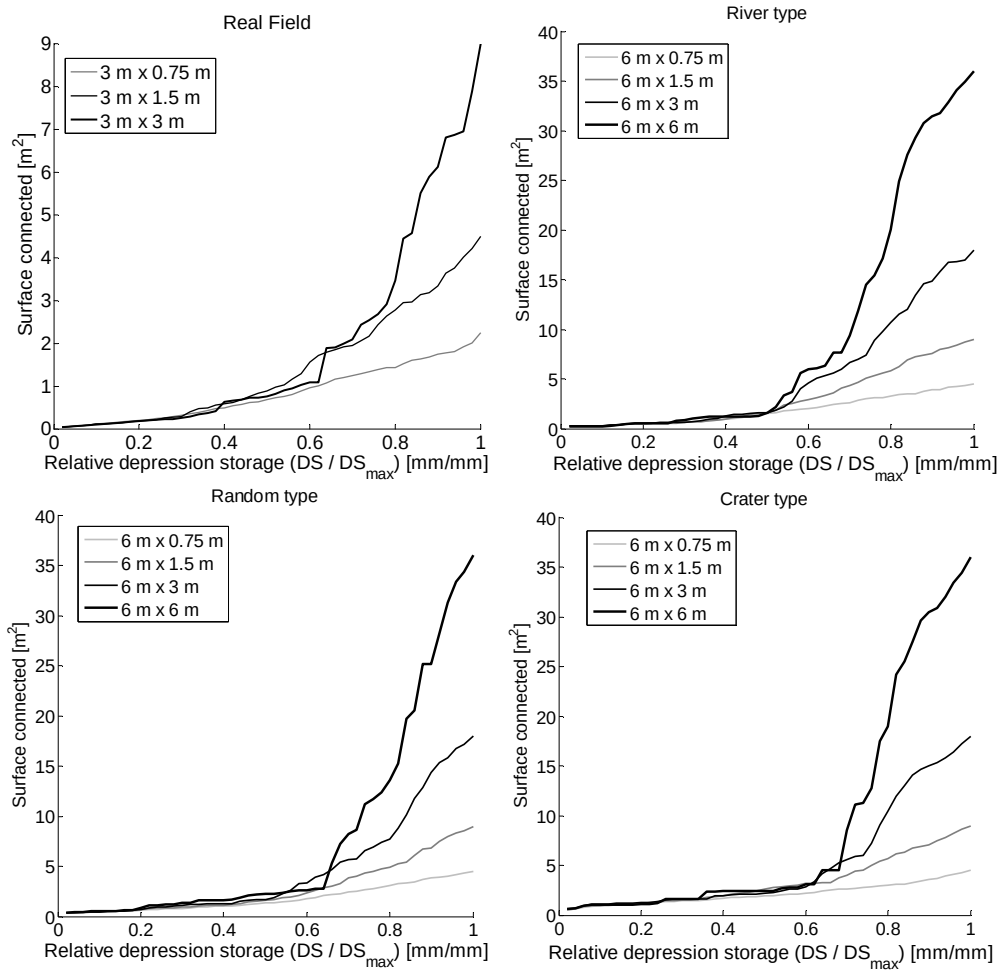

Figure 3-20 Surface of the area connected to the outflow boundary, in absolute units (m^2), as a function of the relative depression storage for the four micro-topography types.

3.6 Conclusions

In this study we investigated the behaviour of overland flow connectivity using the RSCf when changing the scale (length or width) of the area of study. The results reveal that both scale effects and border effects affect overland flow connectivity at the plot scale. The changes in the RSCf with scale were consistent across four

different surfaces with contrasting micro-topography patterns. However, the magnitude of the scale and the border effects differed according to the hydrological response of the micro-topography but could not be related to spatial statistics (e.g. the variogram).

No scale effect but a border effect was observed when changing the width of the plots. Hence, regions of a field with fairly short widths could be considered representative of the functional connectivity of the whole field. Based on the study of the sensitivity of the RSCf to width and length border effects, preferential direction of flows and different predominant mechanisms of connectivity on different micro-topography types could be inferred. This sensitivity to border effects also allowed determining the minimal representative scale (width or length) needed to study the overland flow connectivity, in this study between 0.3 m and 2.5 m depending on the micro-topography type.

A remarkable scale effect was observed in the RSCf when changing the length of the plots. At scales larger than the minimal representative scale, the RSCf showed a great potential to be extrapolated to other scales. For a given degree of filling of the depression storage, connectivity (C) decreased as the plot length increased and the rate of this change of connectivity was inversely proportional to the rate of change in length. This latter observation applied only to the first stage of the RSCf (up to approx. 50–70 % of filling of the maximum depression storage), after which no correlation was found between C and length.

At this first stage of the RSCf, it has been observed that only the depressions close to the outflow boundary are connected. After this first stage, the RSCf shows a quick linear increase of the connectivity of the field, which is consistent with percolation theory. These two well-differentiated stages can potentially not only help extrapolate the whole RSCf to larger scales but also obtain information about the structural connectivity of the field.

Additional research is needed in order to predict the percolation threshold and to test the applicability of extrapolating the whole RSCf to other scales. In order to do so, a larger number of DEMs obtained from a greater variety of real soils and synthetic fields with larger sizes, different boundary conditions and connectivity characteristics must be studied.

CHAPTER 4[2]

[2] Based on: *Peñuela, A., Javaux, M., Bielders, C. L., 2015. How do slope and surface roughness affect plot-scale overland flow connectivity? J. Hydrol. 528,192-205.*

4 How do slope and surface roughness affect plot-scale overland flow connectivity?

4.1 Abstract

Surface micro-topography and slope drive the hydrological response of plots through the gradual filling of depressions as well as the establishment of hydraulic connections between overflowing depressions. Therefore, quantifying and understanding the effects of surface roughness and slope on plot-scale overland flow connectivity is crucial to improve current hydrological modeling and runoff prediction. This study aimed at establishing predictive equations relating structural and functional connectivity indicators in function of slope and roughness. The Relative Surface Connection function (RSCf) was used as a functional connectivity indicator was applied. Three characteristic parameters were defined to characterize the RSCf: the surface initially connected to the outlet, the connectivity threshold and the maximum depression storage (DS_{max}). Gaussian surface elevation fields (6 m × 6 m) were generated for a range of slopes and roughnesses (sill σ and range R of the variogram). A full factorial of 6 slopes (0 to 15%), 6 values of R (50 to 400 mm) and 6 values of σ (2 to 40 mm) was considered, and the RSCf calculated for 10 realizations of each combination. Results showed that the characteristic parameters of the RSCf are greatly influenced by R, σ and slope. At low slopes and high ratios of $\sigma/2R$, the characteristic parameters of the RSCf appear linked to a single component of the surface roughness (R or σ). On the contrary, both R and σ are needed to predict the RSCf at high slopes and low ratios of $\sigma/2R$. A simple conceptualization of surface depressions as rectangles, whose shape was determined by R and σ, allowed deriving simple mathematical expressions to estimate the characteristic parameters of the RSCf in function of R, σ and slope. In the case of DS_{max}, the proposed equation performed better than previous empirical expressions found in the literature which do not account for the horizontal component of the surface roughness. The

proposed expressions allow estimating the characteristic points of the RSCf with reasonable accuracy and could therefore prove useful for integrating plot-scale overland flow connectivity into hydrological models whenever the RSCf presents a well-defined connectivity threshold.

4.2 Introduction

Surface micro-topography strongly affects the spatio-temporal distribution of overland flow at the plot scale (Helming et al., 1998; Darboux and Huang, 2005; Antoine et al., 2009; Frei et al., 2010; Appels et al., 2011; Chu et al, 2013; Yang and Chu, 2013). Overland flow is a spatially distributed process whereby depressions progressively overflow and connect to either nearby depressions or to the outflow boundary (Onstad, 1984; Darboux et al., 2002b; Antoine et al., 2011; Chu et al, 2013). During a rainfall event this process starts when the infiltration capacity becomes lower than the rainfall intensity. On rough micro-topographies and ignoring surface detention (i.e. live water) (Figure 1-2a), the excess rainfall is at first mostly stored in depressions. In this first stage, depressions do not overflow and thus are not yet connected. However, some outflow may occur due to border effects. This initial and limited flow is generated from the depressions directly connected to the system's outlet and from nearby upstream depressions connected to these initially connected depressions (Peñuela et al., 2013). In a second stage, additional upstream micro-depressions get filled, and start to overflow and connect either to nearby depressions or to the outlet. This process results in a gradual and non-linear filling, spilling and connection process. This stage is characterized by a particular phenomenon which consists of a threshold relationship between rainfall excess and overland flow (Figure 1-2a). When the cumulative rainfall excess volume exceeds a certain threshold value, a sharp increase in the generated overland flow is observed as a consequence of the rapid establishment of hydraulic connections between different parts of the system. This threshold phenomenon, which is consistent with

percolation theory (Berkowitz and Ewing, 1998) and characteristic of random media (Berkowitz and Ewing, 1998), has been observed in overland flow at the plot scale (Darboux et al., 2002a; Frei et al., 2010; Peñuela et al., 2013; Yang and Chu, 2013). Around this threshold, the overland flow process evolves from a predominant filling process to a predominant spilling process. This second stage finishes when all the micro-depressions are completely filled. The whole soil surface is then connected to the outlet and overland flow consists exclusively in a spilling process. Neglecting surface detention dynamics, steady state overland flow is reached at this point (Figure 1-2a).

The spatio-temporal distribution of the overland flow process is affected by structural features of the soil micro-topography. For instance, when increasing surface roughness and thus the maximum amount of water that can be stored in surface depressions, the runoff threshold is delayed (Darboux and Huang, 2005; Chu et al., 2013) and total runoff is decreased (Kamphorst et al., 2000; Chu et al., 2013). Surface slope gradient is another important terrain attribute that may interact with surface roughness to affect functional hydrological connectivity. On rough surfaces particularly, slope gradient can dramatically affect the depression storage (Onstad, 1984; Kamphorst et al., 2000), runoff and the development of preferential flow paths (Bracken and Croke, 2007). Changing the slope gradient modifies the balance between water fill and water spill processes and therefore also changes the dynamics and spatial distribution of overland flow. Low slopes favor the filling of depressions. Overland flow is therefore less likely to occur and the occurrence of the above mentioned threshold in runoff is delayed (Yang and Chu, 2013). As slope increases, the volume of water stored in depressions decreases and a higher number of parallel flow paths connecting upslope areas to downslope areas can be identified. This results in higher drainage efficiency, i.e. a spill-dominated regime and an earlier occurrence of the runoff threshold (Yang and Chu, 2013).

Models generally simplify the hydrological representation of the micro-topography using two effective parameters, the maximum depression storage (i.e. maximum volume of water that the soil is able to store in surface depressions; DS_{max}) and the friction factor (i.e. resistance to flow) (Singh and Frevert, 2002; Smith et al., 2007). It has been shown, however, that these simplified representations fail to predict satisfactorily overland flow initiation as well as the gradual nature of the overland flow generation process (Antoine et al., 2011). Moreover, DS_{max} is generally predicted on the sole basis of the vertical variability of surface elevation (random roughness) and sometimes the slope gradient of the soil surface (Cremers et al., 1996; Kamphorst et al., 2000; Kirkby et al., 2002), even though it has been found to be dependent on the micro-topographical configuration of the soil (Antoine et al., 2009).

The objectives of this study were twofold. First, to quantify the effect of soil random roughness and slope on overland flow connectivity, the latter being characterized by the RSCf. Secondly, to determine to what extent the RSCf can be predicted on the basis of structural indicators of soil micro-topography and slope. In order to facilitate the study of the effect of surface morphology on overland flow, infiltration capacity was assumed to be spatially homogeneous and temporally constant and lower than the rainfall intensity. In order to simplify the physical interpretation and identification of the effects produced by the combination of horizontal and vertical variability of surface roughness with slope gradient, the study was performed on Gaussian surface micro-topographies.

4.3 Materials and methods

In order to facilitate discrimination between slope and roughness effects, this study relied on numerically generated topographical fields (see Section 3.3.1). Since surface elevation has been reported as normally distributed (Cremers et al., 1996), synthetic Gaussian fields with different variograms and slopes (Table 4-1) were generated.

4.3.1 Characteristics of the micro-topographies

The method developed by Zinn and Harvey (2003) and adapted by Antoine et al. (2009) was used to generate the topographical fields. The range of values of σ and R were selected so as to reflect extreme but still realistic values observed in real fields (Table 4-1; Onstad, 1984; Zobeck and Onstad, 1987; Darboux et al., 2002a; Vidal Vázquez et al., 2005). The fields were 6 m x 6 m size and the maximum R was 400 mm in order to minimize scale and boundary effects (Appels et al., 2011; Peñuela et al., 2013). R values lower than 50 mm were not considered in order to avoid large inaccuracies caused by the 10 mm/pixel horizontal spatial resolution of the digital elevation models (DEM). In total 216 combinations of R, σ and slope were considered, i.e. 36 flat Gaussian micro-topographical fields x 6 slope gradients. For each combination, 10 replicate fields were generated.

Table 4-1 Characteristics of the Gaussian micro-topographical fields

Size [m x m]		6 x 6
Spatial resolution [mm/pixel]		10
Slope gradient [%]		0, 1, 2, 5, 10 and 15
Variogram	σ [mm]	2, 5, 10, 20, 30 and 40
	R [mm]	50, 100, 150, 200, 300 and 400

4.3.2 Conceptualization of the micro-topography profile

In order to develop a simplified model linking topographical features and connectivity, a schematic representation of the soil surface was used. The soil surface was geometrically conceptualized as a longitudinal profile with rectangular depressions sized according to the variogram of the Gaussian fields (Figure 4-1a). From its definition R represents the minimal distance between points where the difference

of elevation is more likely to be maximal. Therefore, we consider R to be a measure of the mean horizontal distance between the highest points (crests) and the lowest points (depressions) of the micro-topography, i.e. R can be viewed as a measure of the typical size of depressions. σ is a measure of the amplitude of the vertical variations and can therefore be viewed as a proxy for the depression depth. The angle β, given by $\arctan(\sigma/2R)$, is a measure of the shape of micro-depressions. Based on this, the dimensions of the rectangular depressions were defined by a half-length R and height σ. The slope of the profile (α) represents the mean slope of the field (Figure 4-1a). The stored water is represented as an area (A). 1) If $\beta>\alpha$, water stored in the depression is bounded by the base and the two vertical walls of the rectangular depressions (Figure 4-1b). Therefore, A depends not only on σ but also on R. 2) If $\beta<\alpha$, stored water is bounded only by the base and the lower vertical wall of the depressions (Figure 4-1b). Therefore, A depends only on σ.

Based on this schematic representation of the micro-depressions (Figure 4-1), DS_{max} [mm] at 0% slope is given by:

$$\mathrm{DSmax} = \frac{n * A}{L} \qquad \text{Equation 4-1}$$

where A [mm²] is the area occupied by stored water (shadowed areas in Figure 4-1b), L [mm] is the length of the longitudinal profile (Figure 4-1a), and n is the number of depressions which can be calculated as follows:

$$n = \frac{b * L}{2R} \qquad \text{Equation 4-2}$$

where b is a constant representing the proportion of the field occupied by actual depressions, i.e. a correction factor that takes into account the area in between depressions that do not store water and the actual shape of micro-depressions.

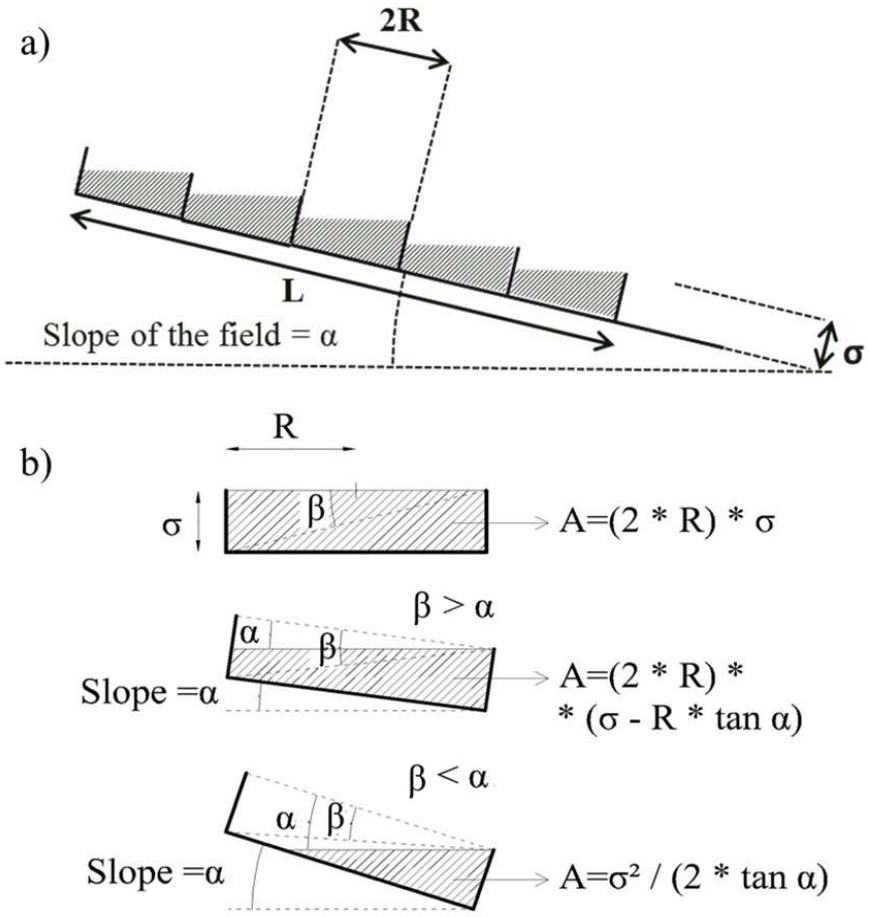

Figure 4-1 Longitudinal profile in the slope direction of soil depressions conceptualized as rectangles. Stored water is represented by the shadowed area (*A*).

Once a certain slope value is applied on the field, using trigonometry to calculate *A*, and after combining Equations 4-1 and 4-2, we obtain the following expressions for DS_{max} [mm]:

$$if\ \alpha = 0 \rightarrow DS_{max,\,\alpha=0} = b * \sigma \qquad \text{Equation 4-3}$$

$$if\ \beta > \alpha\ \rightarrow\ \mathrm{DS_{max,}} = b * (\sigma - R * \tan\alpha)\ \mathrm{DS_{max,\ \alpha=0}} * \left(1 - \frac{\tan\alpha}{2 * \tan\beta}\right)$$

Equation 4-4a

$$if\ \beta < \alpha\ \rightarrow\ \mathrm{DS_{max}} = b * \frac{\sigma^2/(2 * \tan\alpha)}{2 * R} = \mathrm{DS_{max,\ \alpha=0}} * \left(\frac{\tan\beta}{2 * \tan\alpha}\right)$$

Equation 4-4b

where α is the slope angle [rad], R and σ are in mm, β is in rad and b will be obtained after fitting Equation 4-3, Equation 4-4a and Equation 4-4b, to the data.

4.4 Results

For reasons of clarity, only the results of two slope gradients, 1% as representative of low slopes and 10% as representative of high slopes, will be shown in the majority of the graphs.

For high slopes and low surface roughnesses, DS_{max} is very small and hence the surface tends to behave like a flat plane, i.e. the whole surface is initially connected ($C_0 \approx 1$). Hence the gradual process of filling, spilling and connection of micro-depressions cannot be characterized by the RSCf. Consequently, the combinations for which the mean DS_{max} was smaller than 0.01 mm were not further considered (Table 4-2).

Keeping σ constant, one observes a gradual decrease of DS_{max} as R increases (Figure 4-2a and c). In addition, a gradual change in shape of the RSCf is observed as R increases (Figure 4-2b and Figure 4-2d). For high slopes (10% and 15%), this change in shape is quite pronounced. As R increases, the RSCf evolves from a convex to a straighter shape and even becomes concave for the highest values of R.

For all the slope values, one observes a gradual increase of DS_{max} when σ increases, at constant R (Figure 4-3a and c). For low slope values (0%, 1% and 2%), the shape of the normalized RSCf barely changes when σ increases at constant R (Figure 4-3b), indicating that C_0, C_{CT} and RDS_{CT} remain fairly constant. Conversely to low slope values, for high slope values (10% and 15%) a strong change in the shape of the normalized RSCf is observed as σ decreases (Figure 4-3d). This indicates that, when increasing σ, a higher RDS is necessary to reach the CT. Note that for the lowest σ value (2 mm), C_0 is much larger than for all other cases and that CT cannot be defined since the rate of increase of C is higher than the rate of increase of DS as from C_0.

Table 4-2 Combinations of R, σ and slope that were discarded because DSmax< 0.01 mm

Slope	σ	R
2%	2 mm	400 mm
5%	2 mm	150, 200, 300, 400 mm
10%	2 mm	100, 150, 200, 300, 400 mm
	5 mm	200, 300, 400 mm
15%	2 mm	50, 100, 150, 200, 300, 400 mm
	5 mm	150, 200, 300, 400 mm
	10 mm	300, 400 mm

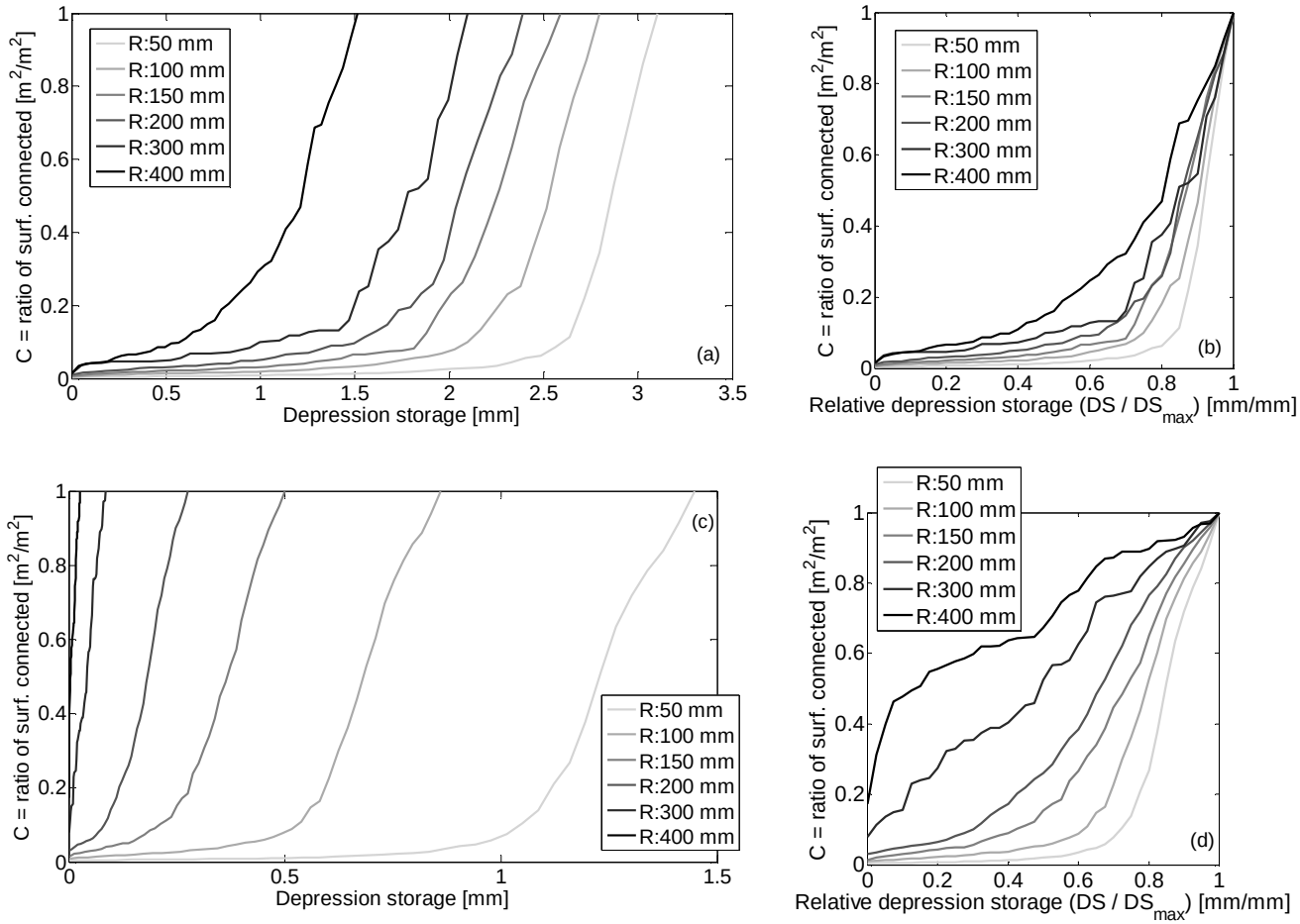

Figure 4-2 Example of effect of range at 1% (a, b) and 10% (c, d) slope on the RSCf (a, c) and the normalized RSCf (b, d). σ is equal to 10 mm. Each curve is the average of 10 replicates. The scales of the x-axes are different in (a) and (c).

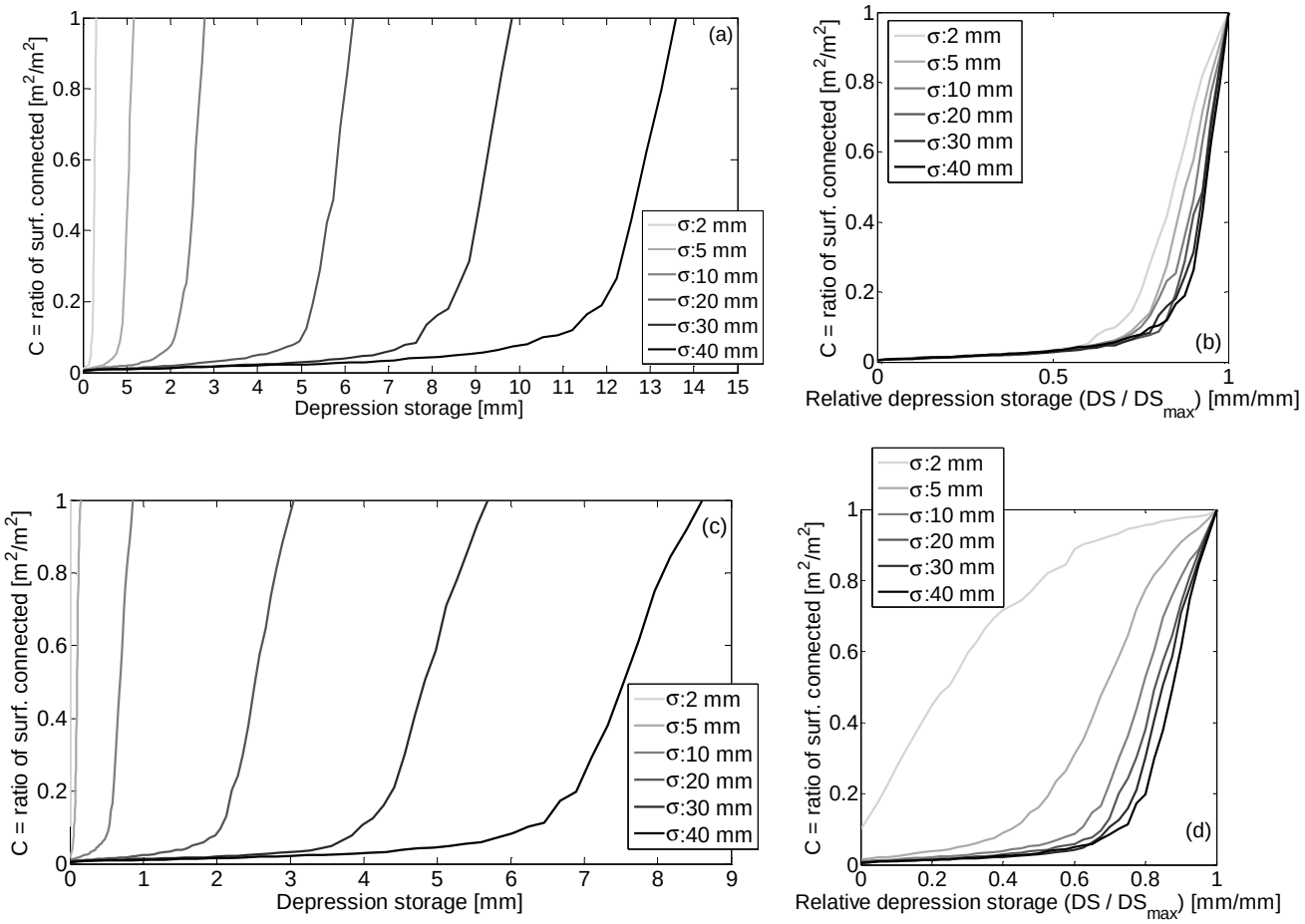

Figure 4-3 Example of effect of sill at 1% (a, b) and 10% (c, d) slope on the RSCf (a, c) and the normalized RSCf (b, d).*R* is equal to 100 mm. Each curve is the average of 10 replicates. The scales of the x-axes are different in (a) and (c).

4.4.1 Ratio of initially connected surface

A gradual increase of C_0 is observed when R increases (Figure 4-4a and Figure 4-4c). This indicates that the fraction of area initially connected to the outlet increases as the horizontal component of the surface roughness increases. The relationship between C_0 and R is approximately linear for low slope values (0%, 1% and 2%) and independent of σ (Figure 4-4b). Since at 1% slope C_0 shows the highest linearity with R and the lowest dependency on σ, the observed values of C_0 for this slope are used to derive an equation relating C_0 and R by means of a linear regression. The equation of this linear regression is given by:

$$C_{0,\alpha=1} = 0.24 * \frac{R}{L} \qquad \text{Equation 4-5}$$

where $C_{0,\alpha=1}$ is C_0 at α = 1% slope, R is in mm and L is the total length of the field in mm.

For high slope values (5%, 10% and 15%), the rate of increase of C_0 with R becomes higher when the slope increases. For all the slope values, the mean values of C_0 remain fairly constant for low values of R irrespective of σ (Figure 4-4d). However, especially for high R and high slope values, an asymptotic decrease of C_0 is observed when increasing σ, tending towards approximately 0.03-0.04 (Figure 4-4d). The asymptotic values of C_0 observed for slopes higher than 1% (Figure 4-4d) seems to tend to the values of C_0 at 1% (Figure 4-4b).

Based on our conceptual representation of surface topography and in order to take into account the trends observed for high slope values as well as the higher values of C_0 observed for low ratios of $\sigma/2R$ (= tanβ), a generalization of Equation 4-5 is proposed. This generalization, similar to the generalization of Equation 4-3 into Equation 4-4a, incorporates in its second term the relationship

between the slope and the shape of the conceptualized micro-depressions (tanα / tanβ). The proposed expression for C_0 is as follows:

$$C_0 = C_{0,\alpha=1} * (1 + \frac{\tan\alpha - 0.01}{2 * \tan\beta})$$

Equation 4-6

where $C_{0,\alpha=1}$ is given by Equation 4-5, α is the slope gradient [rad] and β is in rad. The constant value of 0.01 in the second term on the right corresponds to the tangent of the 1% slope. It is used in order to only consider the first term on the right of Equation 4-6 when the slope is equal to 1%. After expressing tan β as $\sigma/2R$ and replacing $C_{0,\alpha=1}$ by Equation 4-5, Equation 4-6 becomes:

$$C_0 = 0.24 * \frac{R * (\sigma + R * (\tan\alpha - 0.01))}{L * \sigma} = 0.24 * \frac{R}{L} * (1 + \frac{R}{\sigma}(\tan\alpha - 0.01))$$

Equation 4-7

where σ is in mm. With the exception of C_0 at high slope and high σ values, Equation 4-7 allows predicting C_0 with reasonable accuracy over the entire range of R, σ and slope values (NSE = 0.75; Figure 4-4 and Figure 4-5a).

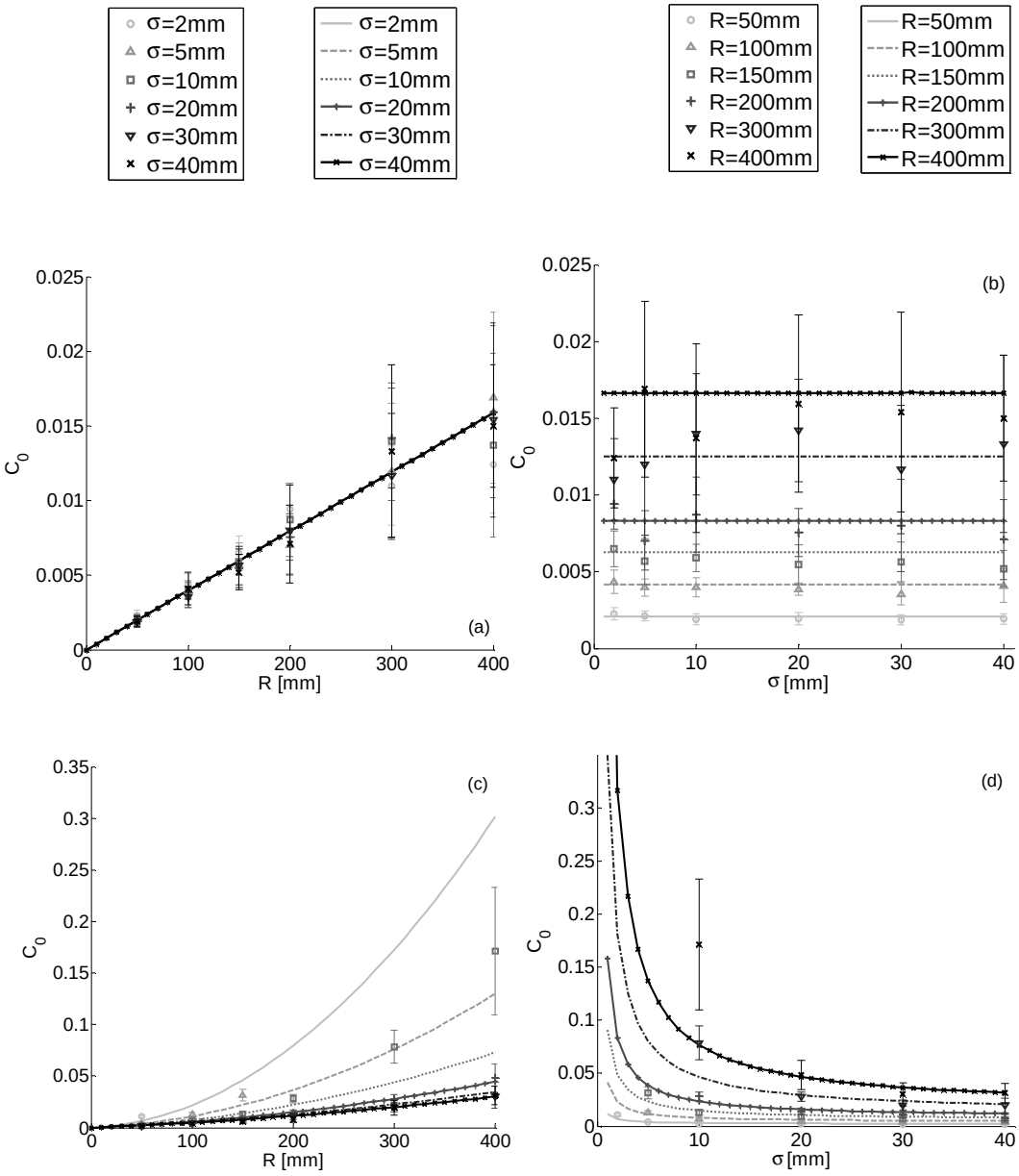

Figure 4-4 Effect of range (a, c) and sill (b, d) on C0 at (a, b) 1% slope and at (c, d) 10% slope. Error bars = standard deviation (n=10). Points correspond to observed values. Lines correspond to the values calculated using Equation 4-7

4.4.2 Connectivity threshold

C_{CT}

C_{CT} appears fairly independent of σ, R and slope (Figure 4-6). C_{CT} values show an important variability that increases with high slope and R values and low σ values. 95% of the observed mean values are comprised between 0.05 and 0.15.

RDS_{CT}

An approximately linear decrease of RDS_{CT} is observed when R increases (Figure 4-7a and c), this decrease being more pronounced for both low σ and high slope values (Figure 4-7c). As R tends to 0, RDS_{CT} converges to a common value which is approximately equal to 0.85. For a given R and for slopes higher than 0%, RDS_{CT} tends to increase asymptotically to a constant value as σ increases (Figure 4-7b and d). This effect is particularly noticeable for high R values. However, RDS_{CT} is not affected by σ in the absence of slope (Figure 4-8b). The values of RDS_{CT} at 0% slope seem to correspond to the asymptotic values observed for slopes higher than 0% (Figure 4-7b).

Since at 0% RDS_{CT} shows the lowest dependency on σ and a linear decrease with increasing R values, the observed values of RDS_{CT} for this slope are used to derive an equation relating RDS_{CT} and R by fitting a linear equation to the observed values:

$$RDS_{CT,\alpha=0} = 0.87 - 0.725 * \frac{R}{1000} \qquad \text{Equation 4-8}$$

where $RDS_{CT,\alpha=0}$ is the RDS_{CT} at the 0% slope in mm and R is in mm. Based on our conceptual representation of surface topography and in order to take into account the trends observed at slopes higher than 0% and the lower values of RDS_{CT} observed for low ratios of $\sigma/2R$ (= $\tan\beta$), a generalization of Equation 4-8 is proposed. This generalization, similar to the generalization of Equation 4-3,

incorporates in its second term the relationship between the slope and the shape of the conceptualized micro-depressions (tanα/tanβ). The proposed expression for RDS_{CT} is as follows:

$$RDS_{CT} = RDS_{CT,\alpha=0} - c * \frac{\tan \alpha}{\tan \beta} \qquad \text{Equation 4-9}$$

where $RDS_{CT,\alpha=0}$ is given by Equation 4-8, α is the slope gradient [rad] and β is in rad. c is obtained after fitting Equation 4-9 to the data. After expressing tan β as $\sigma/2R$, fitting Equation 4-9 to the data and replacing $RDS_{CT,\alpha=0}$ by Equation 4-8, Equation 4-9 becomes:

$$RDS_{CT} = 0.87 - 0.725 * \frac{R}{1000} - 0.1 * \frac{\tan \alpha}{\sigma/2R} \qquad \text{Equation 4-10}$$

where α is the slope angle [rad], R and σ are in mm and c was found to be equal to 0.1. Equation 4-10 is able to efficiently predict the observed values of RDS_{CT} for all the combinations of R, σ and slope (NSE = 0.95; Figure 4-5b, Figure 4-7 and Figure 4-8).

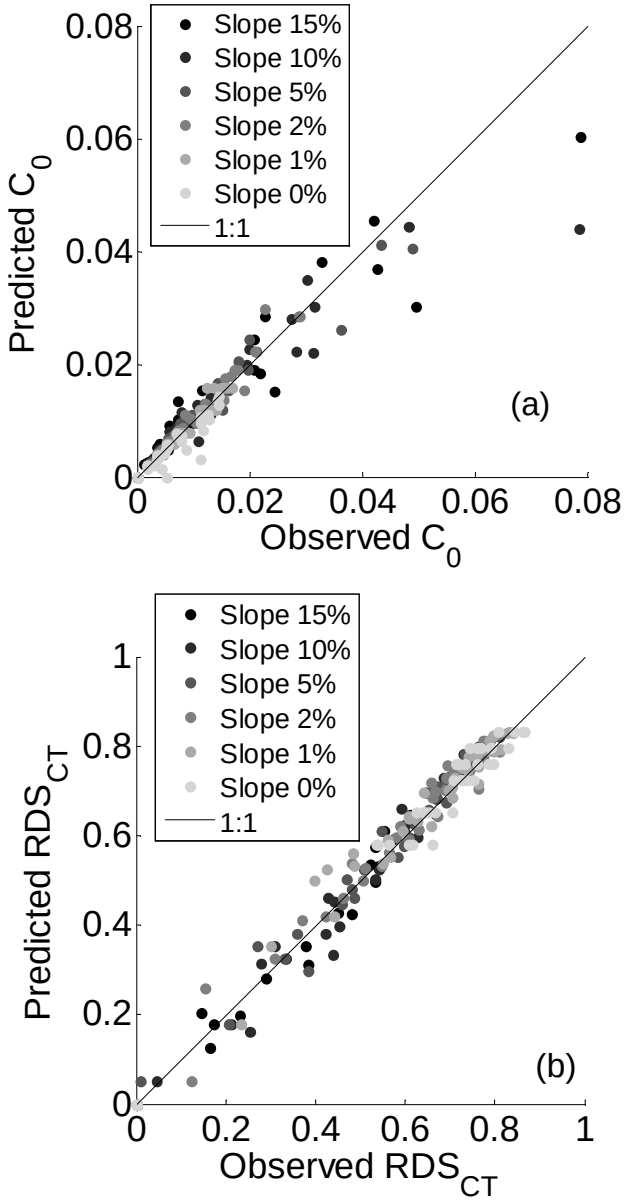

Figure 4-5 Observed versus predicted values for all slope, R and σ combinations for (a) C_0 (Equation 4-7; $R^2 = 0.803$; RMSE = 0.008; NRMSE = 0.63; NSE = 0.75), and (b) RDS_{CT} (Equation 4-10; $R^2 = 0.960$; RMSE = 0.039; NRMSE = 0.07; NSE = 0.95). Each point is the average of 10 replicates.

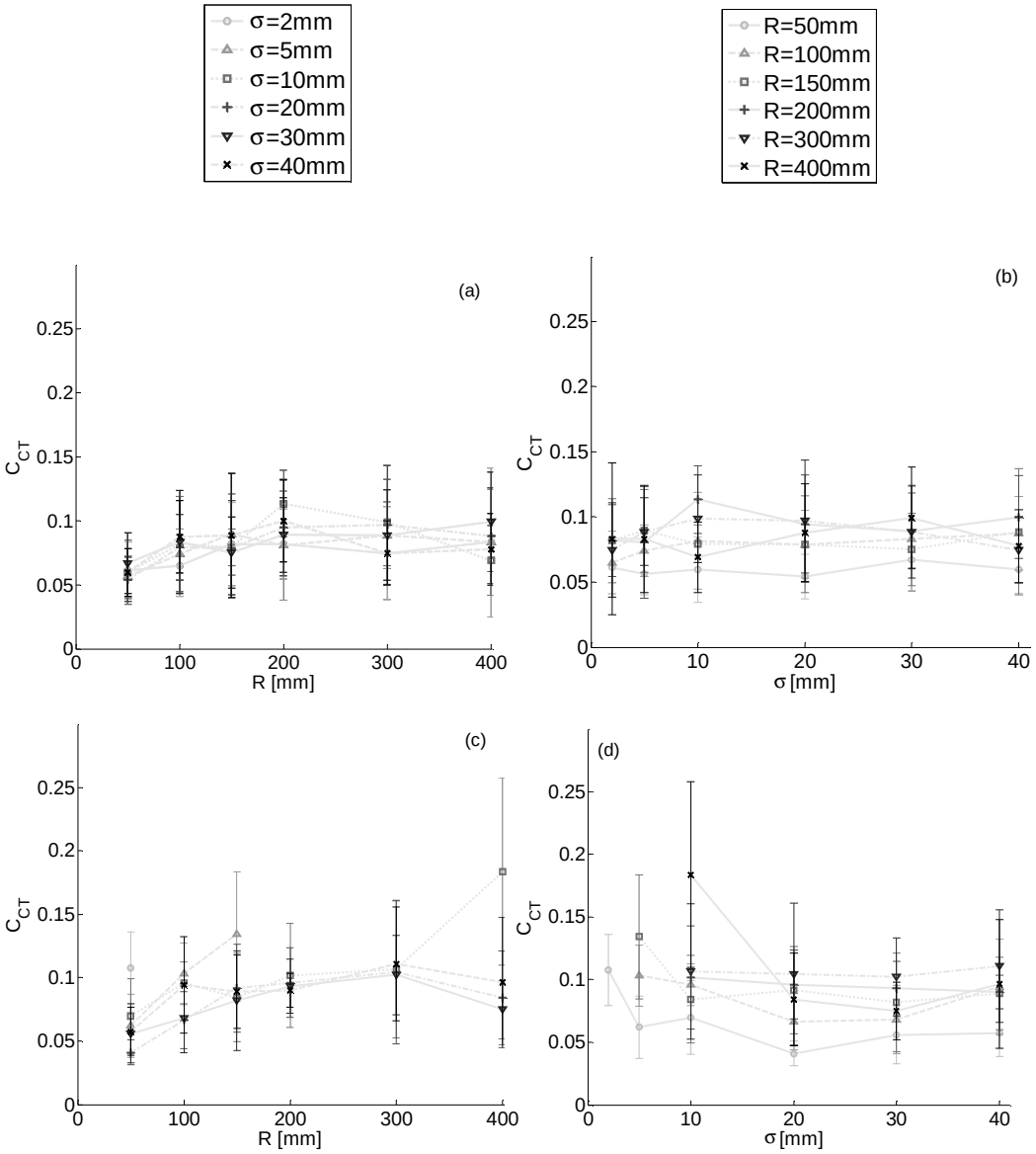

Figure 4-6 Effect of range (a, c) and sill (b, d) on C_{CT} at (a, b) 1% slope and at (c, d) 10% slope. Error bars = standard deviation (n=10). Points correspond to observed values. Gray lines link points of constant R or σ for better visualization of variability.

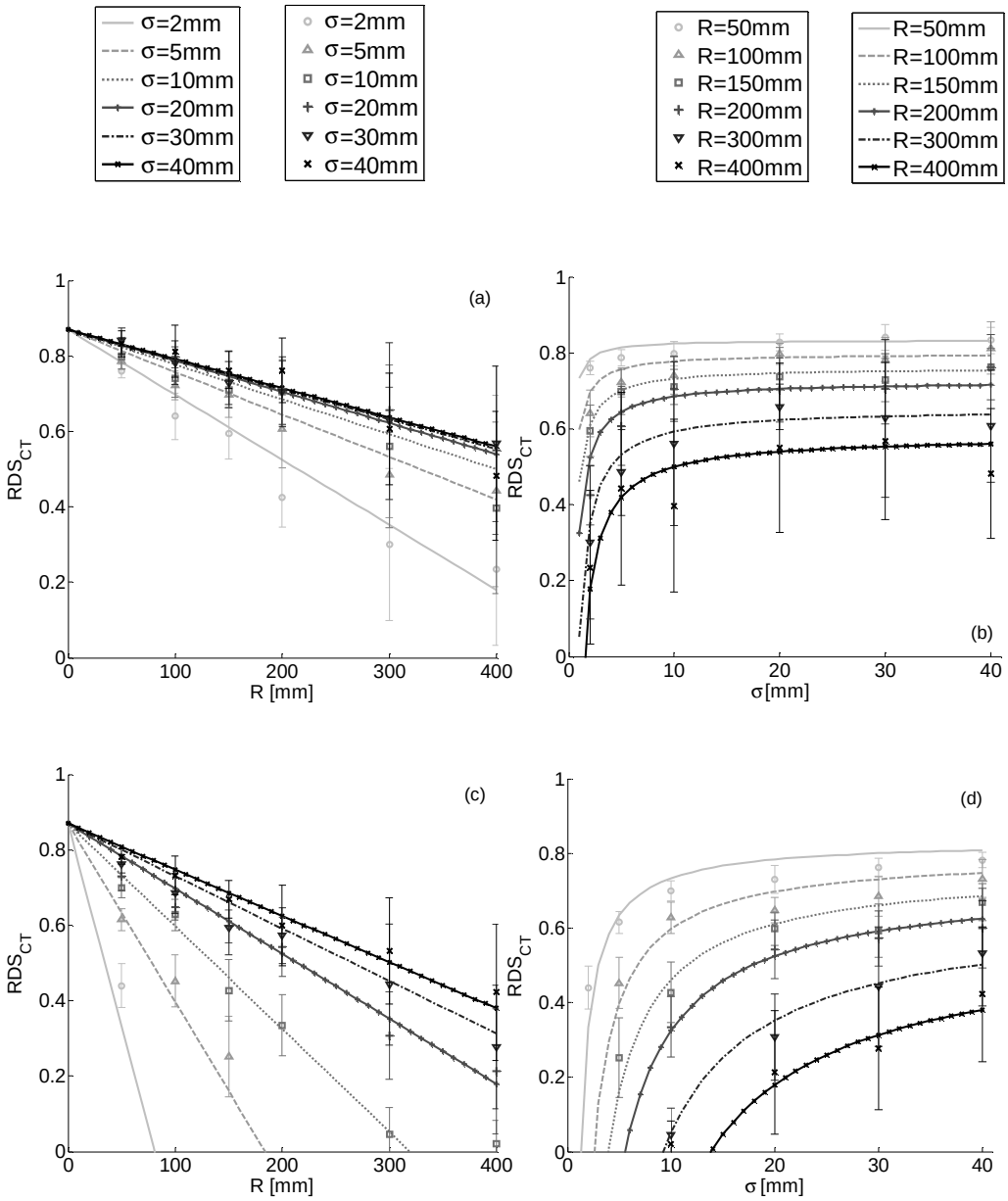

Figure 4-7 Effect of range (a, c) and sill (b, d) on C_{CT} at (a, b) 1% slope and at (c, d) 10% slope. Error bars = standard deviation (n=10). Points correspond to observed values. Lines correspond to the values calculated using Equation 4-10.

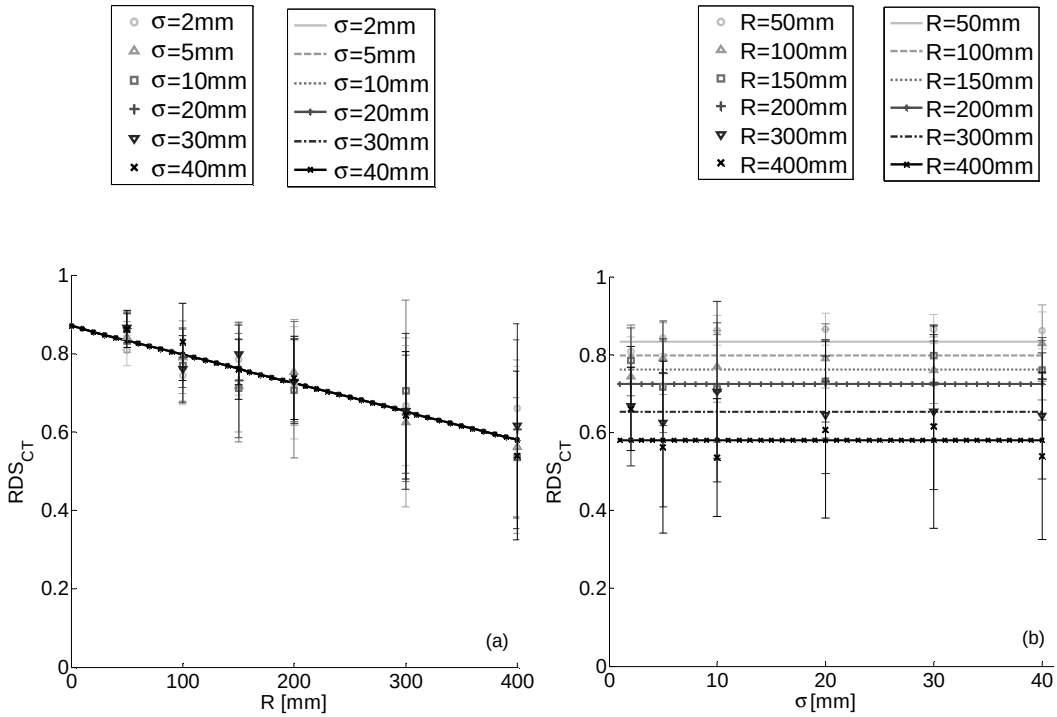

Figure 4-8 Effect of (a) range and (b) sill on RDS_{CT} at 0% slope. Error bars = standard deviation (n=10). Points correspond to observed values. Lines correspond to the values calculated using Equation 4-8 or Equation 4-10.

4.4.3 Maximum depression storage

For DS_{max} an approximately linear decrease is observed when R increases for low slope values (Figure 4-9a), while a more curved and asymptotic decrease of DS_{max} is observed for high slope values (Figure 4-9b). This decrease, which is more pronounced for low values of *R*, tends asymptotically to $DS_{max} = 0$ as *R* increases.

A clear increase of DS_{max} with σ is observed (Figure 4-9b and d), which seems to start at (0, 0) and to be approximately linear for low *R* and low slope values (Figure 4-9b). In particular for the 0% slope the observed linear increase (Figure 4-10b), can be fitted by Equation 4-3

with b equal to 0.36 (Figure 4-10a and b). This linear relation between σ and DS_{max} is, however, not observed for higher slope values and in particular for high values of R. Therefore Equation 4-3 is not able to predict the values of DS_{max} for slopes > 0%.

For slopes > 0%, after fitting Equation 4-4a and Equation 4-4b to the data, we obtain b equal to 0.3 (Figure 4-9). A good correlation between observed and predicted values (NSE=0.96) is obtained for all the combinations of R, σ and slope with the exception of DS_{max} at low slopes, small R and high σ values(Figure 4-11a).

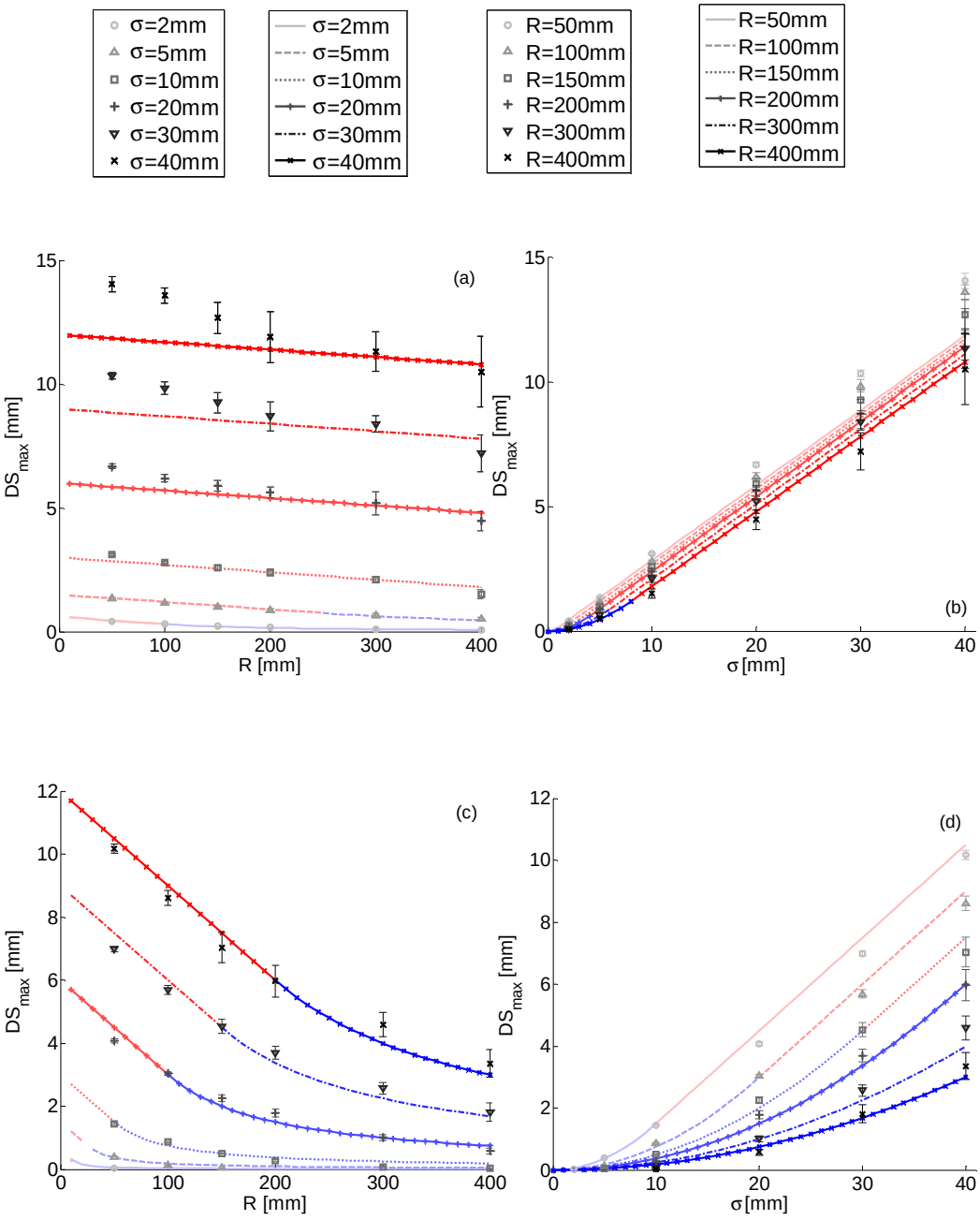

Figure 4-9 Effect of range (a, c) and sill (b, d) on DS_{max} at (a, b) 1% slope and at (c, d) 10% slope. Error bars = standard deviation (n=10). Points correspond to observed values. Red lines correspond to Equation 4-4a and blue lines to Equation 4-4b.

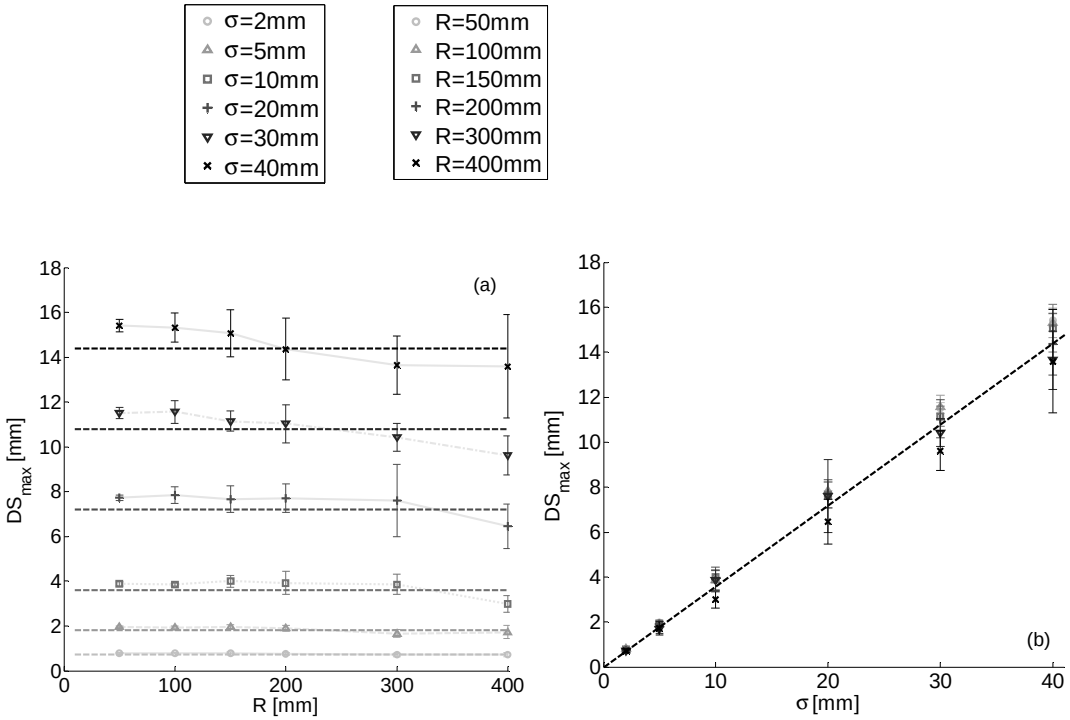

Figure 4-10 Effect of (a) range and (b) sill on DS_{max} at 0% slope. The dashed black line corresponds to Equation 4-3. Error bars = standard deviation (n=10).

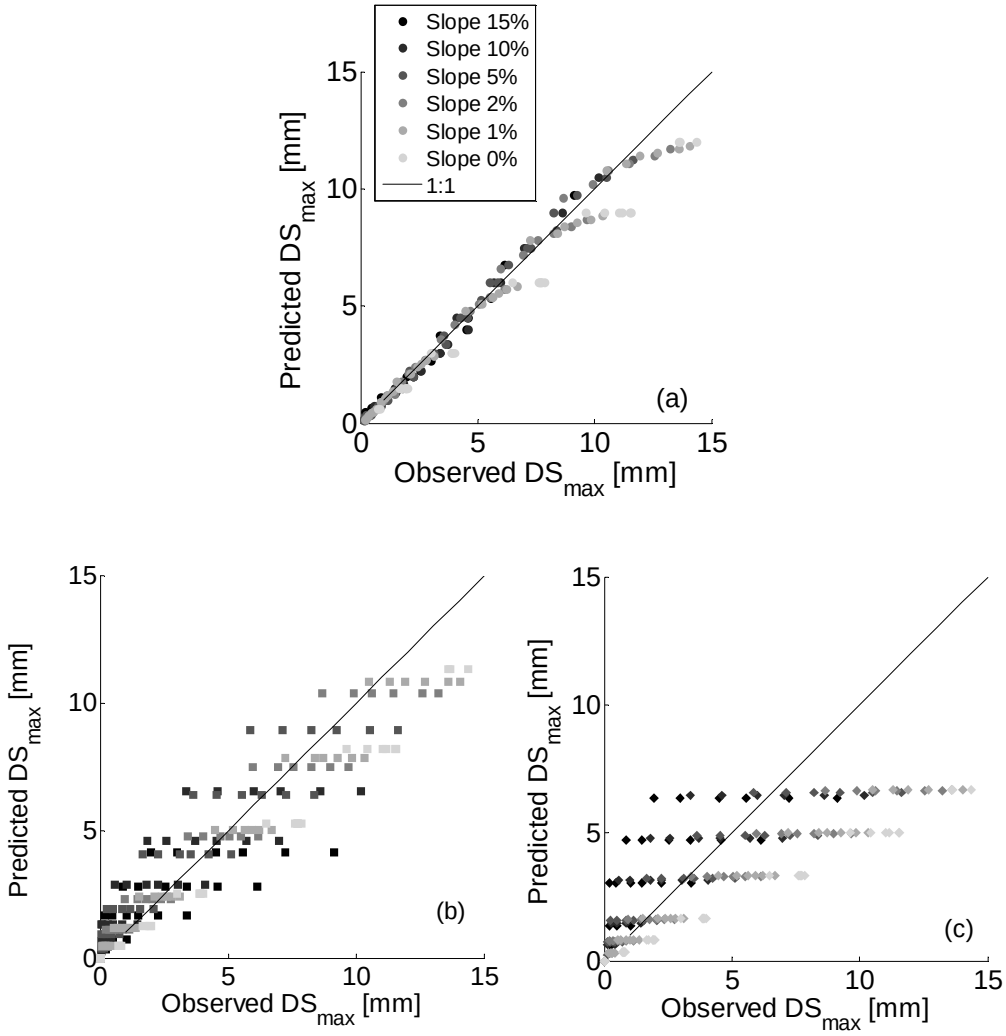

Figure 4-11 Observed versus predicted values of DS_{max} for the different combinations of slope, R and σ using (a) Equation 4-4a and Equation 4-4b (R^2 = 0.975; RMSE = 0.733 mm; NRMSE = 0.17; NSE = 0.96), (b) Kamphorst et al. (2000) (R^2 = 0.892; RMSE = 1.429 mm; NRMSE = 0.34; NSE = 0.86) and (c) Kirkby et al. (2002) (R^2 = 0.698; RMSE = 2.675 mm; NRMSE = 0.63; NSE = 0.53). Each point is the average of 10 replicates.

4.5 Discussion

The results indicate that both the range and sill of the variogram have an important influence on the RSCf, and that the effects depend on the slope of the field. With the exception of C_{CT}, these variations follow clear trends represented by Equation 4-7, Equation 4-10, and Equation 4-4a and Equation 4-4b. In this section we will provide a physical interpretation for the observed effects based on the geometrical conceptualization of the soil surface (Figure 4-1).

4.5.1 Ratio of initially connected surface

C_0 is the area of the depressions connected to the bottom outlet before depressions start filling. This area results from a border effect caused by the bottom outlet (Peñuela et al., 2013). C_0 includes depressions directly connected to the outlet but also upstream depressions connected to the latter depressions. At low slopes, upstream depressions are disconnected from the outlet by crests, and even low crests suffice to block them off from the outlet. At 1% slope Equation 4-5 indicates proportionality between C_0 and R, i.e. between C_0 and the size of depressions. The larger the depressions, the larger the area initially connected to the outlet. The slope of Equation 4-5 (0.24) may be understood conceptually as the proportion of an imaginary rectangular area, 6000 mm wide and R mm long located immediately upstream of the bottom outlet, that is initially connected to the bottom outlet.

In this study, Equation 4-5 was found to also provide a good fit for high slope values but only for high values of σ (Figure 4-4c and Figure 4-4d). With a higher vertical roughness, and hence higher crests surrounding depressions, even at high slope values the wall effect produced by these crests is sufficient to disconnect the upstream areas from the bottom outlet. As the slope further increases, the elevation of the bottom of the upstream depressions becomes higher

than the crests immediately below, and consequently these depressions become connected, resulting in an increase in C_0. This will occur faster for small crests than for large crests. This is reflected in Equation 4-7, which is a generalization of Equation 4-5 based on our conceptual representation of surface topography and which takes into account the relationship between C_0 and 1) the shape of the depressions (β) and 2) the slope of the field (α).

4.5.2 Connectivity Threshold

C_{CT} represents the proportion of area connected to the outlet when the generalized overland flow process starts. C_{CT} values appear fairly independent of σ, R and slope (Figure 4-6). However, this apparent independence might be caused by the high variability of C_{CT} which makes it impossible to identify clear trends. C_{CT} values range between 0.05 and 0.15 with the exception of the combinations of high values of slope and R and low values of σ. Most of the latter combinations were not considered in this study since they correspond to cases where the soil surface barely stores water in depressions (DS_{max}<0.01 mm) and behaves like a flat surface (Table 4-2). Since C_{CT} represents a relative area (connected area at the connectivity threshold divided by total study area) and it is a border effect along the bottom outlet (Peñuela et al., 2013), C_{CT} will tend to 0 as the length of the study area increases.

RDS_{CT} corresponds to the height of stored water needed to initiate the overland flow process. Figure 4-8 and Equation 4-8 and Equation 4-10 indicate that RDS_{CT} is not affected by σ in the absence of slope. A certain slope gradient is needed to facilitate the spilling and connection process of the micro-depressions and hence the occurrence of the connectivity threshold. However, for high σ values when the slope is not high enough to facilitate the spilling process, the system behaves similarly to a 0% slope case. For high σ values and low slopes, Equation 4-10 tends asymptotically to Equation 4-8. Hence, values of RDS_{CT} observed at low slopes are also observed in high slope cases combined with high values of σ.

At first, one might not expect the average horizontal size of the depressions to affect RDS_{CT}. However, Figure 4-7 and Figure 4-8 and Equations 4-8 and 4-10 show a clear decrease of RDS_{CT} with *R*. This decrease, which is linear, becomes more pronounced for high slope values. The increase of slope of the field together with the increase of *R* facilitates the connection between depressions and reduces their capacity to store water. As a consequence, a lower RDS is needed to initiate CT. Surprisingly, this decrease is also observed for the 0% slope case (Figure 4-8a), indicating that an increase in *R* alone is sufficient to decrease the value of RDS needed to initiate the overland process. This can be explained by the fact that as *R* increases, the number of micro-depressions decreases and so the probability that the overland flow gets trapped in poorly connected micro-depressions decreases.

The existence of a single connectivity threshold may appear to contradict previous studies where the hydrograph, especially for rough surfaces characterized by a small number of large depressions, showed a stepwise increase, i.e. the initial flow threshold was followed by a number of other flow thresholds (Chu et al., 2013; Yang and Chu, 2013; Chu et al., 2015; Yang and Chu, 2015). These multiple thresholds resulted from the spilling and connection of individual depressions (Yang and Chu, 2013). In contrast to the present study, the depressions of the rough surfaces were considerably larger in relation to the plot size and fewer, which may explain their marked effect on the hydrograph. Similar to the present study, a more gradual increase of hydrologic connectivity was, however, observed on smooth surfaces with smaller depressions after the first threshold (Chu et al., 2015). We therefore believe that as the size of the study area increases in relation to the size of depressions, and hence a higher number of depressions are present, this stepwise increase will tend to a more continuous rise of the hydrograph and with a single initial threshold. The first major threshold in contributing area coincides with the first significant increase in outlet flow (Chu et al., 2015) and is

therefore analogous to the CT defined in the present study. It must be noted that the stepwise behaviour may also be affected by border effects. As shown by Appels et al. (2011) and Peñuela et al. (2013), when the size of depressions is large compared to the plot size, border effects can significantly affect connectivity. These border effects cause a large area of the field to be connected to the outlet right from the start, i.e. a high C_0, producing a significant decrease of DS_{max}. Moreover, the plot size is not able to represent all the components involved in the connectivity process (Peñuela et al., 2013) causing contrasting micro-topographies to have indistinguishable connectivity behaviours (Appels et al., 2011; Peñuela et al., 2013).

4.5.3 Maximum Depression Storage

DS_{max} has commonly been predicted on the basis of the random roughness value of the soil micro-topography which is generally defined as the standard deviation of the point elevations (e.g., Kamphorst et al., 2000). Figure 4-9 and Figure 4-10 and Equations 4-4a and b confirm that σ greatly affects DS_{max} for all the slopes. In particular for a 0% slope, DS_{max} is a linear function of σ (Equation 4-3, Figure 4-10). The slope coefficient of this linear equation (0.36) reflects the proportion of the surface that stores water but also the difference in shape between the micro-depressions in the Gaussian fields and the rectangular depressions of our conceptual representation of surface micro-topography.

However, a linear relation between DS_{max} and σ is not observed for higher slope values (large α), particularly for high values of R. As discussed above for C_0 and RDS_{CT}, the combination of high slopes and low values of σ facilitates the connection of micro-depressions with the bottom outlet and hence reduces their capacity to store water. Yet, as for RDS_{CT}, the range of the variogram (R) also has an important influence on DS_{max}, except for the 0% slope case (Figure 4-10a). In both cases, this effect can be explained satisfactorily by the relationship between the shape of micro-depressions (β) and the slope

gradient (α). As mentioned in Section 4.4, flatter surfaces (low values of β, in this case caused by high values of R) combined with high slope gradients reduce the relative difference in elevation between the bottom of the micro-depressions and the downstream crests that disconnect them from either other depressions or the bottom outlet.

In general, Equations 4-4a and b fit reasonably well the observed values of DS_{max} except for low slopes, small R and high σ values (Figure 4-9a, b and Figure 4-11a). At 1% slope, low values of R and high values of σ, the conceptual depressions resemble deep, narrow slots, a shape that is unlikely to be found in practice. The value of b (0.3) is lower than the value obtained for the 0% slope in Equation 4-3 (0.36). This may indicate that the proportion of area that stores water is higher for horizontal surfaces than for inclined surfaces and hence Equations 4-4a and b are not valid for the 0% slope case.

In the literature, several empirical expressions have been proposed that relate DS_{max} and structural characteristics of the micro-topography, e.g. Kamphorst et al. (2000) and Kirkby et al. (2002). The expressions of Kamphorst et al. (2000) and Kirkby et al. (2002), which do not account for the horizontal component of the surface roughness, perform less well (NSE = 0.86 and NSE = 0.53, respectively) than the simple conceptual model proposed here when using the present dataset (NSE = 0.96; Figure 4-11). Moreover, random roughness index-based equations imply that for a given random roughness value, DS_{max} decreases linearly with increasing slope and that a threshold slope exists at which DS_{max} is equal to zero. As opposed to the unrealistic zero-DS_{max} threshold slope implied in the random roughness index-based equations (Onstad 1984; Kamphorst, 2000), Equations 4-4b is able to reflect the asymptotical decrease of DS_{max} with slope also observed by Chu et al. (2012).

4.5.4 General discussion

For Gaussian random fields at low slopes and high ratios of $\sigma/2R$ (deep/narrow depressions), overland flow connectivity is controlled by an important process of depression filling and characterized by a marked connectivity threshold. The spilling and rapid connection process starts when micro-depressions are almost full. For these more low connectivity cases, the link between functional connectivity and structural connectivity is represented by a linear relation between the RSCf parameters and a single component (horizontal or vertical) of the surface roughness: between C_0 and R (Equation 4-5), between RDS_{CT} and R (Equation 4-8) and between DS_{max} and σ (Equation 4-3). On the other hand, as the slope increases in combination with low $\sigma/2R$ ratios (wide shallow depressions), the filling and spilling process occurs more gradually with an earlier initiation of CT. In these high connectivity cases, all components of the surface roughness, in the form of β, are needed to define the RSCf parameters (Equation 4-7, 4-10 and 4-4a and b), except for C_{CT}. For cases with very low DS_{max}, the RSCf could not be characterized and hence the above equations do not apply. However, such surfaces essentially behave like fully-connected, flat surfaces and hence can be modelled as such.

It should be noted that, since C_0 and C_{CT} are border effects that tend to 0 as the plot length increases (Peñuela et al., 2013), the RSCf could be characterized only by RDS_{CT} and DS_{max} for long plots. This would greatly facilitate the use of the RSCf as a means to integrate plot-scale hydrological connectivity into hydrological models and to improve the representation of subgrid overland flow generation. A similar methodology to improve the representation of the subgrid overland flow process is implemented in the openLISEM model (De Roo et al., 1996a,b and Baartman et al., 2012). This model takes into account the runoff that takes place before the excess rainfall reaches the maximum depression storage and reflects the gradual nature of overland flow generation. In order to do so it first assumes that runoff generation starts when 10% of the surface is ponded, the depression storage at

this point is referred to as Start Depressional Storage. Second, as from the Start Depressional Storage, it assumes that runoff is generated gradually in a nonlinear way as a function of the depression storage. Finally, after all the depressions are completely filled, i.e. DS_{max} is reached, runoff increases linearly with water height. In order to set the values of both parameters, Start Depressional Storage and DS_{max}, openLISEM uses the random roughness which is a structural indicator of the vertical variability of the micro-topography but which does not consider the horizontal component of this variability. This model also does not consider explicitly the slope gradient of the soil surface to predict the Start Depressional Storage, despite the strong interactions observed between slope, sill and range in the present study.

The results of this study are restricted to cases where the RSCf has a convex shape with a clearly identifiable connectivity threshold, which nevertheless covers a wide range of conditions. However, the combination of either high slopes and low σ or high slopes and high R leads to an RSCf with a straight or concave shape since the RSCf increases very rapidly right from C_0 (i.e. overland flow generation is dominated by a rapid spilling and connection process at the earliest stages of the process). This makes CT more difficult to be visually identified and even to disappear. Results are also restricted to cases where oriented roughness is not present and where the micro-topography has not yet been substantially modified by flowing water, i.e. no preferential flow paths such as rills are present. At scales larger than the minimal representative scale, i.e. when the plot size is large enough in relation to R (Appels et al. 2011; Peñuela et al., 2013), the RSCf and hence the equations presented in this study can be potentially extrapolated to other scales. C_0 and C_{CT}, as border effects will tend to 0 as the scale of study increases and RDS_{CT} and DS_{max} remain constant since they are only affected by scales smaller than the minimal representative scale.

These equations were derived from Gaussian random topographical fields. Although real fields have also been shown to follow this distribution (Cremers et al., 1996), oriented roughness is not represented when generating random topographical fields and hence, additional research on real fields with oriented roughness is needed to confirm these results.

4.6 Conclusions

The results reveal that the range, the sill and slope have marked effects on the parameters defining the RSCf with the exception of C_{CT}. At low slopes and high sill/range ratios (deep depressions), the characteristic parameters of the RSCf are linked to a single component of the surface roughness (range or sill), whereas at high slopes and low sill/range ratios (shallow depressions), both the range and the sill are needed to explain and predict the Relative Surface Connection function. Based on a simple rectangular conceptualization of surface roughness, mathematical expressions in function of the range, the sill and slope were derived in order to predict C_0, RDS_{CT} and DS_{max}. These expressions were able to physically explain and reasonably predict the slope, range and sill effects on the Relative Surface Connection function. For the present dataset, they outperformed relations proposed previously for DS_{max}.

This study shows the potential of linking structural and functional connectivity and of predicting runoff-relevant features of overland flow connectivity by the study of surface roughness. Moreover it opens a new way to predict the DS_{max} of soils by a physical analysis of the soil surface and not by empirical formulas which generally do not take into account the horizontal component of surface roughness.

CHAPTER 5

5 Evolution of overland flow connectivity in bare agricultural plots.

5.1 Abstract

Soil surface roughness not only delays overland flow generation but also strongly affects overland flow distribution and concentration. Studies seeking to find the link between soil roughness and overland flow generation generally aimed at predicting the delay in overland flow generation by means of a single parameter characterizing soil roughness. However, little work has been done to find a link between soil roughness and overland flow characteristics. This is made difficult because soil roughness and hence overland flow characteristics evolve as a result of soil erosion processes, but this evolution may be very different depending on whether diffuse or concentrated erosion dominates. The present study examines the potential of using the concept of structural and functional connectivity to link roughness characteristics to overland flow characteristics. For this purpose, soil roughness of three 2.5-m x 9.4-m agricultural plots exposed to natural rainfall was monitored for a 7-month and 6-month periods in each of 2 years. Different initial roughnesses after tillage were applied each year. Soil micro-topography was characterized by a photogrammetry technique, initially and after each important rainfall event. Soil roughness was characterized by the flow directional variogram, overland flow connectivity by a functional connectivity indicator called the Relative Surface Connection function (RSCf) and overland flow generation by FullSWOF_2D. Whereas the overland flow characteristics were found to be little or moderately correlated to the variogram, the former was found to be highly correlated to the RSCf. Very high correlations observed between DS_{max} and overland flow generation delay not only confirms the important role of depression storage on the delay of overland flow generation but also, it shows the potential of improving the prediction of the overland flow hydrograph

by the use of DS_{max}. However the results of this study show that soil roughness cannot just be considered as a delaying factor for overland flow generation. The development of eroded flow paths at the soil surface not only produces a decrease in DS_{max} but also an increase in connectivity and a higher rate of increase of the runoff ratio, as well as a higher Froude number and higher spatial continuity of flow velocities. These results show the potential of the RSCf to serve as a link between structural connectivity (soil roughness) and overland flow dynamics.

5.2 Introduction

Overland flow generation is a dynamic process greatly influenced by the soil micro-topography (Govers et al., 2000; Darboux et al., 2002b; Frei et al., 2010). When micro-topography elements such as clods, crests and rills are of the same order of magnitude or larger than the water flow depth, the resulting *form roughness* (Abrahams and Parsons, 1990; Govers et al., 2000) is a major factor causing spatial variations in overland flow depth, velocity, and direction (Zhang and Cundy, 1989; Esteves et al., 2000).

On arable land, the initially tilled soil surface is modified by erosion, thereby affecting the process of overland flow generation. When micro-topography elements are randomly distributed, soil roughness is typically characterized by a single parameter (e.g., random roughness; Hansen et al., 1999; Kamphorst et al., 2000; Smith, 2014) and strong links between standard roughness indicators (structural connectivity) and functional connectivity are observed (Chapter 4). For such randomly distributed surfaces, the overland flow process consists of a gradual and spatially distributed process of filling, spilling and connection between micro-depressions (Onstad, 1984; Darboux et al., 2002b). In particular for low slope gradients and rough surfaces, this process is mainly controlled by depression filling, since this type of surface has a high depression storage capacity. This fill-dominated

process delays runoff generation (Darboux and Huang, 2005) and increases overland flow re-infiltration (Puigdefabregas and Sanchez, 1996*)*.

During rainfall, interrill erosion (sheet and splash erosion) tends to smoothen the surface roughness by eroding clods and flattening ridges, and by filling downstream micro-depressions with the produced sediments (Kirkby, 2002; Guzha, 2004). As a consequence, the capacity of micro-depressions to store water and to delay overland flow generation is reduced progressively. For steep enough slopes (Savat and De Ploey, 1982; Govers, 1987; Planchon et al., 1987), once the micro-depression spilling process is initiated, connected depressions tend to form continuous flow paths in the direction of the slope gradient. These preferential flow paths facilitate the overland flow process by routing and concentrating the water flow (Nicolau, 2002; Darboux and Huang, 2005; Moreno-de las Heras et al., 2010), producing an increase in the local flow velocity, erosive power and sediment transport capacity (Govers et al., 2000; Kirkby, 2002) and a low potential for sediment deposition (Helming et al., 1998; Bracken and Croke, 2007). This erosive energy of concentrated overland flow creates eroding flow paths that can be described as incisional (rills which are easily recognized on the soil surface) or dispersive (wide and shallow paths not so easily recognized on the soil surface) (Bracken and Croke, 2007). The initiation of eroding flow paths has been related to the Froude number (Fr). Rill initiation has been reported to occur in the transition from subcritical to supercritical flow (Savat, 1979; Torri et al., 1987; Slattery and Bryan, 1992) and as consequence of local hydraulic jumps occurring in these preferential flow paths (Grant, 1997; Giménez et al., 2004). In turbulent overland flow rill initiation has also been reported to depend on the spatial variability of soil shear strength and the effect of raindrop detachment (Parsons and Wainwright, 2006). In particular, the rilling process and rill network can be modified by the sequence of rainfall events which determine the scour and fill processes in the rills (Luk et al., 1993). In the presence of oriented roughness patterns, the link between

structural and functional connectivity may depend on particular details and directional patterns which cannot be characterized by standard random roughness indicators (Darboux et al., 2002b; Smith, 2014). Yet, these features must be taken into account in order to determine the overland flow characteristics (Parsons and Abrahams, 1992; Bryan, 2000).

Although the processes described above have been extensively studied in the literature, their impact on overland flow connectivity has not, especially in quantitative terms. The objective of this study was therefore twofold. The first objective was to investigate the evolution of overland flow connectivity on bare agricultural plots in response to changes in surface micro-topography under natural rainfall conditions. The second objective was to evaluate to what extent these changes in the RSCf could be linked to the overland flow generation process.

5.3 Materials and methods

5.3.1 Study area

The study site was located at the UCL experimental farm in the Belgian province of Brabant Wallon (50°40'22.0"N 4°38'17.2"E). The weather is maritime temperate with precipitations evenly distributed along the year (800 mm/year) and occasional thunderstorms in spring and summer. The experiments were conducted between April 2013 and October 2014. The experimental plots were laid out on silt loam soils (17.4% clay, 73.0% silt and 10.7% sand) with 10 g/kg of organic carbon and derived from aeolian deposits.

5.3.2 Experimental Set-up

The experiments were conducted on freshly tilled soil surfaces on an agricultural hillslope in three replicate plots 3 m wide and 10 m long. The soil surface was tilled with a rototiller to a depth of 0.1 m, and it

was kept free of vegetation by applying herbicides regularly. Tillage was undertaken in May 2013 and in April 2014, after which the plots were monitored for a period of 7 months in Year 1 and 6 months in Year 2. Table 5-1 summarizes the topographic characteristics of the plots in both years.

Table 5-1 Slope and initial soil roughness of the plots.

	Plot 1	Plot 2	Plot 3
Slope gradient [%]	9.4	6.9	10.7
Initial along-slope variogram			
Year 1: Tillage - May 2013			
Standard deviation (σ) [mm]	9.3	7.3	8.7
Range (R) [mm]	656,4	853.6	673.4
Year 2: Tillage - April 2014			
Standard deviation (σ) [mm]	11.4	13.7	13.8
Range (R) [mm]	438.2	538.4	516.0

The top and the lateral sides of the plots were bounded with rigid plastic sheets driven about 10 cm into the ground and extending 20 cm above the surface. Overland flow was collected at the lower end of each plot in a gutter and discharge was measured every 10 s using a 1-litre capacity tipping bucket (Giboire et al., 2003). Rainfall was measured with an electronic tipping bucket recording rain gauge, each tip corresponding to 0.16 mm of rainfall depth. Because erosion and changes in surface microtopography are better correlated with rainfall erosivity than rainfall amount (Alberts et al., 1995; Antoine et al., 2011), rainfall erosivity (RE in MJ ha^{-1} mm h^{-1}) was calculated as described by Verstraeten et al. (2006).

Cumulative outflow data from Plot 1 in Year 1 could not be calculated since data from three months (Table 5-2) were missing due to technical problems.

5.3.3 Photogrammetric Data Acquisition

Digital elevation models (DEM) of the soil surface were obtained by means of close range digital photogrammetry software called Apero and MicMac v1.0.1 (IGN, Institut Géographique National, France) (Ahmadabadian et al., 2013; Toschi et al., 2013). Despite the limitations of digital photogrammetry, it enables the measurement of micro-topographic surfaces and the characterization of the spatial distribution of erosion and deposition and rill development (Gessesse et al., 2010). Images were taken on a monthly basis or more frequently in case of extreme rainfall events. The photographs were taken vertically from a height of approximately 2 m. A SLR camera with a focal length of 20 mm was used during the study. Each experimental plot including the borders on all sides was covered by a block of approximately 50 photos with an overlap of at least 60% in three strips. To exclude large relief displacements caused by plot border effects during pixel matching (Lane et al., 2003), the area for DEM generation was reduced by 25 cm in advance along the sides and by 30 cm along the top and bottom edges. In order to precisely set the study area, four 20-mm diameter plastic pipes were driven into the ground at each corner of the plots, limiting the effective study area to a width of 2.5 m and length of 9.4 m. A vertical accuracy of ±0.5 mm was obtained with this technique. To reduce the computational requirements for analyzing the DEMs yet keeping sufficient resolution for proper characterization of the soil roughness (Ogilvy and Foster, 1989), the DEMs were interpolated to a 1-cm grid.

5.3.4 Median polishing technique and variogram calculation

Geostatistical characterization of the surface micro-topography can only be performed after removing large-scale variations (or trends). Consequently, data were detrended by using the median polishing technique (Cressie, 1993). The technique estimates the grid elevation

(Y_{ij}) value as the sum of the overall median (m), transect median (r_i), column median (c_j), a row-column interaction $g(i-\bar{\imath})(j-\hat{\jmath})$ and a residual term (R_{ij}):

$$Y_{ij} = m + r_i + c_j + g(i-\bar{\imath})(j-\hat{\jmath}) + R_{ij} \qquad \text{Equation 5-1}$$

where subscripts i and j are the row and column numbers of the grid and i and j are the average row and column number of the grid and g is the slope of the row-column interaction component. As recommended by Cressie (1993), R_{ij} are used to calculate the variogram.

The variogram $\gamma(l)$ (Equation 2.1) was used as a means to characterize soil roughness and as a structural connectivity indicator. Given the high slope gradients of the three studied plots, erosion and sediment transport are expected to most strongly modify the spatial configuration of soil roughness in the slope direction. Especially with the appearance of continuous and parallel roughness elements produced by tillage (Vazquez et al., 2005) or, as in this study, by eroding flow paths in the direction of the slope gradient, the amplitude of the horizontal variability is expected to reflect this continuity by an increase in the range (R). For this reason the variogram will be studied in the slope direction applying a directional tolerance of 30°.

5.3.5 Flow simulation, hydrographs and connectivity length

It is difficult to discriminate between the effects of surface micro-topography and the effects of spatial heterogeneity of soil infiltration on the measured hydrographs. Hence, to assess how surface evolution affects flow properties, overland flow was simulated numerically for each DEM using FullSWOF_2D v1.0.10 (Full Shallow Water equations for Overland Flow; Delestre et al., 2014). FullSWOF_2D solves the 2D shallow water flow equations (full Saint-Venant equations) using finite volumes and numerical methods specifically

developed for hydrological applications with small water heights. Some of its main features are that it proposes two friction models (Manning and Darcy-Weysbach), that water infiltration is based on the Green-Ampt equation and that DEMs can be directly used as input. In this study the Mannning friction model was used. It must be noted that the Saint-Venant equations assume that the fluid velocity is constant along the vertical direction. The fluid velocity is determined as a function of the local gradient slope, given by the DEM, and the friction force, which is a function of the friction factor and the water depth. FullSWOF provides the water height and flow velocity for each grid element.

In this study, since only excess-rainfall is needed to study overland flow, infiltration was not considered explicitly and the application of the model only required the friction factor of Manning as input parameter, in addition to the DEM. According to Chow (1959), Manning values for bare soils are 0.02-0.025 under normal conditions. However, a lower value must be selected in order to represent the effect produced by the micro-roughness and not the form roughness (Abrahams and Parsons, 1990) which is already represented by the DEMs. A minimum Manning value was established by using Equation 5-2 (Strickler, 1923; Yen, 1992) which only considers the grain size effect:

$$n = 0.0474\, d_{50}^{1/6} \qquad \text{Equation 5-2}$$

where d_{50} is the median sediment diameter expressed in metres. For a silt loam, d_{50} = 26 μm, giving approximately n = 0.01. Since the 10 mm spatial resolution of the DEMs is not able to represent explicitly the grain size, the friction factor should be scaled-up in order to represent the effective roughness length (Clifford et al., 1992). Therefore, a Manning coefficient of 0.015, comprised between the maximum (0.02-0.025) and the minimum (0.01) values, was used for the simulations. Up-scaling the friction factor relies on the assumption

that the only effect of the micro-roughness not explicitly represented is a momentum loss but it does not take into account the effect of the micro-roughness on the routing of flow (Lane 2005). We consider that the micro-roughness elements not explicitly represented by the 10 mm spatial resolution have a negligible influence on the routing of flow compared to the influence of the form roughness elements already represented in the DEMs.

For illustration purposes, a constant 60 mm/h excess-rainfall intensity was used to calculate the overland flow hydrographs. Simulations lasted until steady-state was reached. Hydrographs are depicted as the runoff ratio [-] vs. cumulative rainfall [mm]. To facilitate comparison of the hydrographs, five characteristic values were used. Three to characterize the timing or delay of overland flow generation, I_{10}, I_{50}, and I_{90} and two to characterize the rate of increase of the runoff ratio, $S_{10,50}$ and $S_{50,90}$. I_{10}, I_{50}, and I_{90} correspond to the cumulative rainfall needed to reach 10%, 50% and 90% of the maximum runoff, respectively. The maximum outflow occurs when the runoff rate is equal to the rainfall intensity, i.e. when the runoff ratio equals 1. In order to characterize the rate of increase of the hydrograph, the slope of the hydrograph between I_{50} and I_{10}, $S_{10,50} = (0.5 - 0.1)/(I_{50} - I_{10})$, and between I_{90} and I_{50}, $S_{50,90} = (0.9 - 0.5)/(I_{90} - I_{50})$, were calculated.

The flow patterns at steady-state were characterized based on the velocity fields provided by FullSWOF_2D. The connectivity length (ξ), as defined by percolation theory, was used. ξ is defined as the size-weighted average radius of gyration of connected clusters (Keitt et al., 1997). A natural measure of the size of a circular cluster is its radius. However, in general, clusters are not round; they can be irregular, sinuous structures. The radius of gyration, r [mm], is measure of irregular cluster size used in percolation and is defined as:

$$r = 1/\mathrm{n} \sum_{i=1}^{n} \sqrt{(x_i - \bar{x})^2 + (y_i - \bar{y})^2}$$ Equation 5-3

where $\bar{x}$ and $\bar{y}$ are the mean x and y coordinates of lattice cells in the cluster in mm, x_i and y_i are the coordinates of the i^{th} grid cell in the cluster in mm, and n is the total number of cells in the cluster. In this study, in order to differentiate between connected and non-connected clusters, flow velocity fields were first binarized using a threshold equal to the average flow velocity (calculated across all the plots and years). Thus, ξ is a measure of the typical length of continuous high flow velocity areas/paths. Each of the connected clusters was labelled according to their size s. ξ [mm] was calculated by using the following equation:

$$\xi^2 = \frac{\sum_s r_s^2 \, s^2 n_s}{\sum_s s^2 n_s}$$

Equation 5-4

where s is in mm^2, r_s is the radius of gyration in mm of the connected clusters of size s and n_s is the proportion of connected clusters of size s.

The average Froude number for the whole plot surface was calculated at steady state (maximum outflow) as an indicator of the flow erosive power which is expected to increase as overland flow becomes concentrated in preferential and eroding flow paths.

5.3.6 Uncertainty analysis of DEM

Given the importance of achieving repeatable results when studying the evolution of the soil roughness, connectivity and hydrograph, the uncertainty resulting from building the DEMs was assessed. In digital photogrammetry, the quality of the DEM can be affected by the process of acquisition of the reference points, the lens distortion and by the process of identification of homologous points and DEM extraction (Rieke-Zapp and Nearing, 2005; Gessesse et al., 2010). In order to evaluate the uncertainty in scenarios with contrasting hydrological characteristics and connectivity patterns, 8 replicate sets

of images of an eroded surface and then 6 replicate sets of images of the same plot (Plot 1) but freshly tilled surface, were taken at different times of a single, rainless day and with different light conditions. These replicates were used to calculate the mean and the standard deviation (SD) of the parameters defining the variogram, RSCf and hydrograph. The SD compared to the range of variation of the calculated values of the parameters observed in this study will provide a measure of the precision or repeatability of the methodology and the results.

5.4 Results

5.4.1 Climatic conditions

In Year 1, for the first two months, the cumulative rainfall (152 mm) barely generated runoff (Figure 5-1a and Table 5-2). However, at the end of July, after a dry period, an intense thunderstorm (28.3 mm in 30 min; Δ RE = 219 MJ ha^{-1} mm h^{-1}) produced considerable runoff (Figure 5-1a and Table 5-2). In August, a second less intense thunderstorm (14mm in 40 min; Δ RE = 45 MJ ha^{-1} mm h^{-1}) produced additional runoff. From this moment till November, almost no further increase in the cumulative runoff was observed (Figure 5-1a and Table 5-2).

In Year 2, after a relatively dry period in April, a series of rainfall events in May and especially a first thunderstorm (10.2 mm in 30 min; Δ RE = 29 MJ ha^{-1} mm h^{-1}) produced runoff on the three plots (Figure 5-1b and Table 5-2). In early June, an intense thunderstorm (24.1 mm in 40 min; Δ RE = 152 MJ ha^{-1} mm h^{-1}) produced an important increase in the cumulative runoff of the plots. From this moment till September, a series of intense rainfall events generated an important amount of runoff (Figure 5-1b and Table 5-2).

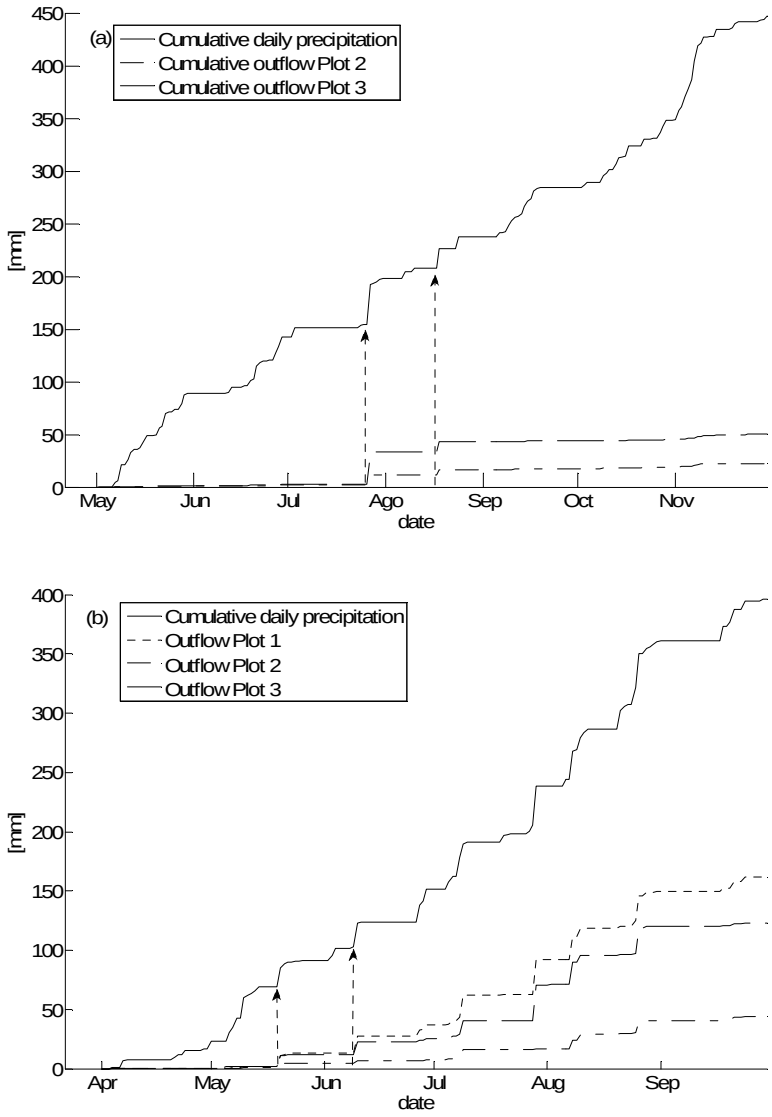

Figure 5-1 Measured cumulative daily precipitation and cumulative outflow from each plot during (a) Year 1 and (b) Year 2. Vertical arrows represent the first two thunderstorms for each year. Cumulative outflow data for Plot 1 in Year 1 could not be plotted because some data was missing.

Table 5-2 Increments of cumulative rainfall energy and rainfall and plot outflow in between successive DEMs.

RE [MJ ha^{-1} mm h^{-1}]	Date	Δ rainfall [mm]	Plot 1 Δ outflow [mm]	Plot 2 Δ outflow [mm]	Plot 3 Δ outflow [mm]
Year 1					
1	8/05/2013	5.7	0	0.3	0.1
36	4/06/2013	83.2	1.2	0.6	1.2
52	17/07/2013	62.7	No data	1.5	1.6
286	2/08/2013	46.3	No data	9.2	30.6
346	6/09/2013	43.7	No data	5.1	9.7
406	21/10/2013	82.2	1.6	1.9	1.4
436	11/11/2013	103.5	2.9	3.5	3.9
Year 2					
1	3/04/2014	0	0	0	0
10	4/05/2014	23.3	0.4	0.4	0.6
52	30/05/2014	68.0	12.6	4.2	11.2
204	17/06/2014	32.0	14.5	2.2	10.6
274	16/07/2014	67.7	34.8	9.5	18.3
404	2/08/2014	47.0	29.9	0.4	30.4
746	3/09/2014	122.7	57.1	24.1	49.1

5.4.2 Uncertainty of characteristic parameters

For the two contrasted micro-topographies, the parameters defining the variogram (Chapter 2), the RSCf (Chapter 2) and the overland flow hydrograph show very low coefficient of variation (CV) values, all of them being equal or below 0.091 (Table 5-3), with the only exception of C_{CT} for the freshly tilled surface and C_0, C_{CT} and RDS_{CT} for the eroded surface (Table 5-3). This means that the parameters are reliably determined from the DEMs.

Table 5-3 Uncertainty of the parameters defining the variogram, RSCf and overland flow hydrograph for two contrasted micro-topographies

			Freshly tilled surface			Eroded surface		
		units	mean	SD	CV	mean	SD	CV
Along-slope variogram	σ	[mm]	9.4	0.1	0.015	9.7	0.1	0.014
	R	[mm]	478.4	15.3	0.027	1057.6	17.2	0.016
RSCf	C_0		0.004	0.0003	0.091	0.019	0.003	0.134
	C_{CT}		0.072	0.020	0.278	0.054	0.026	0.469
	RDS_{CT}		0.500	0.042	0.084	0.080	0.037	0.463
	DS_{max}	[mm]	0.315	0.010	0.031	0.011	0.001	0.074
Overland flow hydrograph	I_{10}	[mm]	0.9	0.022	0.024	0.23	0.004	0.019
	I_{50}	[mm]	1.66	0.043	0.026	0.49	0.010	0.021
	I_{90}	[mm]	2.44	0.047	0.019	0.66	0.008	0.013
	$S_{10,50}$	[mm^{-1}]	0.53	0.029	0.055	1.54	0.059	0.038
	$S_{50,90}$	[mm^{-1}]	0.51	0.031	0.060	2.38	0.108	0.045
	Fr		1.09	0.010	0.011	1.39	0.015	0.011

5.4.3 Soil roughness

In Year 1, up to RE = 52 MJ ha^{-1} mm h^{-1}, the soil roughness distribution did not change and only a slight smoothing of the soil surface was observed (Figure 5-2a and b). With the occurrence of the first thunderstorm, RE = 286 MJ ha^{-1} mm h^{-1}, the DEMs showed a slight change in the spatial soil roughness distribution, and wide and shallow paths appeared on the surface (Figure 5-2c). From RE = 286 MJ ha^{-1} mm h^{-1} till the end (RE = 436 MJ ha^{-1} mm h^{-1}), the DEMs did not show visual changes in roughness (Figure 5-2c and d). The study of the variogram reveals a continuous and slight decrease of σ with RE along the year (approx. 1 mm) for the three plots (Figure 5-4a) while *R* increases (by 300-400 mm) linearly up to RE = 350 MJ ha^{-1} mm h^{-1} for all the plots (Figure 5-4b) except for Plot 3 for which *R* slightly decreases from RE = 286 MJ ha^{-1} mm h^{-1} up to the end of Year 1. From RE = 350 MJ ha^{-1} mm h^{-1} till the end of Year 1, *R* decreased (by 150 mm) for Plot 2 and remained approximately constant for Plot 1 (Figure 5-4b).

In Year 2, significant changes were observed in the DEMs after the occurrence of the first important rainfall events (RE = 52 MJ ha^{-1} mm h^{-1}) (Figure 5-3a and b). Preferential flow paths, but not yet well developed rills, were observed on the soil surface (Figure 5-3b). A subsequent thunderstorm eventually produced the development of a rill network at the surface (Figure 5-3b and c). From RE = 274 MJ ha^{-1} mm h^{-1} till the end of Year 2 (RE = 745 MJ ha^{-1} mm h^{-1}) the spatial configuration of soil roughness barely changed (Figure 5-3d). Additional rills were not observed, but the rills already present became deeper and showed local headcuts. The interrill areas became smoother. The variogram shows an initial pronounced decrease of σ (by 2.8-3.5 mm) up to RE = 52 MJ ha^{-1} mm h^{-1} (Figure 5-4b). After this point till the end of Year 2 (RE = 746 MJ ha^{-1} mm h^{-1}), σ remains fairly constant. A similar but opposite behaviour is observed for *R*. First, a pronounced increase of *R* (by 280-320 mm) is observed up to

RE = 52 MJ ha^{-1} mm h^{-1}. This is followed by a less pronounced increase (by 160-200 mm) up to RE = 274 MJ ha^{-1} mm h^{-1}. From this point till the end, it remains fairly constant with the exception of Plot 1 that continues to increase up to the end of Year 2.

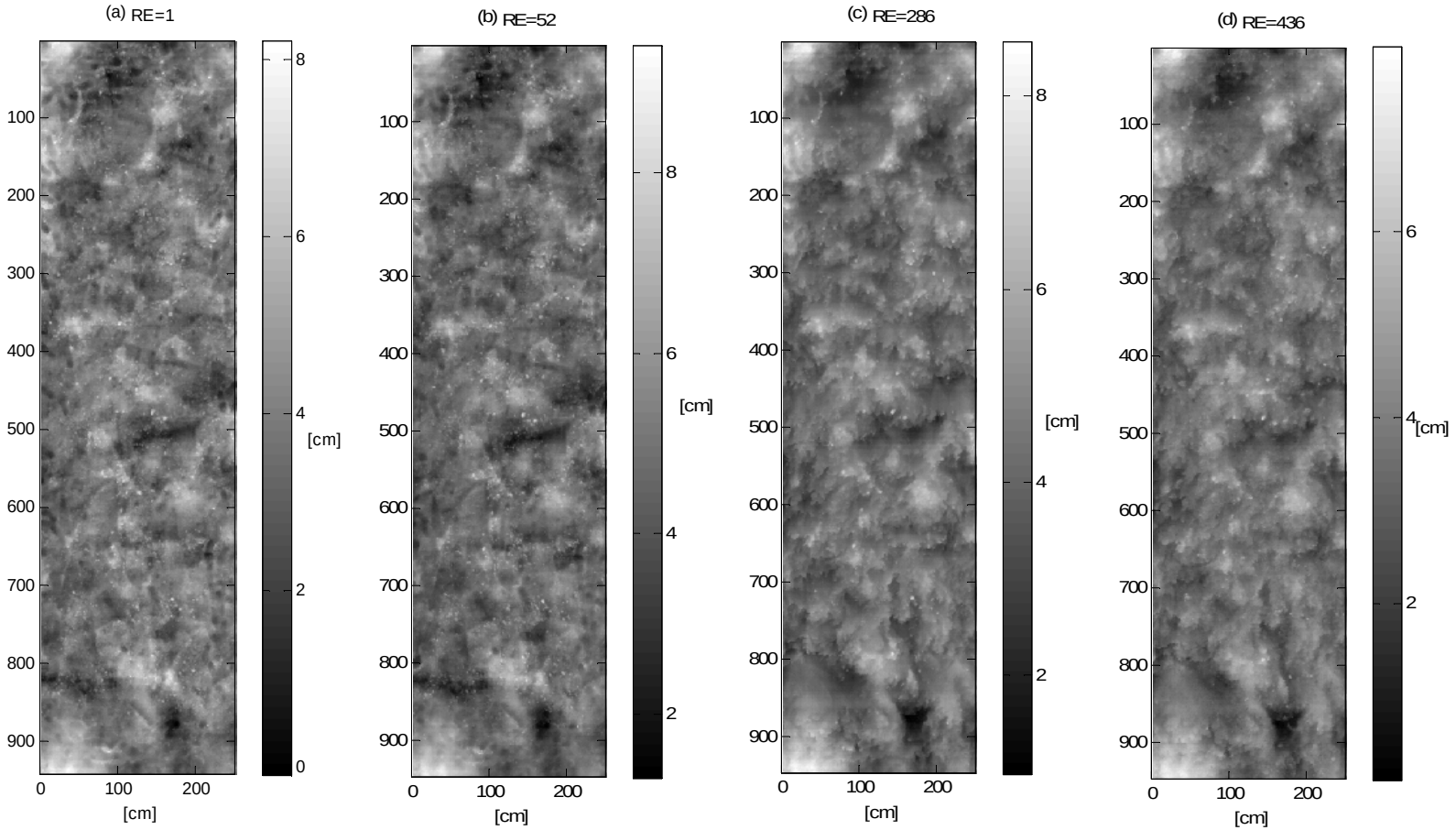

Figure 5-2 Digital elevation models of Plot 1 in Year 1 for (a) RE = 1, (b) RE = 52, (c) RE = 286 and (d) RE = 436. RE in MJ ha^{-1} mm h^{-1}.

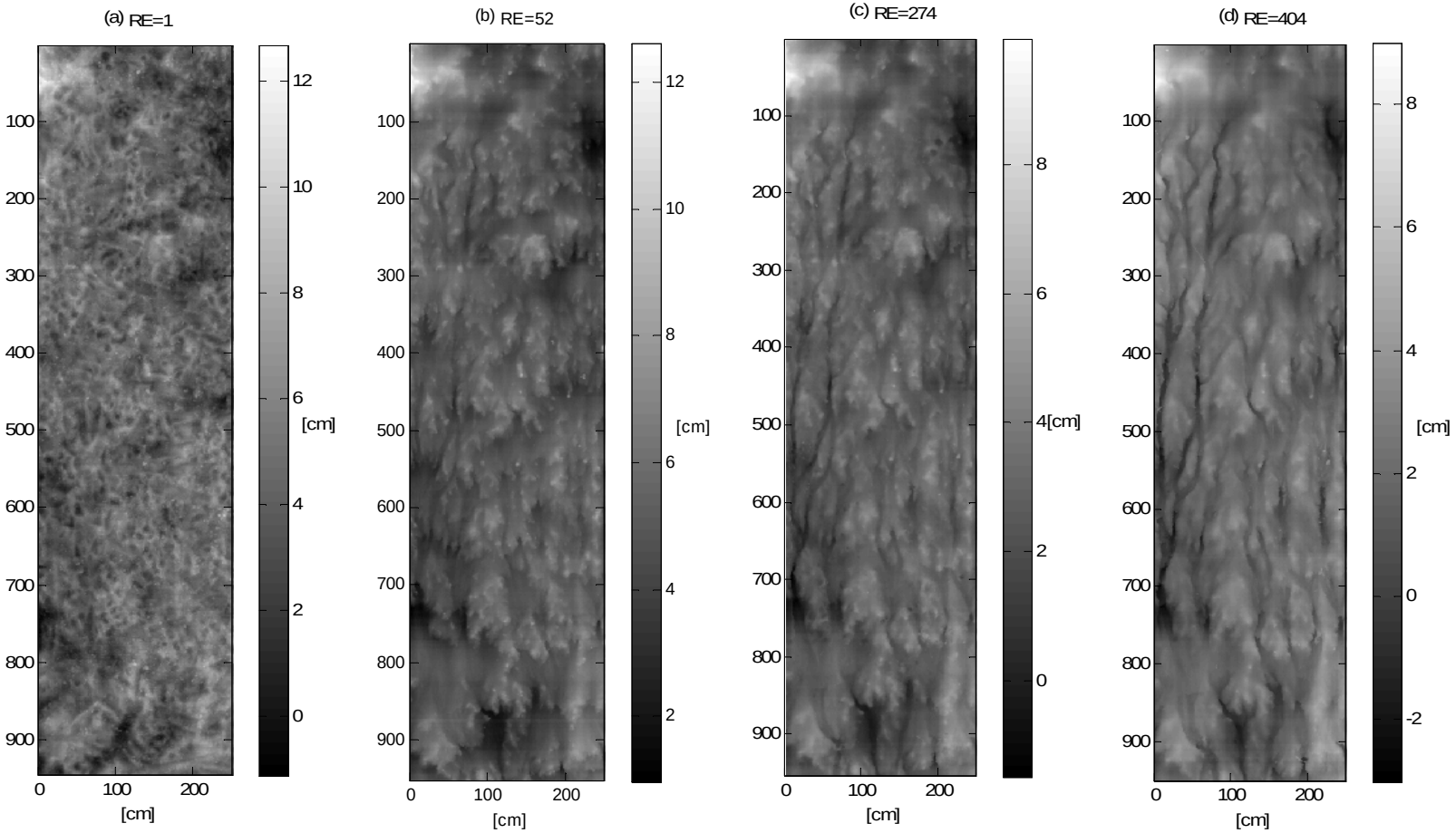

Figure 5-3 Digital elevation models of Plot 1 in Year 2 for (a) RE = 1, (b) RE = 52, (c) RE = 274 and (d) RE = 404. RE in in MJ ha^{-1} mm h^{-1}

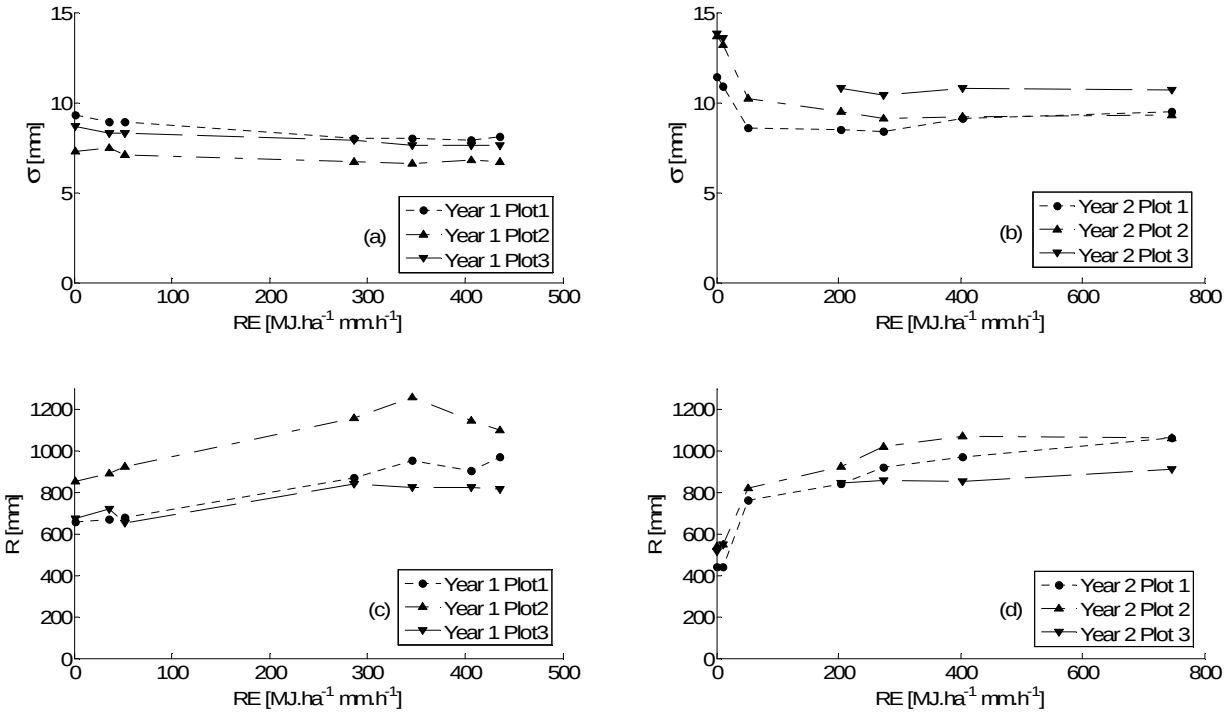

Figure 5-4 Evolution of the sill (expressed as σ) of the along-slope variogram (a) in Year 1 and (c) in Year 2 and evolution the range (R) (b) in Year 1 and (d) in Year 2 as a function of cumulative rainfall erosivity (RE). Data from Plot 3 in Year 2 for RE = 52 is missing. Data of Plot 3 in Year 2 and RE = 52 is missing.

5.4.4 RSCf

In Year 1, for the three plots, a decrease of DS_{max} is observed up to RE = 286 (Figure 5-5a and Figure 5-6g). The shape of the normalized RSCf barely changes, remaining convex for 0 < RE < 52 (Figure 5-5b). After the occurrence of the first thunderstorm (RE = 286), one observes an important change in the shape of the normalized RSCf, from convex to concave (Figure 5-5b). This change is reflected in a decrease of RDS_{CT} by approx. 0.2 units for Plot 2 and 3 and 0.5 units for Plot 1 (Figure 5-6e). For 286 < RE < 346, the four RSCf parameters remained fairly constant (Figure 5-6a, c, e and g) and the shape of the normalized RSCf stays concave (Figure 5-5b). As from RE = 346, a slight increase of DS_{max} is observed (Figure 5-5a and Figure 5-6g) while the shape of the normalized RSCf tends to a less concave shape (Figure 5-5b). Again this change in shape mainly affects RDS_{CT} which shows an increase of 0.1 to 0.2 units depending on the plot (Figure 5-6e). Only small variations are observed for C_0 (Figure 5-6a) as well as for C_{CT} (Figure 5-6c) over the entire range of RE values, with the exception of Plot 1 for which C_{CT} decreases from 0.2 to 0.05.

In Year 2, similar variations were observed as in Year 1, but they occurred more rapidly and were more pronounced. Up to R =52, DS_{max} decreases approximately linearly, after which it remains fairly constant and always below 0.01 mm (Figure 5-6h). For RE < 10, the shape of the normalized RSCf remains convex (Figure 5-5d). Thereafter, there is a rapid shift towards a concave shape following the first thunderstorm. As the season progresses, the RSCf becomes less concave. The behaviour of RDS_{CT} is similar to that of DSmax, with a rapid decrease for RE < 52 (Figure 5-6f). Thereafter, RDS_{CT} values are equal to 0, with the exception of Plot 1 which shows a slight and linear increase up to 0.08 units. As in Year 1, C_0 and C_{CT} are small and not significantly affected by the RE (Figure 5-6b and d).

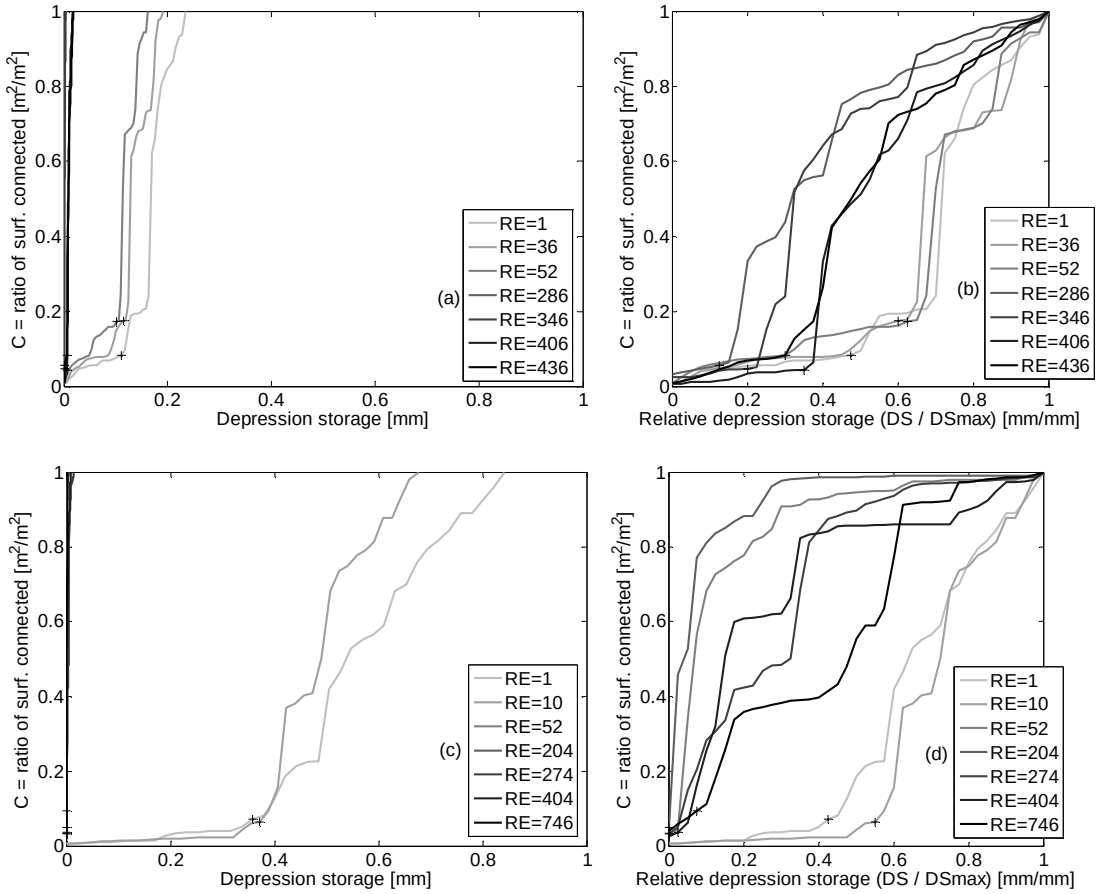

Figure 5-5 Evolution of the RSCf (a, c) and the normalized RSCf (b, d) as a function of the cumulative rainfall erosivity (RE) for Plot 1 in Year 1 (a, b) and Year 2 (b, c). Cross markers represent the connectivity threshold (CT). RE in MJ ha^{-1} mm h^{-1}.

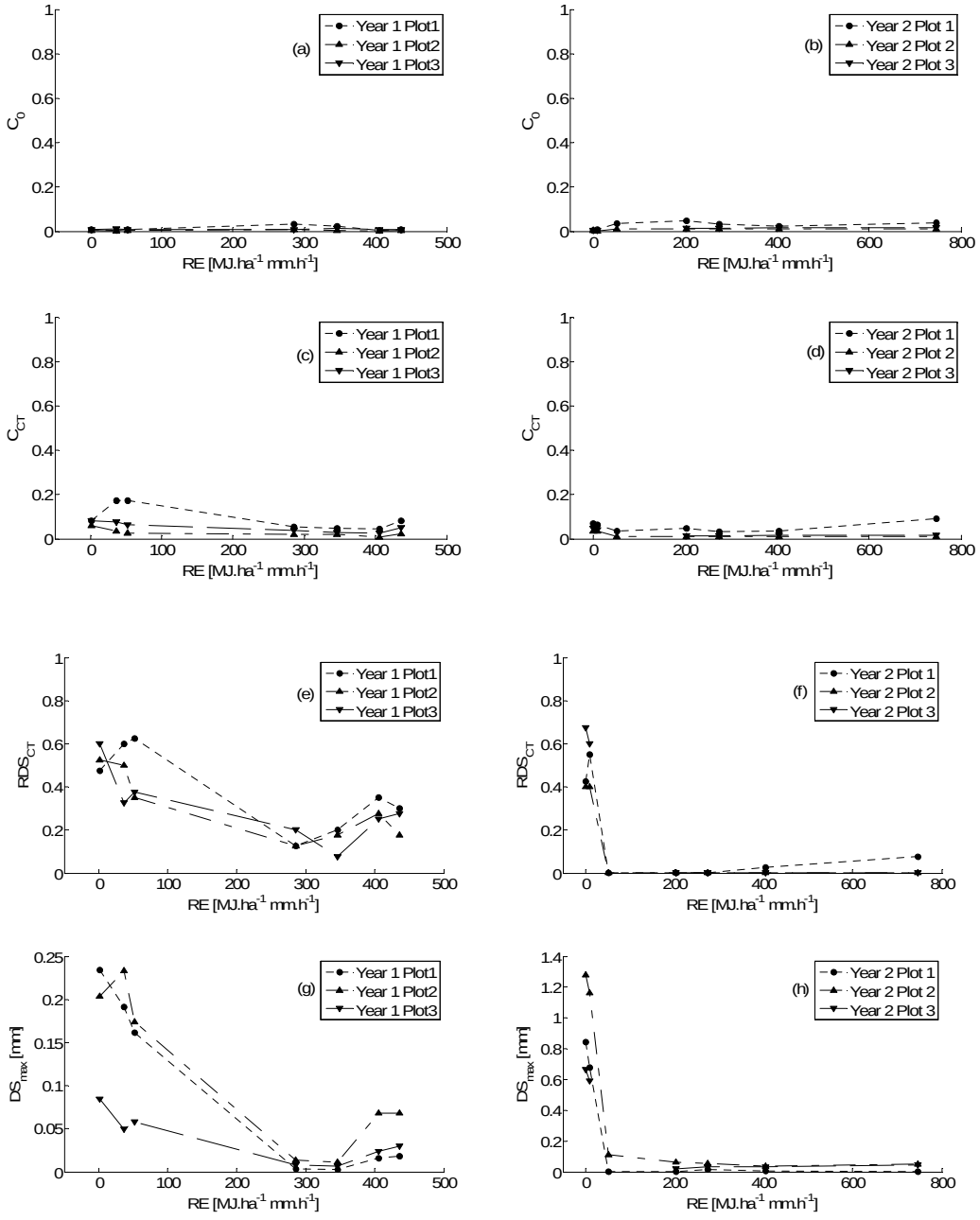

Figure 5-6 Evolution of the RSCf parameters, C_0 (a, b), C_{CT} (c, d), RDS_{CT} (e, f) and DS_{max} (g, h) as a function of the cumulative rainfall erosivity (RE) in Year 1 (a, c, e, g) and Year 2 (b, d, f, h). Data of Plot 3 in Year 2 and RE = 52 is missing.

5.4.5 Overland flow

A value of 0.07 m/s, corresponding approximately to the mean flow velocity at steady state calculated in FullSWOF_2D for all the plots and both years, was used to binarize the overland flow velocity fields at steady state (Figure 5-8 and Figure 5-9) and eventually calculate the connectivity length ξ (Figure 5-7).

In Year 1, after the occurrence of the first thunderstorm (RE = 286 MJ ha^{-1} mm h^{-1}), the continuity of the spatial distribution of the flow velocities increased, i.e. flow paths became better defined and more continuous (Figure 5-8c). This is also indicated by an increase of ξ by 50-60 mm for all three plots (Figure 5-7). Until the end of Year 1 (RE = 436 MJ ha^{-1} mm h^{-1}), well defined continuous flow paths are still observed (Figure 5-8d), and ξ values remain fairly constant, between 223 and 253 mm (Figure 5-7).

In Year 2, before the occurrence of the first thunderstorm (RE = 52 MJ ha^{-1} mm h^{-1}), the discontinuity of flow velocities is higher than for Year 1 (Figure 5-9a). ξ values are more than 100 mm lower in Year 2 than in Year 1 (Figure 5-7). Similarly to Year 1, significant changes are observed in the flow velocity distribution after the occurrence of the first important rainfall event (RE = 52 MJ ha^{-1} mm h^{-1}). Very well defined and highly continuous preferential flow paths appear on the surface (Figure 5-9b), and ξ increases considerably from 47-87 mm up to 224-242 mm. From RE = 52 MJ ha^{-1} mm h^{-1} up to the end of Year 2 (RE = 746 MJ ha^{-1} mm h^{-1}), the spatial configuration of the flow velocities barely changes (Figure 5-9b, c and d). Additionally, the preferential flow paths are slightly wider for RE = 52 MJ ha^{-1} mm h^{-1} (Figure 5-9b).

After the first thunderstorm, overland flow in Year 2 is more concentrated, with less numerous, less tortuous and better defined preferential flow paths, compared to Year 1 (Figure 5-8c and d, and Figure 5-9b, c and d). Despite these visual differences, values of ξ are

fairly similar after the first thunderstorm for both years, ranging from 224 to 259 mm, meaning the connectivity is similar in term of distance for the three experimental plots in Year 1 and 2.

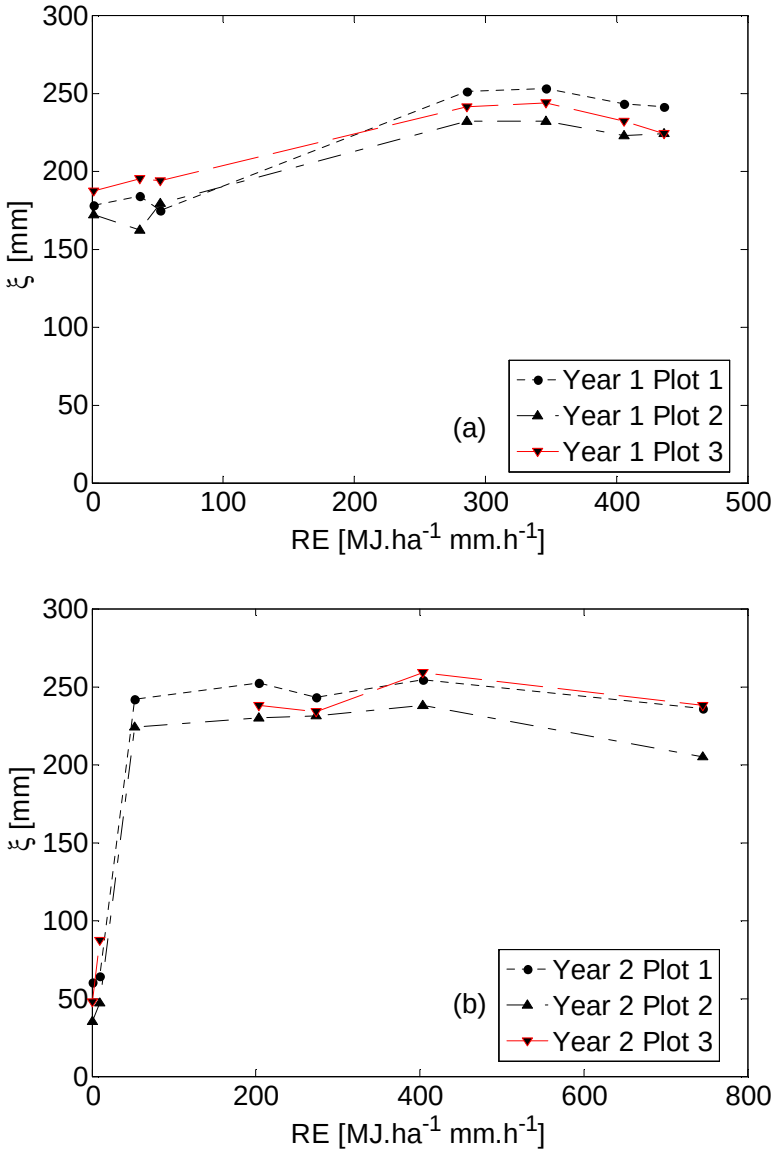

Figure 5-7 Evolution of the connectivity length (ξ) of the overland flow velocity fields for the three experimental plots in (a) Year 1 and (b) Year 2. Data of Plot 3 in Year 2 and RE = 52 is missing.

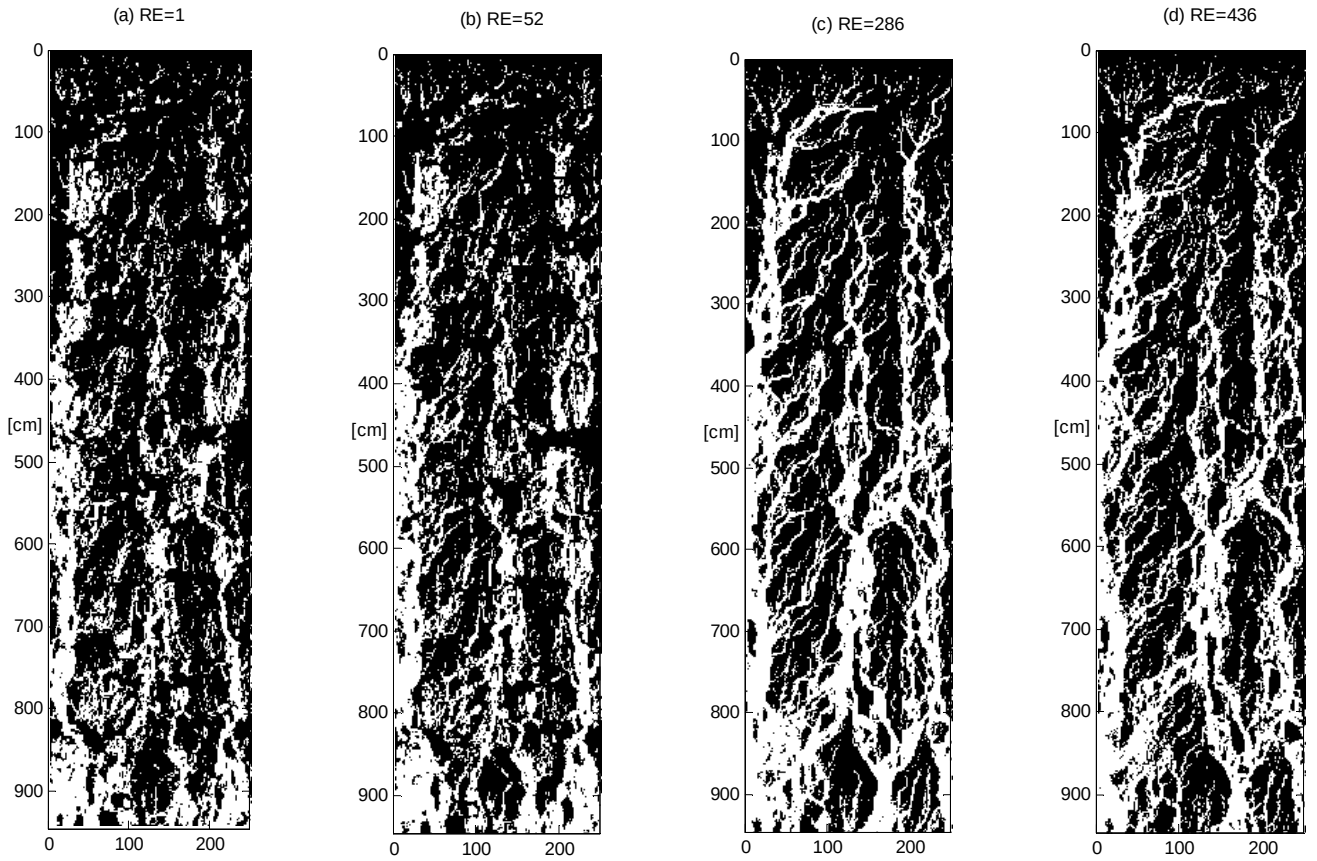

Figure 5-8 Spatial distribution of binarized overland flow velocity fields at steady state of Plot 1 in Year 1 for (a) RE = 1, (b) RE = 52, (c) RE = 286 and (d) RE = 436. RE is in MJ ha^{-1} mm h^{-1}. Flow velocities above 0.07 m/s represented in white and below 0.07 m/s represented in black.

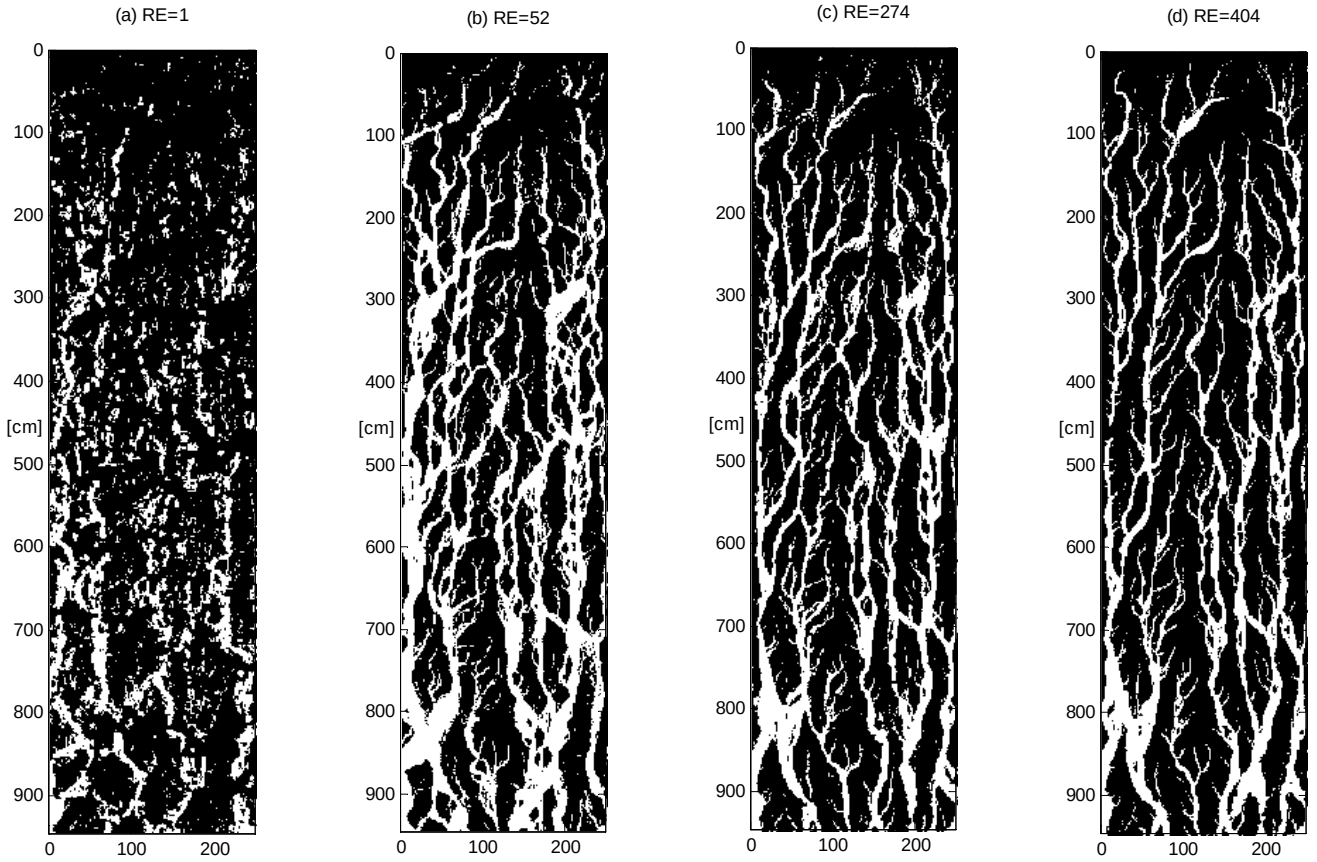

Figure 5-9 Spatial distribution of binarized overland flow velocity at steady state of Plot 1 in Year 2 for (a) RE = 1, (b) RE = 52, (c) RE = 274 and (d) RE = 404. RE is in MJ ha^{-1} mm h^{-1}. Flow velocities above 0.07 m/s represented in white and below 0.07 m/s represented in black.

For the first three DEMs of Year 1 (RE = 1, 36 and 52 MJ ha^{-1} mm h^{-1}), the hydrograph shows an initial plateau (runoff ratio up to 0.09 for Plot 1; Figure 5-10a). This causes a delay in the occurrence of I_{10}, I_{50} and I_{90} as compared to the hydrographs of the later DEMs (from RE = 286 up to 436 MJ ha^{-1} mm h^{-1}) for which this plateau is barely observed. The average values of I_{10}, I_{50} and I_{90} range between 0.5 mm (I_{10}) and 1.5 mm (I_{90}) of cumulative rainfall (Figure 5-10a and Figure 5-11a). The plateau is followed by a rapid increase of the runoff ratio, approximately up to I_{90}, after which the rate of increase levels off as the hydrograph approaches steady state (Figure 5-10a). For the first three hydrographs, the rates of increase of the runoff ratio ($S_{10,50}$ and $S_{50,90}$) range between 2 and 3 (Figure 5-11c) and the mean Fr number ranges between 1 and 1.3 (Figure 5-12a). After the first thunderstorm (RE = 286 MJ ha^{-1} mm h^{-1}), a considerably faster runoff generation is observed (Figure 5-10a). This faster runoff generation is reflected in a short plateau and a decrease of I_{10}, I_{50}, and I_{90}, this decrease being the largest for I_{90} (Figure 5-11a). After RE = 346 MJ ha^{-1} mm h^{-1}, this trend changes and I_{10}, I_{50} and I_{90} increase (Figure 5-10a and Figure 5-11a). Conversely, $S_{10,50}$ and $S_{50,90}$ increase for RE = 286 MJ ha^{-1} mm h^{-1} up to approximately 3.2 and 4.2, respectively, and thereafter decrease slightly down to 3 and 3.5, respectively (Figure 5-11c). The calculated mean Fr numbers increase slightly up to RE = 286 MJ ha^{-1} mm h^{-1}, reaching values between 1.2 and 1.5, and then decrease up to the end of Year 1 to reach values between 1.1 and 1.3 (Figure 5-12a).

In Year 2, similar but more pronounced variations are observed compared to Year 1. At the initial stages (RE $\leq$ 10 MJ ha^{-1} mm h^{-1}) a plateau is observed (runoff ratio up to 0.03 for Plot 1; Figure 5-10b). This plateau extends up to 1 mm of cumulative rainfall and thereby markedly delays the occurrence of I_{10}, I_{50} and I_{90}. The values of I_{10}, I_{50} and I_{90} are larger than in Year 1 and range between 1.5 mm and 4 mm (Figure 5-10b and Figure 5-11b). $S_{10,50}$ and $S_{50,90}$ are initially approximately equal to 1 (Figure 5-11c), and the mean Froude number ranges between 0.9 and 1.2 (Figure 5-12b). After the first thunderstorm (RE = 52 MJ ha^{-1} mm h^{-1}), a considerably faster runoff

generation is again observed (Figure 5-10b). The initial plateau practically disappears and an important decrease of I_{10}, I_{50}, and I_{90} is observed. The average values of I_{10}, I_{50}, and I_{90} after the first thunderstorm are very similar to Year 1 and range between 0.25 mm (I_{10}) and 1 mm (I_{90}). After RE = 52 MJ ha^{-1} mm h^{-1} these values remain constant up to end of Year 2. As for Year 1, $S_{10,50}$ and $S_{50,90}$ increase strongly after the first thunderstorm (RE = 52 MJ ha^{-1} mm h^{-1}) up to approximately 3.8 and 3.5, respectively (Figure 5-11d), and remain fairly constant thereafter. An increase of Fr number is also observed after the first thunderstorm, this increase being more important than in Year 1. The maximum values are fairly similar for both years and range from 1.2 to 1.5. For both years, it must be noted that the highest Fr values are obtained for Plot 1 and Plot 3 which have the highest slope gradients and the lowest Fr for Plot 2, which has the lowest slope gradient (Figure 5-12 and Table 5-1).

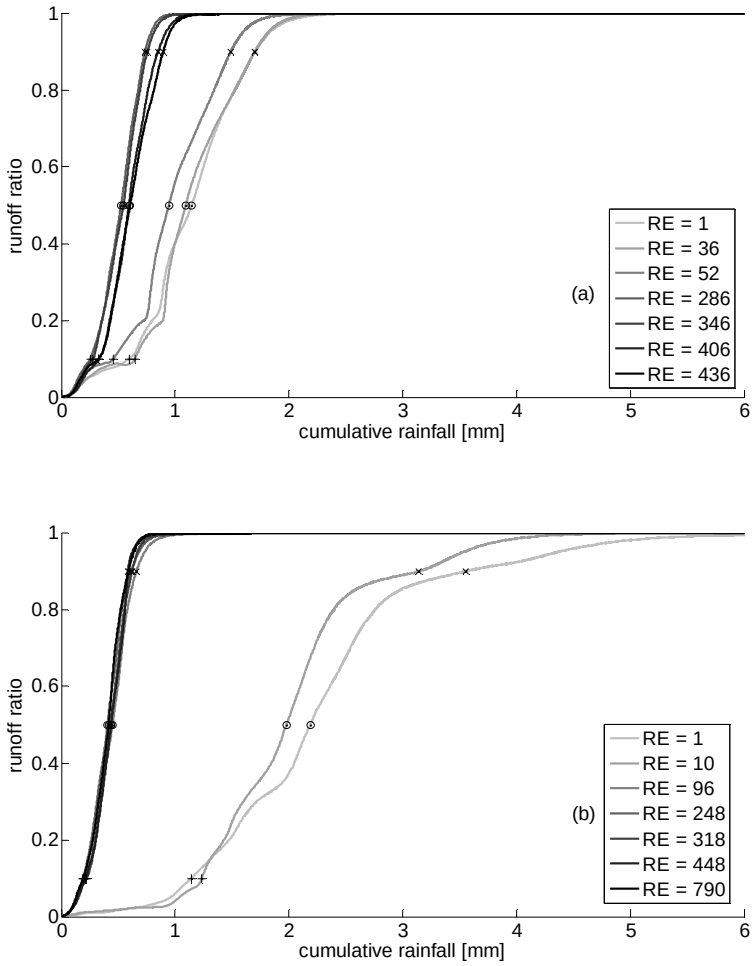

Figure 5-10 Evolution of the overland flow hydrograph for Plot 1 in (a) Year 1 and (b) Year 2 simulated on the basis of DEMs characterized after increasing amounts of rainfall erosivity (RE). Cross markers represent I_{10}, open circles I_{50} and the x markers represent I_{90}. RE is in MJ ha^{-1} mm h^{-1}.

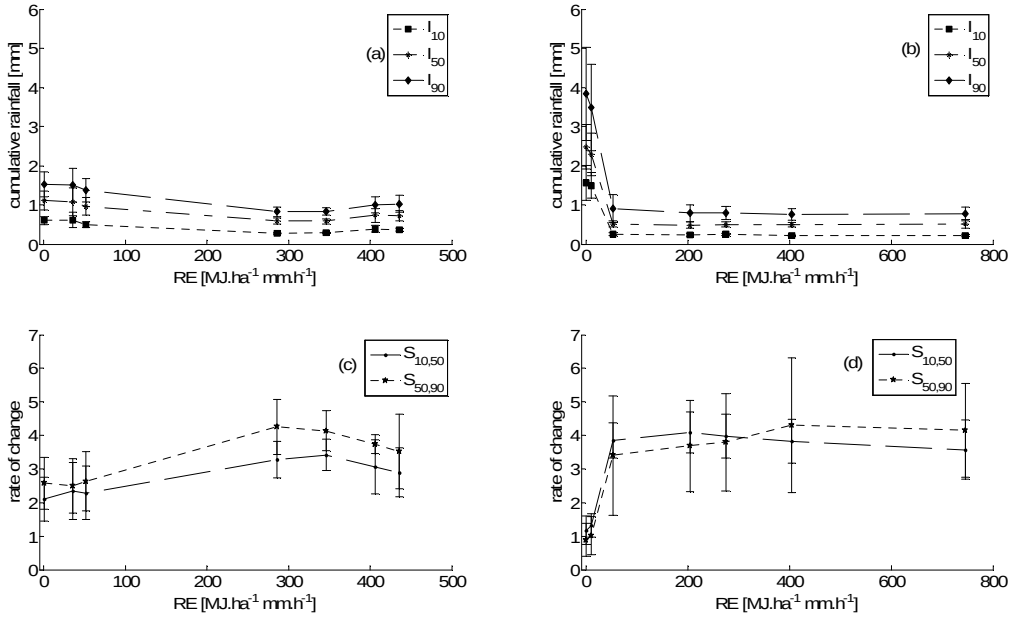

Figure 5-11 Evolution of the overland flow hydrograph characteristic points, I_{10}, I_{50} and I_{90} (a, b) and $S_{10,50}$ and $S_{50,90}$ (c, d), as a function of the cumulative rainfall erosivity (RE) in Year 1 (a, c) and Year 2 (b, d). Each point is the average of the three plots. Error bars are one standard deviation

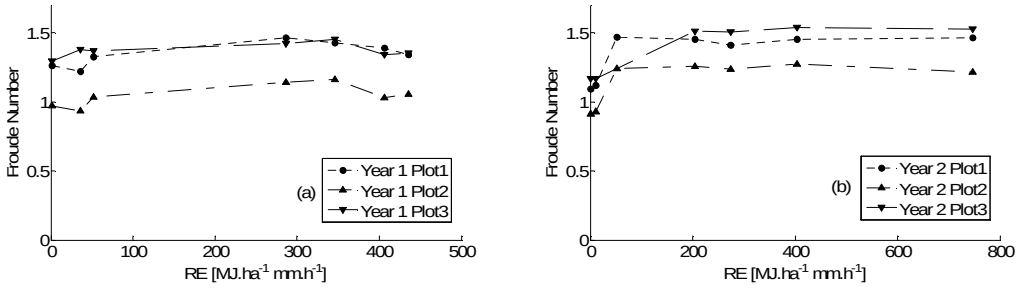

Figure 5-12 Evolution of the Froude number for the three experimental plots as a function of the cumulative rainfall erosivity (RE) in Year 1 (a) and Year 2 (b).

5.4.6 Correlation between variogram, RSCf and hydrograph characteristic parameters

Whereas low correlations are observed between variogram parameters and C_0 and C_{CT}, moderate, high and very high correlations are observed between variogram parameters and RDS_{CT} and DS_{max} (Table 5-4), with the only exception of σ, which is weakly correlated to RDS_{CT}. The parameters defining the overland flow hydrograph, though little to moderately correlated to variogram parameters (Table 5-5), show good correlation with some of the RSCf parameters. Very high correlations are found between DS_{max} and I_{10}, I_{50} and I_{90} (Table 5-4 and Figure 5-13), and high correlations between RDS_{CT} or DS_{max} with $S_{10,50}$ and $S_{50,90}$, with the exception of RDS_{CT} and $S_{50,90}$ (Table 5-4). Low and very low correlations are observed between the hydrograph parameters and C_0 and C_{CT}, with the only exception of C_0 with $S_{10,50}$, $S_{50,90}$ and Fr. Regarding the correlation between the RSCf parameters and $S_{10,50}$ and $S_{50,90}$ for each of the plots, the best correlations are found between DS_{max} and $S_{50,90}$ (Plot 1 ρ = 0.79, Plot 2 ρ = 0.85 and Plot 3 ρ = 0.91), RDS_{CT} and $S_{10,50}$ (Plot 1 ρ = 0.88, Plot 2 ρ = 0.90 and Plot 3 ρ = 0.91; Figure 5-14a) and RDS_{CT} and Fr (Plot 1 ρ = 0.79, Plot 2 ρ = 0.95 and Plot 3 ρ = 0.96; Figure 5-14b).

In this study, the parameter DS_{CT} (see Section 2.1) is not considered given the very high correlation observed between DS_{CT} and DS_{max} (ρ = 0.97; Figure 5-15).

Table 5-4 Coefficients of correlation (ρ), between the RSCf parameters and the parameters defining the variogram and the overland flow characteristics for both years.

	Variogram		Overland flow hydrogram						
	σ	R	I_{10}	I_{50}	I_{90}	$S_{10,50}$	$S_{50,90}$	Fr	ξ
C_0	-0.09	0.19	-0.46	-0.49	-0.46	0.72	0.67	0.62	0.48
C_{CT}	0.03	-0.42	0.14	0.14	0.14	-0.22	-0.16	0.00	0.22
RDS_{CT}	0.18	-0.61	0.66	0.66	0.58	-0.75	-0.57	-0.55	0.71
DS_{max}	0.72	-0.69	0.97	0.98	0.99	-0.76	-0.73	-0.64	0.94

Table 5-5 Coefficients of correlation (ρ), between the variogram and the overland flow characteristics for both years

	Overland flow hydrogram						
	I_{10}	I_{50}	I_{90}	$S_{10,50}$	$S_{50,90}$	Fr	ξ
σ	0.67	0.62	0.65	-0.28	-0.49	-0.10	-0.64
R	-0.69	-0.67	-0.67	0.48	0.54	0.14	0.75

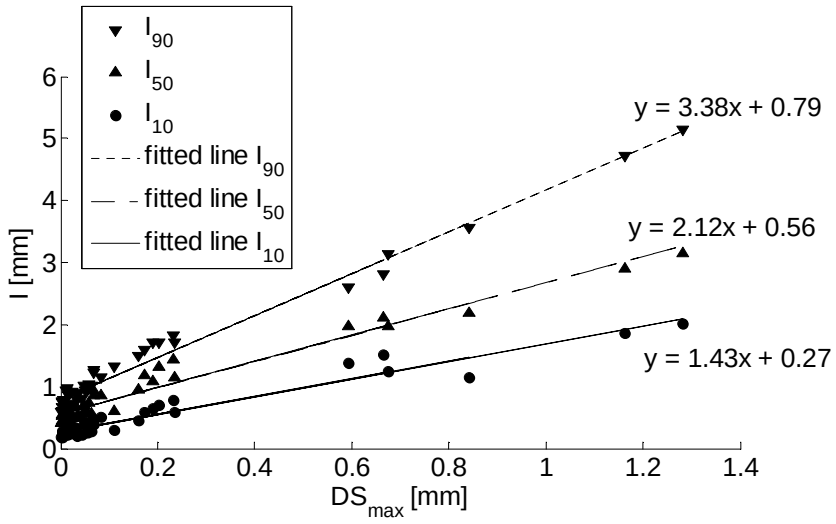

Figure 5-13 Linear regression between DS_{max} and I_{10} (R^2 =0.94), I_{50} (R^2 =0.95) and I_{90} (R^2 =0.98) for both years.

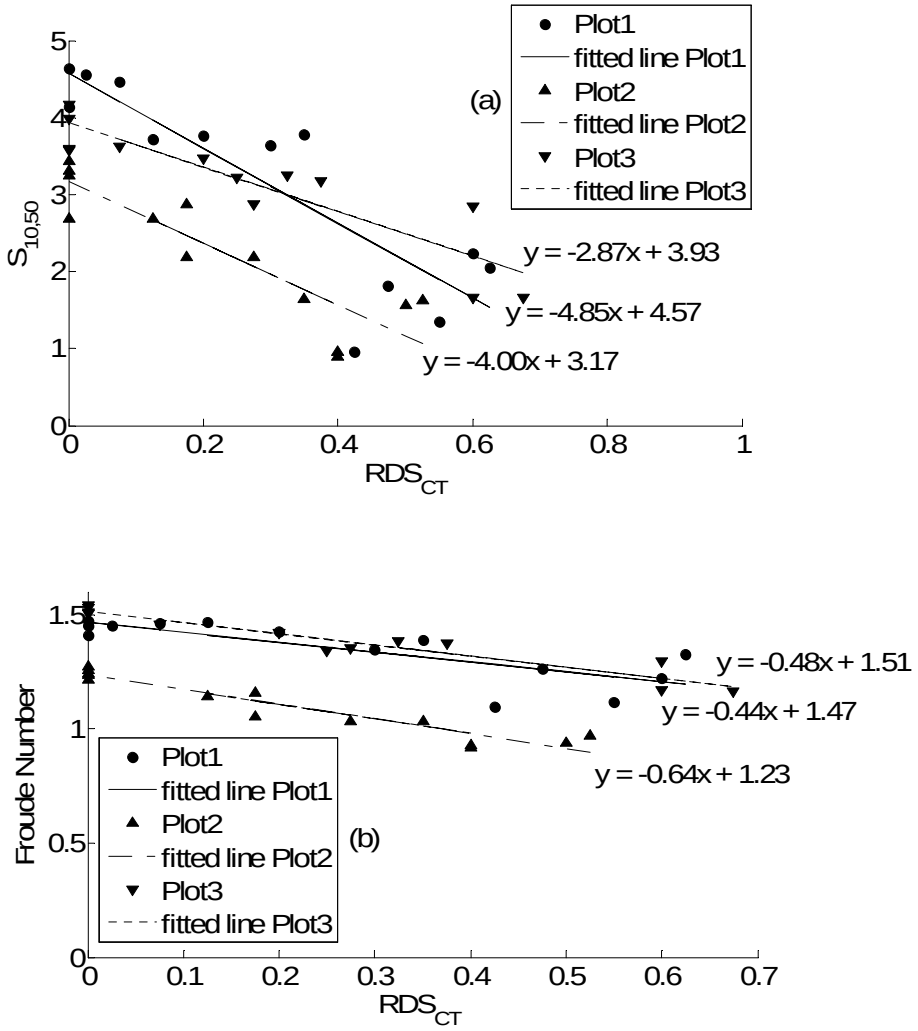

Figure 5-14 Linear regression between RDS$_{CT}$ and (a) $S_{10,50}$ (Plot 1 R^2 =0.78, Plot2 R^2 =0.81, Plot 3 R^2 =0.82) and (b) Fr (Plot 1 R^2 =0.63, Plot2 R^2 =0.90, Plot 3 R^2 =0.93) for both years.

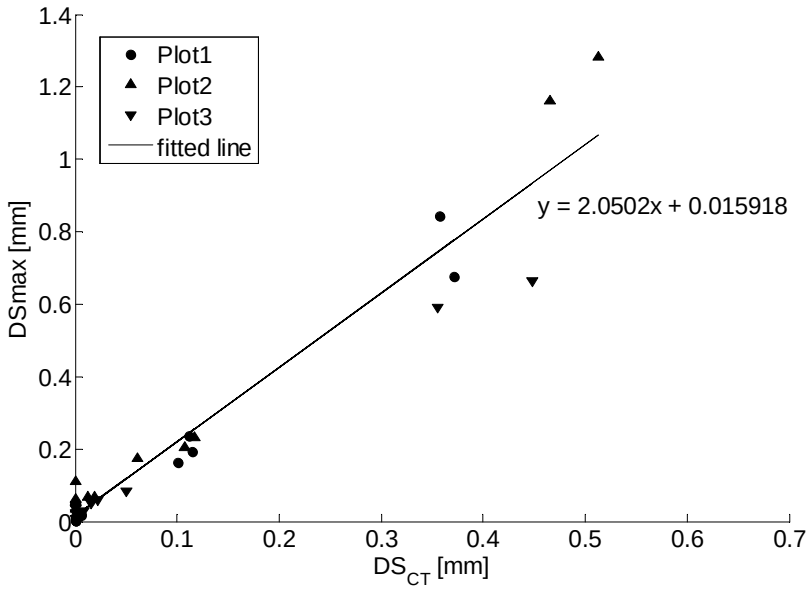

Figure 5-15 Linear regression between DS_{CT} and DS_{max} for both years (R^2 = 0.94).

These changes in overland flow generation and connectivity were also accompanied by changes in the spatial distribution and the spatial continuity of overland flow velocities (Figure 5-8 and Figure 5-9). For both years, the stages with the lowest continuity of flow velocities (Figure 5-8a, b and Figure 5-9a) correspond to the lowest connectivity length and the highest values of RDS_{CT} and DS_{max}. On the contrary, the highest continuity of flow velocities (Figure 5-8c and Figure 5-9b) corresponds to the highest connectivity length and lowest values of RDS_{CT} and DS_{max}. Among the RSCf parameters, DS_{max} shows the highest correlation with the continuity of flow velocities, as represented by ξ (Plot 1 ρ = 0.98, Plot 2 ρ = 0.97 and Plot 3 ρ = 0.96).

5.5 Discussion

5.5.1 Uncertainty

The low CV of the calculated parameters defining the variogram, the RSCf and the overland flow hydrograph (Table 5-3), coupled with the high vertical accuracy (±0.5 mm) demonstrate that the methodology that was used to generate the DEMs is appropriate for the study of the evolution of soil roughness, overland flow generation and overland flow connectivity. Whenever higher values of CV are observed, e.g. C_0, C_{CT} and RDS_{CT} (Table 5-3), this corresponds to cases for which the mean value of the parameters was nearly 0, the SD still being very low in comparison to the range of variation of these parameters (Figure 4-6, Figure 5-11 and Figure 5-12).

5.5.2 Soil roughness evolution

Despite similar total cumulative rainfall and erosivity values for Year 1 and Year 2 (Table 5-2), important differences were observed between both years regarding the evolution of the DEMs, variograms and outflows of the plots. This can be attributed to differences in intra-annual rainfall distribution. In Year 1, most runoff was produced after the occurrence of the first thunderstorm in July (Figure 5-1a and Table 5-2). The DEMs did not show important changes (Figure 5-2). The variogram parameters (σ and R) evolved linearly with cumulative RE, this trend not being modified by the occurrence of the first thunderstorm (RE = 286 MJ ha^{-1} mm h^{-1}) (Figure 5-4a and b). The surface evolved mostly as a result of splash and sheet erosion, and no marked rills developed. On the contrary, in Year 2, several important runoff episodes occurred as from the first thunderstorms in May (Figure 5-1b and Table 5-2). This was accompanied by important changes in the DEMs, in particular the development of incisional flow paths (rills), which was reflected in a sharp decrease of σ and increase in R (Figure 5-4c and d). The occurrence of this sharp break in Year 2 but not in Year 1 does not seem to be related to the rainfall

characteristics of the first thunderstorm since the first thunderstorm in Year 2 (10.2 mm in 30 min; Δ RE = 29 MJ ha^{-1} mm h^{-1}) had a lower total rainfall and RE than the first thunderstorm of Year 1 (28.3 mm in 30 min; Δ RE =219 MJ ha^{-1} mm h^{-1}; Figure 5-1 and Table 5-2). Given that the soil type and slope gradient were the same in both years, two factors are proposed to explain these differences: soil moisture content and initial roughness. As reported in the literature, a low initial water content increases aggregate slaking and breakdown and hence soil detachment and surface sealing, causing significantly more runoff and erosion compared to initially wet soils (Le Bissonnais et al., 1989; Govers et al., 1990). However, the dry period preceding the first thunderstorm was longer in Year 1 (July; Figure 5-1a) compared to Year 2 (May; Figure 5-1b). Therefore this factor can hardly explain the observed differences between Year 1 and Year 2. Roughness elements tend to concentrate the flow along depressions, increasing the erosion and sediment transport capacity of the flow (Govers et al., 2000; Kirkby, 2002; Gomez and Nearing, 2005). Hence, the higher initial roughness of Year 2 (Table 5-1) compared to Year 1 may explain the observed differences in initial evolution of the DEMs. A practical implication obtained from these results is that the initial tillage and hence soil roughness on an agricultural field may have an important influence on the subsequent evolution of the soil surface. Higher initial roughness may facilitate the occurrence of rill erosion. However, this statement must be taken carefully since stronger surface sealing developed on initial low roughness surfaces can also facilitate subsequent erosion processes.

In Year 2, the occurrence of high intensity rainfalls and significant runoff after the second thunderstorm (Figure 5-1b and Table 5-2) did not significantly affect the soil roughness and the rill network pattern (Figure 5-3c and d). This may be because the rill network density can only increase up to a certain limit since the runoff-capturing dynamics of existing rills impedes the formation of new rills (Favis-Mortlock et al., 2000; Mancilla et al., 2005). Once rills are in place, high intensity rainfalls only deepen rills (Figure 5-3d) or create rill headcuts

(Merritt, 1984). According to Luk et al. (1993), sediment deposition in rills can potentially occur during low intensity rainfall events, infilling the rills and hence modifying the rill network.

5.5.3 Evolution of overland flow connectivity

These changes in soil roughness were accompanied by changes in overland flow connectivity as reflected by the RSCf and more specifically by changes in DS_{max} (Figure 5-5a, Figure 5-5c, Figure 5-6g and Figure 5-6h) and in the shape of the normalized RSCf (Figure 5-5b, Figure 5-5d, Figure 5-6e and Figure 5-6f). In the first stages, before erosion creates flow oriented elements at the soil surface, roughness elements are randomly distributed. At these stages, the decrease of σ is accompanied by a decrease of DS_{max} (Figure 5-5a, Figure 5-5c, Figure 5-6g and Figure 5-6h), and σ and DS_{max} show a good correlation (Table 5-4). When the roughness pattern remains the same, but the mean random roughness or the mean standard deviation of surface elevation changes, it is expected that the volume of stored water needed to overflow depressions will change but not the way overland flow is distributed over the surface. In other words, the overland flow connectivity process will change in terms of absolute time but not in terms of space. As for soil roughness, for both years, we observe the most significant variations on the RSCf right after the first thunderstorms with an important decrease of RDS_{CT} and DS_{max} (Figure 5-6e, f, g and h). In both years this critical change in connectivity is accompanied by important changes in the soil roughness reflected in the variogram (Figure 5-4) and visually by the development of dispersive flow paths in Year 1 (Figure 5-2c) and incisional flow paths in Year 2 (Figure 5-3b). This shows that a higher connectivity and a change in the overland flow pattern (Figure 3-2) does not always imply the presence of incisional flow paths, such as in Year 2 (Figure 5-3), but that connectivity can also be produced by dispersive flow paths, such as in Year 1 (Figure 5-2).

5.5.4 Link between the RSCf and overland flow

Whereas the overland flow hydrograph was found to be little or moderately correlated to the variogram (Table 5-5), the former was found to be highly correlated to the RSCf and specifically with DS_{max} and RDS_{CT}. The very high correlation between DS_{max} and I_{10}, I_{50}, and I_{90} (ρ =0.97, ρ =0.97 and ρ =0.99, respectively; Figure 5-13) indicates that, as expected, the process of filling of micro-depressions is strongly related to the delay of overland flow generation (Darboux et al, 2002b). The high correlation between RDS_{CT} and both $S_{10,50}$ and Fr, shows that the shape of the RSCf can be linked to the overland flow characteristics. Convex shapes of the normalized RSCf or high values of RDS_{CT} can be related to a lower initial (first half of the hydrograph) rate of increase of overland flow generation (less "flashy" hydrographs), and to lower values of Fr number and hence to less erosive energy. On the contrary, concave shapes or low values of RDS_{CT} can be linked to a higher initial rate of increase of overland flow generation (more "flashy" hydrographs) as well as to higher Fr numbers and hence to higher erosive energy.

This confirms that the study of connectivity and the use of functional connectivity indicators, such as the RSCf, can be potentially used to improve the prediction of the overland flow hydrograph and that the analysis of the soil roughness alone may not be enough. Not only can DS_{max} be used as predictor of the delay of overland flow generation but, given the strong link between Fr and RDS_{CT}, the change in the shape of the normalized RSCf from a convex to a concave shape can potentially be used for the identification of emergent connectivity, more "flashy" runoff generation and increased erosive energy. The high correlation between DS_{max} and ξ also reveals a significant link between overland flow connectivity and the spatial continuity of flow velocities. It must be noted that given the differential nature of the Saint-Venant equations, FullSWOF_2D may not be able to reproduce abrupt breaks in the flow velocity fields. Hence the continuity of the simulated flow velocities may be higher than in reality. Nevertheless,

we consider that this artefact do not affect the study of the evolution of continuity on the flow velocity fields in relative terms.

5.6 Conclusions

This study investigated the evolution of overland flow connectivity as a function of the cumulative rainfall erosivity under the influence of different erosion processes in bare agricultural plots and how this connectivity is linked to soil roughness and overland flow generation. Overland flow connectivity was characterized by the RSCf (RDS_{CT} and DS_{max}), soil roughness by the variogram parameters (σ and R) and overland flow generation by characteristic points of the simulated hydrograph (I_{10}, I_{50}, I_{90}, $S_{10,50}$, $S_{50,90}$ and Fr). The very high correlation between, I_{10}, I_{50}, and I_{90} and DS_{max} not only confirms the important role of depression storage on the delay of overland flow generation but also, it shows the potential of improving the prediction of the overland flow hydrograph by the use of DS_{max}. However the results of this study show that soil roughness cannot solely be considered as an attenuation factor for overland flow generation. The development of eroded flow paths at the soil surface not only produces a decrease in DS_{max} but also a higher concavity of the normalized RSCf, which is reflected in the first half of the hydrograph by a higher rate of increase of the runoff ratio, as well as a higher Froude number and a higher spatial continuity of the flow velocities, reflected by the connectivity length. The high correlation between the shape of the RSCf, mainly influenced by RDS_{CT}, and both Fr and $S_{10,50}$ shows the potential of the RSCf to serve as a link between structural connectivity (soil roughness) and overland flow generation by providing information about overland flow characteristics, such as erosion energy and rate of increase of the overland flow hydrograph.

CHAPTER 6

6 General conclusions and perspectives

6.1 General conclusions

Distributed hydrological models typically estimate spatial and temporal distribution of water fluxes between elementary grid elements. For computational reasons, the spatial distribution of soil properties, such as the micro-topography, cannot be explicitly represented at the subgrid scale and thus is encompassed into effective simplified functions or parameters. However, this representation is generally oversimplified and hydrological models conceptualize these soil properties as a single constant parameter, such as the random roughness value. However, a single parameter is not able to represent the subgrid spatial variability of the roughness patterns. As a consequence, the effect produced by these soil properties on the water fluxes is also oversimplified not only spatially but also temporally.

In hydrological models the random roughness value is related to the overland flow generation process by the maximum depression storage, which is assumed to determine the moment when runoff occurs. By only considering the maximum depression storage, the process of overland flow generation is conceptualized as a process of filling and spilling of a bucket. The filling is assumed to be spatially uniform and the spilling to be temporally instantaneous. However, at the subgrid scale, water flows from one depression to another, progressively connecting them to each other and eventually to the outlet of the system. In order to represent the spatial and temporal distribution of this process in a simplified manner but still capturing and quantifying the runoff relevant features of the process, the concept of hydrological connectivity must be applied. Hydrological connectivity can be seen as a concept in between the oversimplified representation of a process by a single parameter and the complete representation of the process. This concept, and more specifically the use of process-based subgrid

connectivity indicators, could potentially improve the performance of hydrological models in an efficient way.

Among the different connectivity indicators, a functional overland flow connectivity indicator, the so-called the Relative Surface Connection function (RSCf) based on the concept of "volume to breakthrough" has shown to perform better than other indicators (Antoine et al., 2009). It expresses the ratio of the area of the grid connected to the outlet as a function of the depression storage. The RSCf has shown a great potential to be integrated in hillslope or watershed models as a descriptive function of the subgrid overland flow dynamics in order to improve their prediction ability (Antoine et al., 2009, 2011). Yet several issues needed to be addressed before it can successfully be integrated. Some of these issues have been dealt with in this thesis and the main outcomes are detailed below.

1) How do changes in spatial scale affect the RSCf? (Chapter 3)

As a process-based connectivity indicator, the RSCf is scale-dependent, therefore extra attention must be paid in order to select an appropriate size of the grid cell. The size must be large enough to fully represent the process of overland flow connectivity, i.e. all the components and the relationships between them must be represented, and to minimize border effects. Depending on the type of micro-topography, the RSCf was affected in both its shape and the maximum depression storage by changes in grid cell size. This dependence on grid cell size, mainly produced by border effects, indicates that there is a minimal scale to study overland flow connectivity. At scales lower than this minimal scale, virtual boundaries alter the overland flow process either by blocking or by facilitating the connection of the different parts of the micro-topography to the outlet. At scales larger than the minimal one and as we increase the scale of study, these border effects tend to disappear and the maximum depression storage tends asymptotically to a constant value. Moreover, the RSCf tends to a particular shape common for all the contrasting micro-topographies

tested in Chapter 3. As we increase the scale of study, the first part of the function (up to approx. 50-70% of the maximum depression storage) tends to disappear (the ratio of area connected tends to 0) and in the last part (starting at approx. 50-70% of the maximum depression storage) the RSCf increases approximately linearly up to the end. The decrease of the ratio of area initially connected to the outlet as the scale of study increases indicates that for large enough areas this first part would tend to 0 (Figure 6-1). Therefore, the parameterization of the RSCf could be reduced to two values, the depression storage needed to reach the initiation of the overland flow connectivity process (RDS_{CT}; Figure 6-1) and the maximum depression storage.

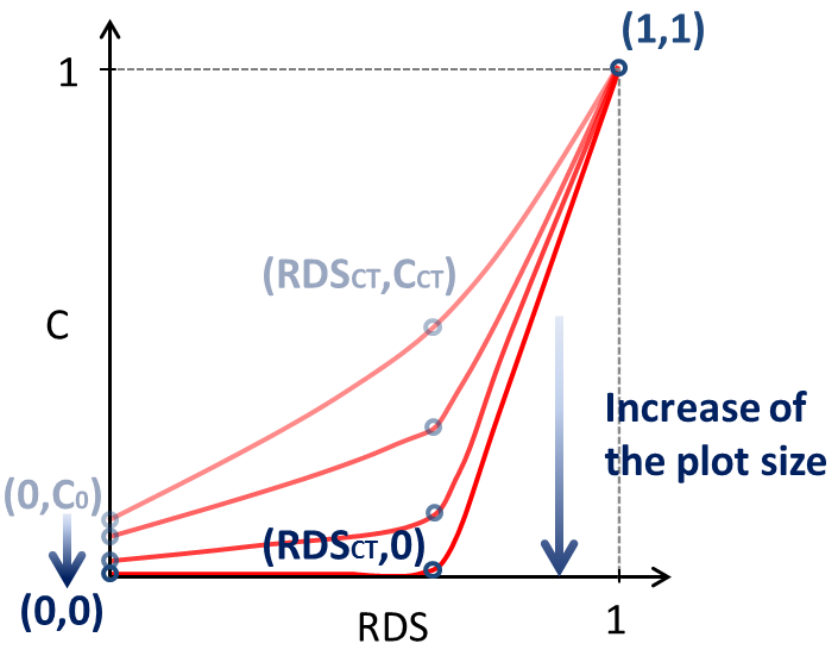

Figure 6-1 Parameterization of the normalized RSCf as the plot size increases.

Once the border effects become negligible, different constant values of maximum depression storage were observed between contrasting micro-topographies. One could also have expected a different shape of the normalized RSCf representing a different evolution of the

overland flow connectivity process for each of the contrasting micro-topographies. However, despite having contrasted roughness patterns, this was not observed, probably because the micro-topographies that were tested in Chapter 3 all had randomly distributed roughness and hence did not present predominant flow oriented micro-topography elements. As shown in Chapter 5, flow oriented elements as well as high slope gradients strongly modify the overland flow connectivity process by facilitating the overland flow process and routing water flow to the outlet and hence (Figure 3-2).

For high slopes and when flow oriented elements predominate on the soil surface, one can expect different scale effects because the flow connectivity process is modified. We expect the presence of preferential flow paths in the direction of the slope to attenuate the scale effect produced by reducing the plot width. When preferential flow paths are predominantly parallel to the slope and hence to the lateral boundaries, these boundaries are less likely to obstruct the connecting paths for narrower plots and hence to modify the connectivity process and the maximum depression storage value (Figure 6-2).

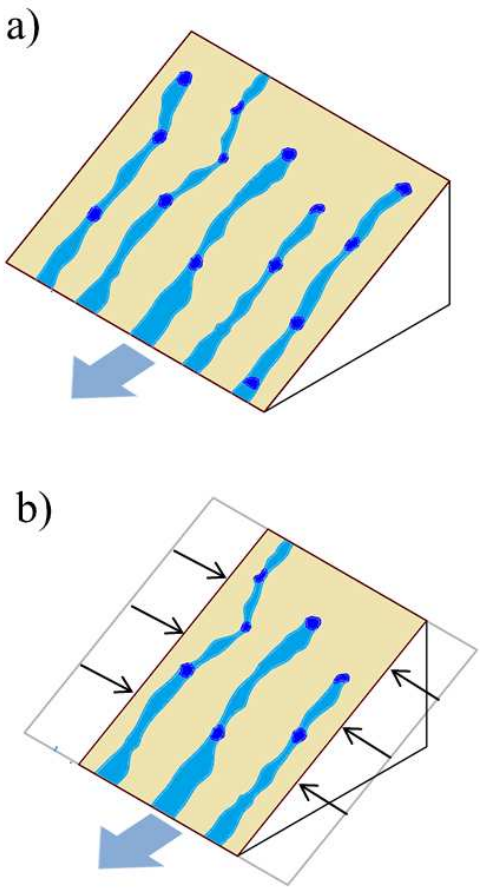

Figure 6-2 Schematic representation of the predominant spilling process and overland flow pattern predominantly parallel to the slope (a) for the original plot size and (b) after reducing the plot width. Reducing the width does not modify the connections that existed before reducing the width. Stored water in micro-depressions in dark blue. Preferential flow paths in light blue.

2) How is the RSCf affected by surface roughness and slope? (Chapter 4)

In order to facilitate the future integration of the RSCf into hydrological models, the RSCf was parameterized. Variations of these parameters were evaluated and quantified as a function of variations of the variogram, a structural indicator that characterizes both the vertical and horizontal variability of the point elevations.

In randomly distributed synthetic surfaces, the characteristic parameters of the RSCf are greatly influenced by the DEM variogram and slope. At low slopes and with deep depressions, the characteristic parameters of the RSCf appear linked to a single component of the surface roughness. On the contrary, more complex interactions between the slope and the vertical and horizontal component of the variogram are observed for high slopes and shallow depression. This indicates that for scenarios with lower connectivity, i.e. overland flow dominated by depression filling, there is simple link between structural and functional connectivity. An example of such a simple link is the often reported link between random roughness and maximum depression storage, which does not take into account the horizontal variability of the surface roughness. On the other hand, for high connectivity scenarios, i.e. depression spilling-dominated processes, this simplification is not valid and structural and functional connectivity are linked by more complex interactions between both components of the variogram, vertical and horizontal, as well as slope.

3) Can the RSCf be predicted on the basis of structural indicators of soil micro-topography and slope? (Chapter 4)

Based on a simple conceptualization of surface roughness as rectangular depressions, mathematical expressions in function of variogram and slope were derived in order to predict the characteristic parameters of the RSCf. These expressions were able to physically explain and reasonably predict the effect of soil roughness and slope on the RSCf, not only in low connectivity scenarios but also in high connectivity ones. Moreover, they performed better than previous empirical expressions found in the literature that are based on random roughness and which do not account for the spatial variability of surface roughness.

This not only shows the value of the RSCf in linking structural and functional connectivity, but also highlights the potential of using

physically-based yet simple conceptualizations of the surface as a new way to predict functional characteristics of flow processes instead of using purely empirical formulas. Based on the results, the DEM variogram can be used as a means to predict runoff-relevant features of overland flow connectivity, such as the maximum depression storage or the connectivity threshold, in randomly distributed subgrid micro-topographies. Several technologies exist for deriving the variogram for real surfaces, including the photogrammetric technique used in the present thesis.

4) How does the RSCf evolve on eroding surfaces? (Chapter 5)

Before erosion starts creating preferential flow paths at the soil surface, i.e. when the soil roughness elements are still randomly distributed, the normalized RSCf is characterized by a convex shape that remains pretty much the same even when low intensity rainfall events produce a decrease in the maximum depression storage. This convex shape, characterized by an initial low increase of connectivity followed by a sharp increase in connectivity at the connectivity threshold, is indicative of a poorly connected surface for which runoff generation and transfer is dominated by depression filling and where patterns of flow are not well defined. After erosion creates directional flow paths on the surface, not only is a decrease of maximum depression storage observed but also a change in the shape of the normalized RSCf, from convex to concave. The connectivity threshold occurs earlier, i.e. for a lower value of depression storage. This can be interpreted as a change in the process of overland flow connectivity, from a depression filling-dominated, low connectivity scenario, to a spilling-dominated high connectivity one where flow patterns are well defined.

5) To what extent do these changes in the RSCf reflect changes in the hydrological response? (Chapter 5)

Very high correlations observed between the maximum depression storage and the delay in overland flow generation confirm the important role of micro-depression storage capacity on overland flow generation. However, the results of this study show that soil roughness is not simply an attenuating factor but that it can also act as an intensification factor for overland flow generation. When the maximum depression storage decreases but the shape of the normalized RSCf barely changes, a shorter delay in overland flow generation is observed. However, when this decrease of the maximum depression storages is accompanied by a change in the RSCf shape from convex to concave, not only is a shorter delay observed but also a higher rate of increase of the runoff ratio, a higher Froude number and higher spatial continuity of the flow velocity field. The high correlation between the shape of the RSCf and both Fr and the rate of increase of the hydrograph confirms the RSCf's value for serving as a link between structural connectivity (soil roughness) and overland flow generation even when flow oriented elements appear on the surface. Therefore integrating the RSCf in hydrological models may not only improve the overland flow prediction ability of such models but it also provides hydrological models with information about overland flow characteristics, such as flow velocities continuity and erosion energy.

Surprisingly, high connectivity overland flow scenarios characterized by a concave normalized RSCf have been observed both for eroded surfaces characterized by flow oriented elements (Chapter 5) and for surfaces characterized by randomly distributed shallow depressions and high slopes (Chapter 4). This indicates that despite strong differences in structural connectivity between micro-topographies (one randomly distributed and the other one flow oriented), the effect of high slope gradients can "hide" the effect of soil roughness on water flow. As observed by Abrahams et al. (1988) in experimental rainfall experiments, the slope gradient and more specifically the existence of a slope threshold can greatly modify the runoff generation process. In this study, high slope gradients do not only decrease the

capacity of the depressions to store water but also modify the interaction between depressions and their connection pattern. Soil roughness, when the slope is steep enough, instead of acting as a barrier, concentrates the flow in the slope direction and hence increases the connectivity (Figure 3-2). Therefore, whether a soil surface is well connected or not would depend not only on the spatial organization of the roughness elements but also on the slope and the interaction between roughness and slope. These dynamics that cannot be captured by standard roughness indicators are well captured by the RSCf.

6.2 Limitations and Perspectives

Although being very promising, there are a number of open research questions and issues that needs to be addressed in the future before the RSCf can successfully be integrated in hydrological models.

While mathematical expressions were derived that allow to predict the RSCf in function of the variogram parameters and slope, these equations are limited to homogeneous (no large-scale variations) random topographical fields characterized by a Gaussian variogram. Although some real fields have also been shown to follow a Gaussian distribution, they may present different types of variograms, possibly making the obtained equations invalid. Moreover, additional equations should be derived in order to predict the RSCf when oriented roughness elements appear at the surface.

In order to quantify and facilitate the integration of the RSCf into hydrological models, the RSCf was parameterized making an important assumption, the existence of only one connectivity threshold. This assumption, observed in the studied micro-topographies (uniform surfaces without important large-scale variations), may not be valid as we increase the scale of study and large-scale variations or elements appear on the surface. These large elements, such as large depressions, may disconnect large parts of the

field, which when connected may produce successive sharp increases in the ratio of area connected (stepwise behaviour) after the occurrence of the considered connectivity threshold.

Therefore, additional research on real fields, with different types of variograms, large-scale variations and oriented roughness is needed to confirm and improve these results.

Another important limitation that may appear as we increase the scale of study is the existence of internal and lateral slopes. This is not treated by the RSCf, which is calculated assuming that a single and general slope exists and that this slope is oriented such that the lower points are located at the outlet. Therefore the presence of internal and lateral slopes, at the subgrid scale, may produce important changes in the RSCf. In order to solve this limitation, we would suggest, for future studies, to account for connectivity not only at the bottom but also at the lateral boundaries of the study area.

There is also the issue of infiltration. The two assumptions used to calculate the RSCf, rainfall intensity is always higher than the infiltration capacity and that rainfall is spatially uniform, ensures that runoff is generated uniformly and that depression storage never decreases. But in practice, infiltration and rainfall are highly variable in time and space and likely to affect the runoff generation process. For instance, soil crusting can modify the infiltration capacity of the soil and create spatial patterns. In addition, since the process of crusting is affected by soil roughness, infiltration capacity would be spatially correlated to the spatial distribution of the roughness elements, such as depressions or rills. This would affect the micro-depressions filling and spilling process both in time and space, and hence the calculation of the RSCf. Therefore this variability should ultimately be taken into account.

Another limitation that needs to be overcome to improve the prediction of overland flow hydrographs is the introduction of the

surface detention component into the RSCf. Although good correlations are observed between the RSCf parameters and the overland flow hydrograph, the obtained linear regressions are dependent on boundary conditions, such as the spatial variability of infiltration and rainfall and the rainfall intensity. The results obtained in this study were limited to constant and uniform excess rainfall of 60 mm/h and infiltration uniformly distributed.

As mentioned above, similar connectivity scenarios characterized by a concave normalized RSCf have been observed both in eroded surfaces characterized by flow oriented elements (Chapter 5) and in surfaces characterized by randomly distributed shallow depressions and high slopes (Chapter 4). However, it is unknown if they both also have similar hydrological responses, i.e. similar hydrographs, despite their strong differences in structural connectivity. In order to clarify this question, overland flow hydrographs of surfaces with similar RSCf, in terms of shape and maximum depression storage, but contrasting structural connectivity should be calculated and compared.

Whereas a previous attempt to introduce the detention component into the RSCf, the weighted-surface procedure (Antoine et al., 2011), showed promising results, it considered soil roughness only as a delaying factor. This procedure consisted in dividing the micro-topographical field into parallel independent strips with the same slope. Each time a rainfall increment induces an increase of the depression storage, an additional strip is activated whose size is given by the RSCf. Thus this procedure assumes that in the absence of depression storage, i.e. a flat surface, the whole surface will be activated at the same time. The fastest runoff generation would therefore be generated on flat surfaces, when soil roughness does not produce any delay. However, soil roughness can be an intensification factor for overland flow generation. The hydrograph of Plot 1 in Year 2 and RE = 274 MJ ha^{-1} mm h^{-1} (maximum depression storage = 0.01 mm), when eroded preferential flow paths developed after the first two important thunderstorms, was compared to the hydrograph of a

flat surface with the same size, slope and excess rainfall intensity (60 mm/h) and the weighted-surface procedure hydrograph. The comparison shows a quicker runoff generation in the eroded surface (Figure 6-3). Therefore, the weighted-surface procedure must be improved in order to reflect the increase in connectivity produced by the presence of preferential flow paths at the soil surface.

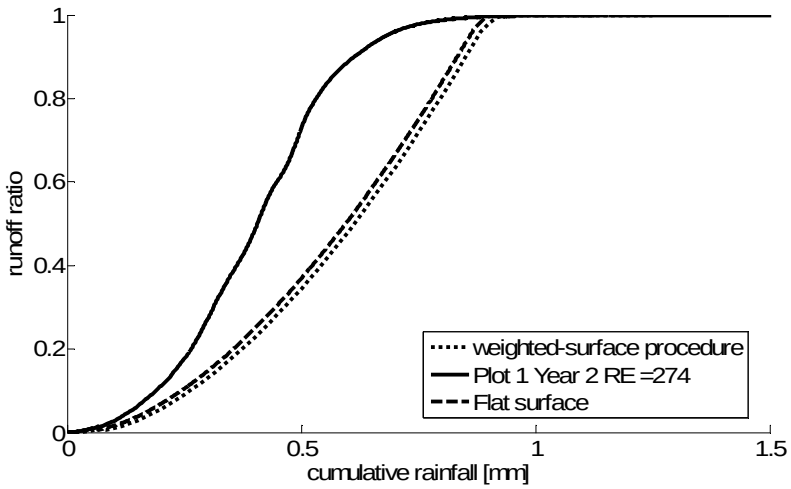

Figure 6-3 Comparison of the simulated overland flow hydrograph of a flat surface, a hydrograph based on the weighted-surface procedure applied to the DEM for Plot 1 in Year 2 and RE = 274 and the simulated hydrograph based on the DEM for Plot 1 in Year 2 and RE = 274. In the three hydrographs the same slope gradient, the same plot size and the same constant rainfall excess is used. RE in MJ ha^{-1} mm h^{-1}.

Another possible approach to introduce the RSCf into hydrological models could be to implement the subgrid variability of overland flow in a similar manner as for instance the Probability Density Model (PDM; Moore, 2007), which implements the subgrid variability of the "soil absorption capacity" as a probability density curve. Alternatively, one may use the parameters defining the RSCf as a means to reflect the progressive non-linear nature of overland flow generation, similar to the openLISEM model, where the runoff initiation ('Start Depressional Storage') would correspond to the here

defined connectivity threshold and where the steady state would correspond to the here predicted maximum depression storage.

Though technological developments have made it possible to obtain high resolution DEMs and to calculate the resulting RSCf fairly easily, the application of the results and findings of this study on agricultural fields by farmers remains still complex. In order to facilitate the use of the RSCf, it would be desirable to identify easily measurable properties of the soil surface that could be used in order to predict the RSCf. As shown in Chapter 4, the size and shape of the micro-depressions and the slope gradient of the field are strongly related to the maximum depression storage and the shape of the RSCf in Gaussian random topographical fields. Therefore, it may be possible to predict these two RSCf parameters by measuring the average size and shape of the micro-depressions at the field surface and the general slope of the field. However, this may be not applicable when oriented roughness elements, such as rills, appear on the surface. In this case, we propose to investigate the influence of other easily measurable properties characterizing the rill network, e.g. rill density, on the RSCf. Another possible approach could be the creation of a database and a guide including images of different types of soil roughnesses, which could be used to identify the type of soil in-situ, and their characteristic RSCf as a function of the slope gradient.

APPENDICES

A. Effect soil roughness and slope on the RSCf

In this section, we show the effect of the soil roughness (sill σ and range R of the variogram) and slope on the RSCf. For this purpose, Gaussian surface elevation fields (6 m × 6 m) were used. The results shown correspond to 6 values of R (50 to 400 mm), 6 values of σ (2 to 40 mm) and 3 slopes (0%, 2%, 5% and 15%) being the RSCf calculated for 10 realizations of each combination. See chapter 4 for details.

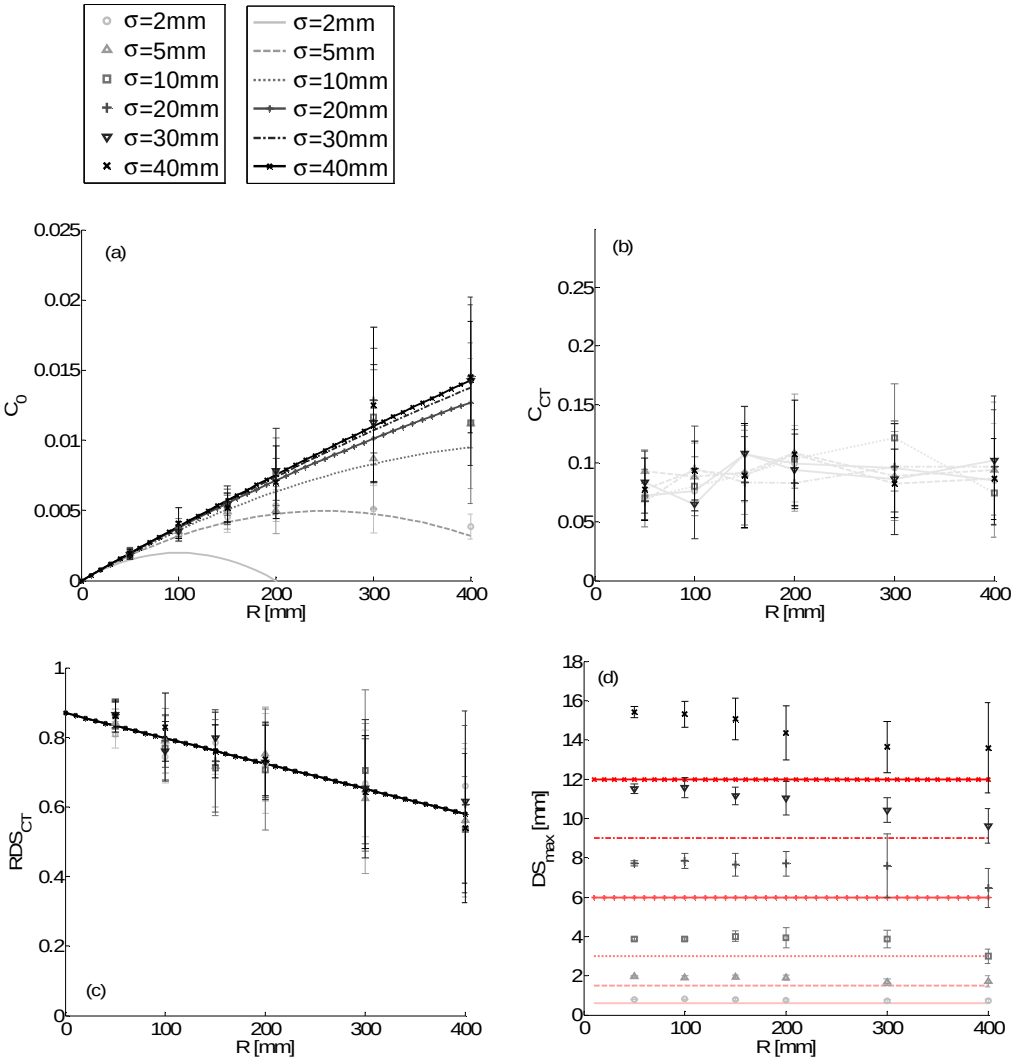

Figure A-1 Effect of range on (a) C_0, (b) C_{CT}, (c) RDS_{CT} and (d) DS_{max} at 0% slope. Error bars = standard deviation (n=10). Points correspond to observed values. Lines correspond to the values calculated using (a) Equation 4-7, (c) Equation 4-10 and (d) Equation 4-4. Red lines correspond to Equation 4-4a and blue lines to Equation 4-4b.

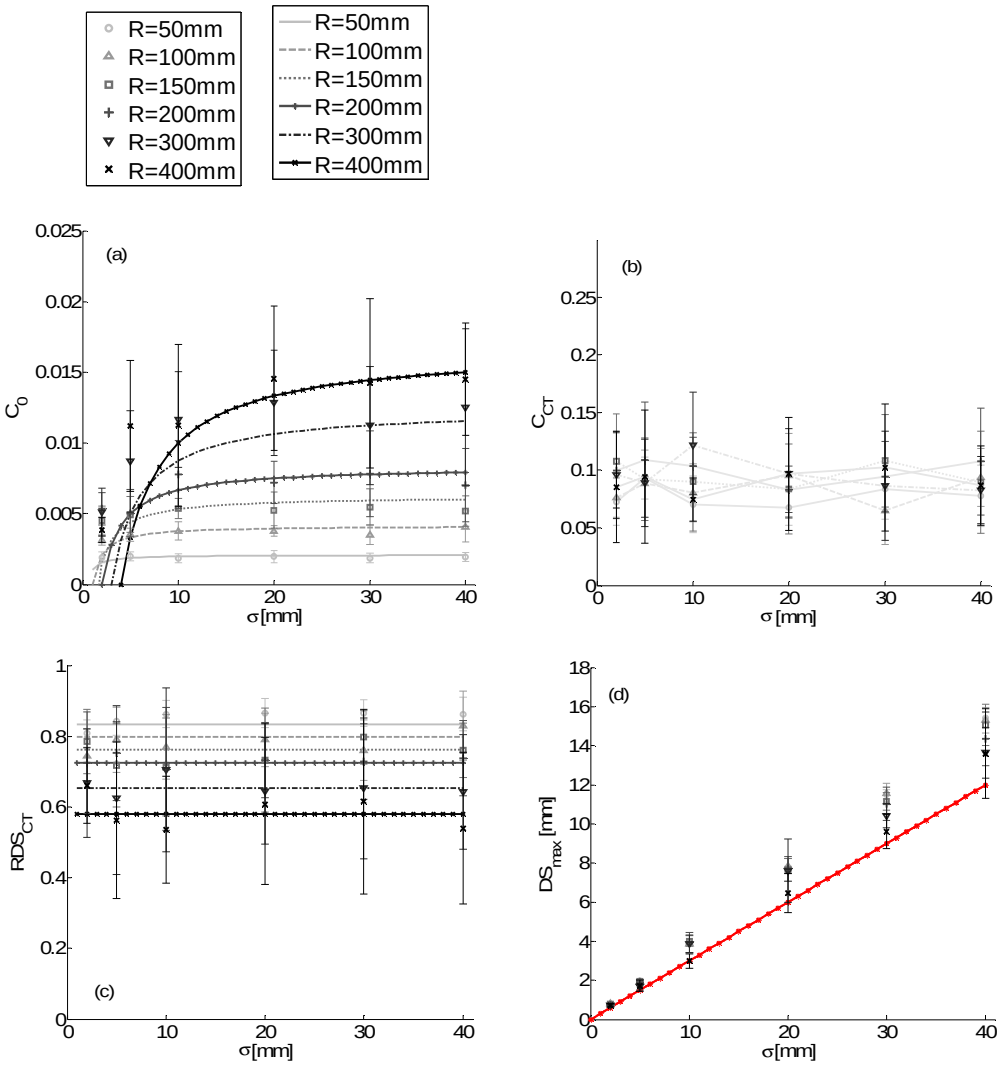

Figure A-2 Effect of sill on (a) C_0, (b) C_{CT}, (c) RDS_{CT} and (d) DS_{max} at 0% slope. Error bars = standard deviation (n=10). Points correspond to observed values. Lines correspond to the values calculated using (a) Equation 4-7, (c) Equation 4-10 and (d) Equation 4-4. Red lines correspond to Equation 4-4a and blue lines to Equation 4-4b.

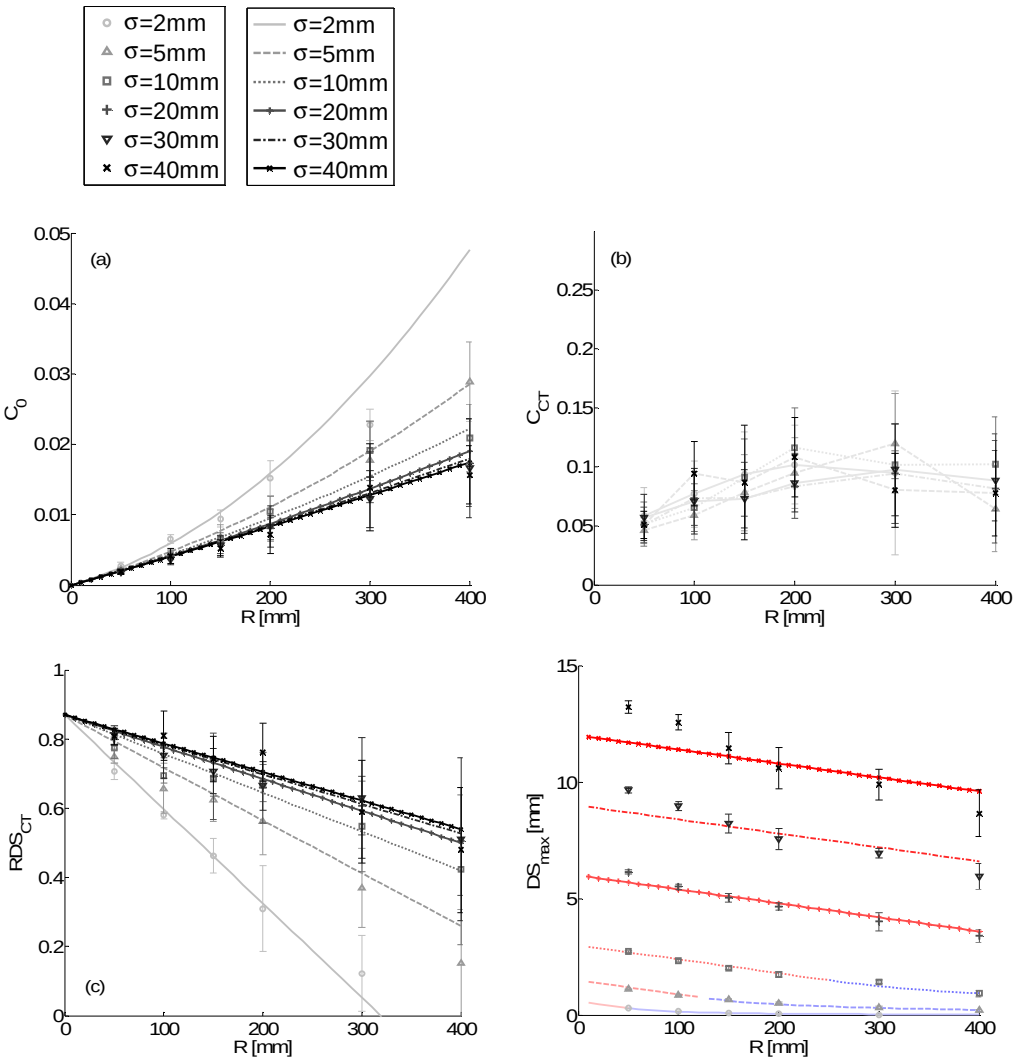

Figure A-3 Effect of range on (a) C_0, (b) C_{CT}, (c) RDS_{CT} and (d) DS_{max} at 2% slope. Error bars = standard deviation (n=10). Points correspond to observed values. Lines correspond to the values calculated using (a) (a) Equation 4-7, (c) Equation 4-10 and (d) Equation 4-4. Red lines correspond to Equation 4-4a and blue lines to Equation 4-4b

.

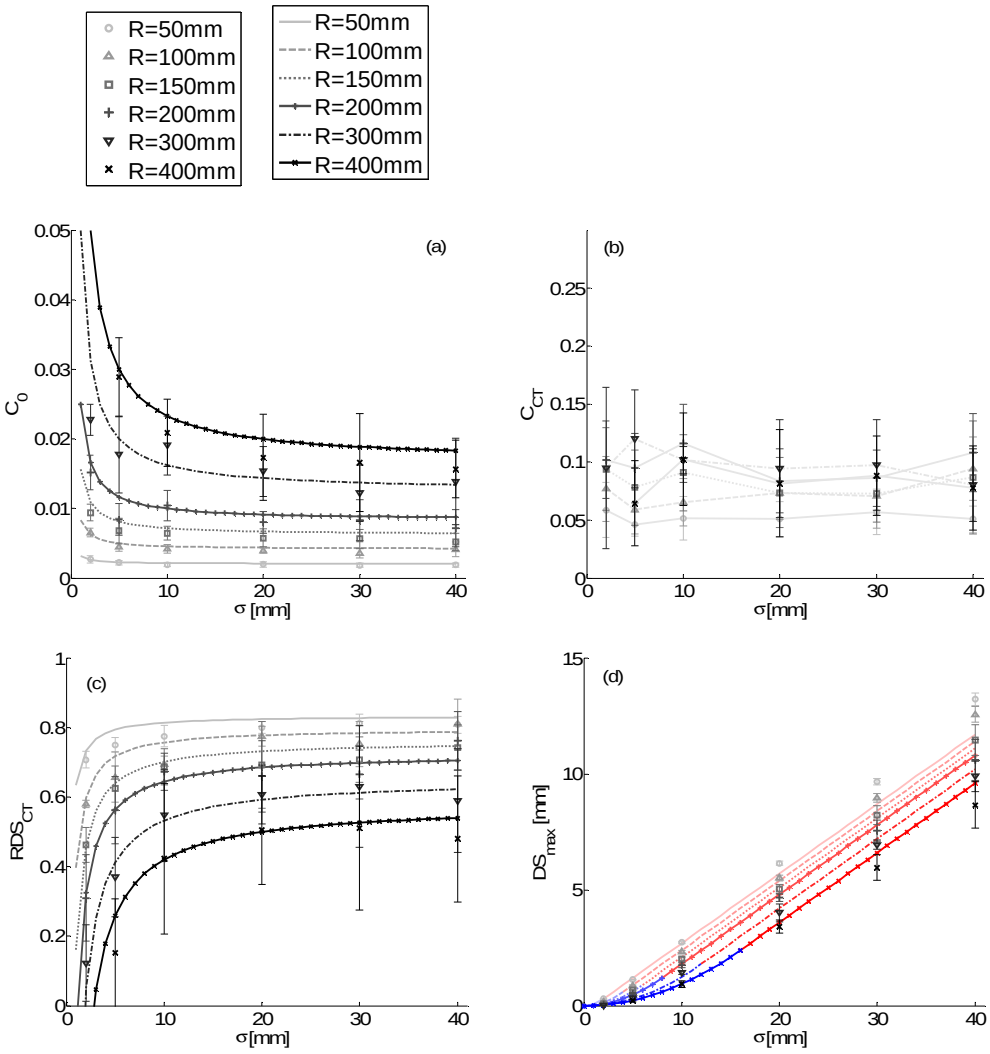

Figure A-4 Effect of sill on (a) C_0, (b) C_{CT}, (c) RDS_{CT} and (d) DS_{max} at 2% slope. Error bars = standard deviation (n=10). Points correspond to observed values. Lines correspond to the values calculated using (a) (a) Equation 4-7, (c) Equation 4-10 and (d) Equation 4-4. Red lines correspond to Equation 4-4a and blue lines to Equation 4-4b.

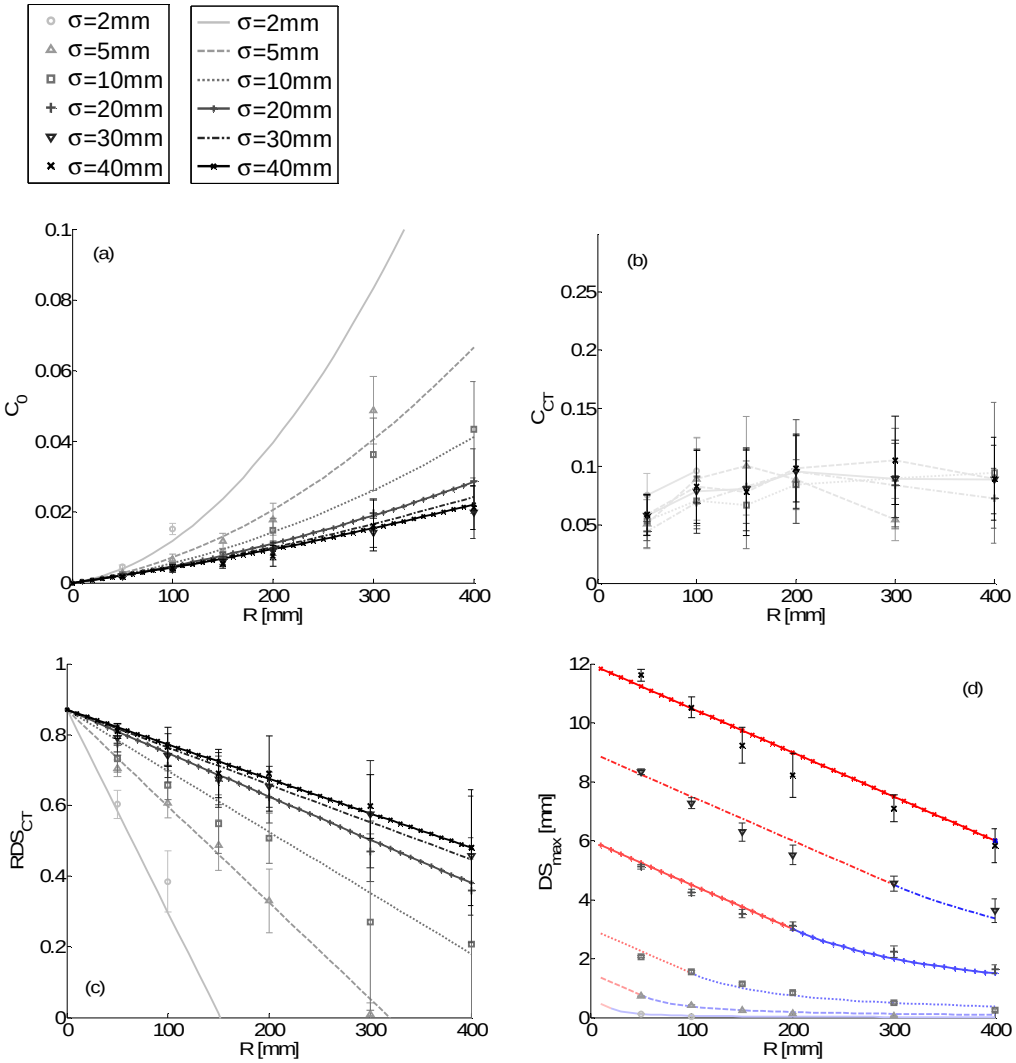

Figure A-5 Effect of range on (a) C_0, (b) C_{CT}, (c) RDS_{CT} and (d) DS_{max} at 5% slope. Error bars = standard deviation (n=10). Points correspond to observed values. Lines correspond to the values calculated using(a) Equation 4-7, (c) Equation 4-10 and (d) Equation 4-4. Red lines correspond to Equation 4-4a and blue lines to Equation 4-4b.

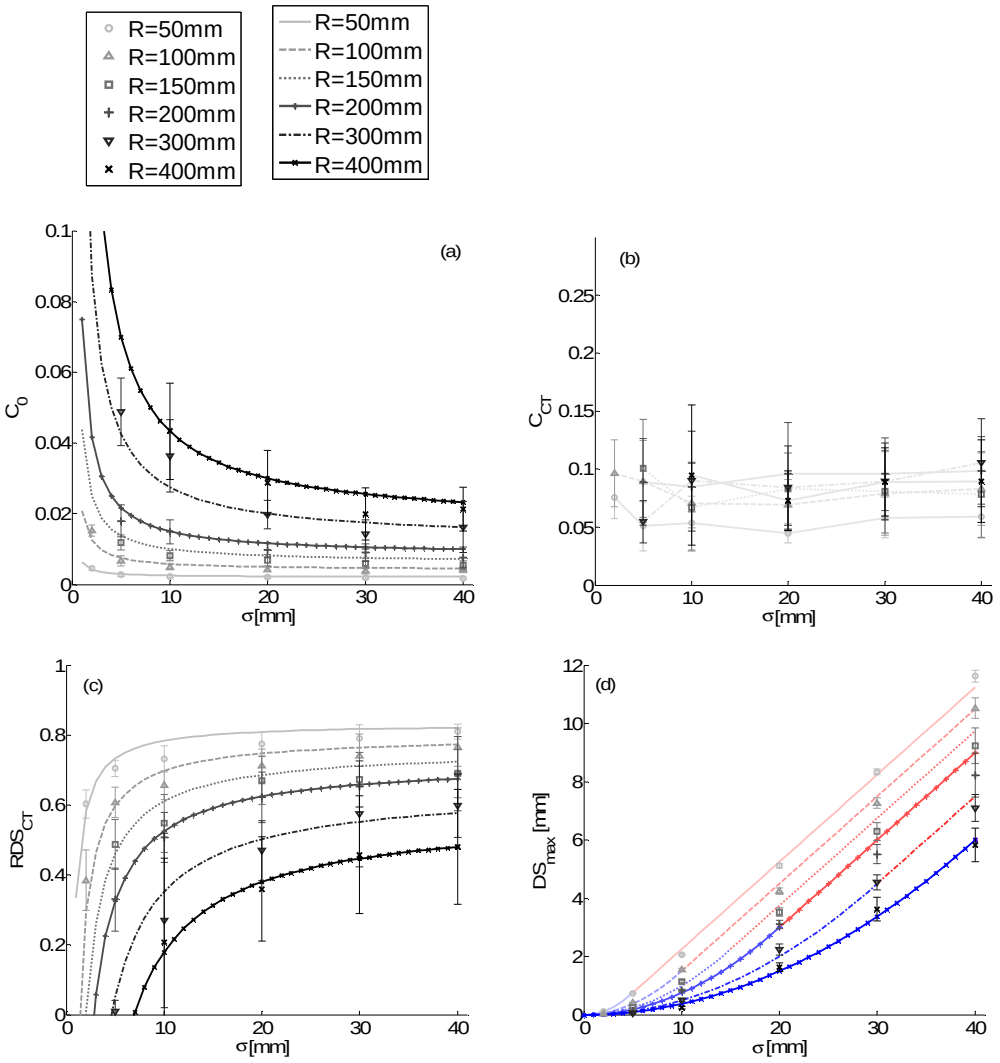

Figure A-6 Effect of sill on (a) C_0, (b) C_{CT}, (c) RDS_{CT} and (d) DS_{max} at 5% slope. Error bars = standard deviation (n=10). Points correspond to observed values. Lines correspond to the values calculated using(a) Equation 4-7, (c) Equation 4-10 and (d) Equation 4-4. Red lines correspond to Equation 4-4a and blue lines to Equation 4-4b.

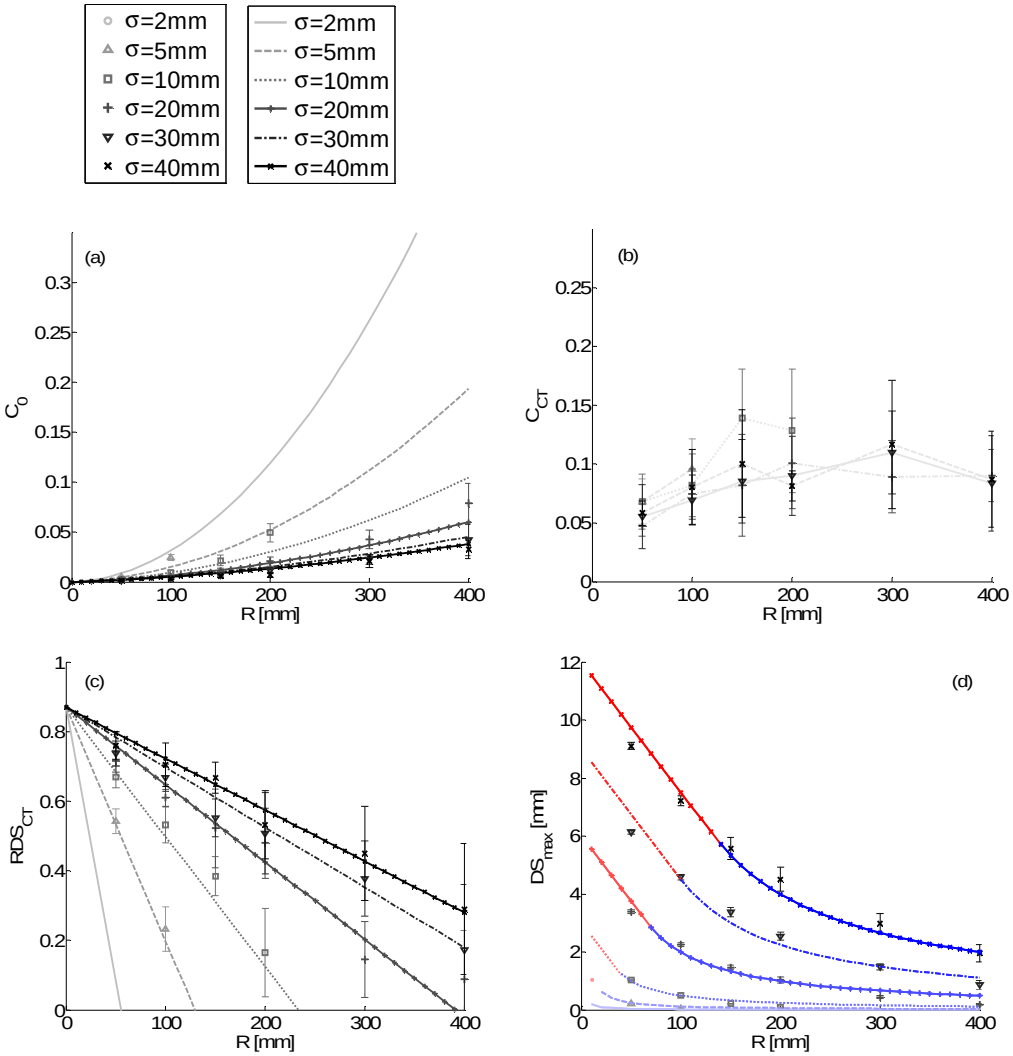

Figure A-7 Effect of range on (a) C_0, (b) C_{CT}, (c) RDS_{CT} and (d) DS_{max} at 15% slope. Error bars = standard deviation (n=10). Points correspond to observed values. Lines correspond to the values calculated using(a) Equation 4-7, (c) Equation 4-10 and (d) Equation 4-4. Red lines correspond to Equation 4-4a and blue lines to Equation 4-4b.

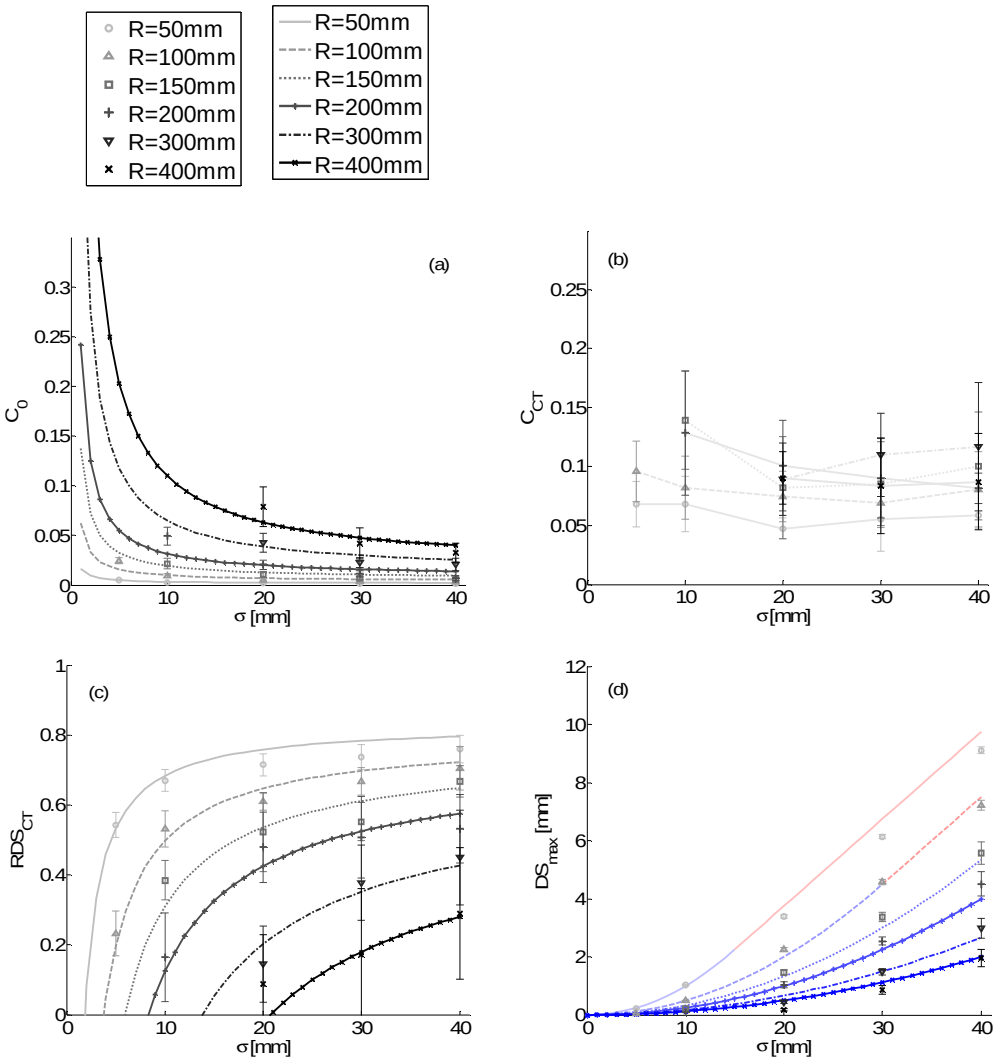

Figure A-8 Effect of sill on (a) C_0, (b) C_{CT}, (c) RDS_{CT} and (d) DS_{max} at 15% slope. Error bars = standard deviation (n=10). Points correspond to observed values. Lines correspond to the values calculated using(a) Equation 4-7, (c) Equation 4-10 and (d) Equation 4-4. Red lines correspond to Equation 4-4a and blue lines to Equation 4-4b.

B. Uncertainty of the parameters defining the variogram, the RSCf, the overland flow hydrograph and Fr

In this section, we show the values of the parameters of the variogram, the RSCf and the overland flow hydrogram obtained in the uncertainty analysis for two contrasting micro-topographies of Plot 1. . The DEM was acquired by photogrammetry on 8 (eroded surface) and 6 (freshly tilled surface) occasions within a single, non-rainy day for each surface. See Section 5.3.6 for details. We show the values obtained for each replicate as well as the mean value, the standard deviation (SD) and the coefficient of variability (CV).

Table-B-1 Values of the parameters defining the variogram for each replicate DEM and mean value, SD and CV for each of two contrasted micro-topographies

Eroded surface	R [mm]	σ [mm]	Freshlytilled surface	R [mm]	σ [mm]
Replicate 1	1039.9	9.5	Replicate 1	498.9	9.2
Replicate 2	1084.8	9.8	Replicate 2	492.6	9.3
Replicate 3	1064.5	9.8	Replicate 3	471.8	9.4
Replicate 4	1051.2	9.6	Replicate 4	459	9.4
Replicate 5	1054.3	9.6	Replicate 5	480.5	9.6
Replicate 6	1078.5	9.8	Replicate 6	467.6	9.5
Replicate 7	1050.7	9.5			
Replicate 8	1036.5	9.6			
Mean	1057.6	9.7	Mean	474.3	9.4
SD	17.2	0.1	SD	12.8	0.1
CV	0.016	0.014	CV	0.027	0.015

Table B-2 Values of the parameters defining the RSCf for each replicate and mean value, SD and CV for each of two contrasted micro-topographies

Freshlytilled surface	C_0	C_{CT}	RDS_{CT}	DS_{max} [mm]	Eroded surface	C_0	C_{CT}	RDS_{CT}	DS_{max} [mm]
Replicate 1	0.004	0.043	0.440	0.315	Replicate 1	0.021	0.054	0.120	0.009
Replicate 2	0.004	0.055	0.480	0.306	Replicate 2	0.015	0.052	0.080	0.011
Replicate 3	0.004	0.077	0.520	0.319	Replicate 3	0.019	0.044	0.080	0.011
Replicate 4	0.004	0.088	0.560	0.310	Replicate 4	0.021	0.000	0.000	0.012
Replicate 5	0.003	0.096	0.480	0.332	Replicate 5	0.018	0.075	0.120	0.011
Replicate 6	0.004	0.076	0.520	0.306	Replicate 6	0.023	0.084	0.080	0.012
					Replicate 7	0.017	0.063	0.080	0.012
					Replicate 8	0.022	0.065	0.080	0.012
Mean	0.004	0.072	0.500	0.315	Mean	0.019	0.054	0.080	0.011
SD	0.000	0.020	0.042	0.010	SD	0.003	0.026	0.037	0.001
CV	0.091	0.278	0.084	0.031	CV	0.134	0.469	0.463	0.074

Table B-3 Values of the parameters defining the overland flow hydrograph and Fr for each replicate and mean value, SD and CV for each of two contrasted micro-topographies

Freshlytilled surface	I_{10} [mm]	I_{50} [mm]	I_{90} [mm]	$S_{10,50}$	$S_{50,90}$	Fr	Eroded surface	I_{10} [mm]	I_{50} [mm]	I_{90} [mm]	$S_{10,50}$	$S_{50,90}$	Fr
Replicate 1	0.88	1.58	2.42	0.57	0.47	1.10	Replicate 1	0.23	0.47	0.64	1.62	2.32	1.40
Replicate 2	0.93	1.66	2.39	0.55	0.55	1.08	Replicate 2	0.23	0.49	0.65	1.55	2.50	1.39
Replicate 3	0.91	1.67	2.45	0.52	0.51	1.08	Replicate 3	0.22	0.50	0.65	1.44	2.54	1.41
Replicate 4	0.92	1.68	2.41	0.53	0.55	1.08	Replicate 4	0.23	0.49	0.66	1.53	2.39	1.38
Replicate 5	0.89	1.69	2.50	0.50	0.50	1.10	Replicate 5	0.23	0.49	0.66	1.53	2.38	1.39
Replicate 6	0.89	1.69	2.50	0.50	0.50	1.09	Replicate 6	0.22	0.47	0.65	1.61	2.22	1.40
							Replicate 7	0.23	0.50	0.66	1.50	2.43	1.37
							Replicate 8	0.23	0.49	0.67	1.52	2.28	1.37
Mean	0.90	1.66	2.44	0.53	0.51	1.09	Mean	0.23	0.49	0.66	1.54	2.38	1.39
SD	0.022	0.043	0.047	0.029	0.031	0.010	SD	0.004	0.010	0.008	0.059	0.108	0.015
CV	0.024	0.026	0.019	0.055	0.060	0.010	CV	0.019	0.021	0.013	0.038	0.045	0.011

C. Digital elevation models

In this section, we show the evolution of the different digital elevation models (DEM) for Plot 1, Plot 2 and Plot 3 in Year 1 and Year 2. See chapter 5 for details.

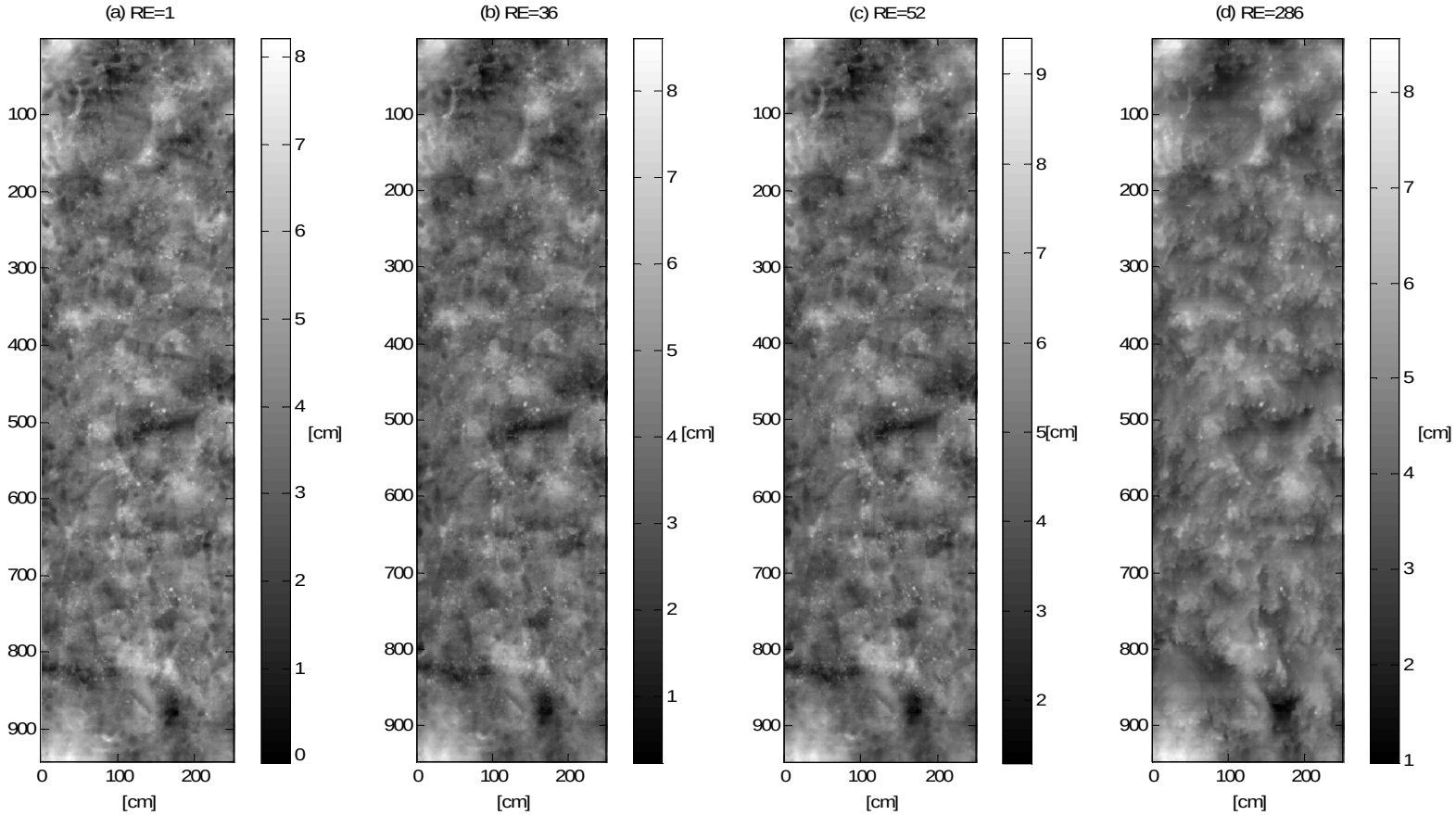

Figure C-1 DEMs of Plot 1 in Year 1 for (a) RE = 1, (b) RE = 36, (c) RE = 52 and (d) RE = 286. RE in MJ ha^{-1} mm h^{-1}

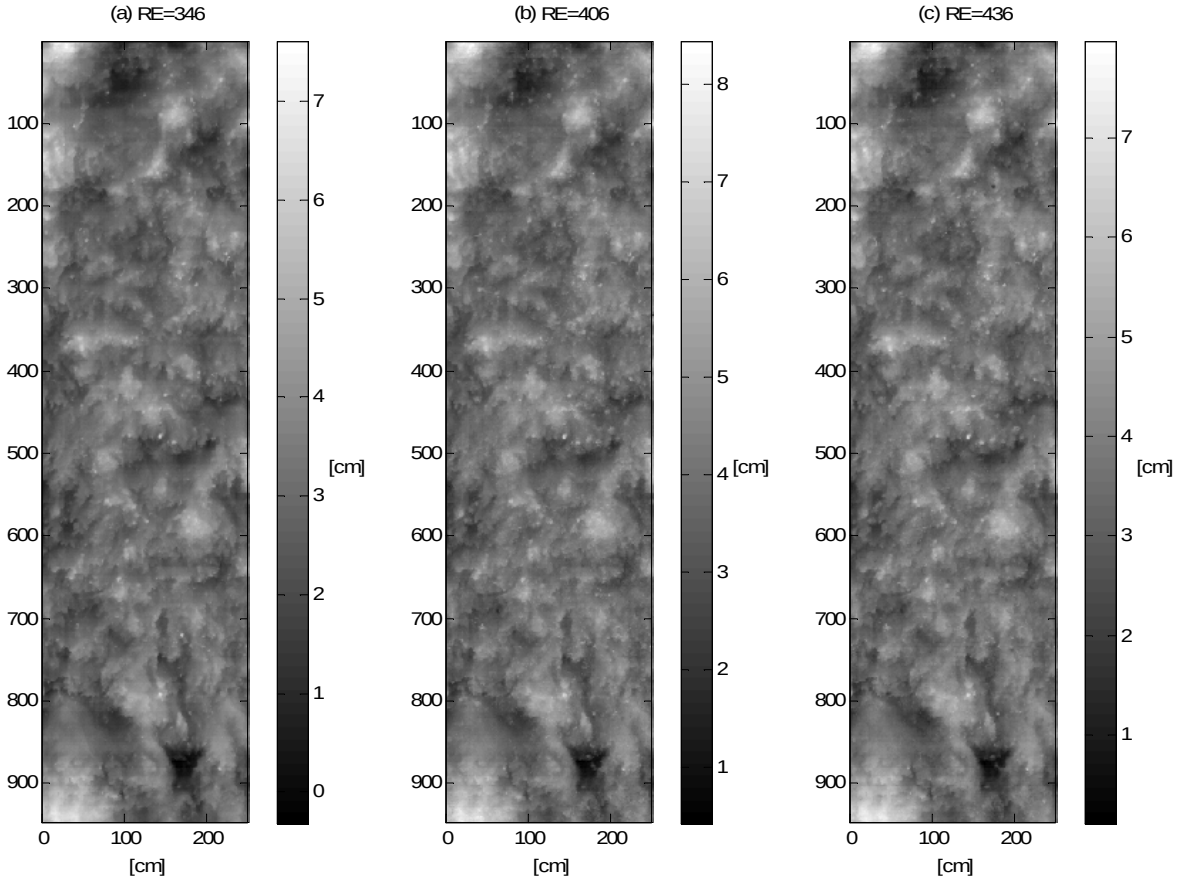

Figure C-2 DEMs of Plot 1 in Year 1 for (a) RE = 346, (b) RE = 406 and (c) RE = 436. RE in MJ ha^{-1} mm h^{-1}

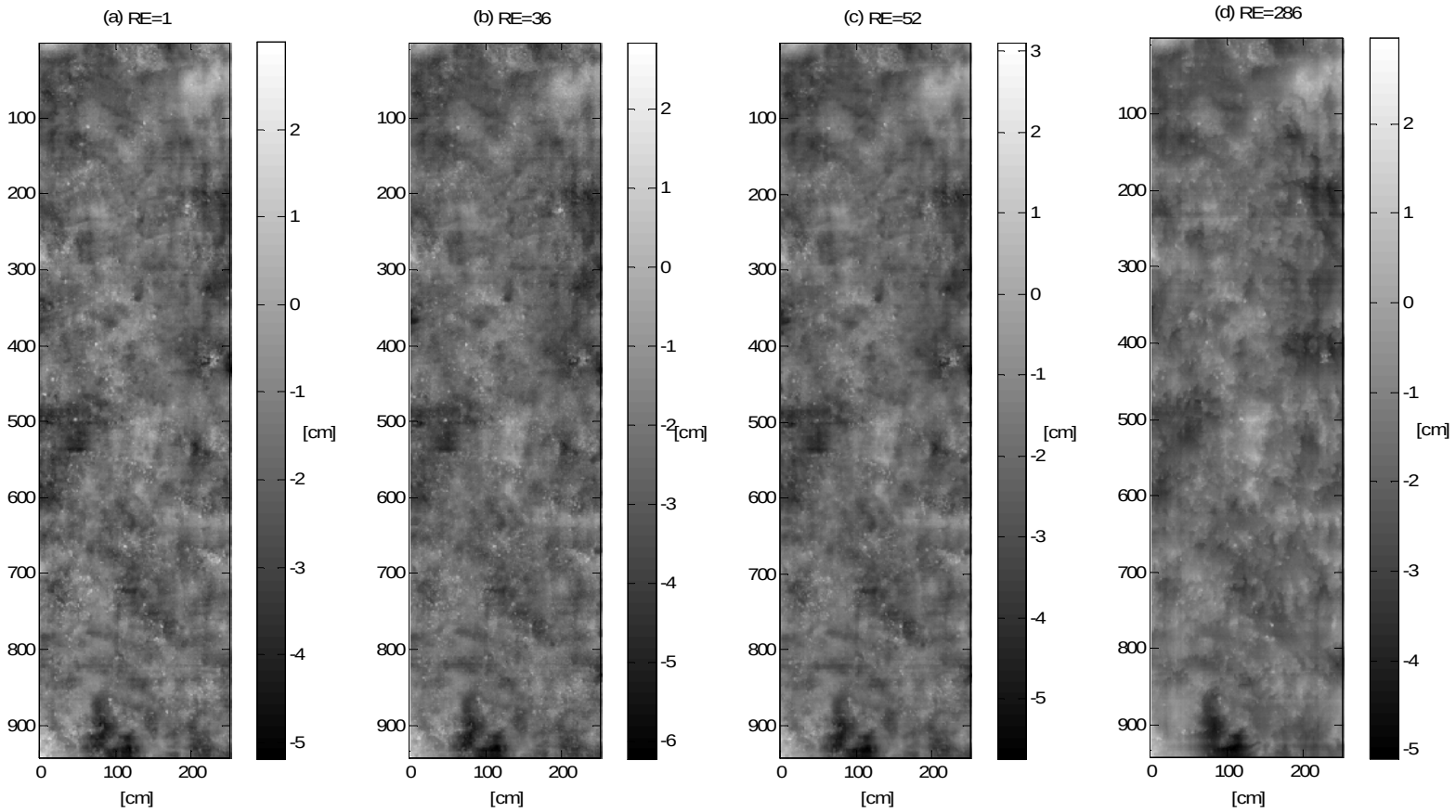

Figure C-3 DEMs of Plot 2 in Year 1 for (a) RE = 1, (b) RE = 36, (c) RE = 52 and (d) RE = 286. RE in MJ ha^{-1} mm h^{-1}

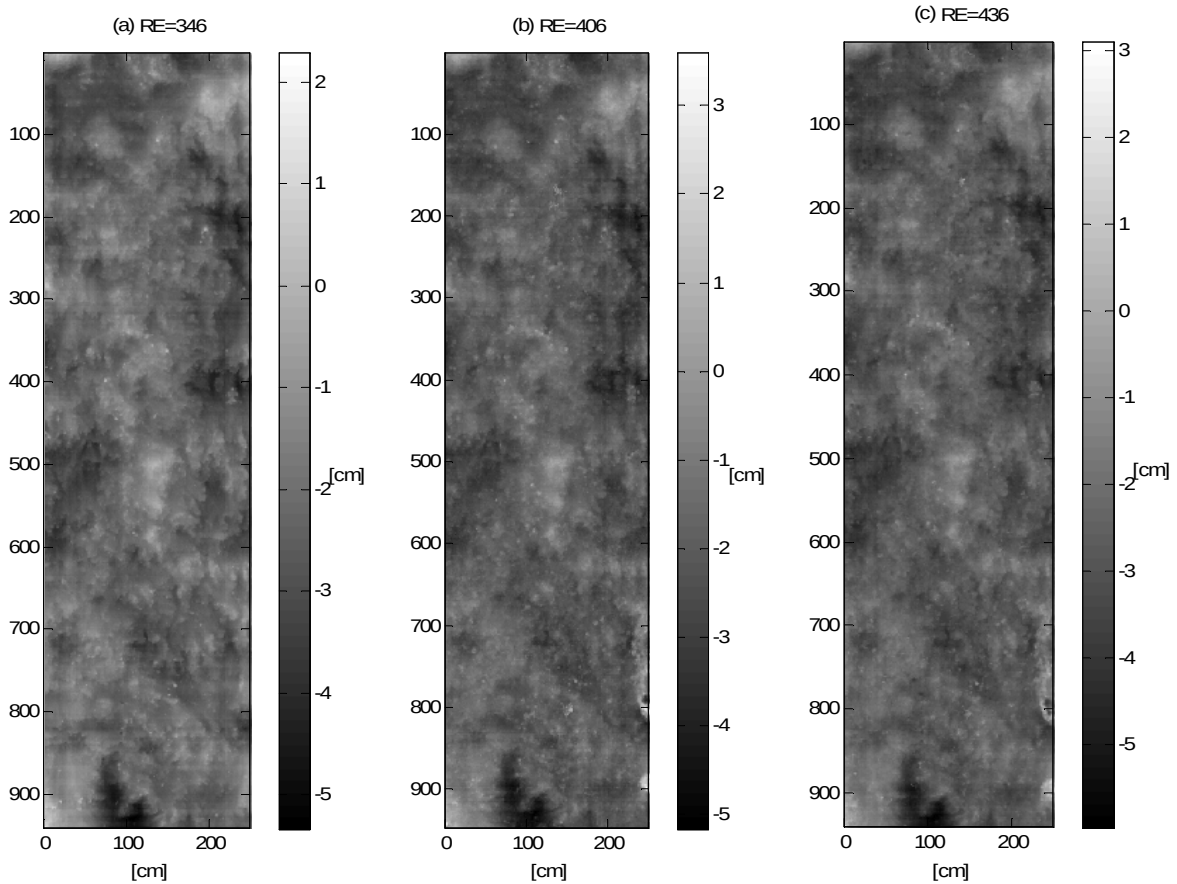

Figure C-4 DEMs of Plot 2 in Year 1 for (a) RE = 346, (b) RE = 406 and (c) RE = 436. RE in MJ ha^{-1} mm h^{-1}

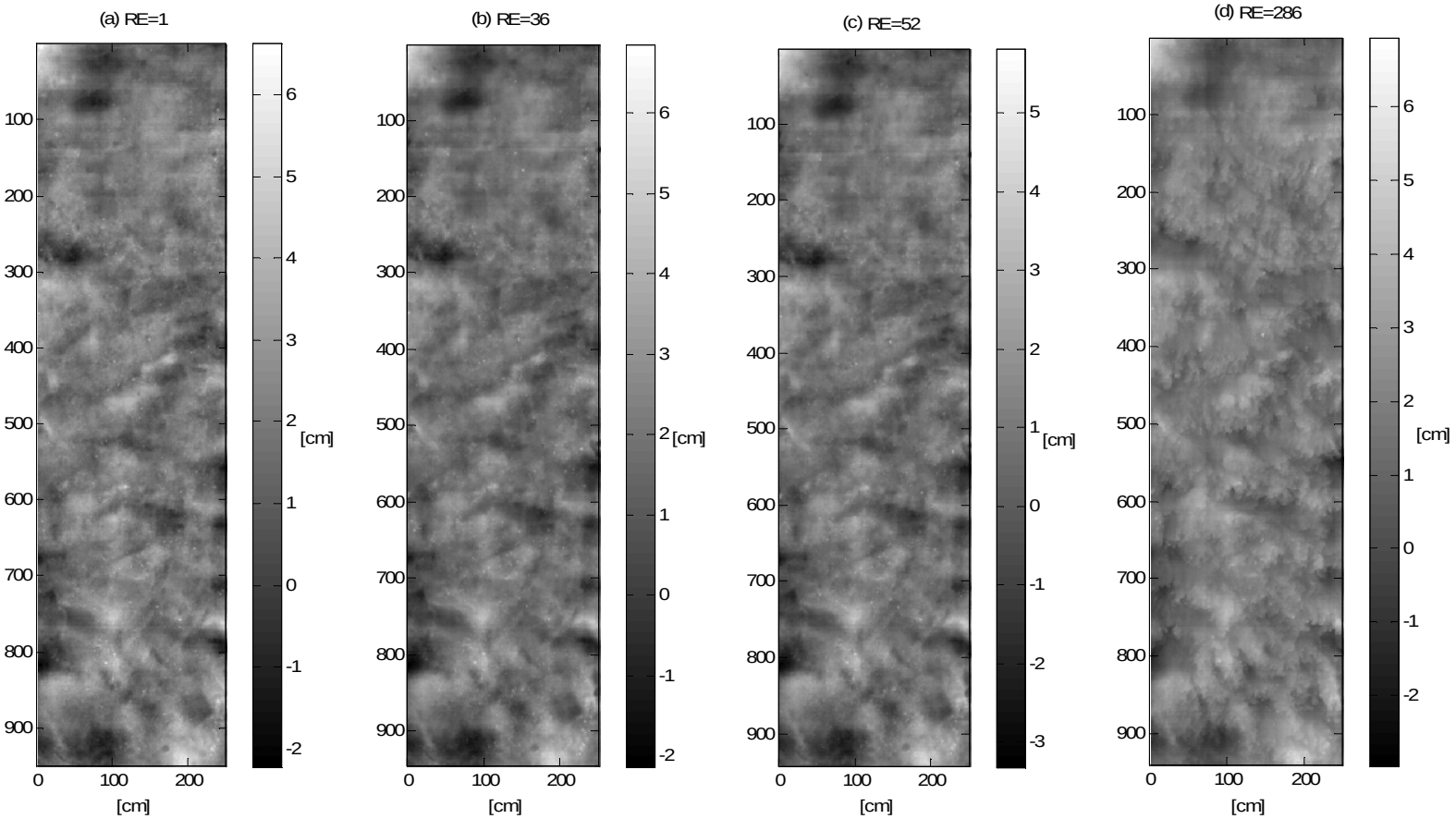

Figure C-5 DEMs of Plot 3 in Year 1 for (a) RE = 1, (b) RE = 36, (c) RE = 52 and (d) RE = 286. RE in MJ ha^{-1} mm h^{-1}

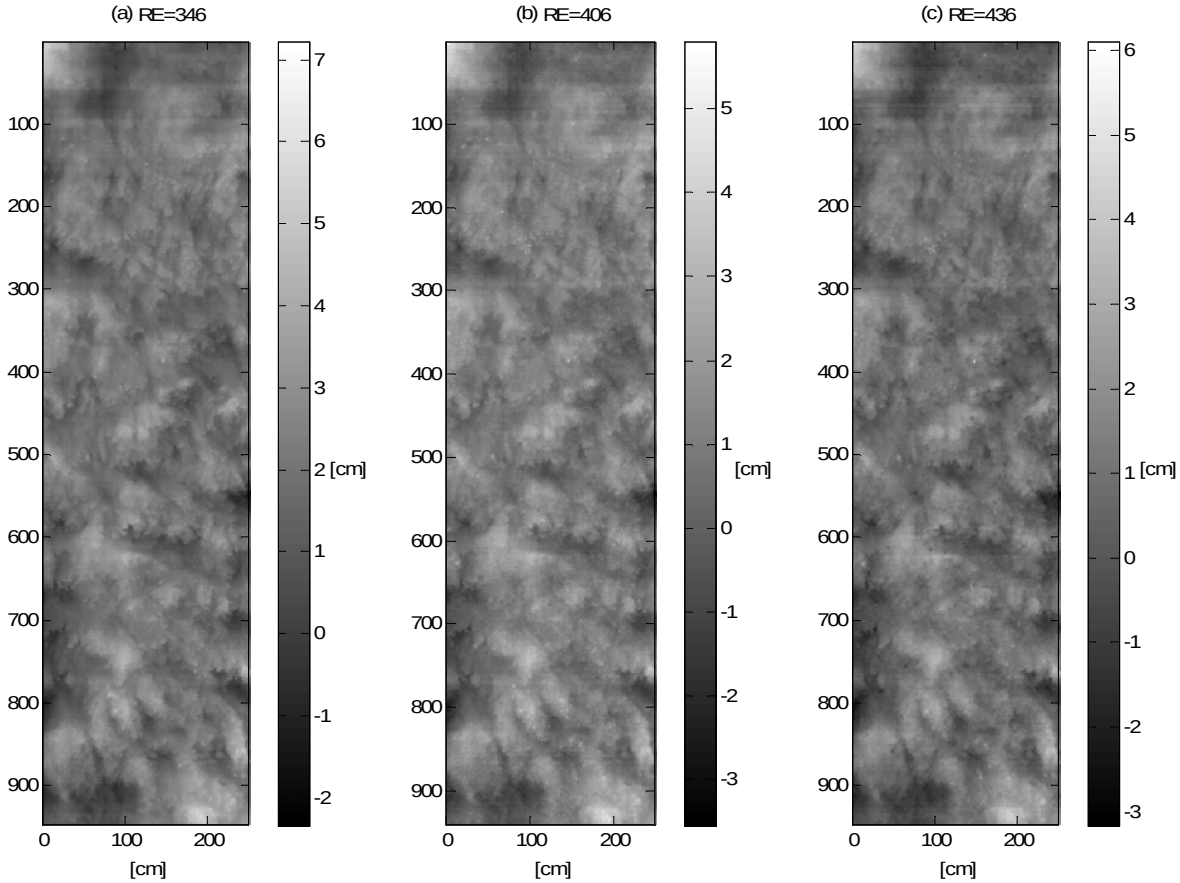

Figure C-6 DEMs of Plot 3 in Year 1 for (a) RE = 346, (b) RE = 406 and (c) RE = 436. RE in MJ ha^{-1} mm h^{-1}

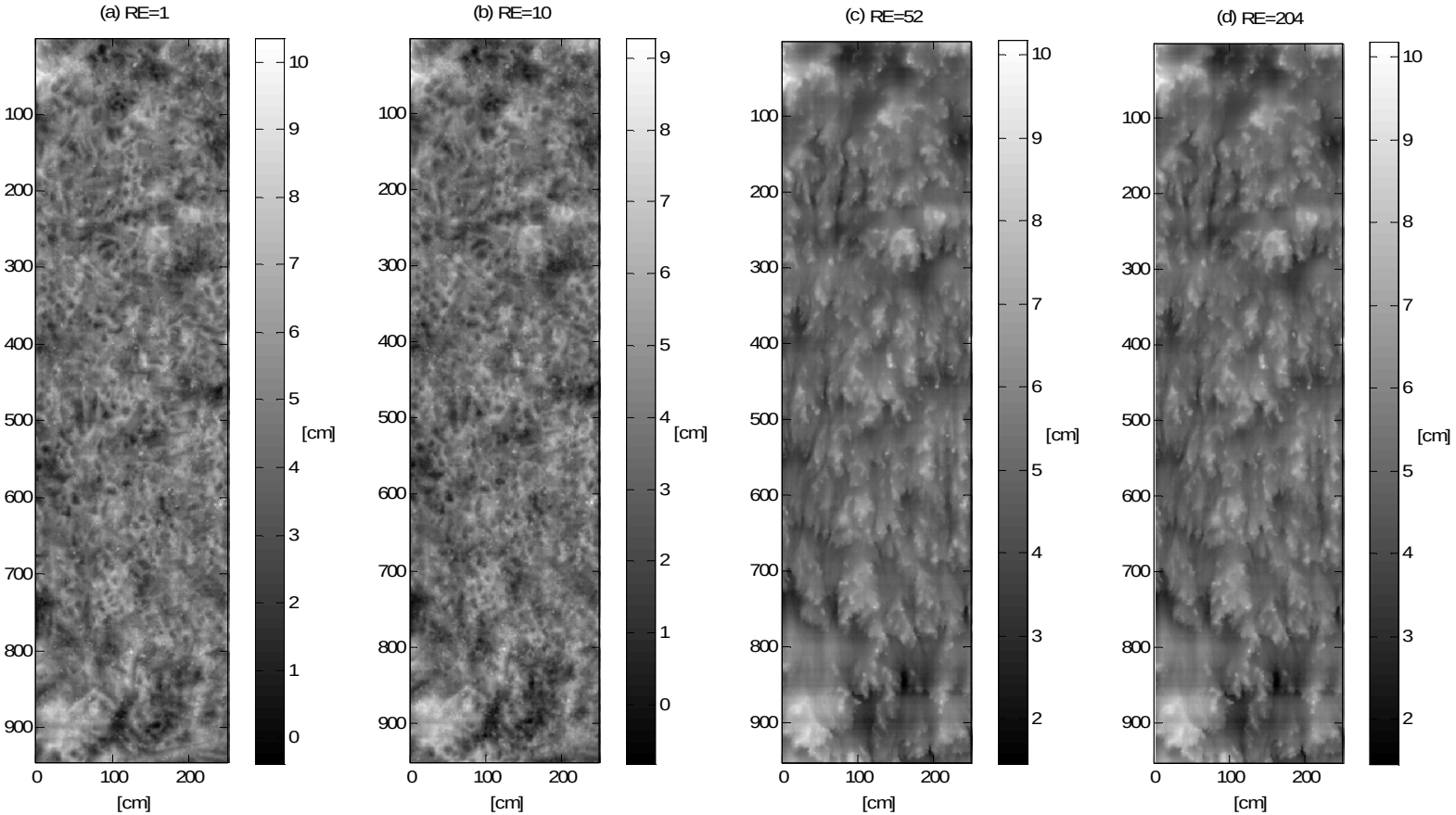

Figure C-7 DEMs of Plot 1 in Year 2 for (a) RE = 1, (b) RE = 10, (c) RE = 52 and (d) RE = 204. MJ ha^{-1} mm h^{-1}

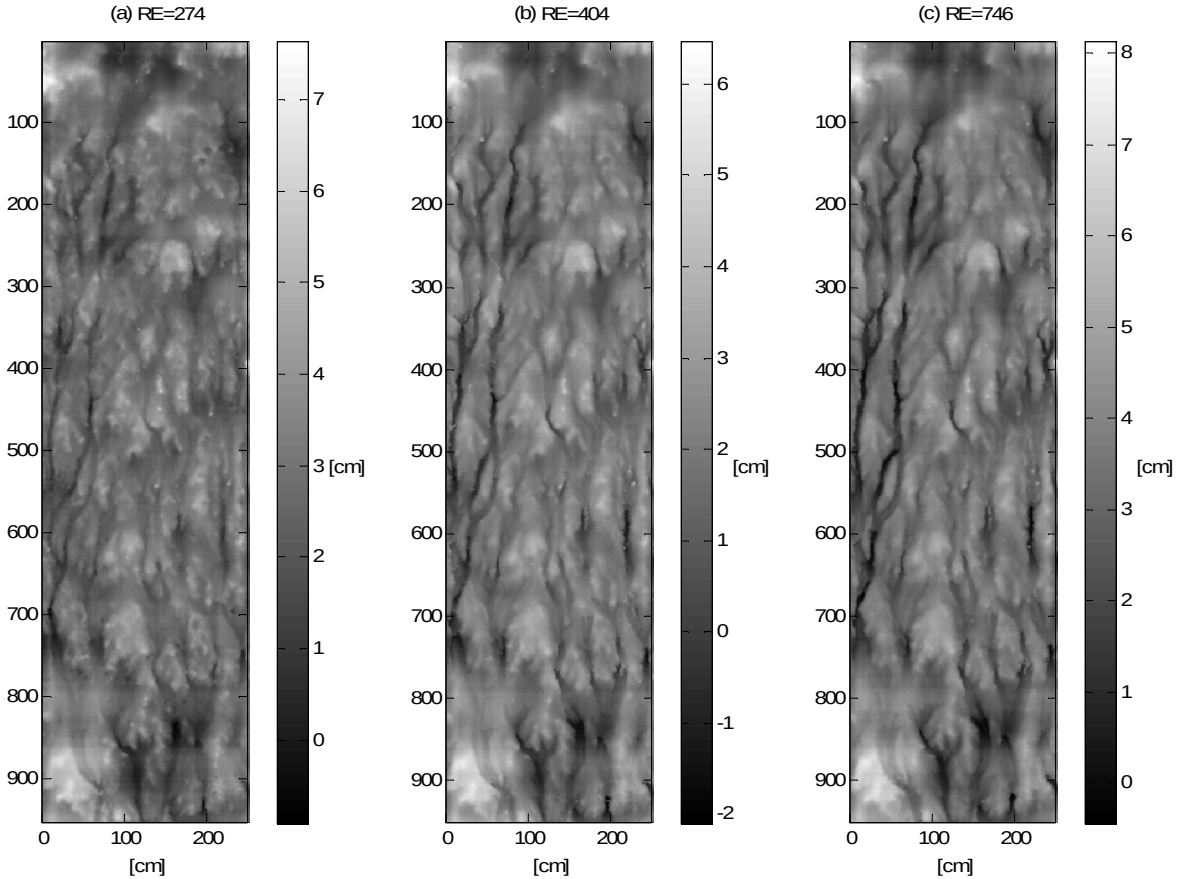

Figure C-8 DEMs of Plot 1 in Year 2 for (a) RE = 274, (b) RE = 404 and (c) RE = 746. RE in MJ ha^{-1} mm h^{-1}

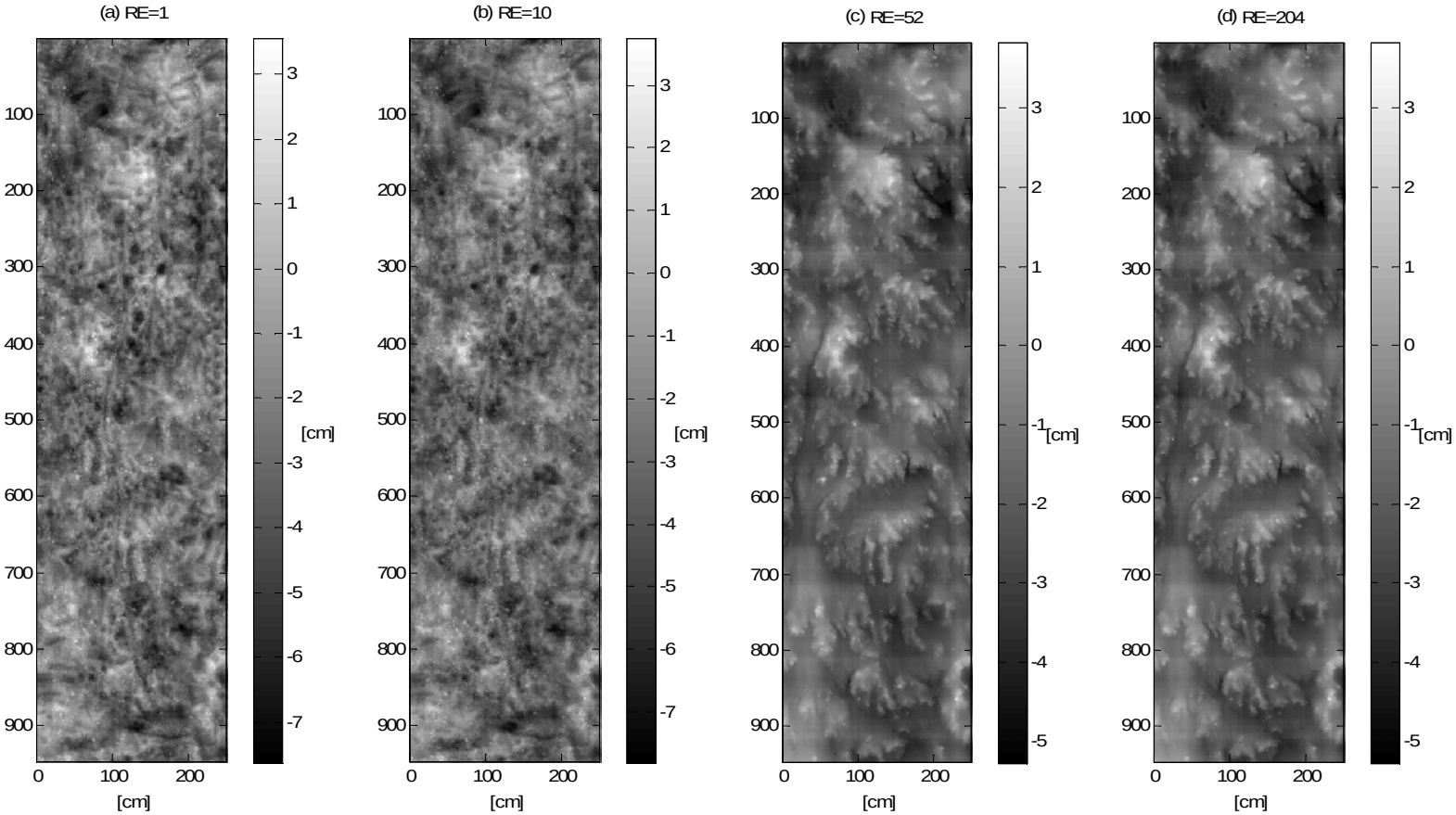

Figure C-9 DEMs of Plot 2 in Year 2 for (a) RE = 1, (b) RE = 10, (c) RE = 52 and (d) RE = 204. RE in MJ ha^{-1} mm h^{-1}

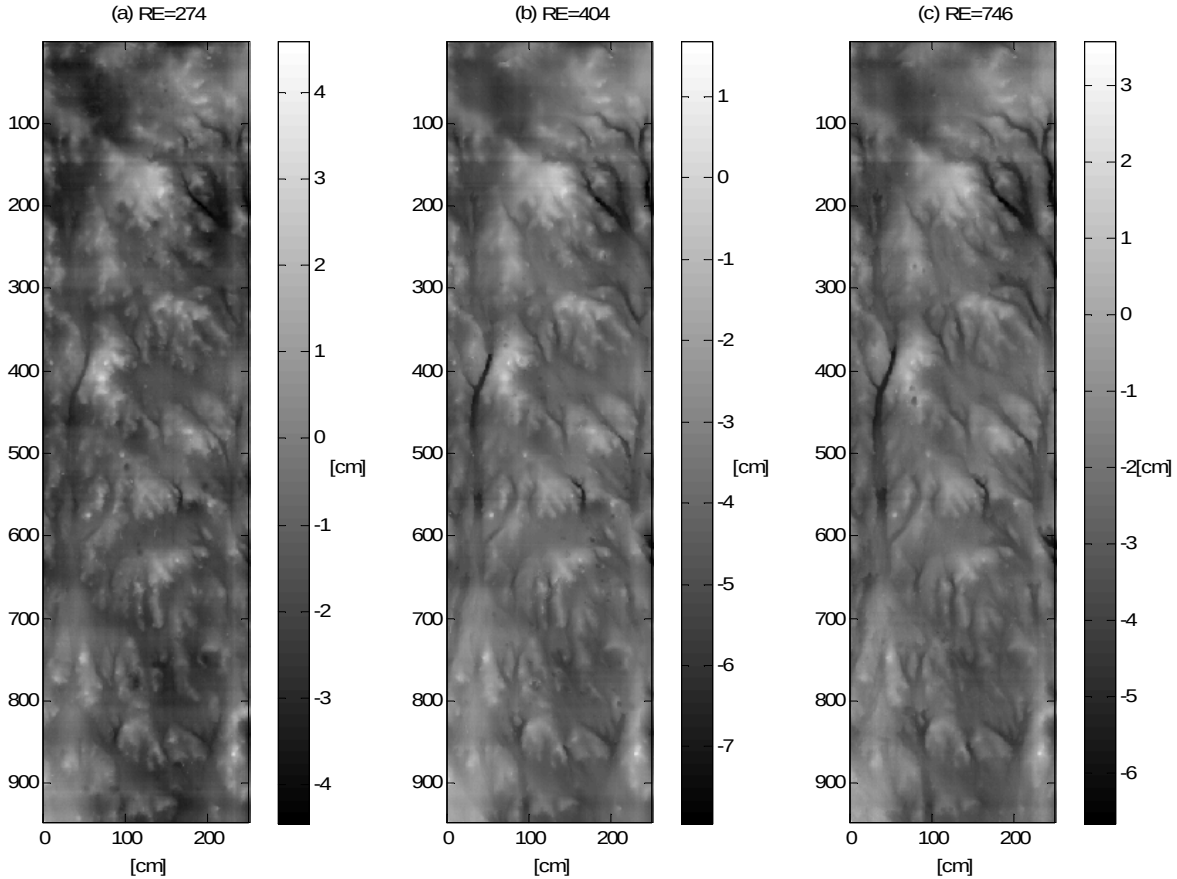

Figure C-10 DEMs of Plot 2 in Year 2 for (a) RE = 274, (b) RE = 404 and (c) RE = 746. RE in MJ ha^{-1} mm h^{-1}

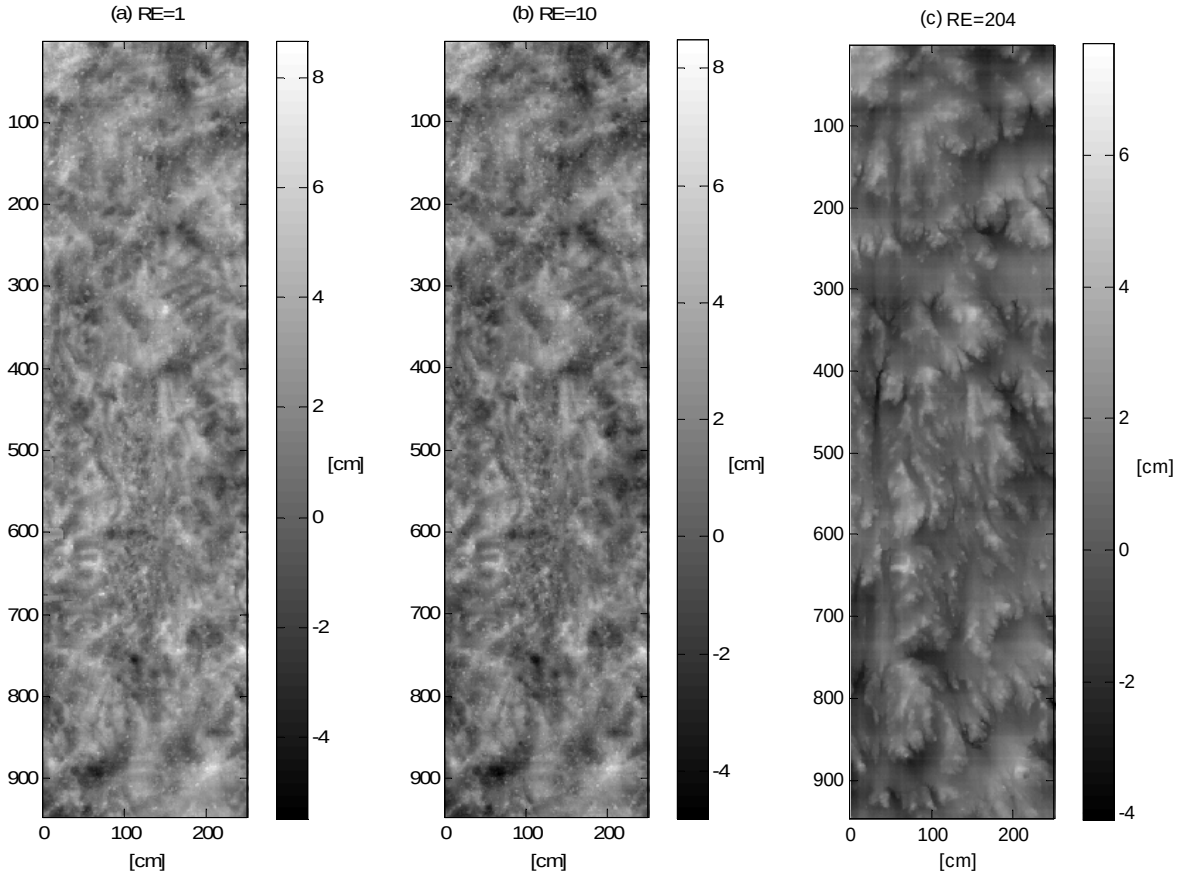

Figure C-11 DEMs of Plot 3 in Year 2 for (a) RE = 1, (b) RE = 10, and (c) RE = 204. RE in MJ ha^{-1} mm h^{-1}

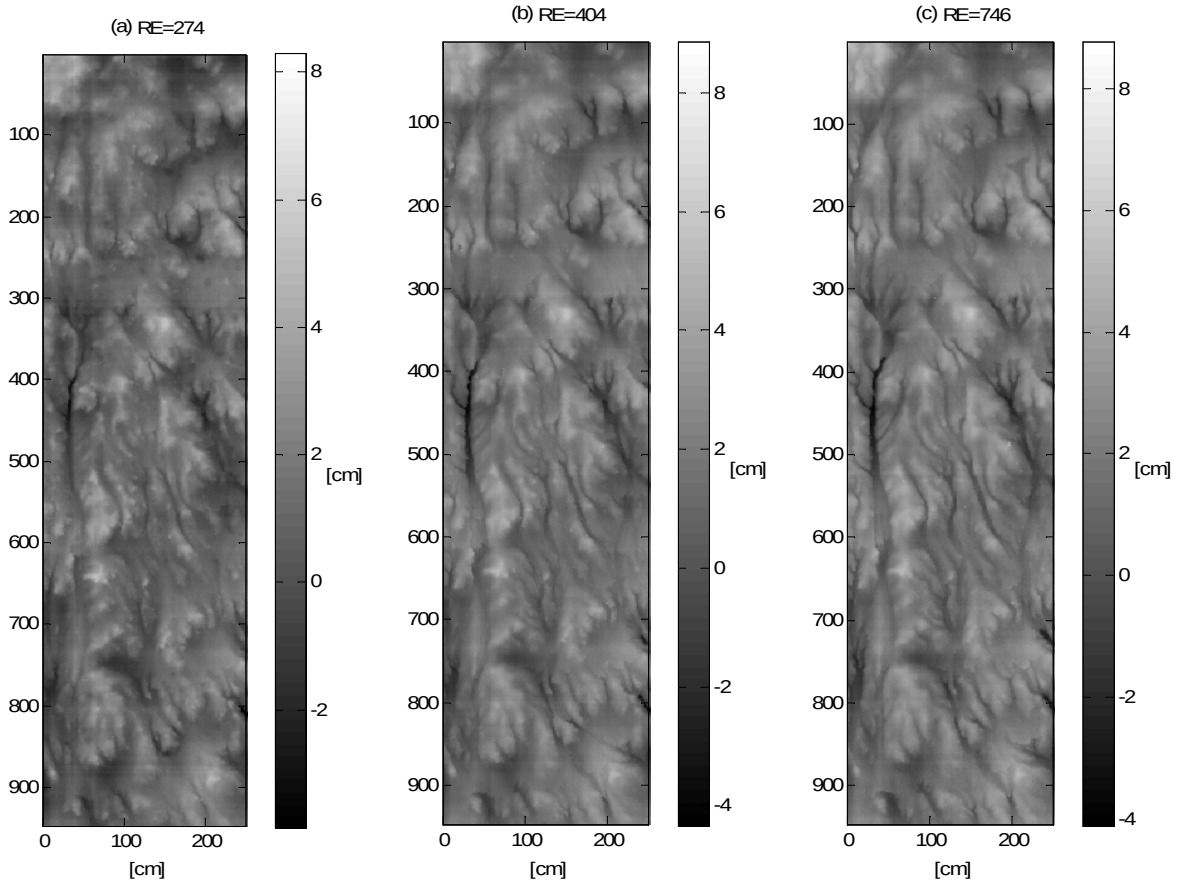

Figure C-12 DEMs of Plot 3 in Year 2 for (a) RE = 274, (b) RE = 404 and (c) RE = 746. RE in MJ ha^{-1} mm h^{-1}

D. Spatial distribution of overland flow velocities

In this section, we show the evolution of the spatial distribution of overland flow velocities for Plot 1, Plot 2 and Plot 3 in Year 1 and Year 2. See chapter 5 for details.

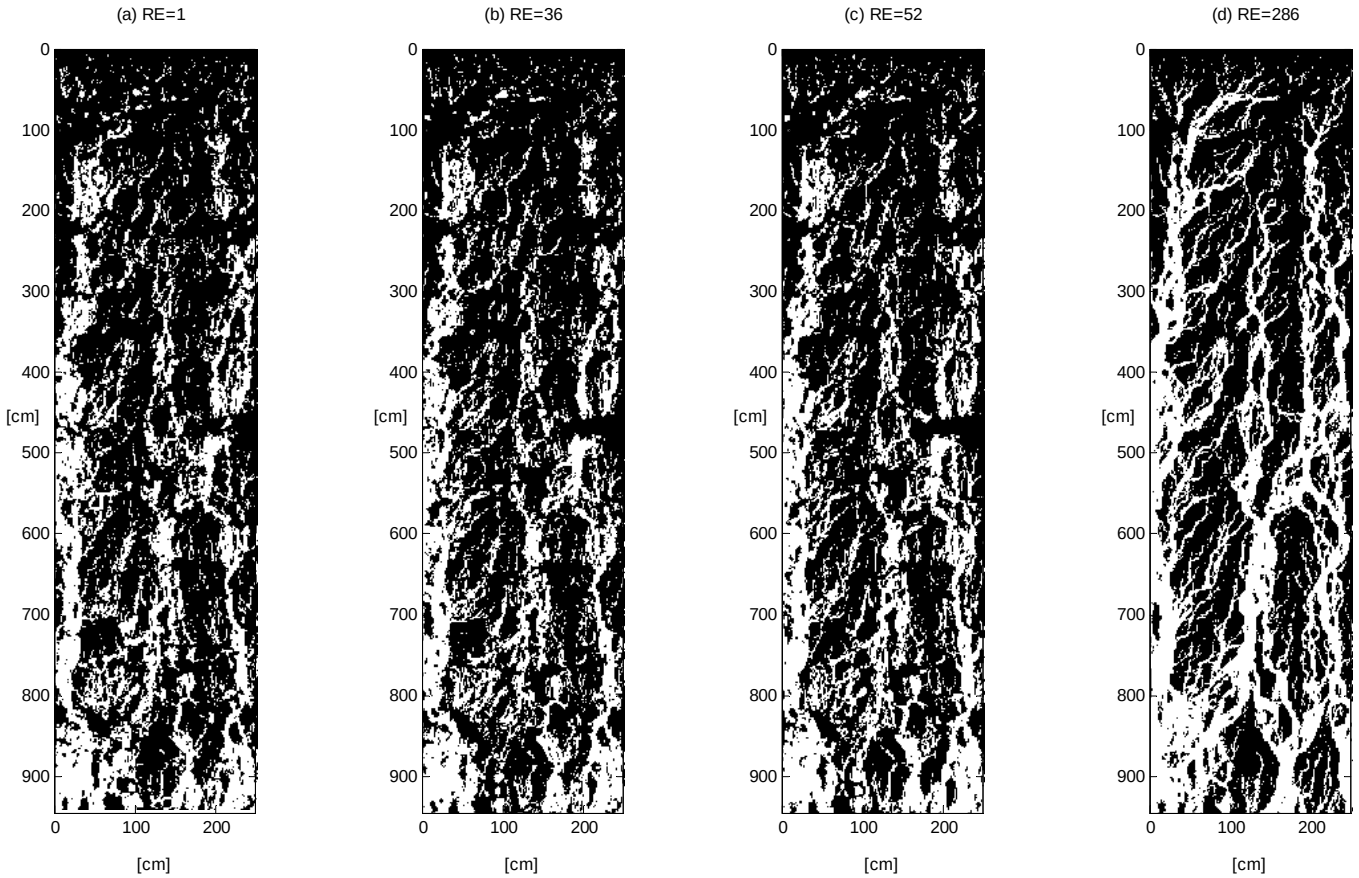

Figure D-1 Spatial distribution of binarized overland flow velocities of Plot 1 in Year 1 for (a) RE = 1, (b) RE = 36, (c) RE = 52 and (d) RE = 286. RE in MJ ha^{-1} mm h^{-1}. Flow velocities above 0.07 m/s represented in white and below 0.07 m/s represented in black.

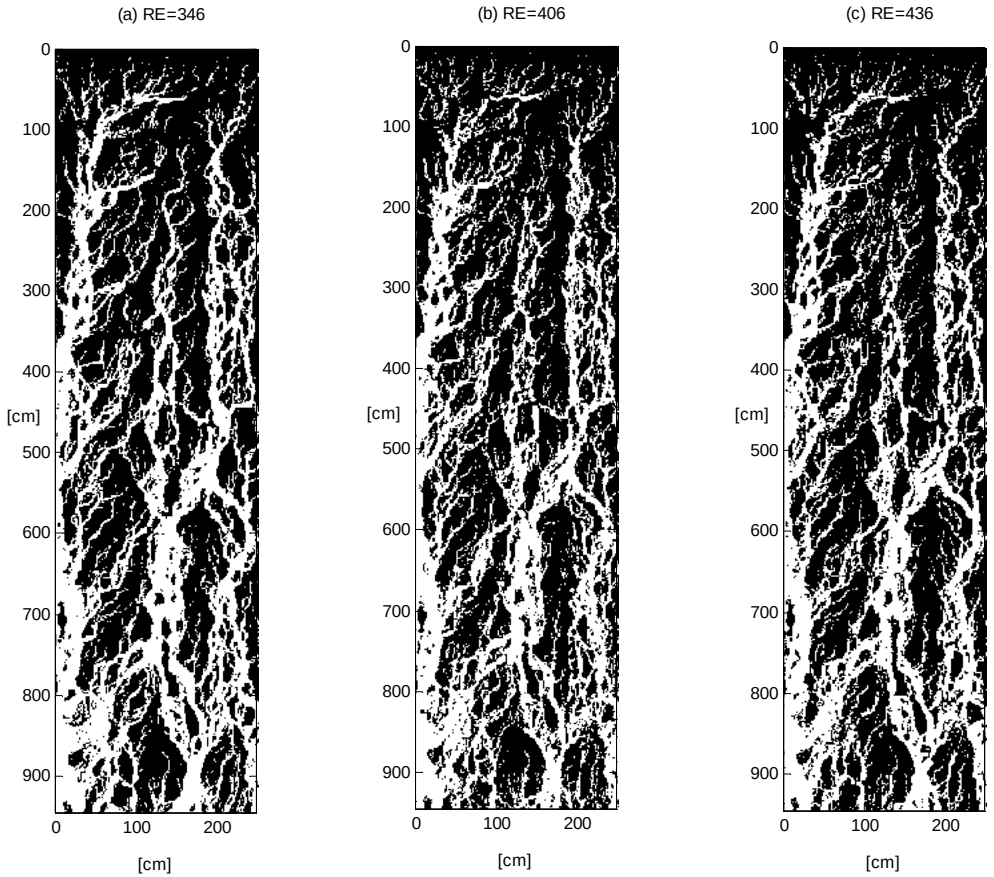

Figure D-2 Spatial distribution of binarized overland flow velocity fields at steady state of Plot 1 in Year 1 for (a) RE = 346, (b) RE = 406, (c) RE = 436 and (d) RE = 436. RE is in MJ ha^{-1} mm h^{-1}. Flow velocities above 0.07 m/s represented in white and below 0.07 m/s represented in black.

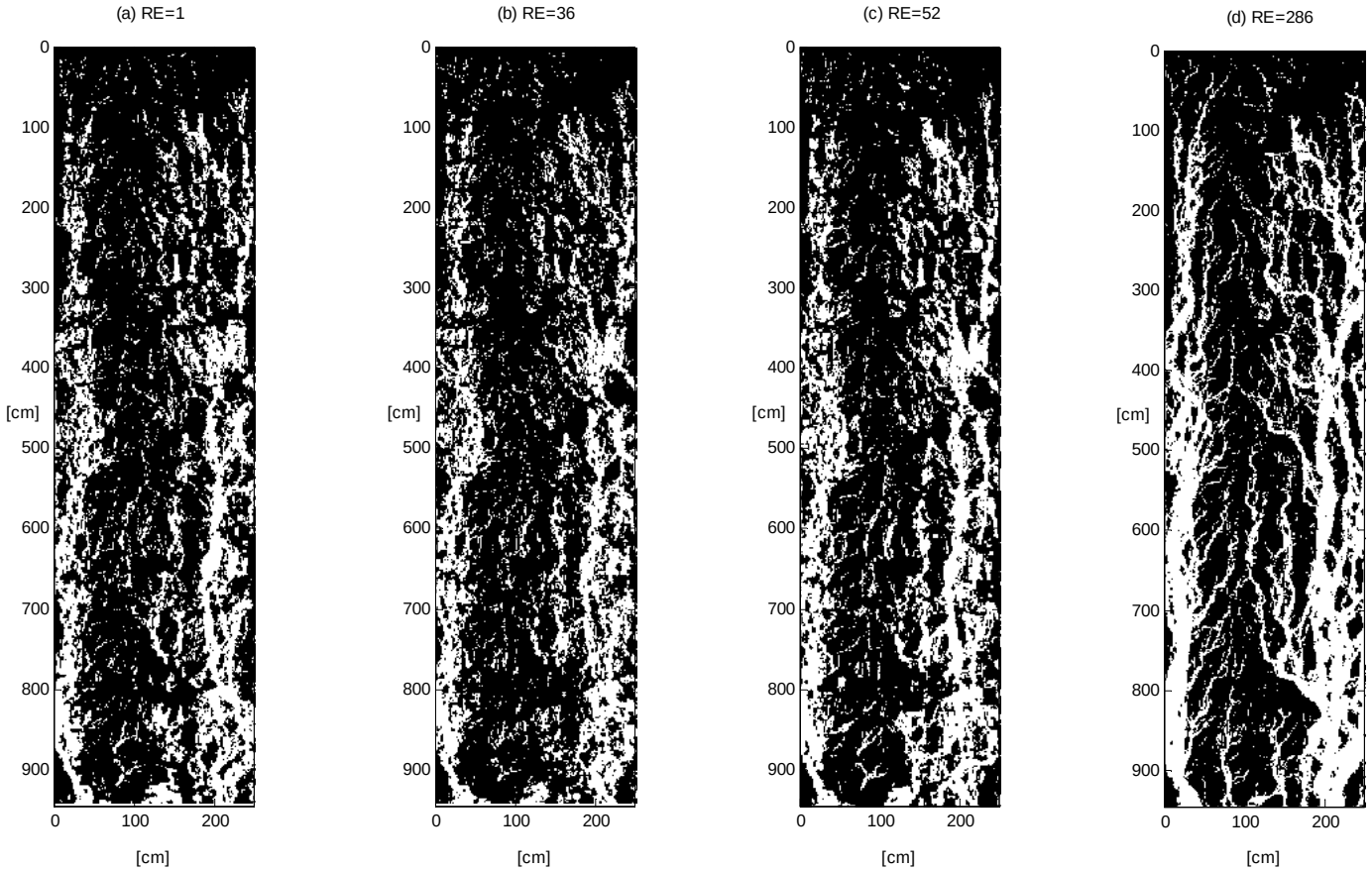

Figure D-3 Spatial distribution of binarized overland flow velocities of Plot 2 in Year 1 for (a) RE = 1, (b) RE = 36, (c) RE = 52 and (d) RE = 286. RE in MJ ha^{-1} mm h^{-1}. Flow velocities above 0.07 m/s represented in white and below 0.07 m/s represented in black.

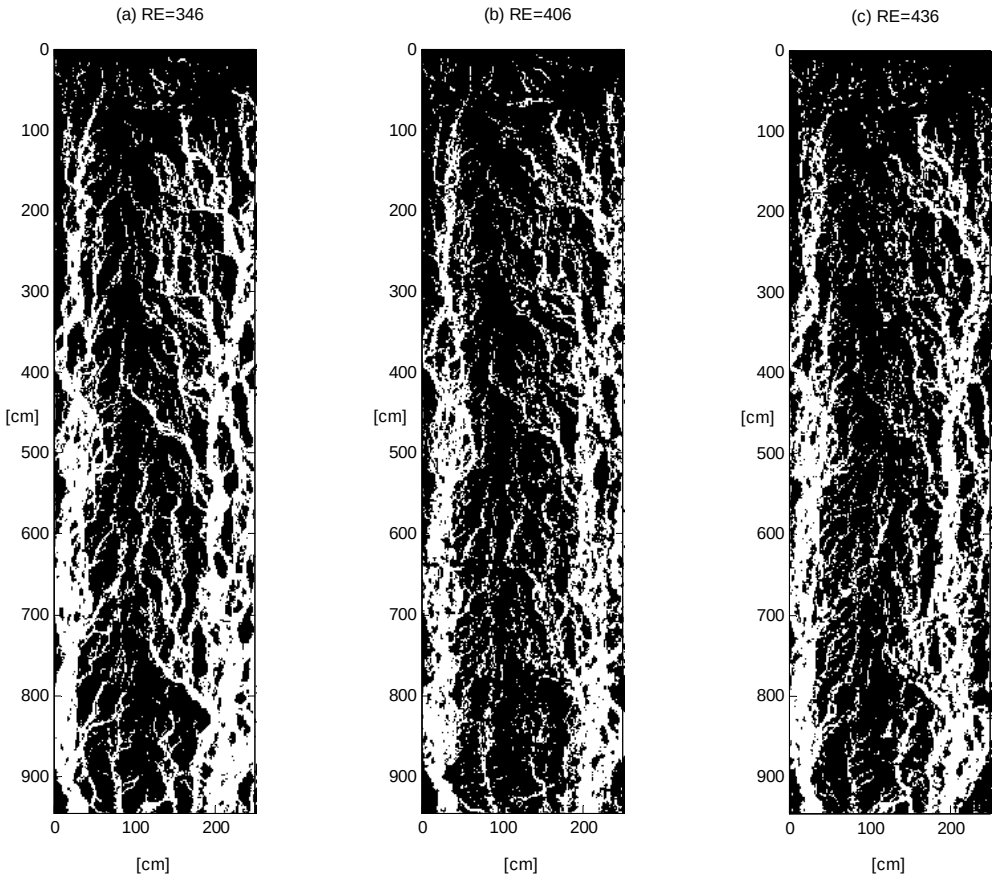

Figure D-4 Spatial distribution of binarized overland flow velocities of Plot 2 in Year 1 for (a) RE = 346, (b) RE = 406 and (d) RE = 436. RE in MJ ha^{-1} mm h^{-1}. Flow velocities above 0.07 m/s represented in white and below 0.07 m/s represented in black.

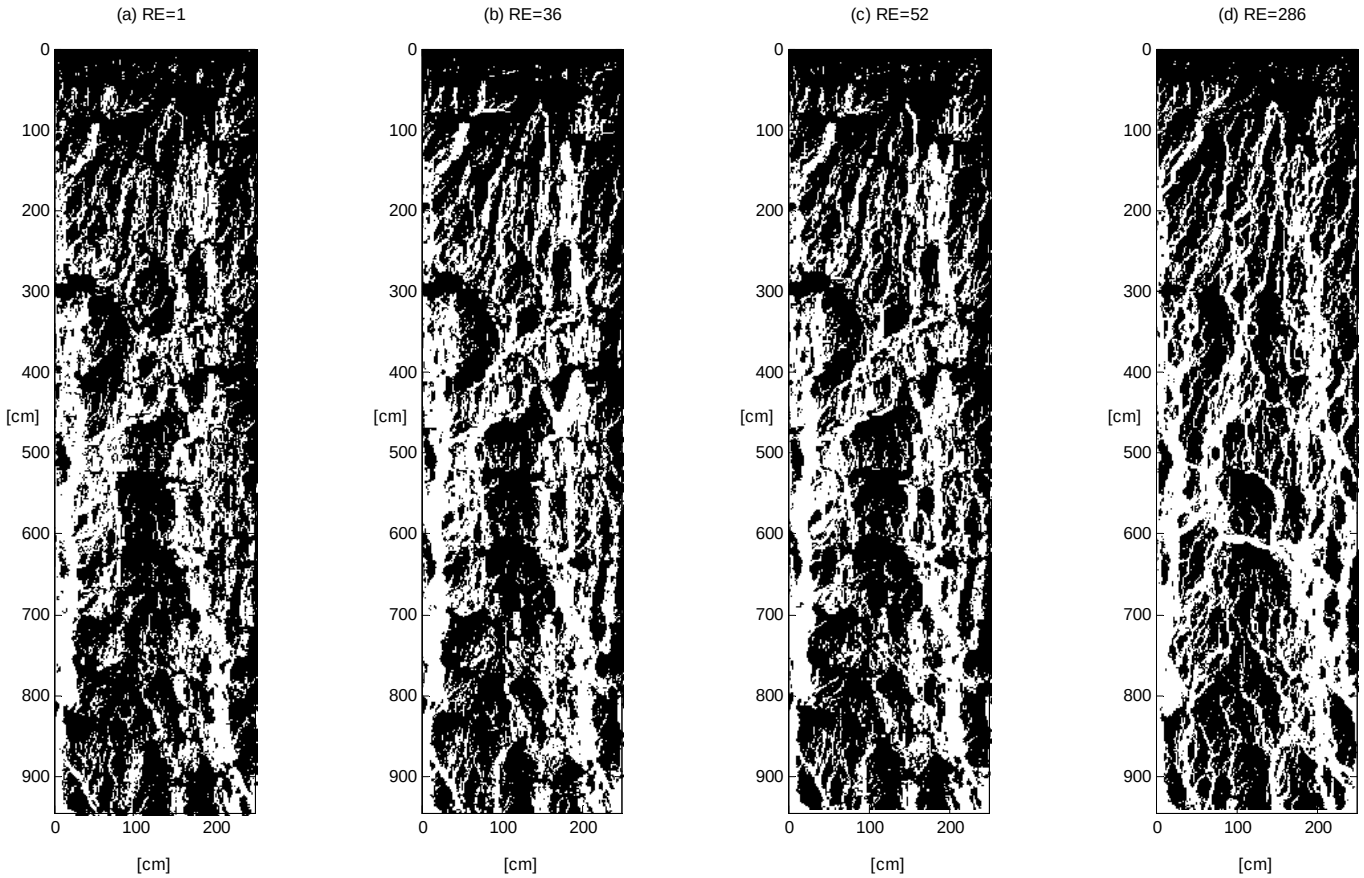

Figure D-5 Spatial distribution of binarized overland flow velocities of Plot 3 in Year 1 for (a) RE = 1, (b) RE = 36, (c) RE = 52 and (d) RE = 286. RE in MJ ha^{-1} mm h^{-1}. Flow velocities above 0.07 m/s represented in white and below 0.07 m/s represented in black.

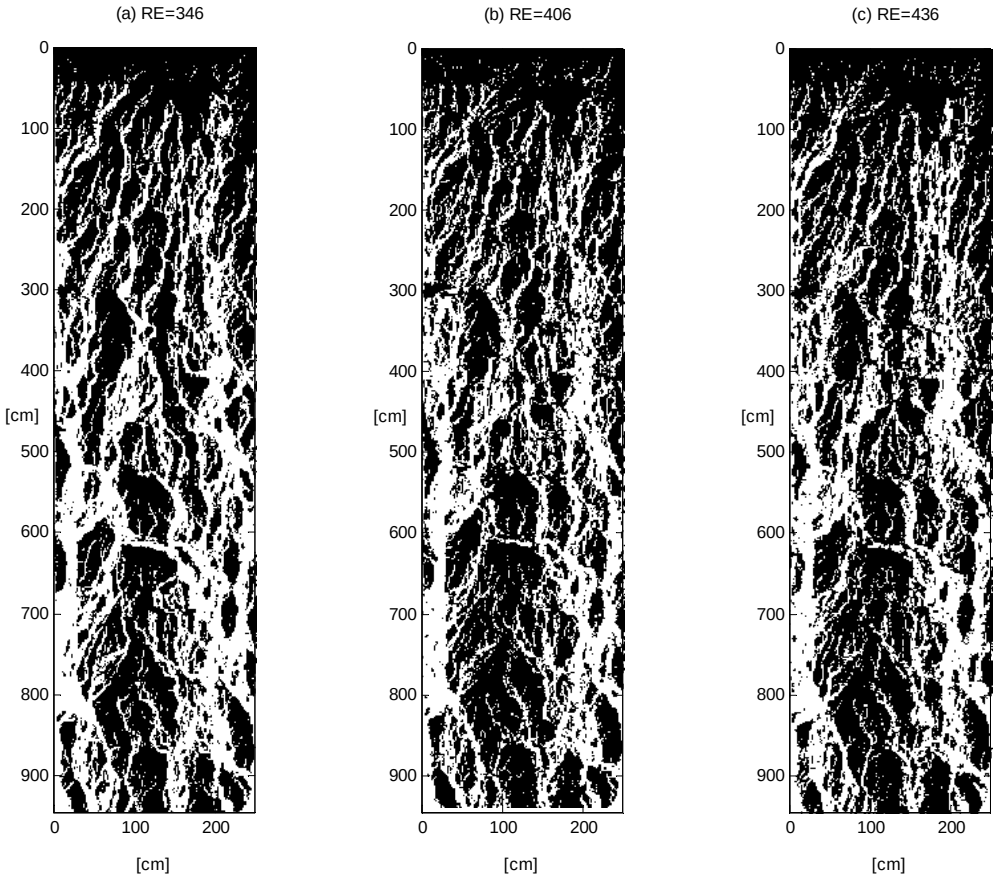

Figure D-6 Spatial distribution of binarized overland flow velocities of Plot 3 in Year 1 for (a) RE = 346, (b) RE = 406 and (d) RE = 436. RE in MJ ha^{-1} mm h^{-1}. Flow velocities above 0.07 m/s represented in white and below 0.07 m/s represented in black.

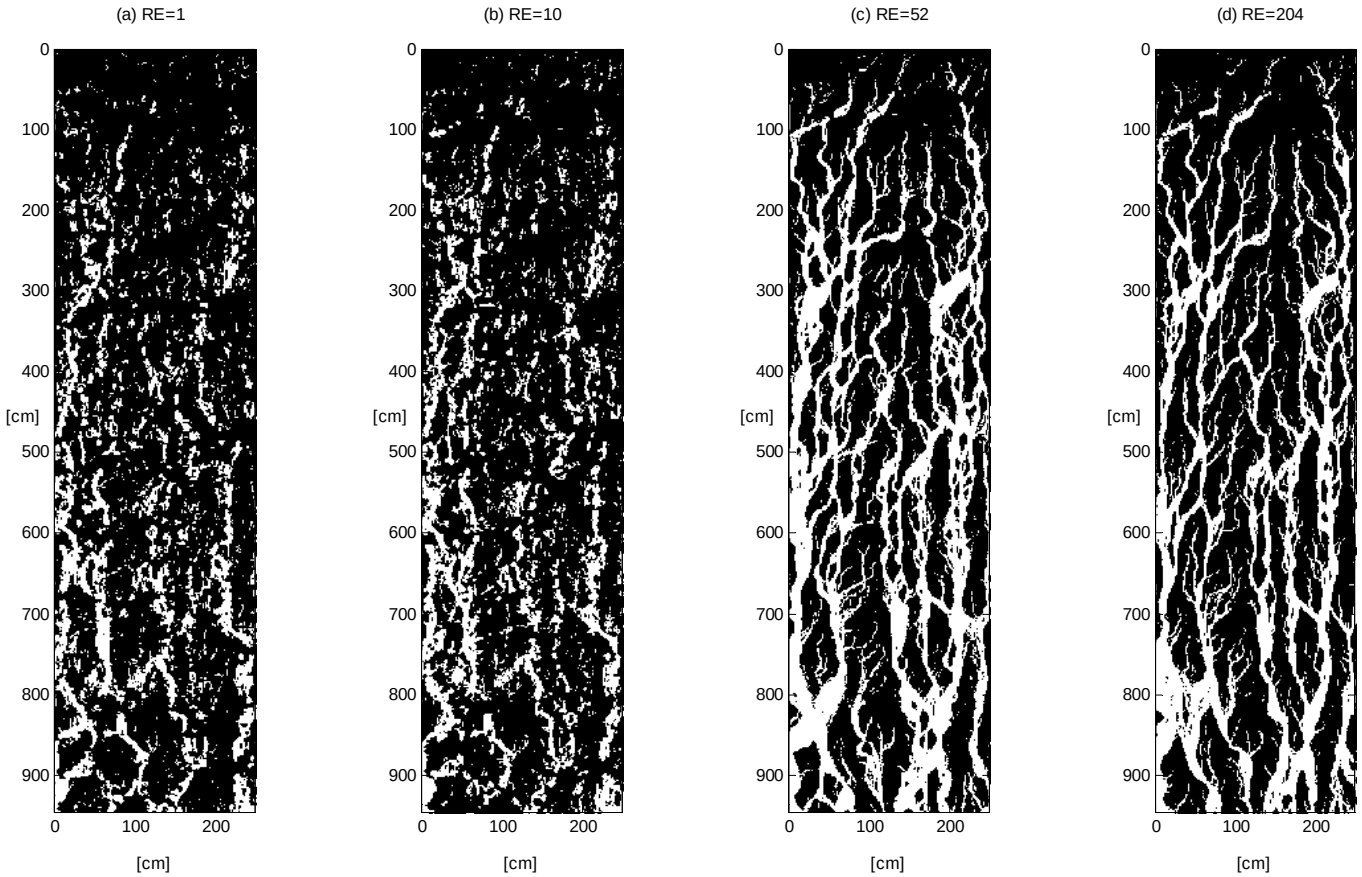

Figure D-7 Spatial distribution of binarized overland flow velocities of Plot 1 in Year 2 for (a) RE = 1, (b) RE = 10, (c) RE = 52 and (d) RE = 204. RE in MJ ha^{-1} mm h^{-1}. Flow velocities above 0.07 m/s represented in white and below 0.07 m/s represented in black.

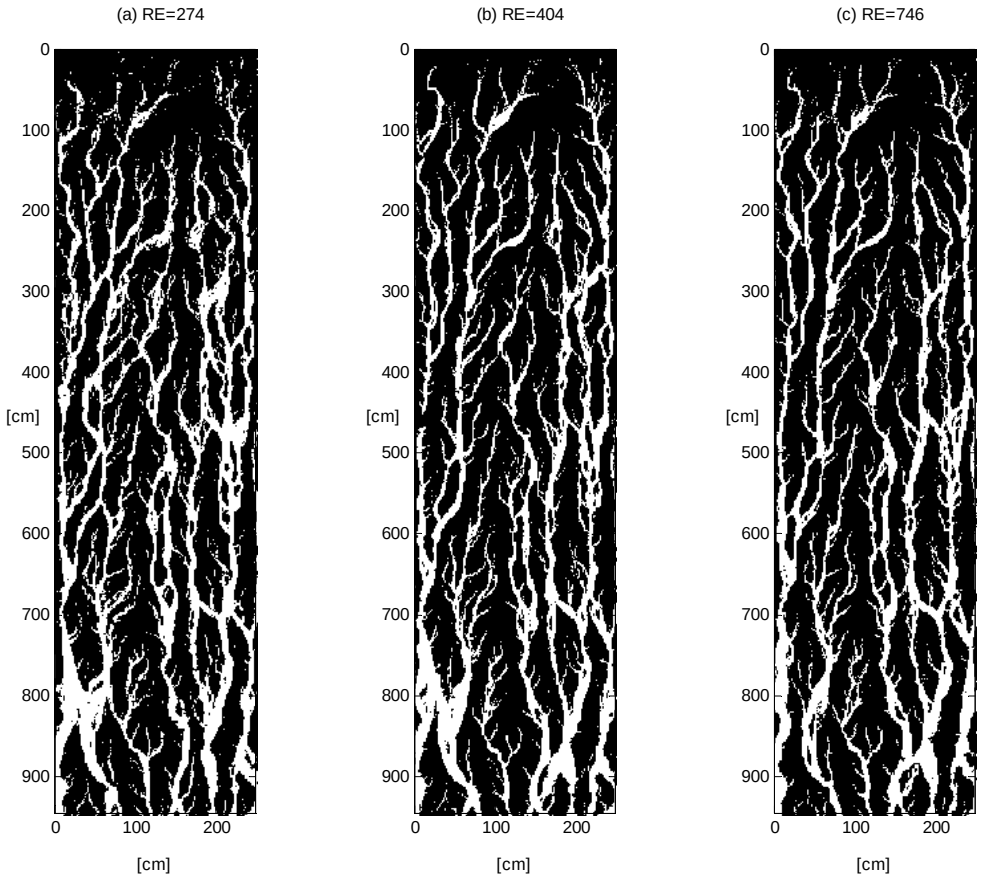

Figure D-8 Spatial distribution of binarized overland flow velocities of Plot 1 in Year 2 for (a) RE = 274, (b) RE = 404 and (c) RE = 746. RE in MJ ha^{-1} mm h^{-1}. Flow velocities above 0.07 m/s represented in white and below 0.07 m/s represented in black.

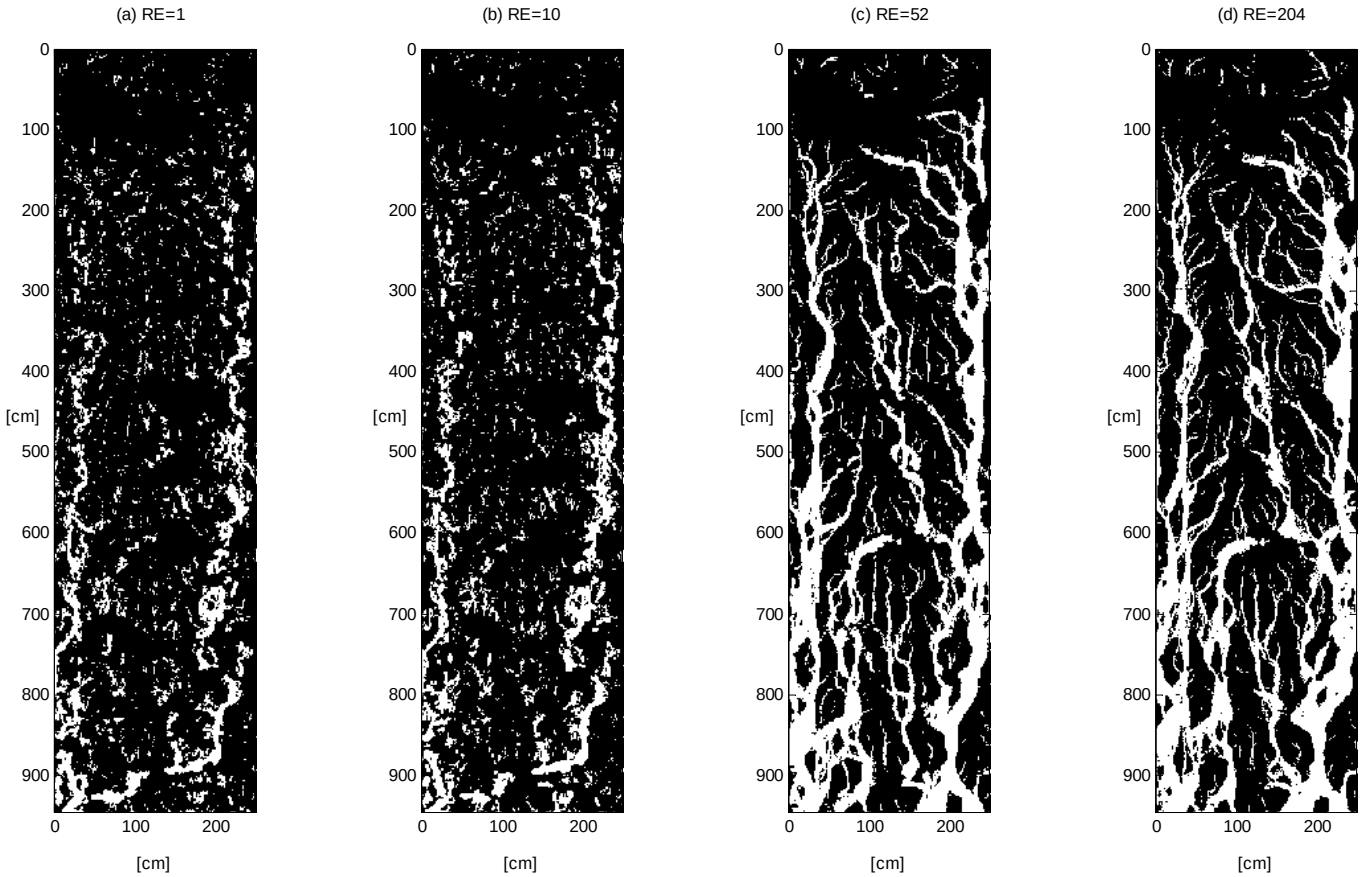

Figure D-9 Spatial distribution of binarized overland flow velocities of Plot 2 in Year 2 for (a) RE = 1, (b) RE = 10, (c) RE = 52 and (d) RE = 204. RE in MJ ha^{-1} mm h^{-1}. Flow velocities above 0.07 m/s represented in white and below 0.07 m/s represented in black.

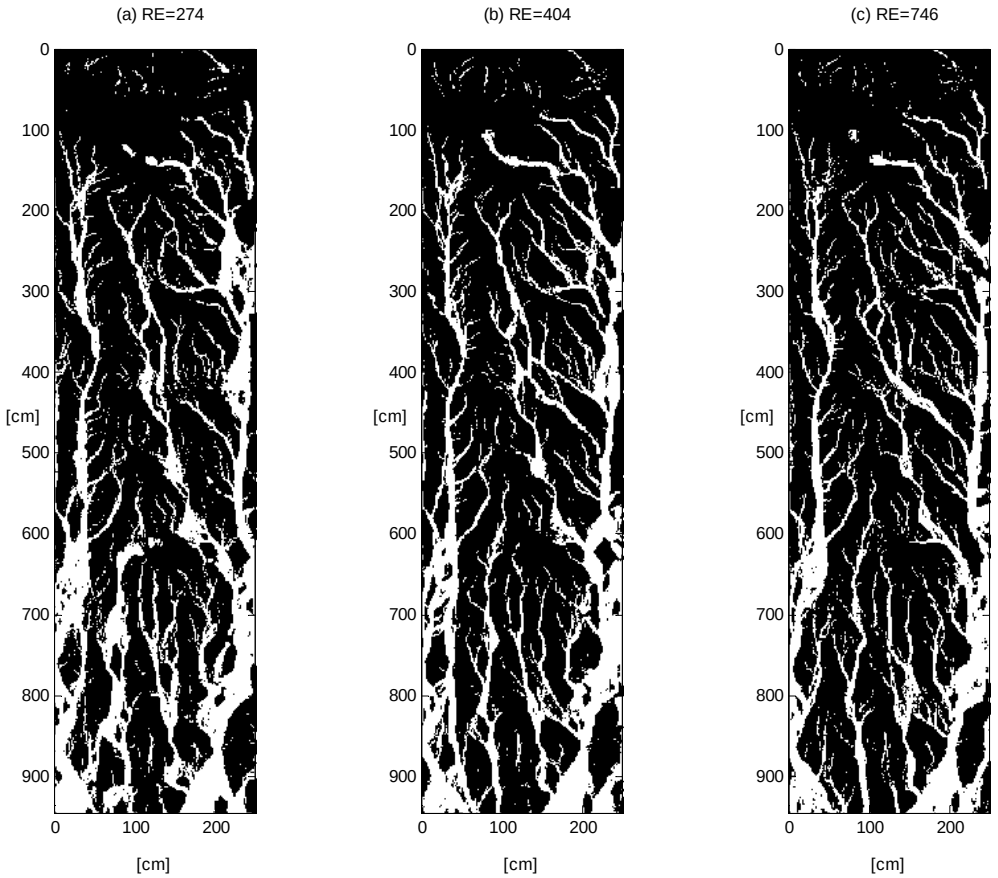

Figure D-10 Spatial distribution of binarized overland flow velocities of Plot 2 in Year 2 for (a) RE = 274, (b) RE = 404 and (c) RE = 746. RE in MJ ha^{-1} mm h^{-1}. Flow velocities above 0.07 m/s represented in white and below 0.07 m/s represented in black.

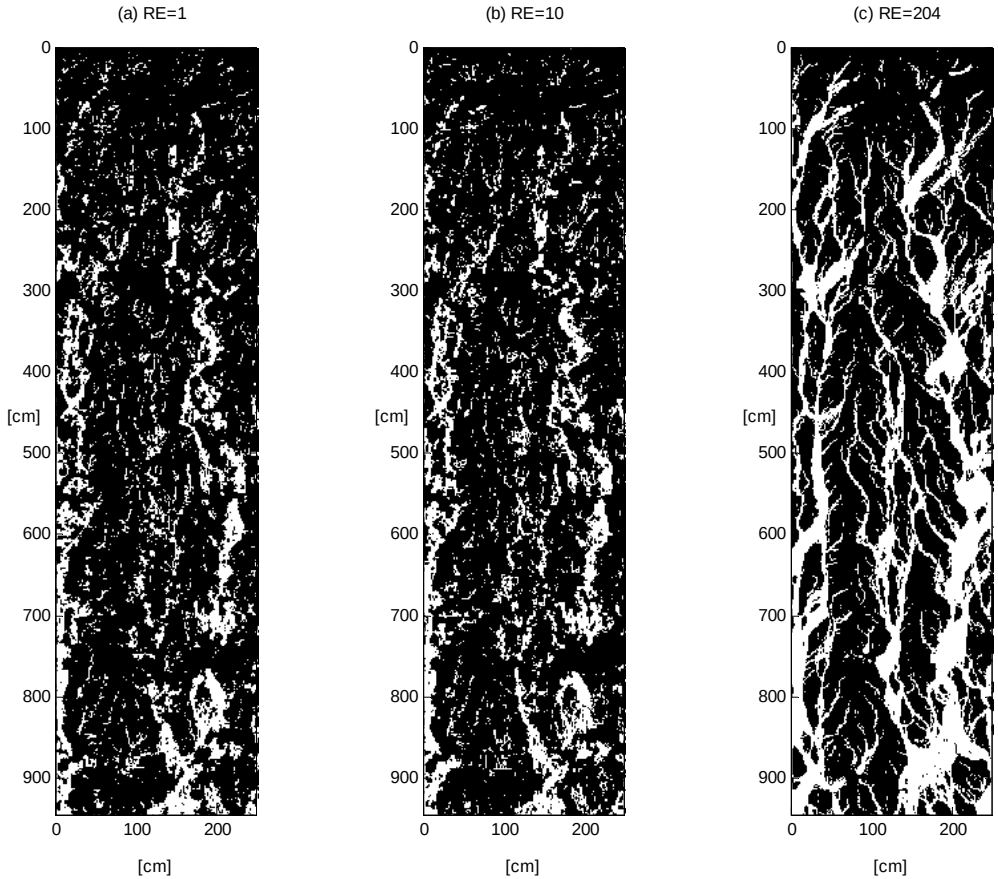

Figure D-11 Spatial distribution of binarized overland flow velocities of Plot 3 in Year 2 for (a) RE = 1, (b) RE = 10, and (c) RE = 204. RE in MJ ha^{-1} mm h^{-1}. Flow velocities above 0.07 m/s represented in white and below 0.07 m/s represented in black.

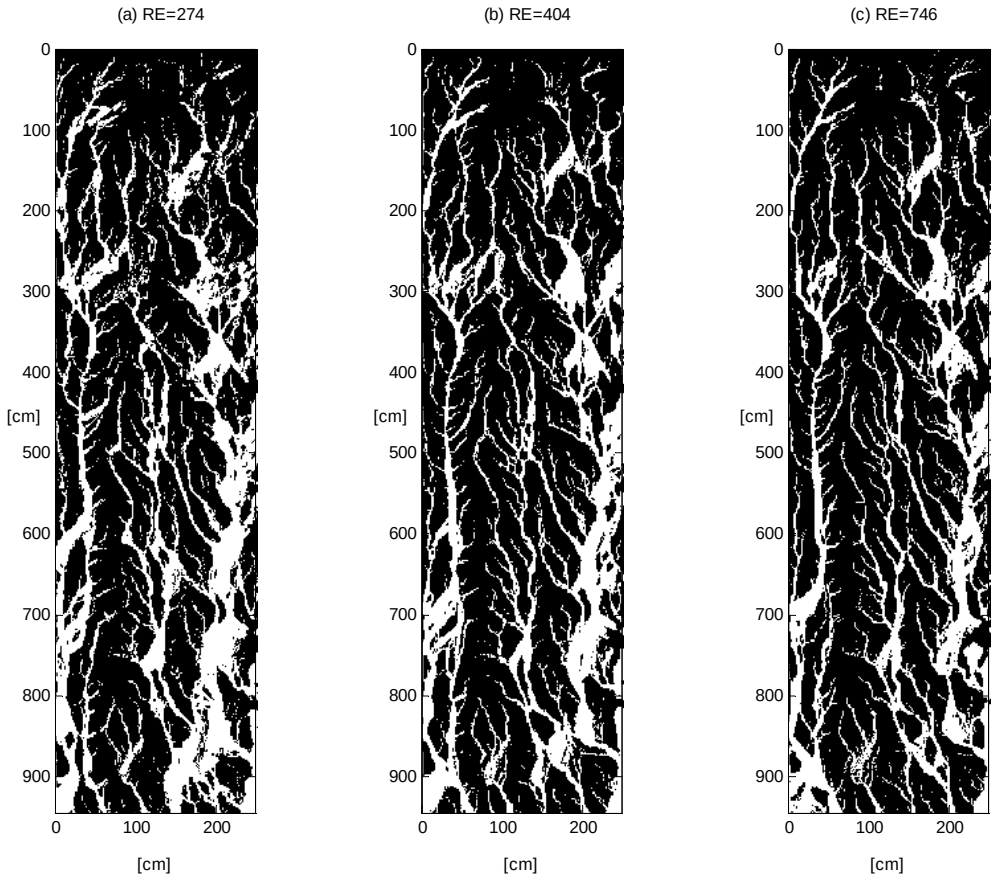

Figure D-12 Spatial distribution of binarized overland flow velocities of Plot 3 in Year 2 for (a) RE = 274, (b) RE = 404 and (c) RE = 746. RE in MJ ha^{-1} mm h^{-1}. Flow velocities above 0.07 m/s represented in white and below 0.07 m/s represented in black.

E. RSCf evolution

In this section, we show the evolution of the RSCf for Plot 2 and Plot 3 in Year 1 and Year 2.

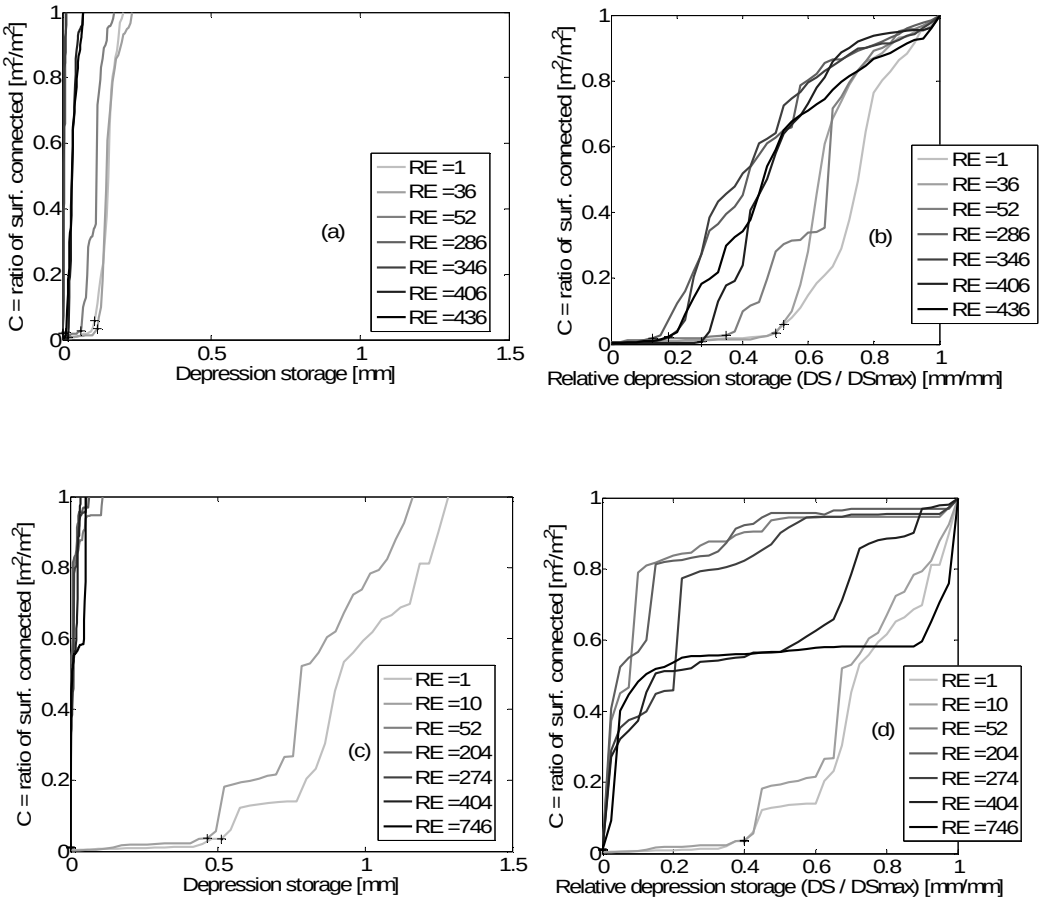

Figure E-1Evolution of the RSCf (a, c) and the normalized RSCf (b, d) as a function of the cumulative rainfall erosivity (RE) for Plot 2 in Year 1 (a, b) and Year 2 (b, c). Cross markers represent the connectivity threshold (CT). RE is in MJ ha^{-1} mm h^{-1}h

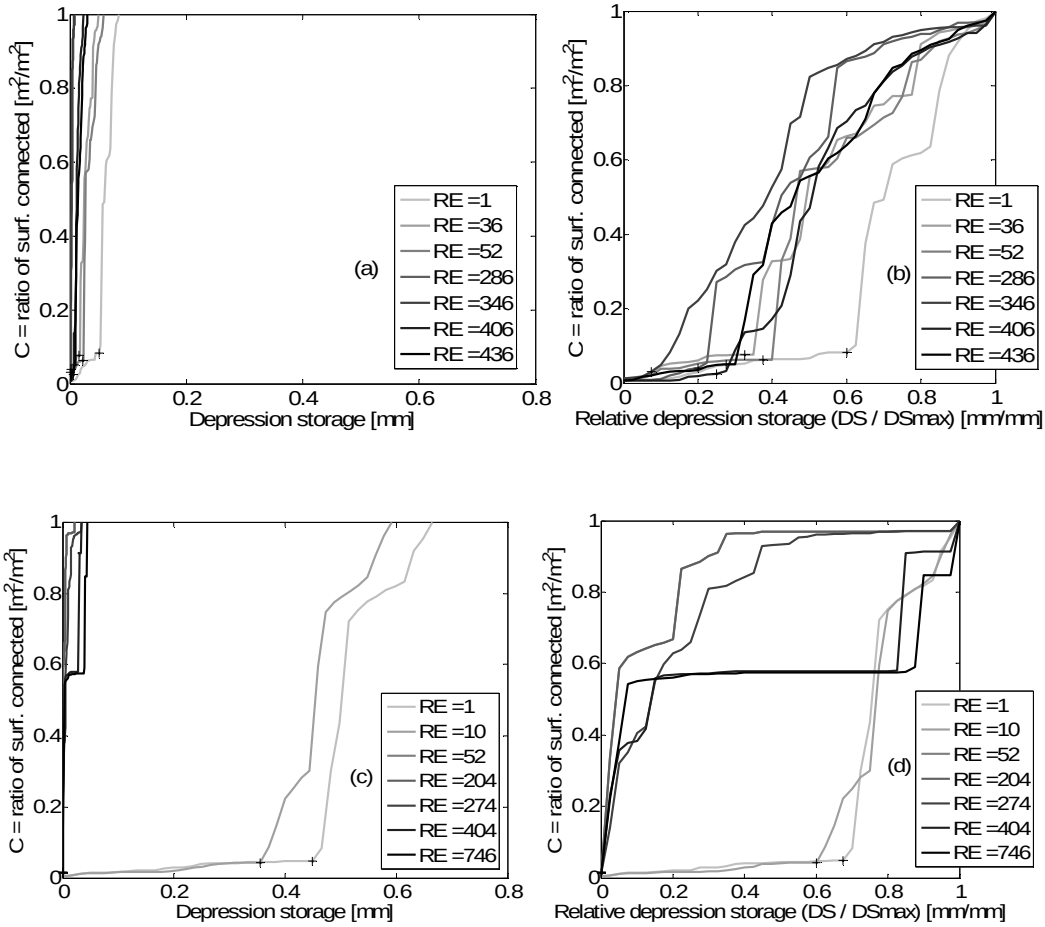

Figure E-2 Evolution of the RSCf (a, c) and the normalized RSCf (b, d) as a function of the cumulative rainfall erosivity (RE) for Plot 3 in Year 1 (a, b) and Year 2 (b, c). Cross markers represent the connectivity threshold (CT). RE is in MJ ha^{-1} mm h^{-1}h

F. Overland flow hydrographs evolution

In this section, we show the evolution of the overland flow hydrographs for Plot 2 and Plot 3 in Year 1 and Year 2.

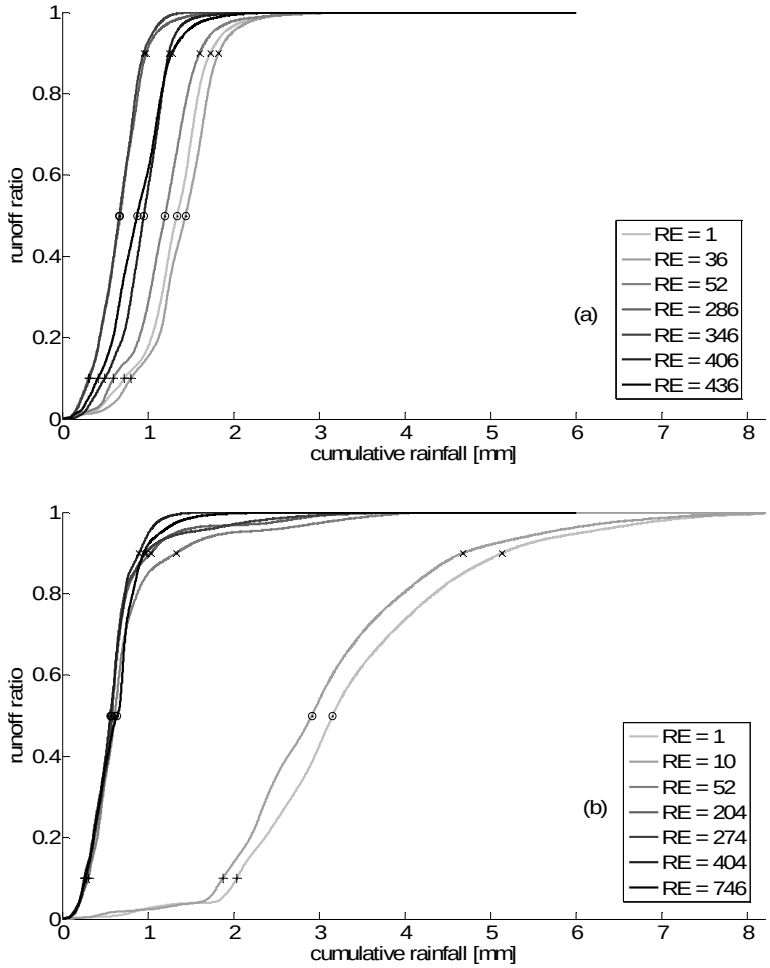

Figure F-1Evolution of the overland flow hydrograph for Plot 2 in Year 1 (a) and Year 2 (b) simulated on the basis of DEMs characterized after increasing amounts of rainfall erosivity (RE). Cross markers represent I_{10}, open circles I_{50} and x I_{90}. RE is in MJ ha^{-1} mm h^{-1}.

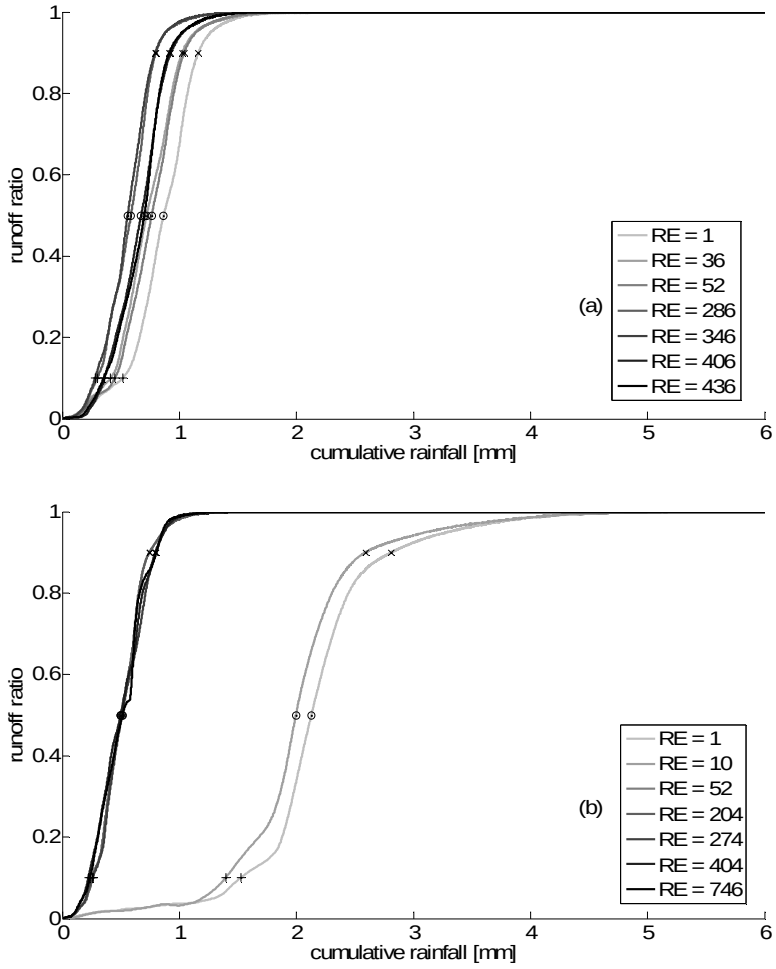

Figure F-2 Evolution of the overland flow hydrograph for Plot 3 in Year 1 (a) and Year 2 (b) simulated on the basis of DEMs characterized after increasing amounts of rainfall erosivity (RE). Cross markers represent I_{10}, open circles I_{50} and x I_{90}. RE is in MJ ha^{-1} mm h^{-1}

Bibliography

Abrahams A.D.., Parsons A.J., Luk, S., 1988. Hydrologic and sediment responses to simulated rainfall on desert hillslopes in southern Arizona. Catena, 15 (2), 103-117.

Abrahams A.D., Parsons A.J., 1990.Determining the mean depth of flow in field studies of flow hydraulics. Water Resour Res 26:501–503.

Ahmadabadian A.H., Robson S., Boehm J., Shortis M., Wenzel K., Fritsch D., 2013. A comparison of dense matching algorithms for scaled surface reconstruction using stereo camera rigs. ISPRS Journal of Photogrammetry and Remote Sensing 78: 157–167.

Alberts, E.E., Nearing, M.A., Weltz, M. A.,Risse, L.M., Pierson,F.B., Zhang, X.C., Laflen J.M.,Simanton. J.R., 1995. Ch 7 Soil Component. In: D.C. Flanagan and M.A. Nearing (Editors), Technical Documentation – USDA Water Erosion Prediction Project (WEPP). U.S. Dep. Agric., West Lafayette, Ind. Nat. Soil Eosion Res. Lab. Report No. 10.

Ali, G.A. and Roy, A.., 2009. Revisiting hydrologic sampling strategies for an accurate assessment of hydrologic connectivity in humid temperate systems. Geography Compass 3/1 (2009):350-374.

Ali, G.A., Roy, A.G., 2010. Shopping for hydrologically representative connectivity metrics in a humid temperate forested catchment. Water Resources Research 46, W12544.

Ali, G.A., L'Heureux, C., Roy, A.G., Turmel, M.C., Courchesne, F., 2011. Linking spatial patterns of perched groundwater storage and stormflow generation processes in a headwater forested catchment.Hydrol. Process. 25, 3843–3857.

Ambroise, B., 2004. Variable 'active' versus 'contributing' areas or periods: a necessary distinction. Hydrological Processes, 18(6):1149–1155

Appels, W.M., Bogaart, P.W., van der Zee, S.E.A.T.M., 2011. Influence of spatial variations of microtopography and infiltration on surface runoff and field scale hydrological connectivity. Adv. Water Resour. 34, 303–313. doi:10.1016/j.advwatres.2010.12.003

Antoine, M., Javaux, M., Bielders, C., 2009. What indicators can capture runoff-relevant connectivity properties of the micro-topography at the plot scale? Adv. Water Resour. 32, 1297–1310. doi:10.1016/j.advwatres.2009.05.006

Antoine, M., Javaux, M., Bielders, C.L., 2011. Integrating subgrid connectivity properties of the micro-topography in distributed runoff models, at the interrill scale. J. Hydrol. 403, 213–223. doi:10.1016/j.jhydrol.2011.03.027

Antoine, M., Chalon, C., Darboux, F., Javaux, M., Bielders, C., 2012. Estimating changes in effective values of surface detention, depression storage and friction factor at the interrill scale, using a cheap and fast method to mold the soil surface micro-topography, Catena, 91, 10–20.

Baartman J.E., Jetten V.G., Ritsema C.J., de Vente J., 2012. Exploring effects of rainfall intensity and duration on soil erosion at the catchment scale using openLISEM: Prado catchment, SE Spain. Hydrological Processes 26: 1034–1049.

Berkowitz, B., Balberg, I., 1993. Percolation theory and its application to groundwater hydrology, Water Resour. Res., 29, 775–794, doi:10.1029/92WR02707.

Berkowitz, B., Ewing, R.P., 1998. Percolation Theory and Network Modeling Applications in Soil Physics.Surv.Geophys. 19, 23–72. doi:10.1023/A:1006590500229.

Betson, R.P., 1964. What is watershed runoff? J. Geophys. Res. 69(8): 1541-1551

Beven, K.J., Binley, A.M., 1992. The future of distributed models: Model calibration and predictive uncertainty, Hydrological Processes, 6, 279-298.

Bracken, L.J., Croke, J., 2007. The concept of hydrological connectivity and its contribution to understanding runoff-dominated geomorphic systems.Hydrol.Process. 21, 1749–1763. doi:10.1002/hyp.6313

Bracken, L.J., Wainwright, J., Ali, G.A., Tetzlaff, D., Smith, M.W., Reaney, S.M., Roy, A.G., 2013. Concepts of hydrological connectivity: Research approaches, pathways and future agendas. Earth-Sci. Rev. 119, 17–34. doi:10.1016/j.earscirev.2013.02.001.

Bryan, R. B., 2000, Soil erodibility and processes of water erosion on hillslope, Geomorphology, Volume 32, Issues 3–4, Pages 385-415, ISSN 0169-555X.

Callow, J.N., Smettem, K.R.J., 2009. The effect of farm dams and constructed banks on hydrologic connectivity and runoff estimation in agricultural landscapes. Environmental Modelling & Software 24, 959–968.

Cammeraat, L.H., 2002. A review of two strongly contrasting geomorphological systems within the context of scale. Earth Surface Processes and Landforms 27, 1201–1222.

Cerdà, A., 1998. The influence of geomorphological position and vegetation cover on the erosional and hydrological processes on a Mediterranean hillslope. Hydrol.Process.12, 661–671.

Cerdan, O., Le Bissonnais, Y., Govers, G., Lecomte, V., van Oost, K., Couturier, A., King, C., Dubreuil, N., 2004.Scale effect on runoff from experimental plots to catchments in agricultural areas in Normandy. Journal of Hydrology, 299(1-2):4–14.

Chow, V.T., 1959, Open-channel hydraulics: New York, McGraw-Hill, 680 p.

Chu, X., Yang, J., Chi, Y., 2012. Quantification of soil random roughness and surface depression storage: Methods, applicability, and limitations. Trans. ASABE 55(5): 1699-1710.

Chu, X., Nelis, J., and Rediske, R., 2013. Preliminary Study on the Effects of Surface Microtopography on Tracer Transport in a Coupled Overland and Unsaturated Flow System. J. Hydrol. Eng., 18(10), 1241–1249.

Chu, X., Padmanabhan, G., Bogart, B., 2015.Microrelief-Controlled Overland Flow Generation: Laboratory and Field Experiments.Applied and Environmental Soil Science, Vol. 2015, Article ID 642952, http://dx.doi.org/10.1155/2015/642952.

Clifford, N.J., Robert, A., Richards, K.S., 1992. Estimation of flow resistance in gravel-bedded rivers: a physical explanation of the multiplier of roughness length. Earth Surface Processes and Landforms, 17, 111–126.

Cremers, N.H.D.T., Van Dijk, P.M., De Roo, A.P.J., Verzandvoort, M.A., 1996. Spatial and Temporal Variability of Soil Surface Roughness and the Application in Hydrological and Soil Erosion Modelling.Hydrol.Process. 10, 1035–1047.

Cressie, N., 1993, Statistics for spatial data, Wiley Interscience.

Darboux, F., Davy, P., and Gascuel-Odoux, C. 2002a. Effect of depression storage capacity on overland-flow generation for rough horizontal surfaces: Water transfer distance and scaling. Earth Surface Processes and Landforms, 27(2):177–191.

Darboux, F., Davy, P., Gascuel-Odoux, C., Huang, C, 2002b. Evolution of soil surface roughness and flowpath connectivity in overland flow experiments. Catena, 46(2-3):125–139.

Darboux, F., Huang, C., 2005. Does Soil Surface Roughness Increase or Decrease Water and Particle Transfers? Soil Sci. Soc. Am. J. 69, 748. doi:10.2136/sssaj2003.0311

Deasy, C., Brazier, R.E., Heathwaite, A.L., Hodgkinson, R., 2009. Pathways of runoff and sediment transfer in small agricultural catchments, Hydrol. Process., 23(9), 1349–1358.

Delestre, O., Cordier, S., Darboux, F., Du, M., James, F., Laguerre, C., Lucas, C., Planchon, O., 2014. FullSWOF: a software for overlandflow simulation. In Gourbesville, P., Cunge, J., and Caignaert, G., editors,Advances in Hydroinformatics. SIMHYDRO 2012 – New Frontiers of Simulation, pages 221–231, Nice, France. Société Hydrotechnique de France (SHF), the University of Nice-Sophia Antipolis (UNS), the International Association for Hydraulic Research (AIHR) and the Association Française de Mécanique (AFM), Springer

De Roo, A.P.J., Wesseling, C.G., Ritsema, C.J., 1996a. LISEM: a single event physically-based hydrologicand soil erosion model for drainage basins: I. Theory, input and output. Hydrological Processes 10 (8),1107–1117.

De Roo, A.P.J., Offermans, R.J.E., Cremers, N.H.D.T., 1996b. LISEM: a single event physically-basedhydrologic and soil erosion model for drainage basins: II. Sensitivity analysis, validation and application. Hydrological Processes 10 (8), 1119–1126.

Devito, K., Creed, I., Gan, T., Mendoza, C., Petrone, R., Silins, U., Smerdon, B., 2005. A framework for broad-scale classification of hydrologic response units on the boreal plain: Is topography the last thing to consider?, Hydrol. Processes, 19, 1705–1714, doi:10.1002/hyp.5881.

Di Domenico, A., Laguardia, G., Fiorentino, M., 2007. Capturing critical behaviour in soil moisture spatio-temporal dynamics. Advances in Water Resources 30 (3), pp. 543 – 554.

Dunne, T. and Black, R.D., 1970. Partial area contributions to storm runoff in a small New England watershed. Water Resour. Res. 6(5): 1296-1311.

Dunne, T., Moore, T.R., Taylor, C.H., 1975. Recognition and prediction of runoff-producing zones in humid regions. Hydrological Sciences Bulletin. v.XX, 3, 609-623.

Dunne, T., Aubry, B.F. 1986. Evaluation of Horton's theory of sheetwash and rill erosion on the basis of field experiments, In: Hillslope Processes (ed. A. D. Abrahams), Geo. Allen & Unwin, London, 31-53, 1986. Reproduced as Paper 44 in Benchmark Papers in Hydrology: Hydro-geomorphology, Erosion, and Sedimentation, (ed. M.J. Kirkby), International Association of Hydrological Science (2011)

Esteves M., Faucher X., Galle S., Vauclin M., 2000. Overland flow and infiltration modelling for small plots during unsteady rain: numerical results versus observed values J Hydrol, 228 (3–4), pp. 265–282

Favis-Mortlock, D.T., Boardman, J., Parsons, A.J., Lascelles, B., 2000. Emergence and erosion: a model for rill initiation and development. Hydrological Processes 14(11-12), 2173-2205.

Fiedler, F.R., Ramirez, J.A., 2000.A numerical method for simulating discontinuous shallow flow over an infiltrating surface Int J Numer Methods Fluids, 32 (2), pp. 219–239.

Flanagan, D.C., Nearing, M.A., eds. 1995. USDA Water Erosion Prediction Project hillslope and watershed model documentation. NSERL Report No. 10. West Lafayette, Ind.: USDA-ARS National Soil Erosion Research Laboratory.

Gessesse, G.D., Fuchs H., Mansberger R., Klik A., Rieke-Zapp D., 2010. Assessment of erosion, deposition and rill development on irregular soil surfaces using close rang digital photogrammetry, Photogramm. Rec., 25, 299–318, doi:10.1111/j.1477-9730.2010.00588.x.

Giboire, G., Soh, A., Renmeester, G., Bielders, C.L.,Persoons, E., 2003. Tipping bucket with splitter device to monitor runoff and suspended sediment charge. p. 231–237. InCornelis, W.M., Gabriels, D. (eds.), International Symposium on 25 Years of Assessment of Erosion. Ghent University, Faculty of Bioscience Engineering, Ghent.

Giménez, R., Planchon O., Silvera N., Govers, G., 2004. Longitudinal velocity patterns and bed morphology interaction in a rill, Earth Surf. Processes Landforms, 29(1), 105–114, doi:10.1002/esp.1021

Gomez, J.A., Nearing, M.A., 2005. Runoff and sediment losses from rough and smooth soil surfaces in a laboratory experiment. Catena, 59, 253-266.

Govers, G., 1987. Spatial and temporal variability in rill development processes at the Huldenberg Experimental Site. In: Bryan (ed.): Rill Erosion − Processes and Significance; Catena Supplement 8, 17−34.

Govers, G., Everaert, W., Poesen, J., Rauws, G., Ploey, D.J., Lautridol, J.P., 1990. A long flume study of the dynamic factors affecting the resistance of a loamy soil to concentrated flow erosion. Earth Surface Processes and Landforms 15: 313–328.

Govers, G., Takken, I., Helming, K., 2000.Soil roughness and overland flow.Agron. Sustain. Dev., 20 2, 131-146.

Grant G.E., 1997. Critical flow constrains flow hydraulics in mobile-bed streams: a new hypothesis. Water Resources Research 33: 349–358.

Gustafson, E.J., 1998. Quantifying landscape spatial pattern: What is the state of the art? Ecosystems, 1(2):143–156.

Guzha, A.C., 2004. Effects of tillage on soil microrelief, surface depression storage and soil water storage. Soil Till. Res. 76:105–114.

Flanagan, D.C., Nearing, M.A., 1995. USDA Water Erosion Prediction Project hillslope and watershed model documentation. NSERL Report No. 10. West Lafayette, Ind.: USDA-ARS National Soil Erosion Research Laboratory

Frei, S., Lischeid, G., Fleckenstein, J.H., 2010. Effects of micro-topography on surface–subsurface exchange and runoff generation in a virtual riparian wetland — A modeling study. Adv. Water Resour., Special Issue on ground water-surface water interactions GW-SW Interactions 33, 1388–1401. doi:10.1016/j.advwatres.2010.07.006

Fryirs, K.A., Brierley, G.J., Preston, N.J., Kasai, M., 2007. Buffers, barriers and blankets: The (dis)connectivity of catchment-scale sediment cascades. Catena, 70(1):49–67.

Flügel, W.A., 1995. Delineating hydrological response units by geographical information system analyses for regional hydrological modeling using PRMS/MMS in the drainage basin of the river Brol, Germany, Hydrol. Processes, 9, 423–436, doi:10.1002/hyp.3360090313

Hairsine, P.B., Croke, J.C., Matthews, H., Fogarty, P., Mockler, S.P., 2002. Modelling plumes of overland flow from roads and logging tracks. Hydrological Processes 16, 2311–2327.

Hansen, B., Schjønning, P., Sibbesen, E., 1999. Roughness indices for estimation of depression storage capacity of tilled soil surfaces. Soil Till. Res. 52, 103–111.

Harel, M.A., Mouche E., 2013. 1-D steady state runoff production in light of queuing theory: Heterogeneity, connectivity, and scale, Water Resour. Res., 49, 7973–7991

Heathwaite, A. L., Quinn, P.F., Hewett, C.J.M., 2005. Modellingand managing critical source areas of diffuse pollution from agricultural land using flow connectivity simulation. Journal of Hydrology, 304(1-4):446–461.

Helming, K., Romkens, M.J.M., Prasad, S.N. et al., 1998. Surface roughness related processes of runoff and soil loss: a flume study. Soil Sci. Soc. Am. J. 62, 243–250.

Hewlett, J.D., Hibbert, A.R., 1967. Factors affecting the response of small watersheds to precipitation in humid areas. In Sopper, W.E. and Lull, H.W. (Eds): Forest Hydrology. Proc. Int. Symp. on Forest Hydrol., Penn. State Univ., University Park, Pennsylvania, pp. 275-290.

Hopp, L., McDonnell, J.J., 2009. Connectivity at the hillslope scale: Identifying interactions between storm size, bedrock permeability, slope angle and soil depth. J. Hydrol. 376 (3–4), 378–391.

Horton, R.E., 1933. The role of infiltration in the hydrologic cycle. Trans. Am. Geophys. Union 14:446-460.

James, A.L., Roulet, N.T., 2007. Investigating hydrologic connectivity and its association with threshold change in runoff response in a temperate forested watershed. Hydrological Processes 21(25): 3391-3408.

Janzen D., McDonnell, J.J., 2015. A stochastic approach to modelling and understanding hillslope runoff connectivity dynamics, Ecological Modelling, 298, 64-74

Jones, O.D., Sheridan, G.J., Lane, P.N., 2013. Using queuing theory to describe steady-state runoff–runon phenomena and connectivity under spatially variable conditions. Water Resources Research 49, 7487–7497.

Julien, P.Y., Moglen, G.E., 1990. Similarity and length scale for spatially varied overland flow. Water Resources Research., 26, 1819–1832.

Kamphorst, E.C., Jetten, V., Guérif, J., Pitkänen, J., Iversen, B.V., Douglas, J.T., Paz, A., 2000. Predicting Depressional Storage from Soil Surface Roughness. Soil Sci. Soc. Am. J. 64, 1749. doi:10.2136/sssaj2000.6451749x

Kirkby, M., Bracken, L., Reaney, S., 2002. The influence of land use, soils and topography on the delivery of hillslope runoff to channels in SE Spain Earth Surface Processes and Landforms, 27 (13), 1459–1473.

Knudby, C., Carrera, J. 2005. On the relationship between indicators of geostatistical, flow and transport connectivity. Advances in Water Resources, 28(4):405–421.

Laloy, E., Bielders, C.L., 2008. Plot scale continuous modelling of runoff in a maize cropping system with dynamic soil surface properties.J. Hydrol. 349, 455–469.

Lane, L.J., and M.A. Nearing, eds. 1989. USDA Water Erosion Prediction Project: Hillslope profile model documentation. NSERL Report No. 2. West Lafayette, Ind.: USDA-ARS National Soil Erosion Research Laboratory.

Lane, S.N., Brookes, C.J., Kirkby, M.J., Holden, J., 2004. A network-index based version of TOPMODEL for use with high-resolution digital topographic data. Hydrological Processes 18, 191–201.

Lane, S.N., 2005. Roughness – time for a re-evaluation?. Earth Surf. Process. Landforms, 30, 251-253.

Langhans, C., Govers, G., Diels, J., Leys, A., Clymans, W., Van den Putte, A., and Valckx, J., 2011. Experimental rainfall-runoff data: Reconsidering the concept of infiltration capacity, J. Hydrol., 399, 255–262..

Larsen, L.G., Choi, J., Nungesser, M.K., Harvey, J.W., 2012. Directional Connectivity in Hydrology and Ecology. Ecological Applications 22 (8), 2204–2220.

Le Bissonnais, Y., Bruand, A., Jamagne, M. 1989. Laboratory experimentalstudy of soilcrusting:Relationbetweenaggregate breakdownmechanismsand cruststructure. Catena, 16, 377-392.

Lehmann, P., Hinz, C., McGrath,G., Tromp-van Meerveld, H.J, McDonnell, J.J., 2007. Rainfall threshold for hillslope

outflow:an emergent property of flow pathway connectivity. Hydrology and Earth System Sciences, 11, 1047-1063,.

Lexartza-Artza, I., Wainwright J., 2009. Hydrological Connectivity: Linking concepts with practical implications. Catena, 79, 146-152.

Ludwig, B., Boiffin, J., Auzet, A.V., 1995. Hydrological structure and erosion damage caused by concentrated flow in cultivated catchments. Catena, 25 (1), pp. 227–252.

Ludwig, J.A., Wilcox, B.P., Breshears, D.D., Tongway, D.J., Imeson, A.C., 2005. Vegetation patches and runoff-erosion as interacting ecohydrological processes in semiarid landscapes. Ecology 86, 288–297.

Luk, S., Abrahams, A.D., Anthony J. Parsons, 1993. Sediment sources and sediment transport by rill flow and interrill flow on a semi-arid piedmont slope, southern Arizona, Catena, 20 (1–2), pp. 93-111.

Mancilla, G. A., Chen, S., McCool, D.K., 2005. Rill density prediction and flow velocity distribution on agricultural areas in the Pacific Northwest. Soil and Tillage Research, 84, 54-66. http://dx.doi.org/10.1016/j.still.2004.10.002

McGlynn, B.L., McDonnell, J.J., 2003. Quantifying the relative contributions of riparian and hillslope zones to catchment runoff. Water Resources Research 39 (11) (Article Number: 1310).

Meerkerk, A.L., van Wesemael, B., Bellin, N., 2009. Application of connectivity theory to model the impact of terrace failure on runoff in semi-arid catchments.Hydrological Process 23, 2792–2803.

Merritt, E., 1984. The identification of four stages during micro-rill development. Earth Surface Processes and Landforms 9:493-496.

Moore, R. J., 2007.The PDM rainfall-runoff model. Hydrology and Earth System Sciences, 11 (1): 483-499.

Moreno-de las Heras, M., Nicolau, J.M., Merino-Martín, L., Wilcox, B.P., 2010. Plot-scale effects on runoff and erosion along a slope degradation gradient. Water Resources Research;46:W04503.

Morgan R.P.C., Quinton J.N., Smith R.E., Govers G., Poesen J. A., Auerswald K., Chisci G., Torri D., Styczen M.E., 1998. The European Soil Erosion Model (EUROSEM): A dynamic

approach for predicting sediment transport from fields and small catchments. Earth Surface Processes and Landforms 23: 527–544

Mueller, E.N., Wainwright, J., Parsons, A.J., 2007. Impact of connectivity on the modeling of overland flow within semiarid shrubland environments. Water Resources Research, 43(9):W09412.

Nicolau, J.M., 2002. Runoff generation and routing on artificial slopes in a Mediterranean–continental environment: The Teruel coal field, Spain. Hydrological Processes 16, 631–647.

Ogilvy A., Foster J.M., 1989. Rough surfaces: Gaussian or exponential statistics? J. Phys. D: Appl. Phys.;22:1243–1251.

Onstad, C.A., 1984. Depressional storage on tilled soil surfaces. Trans. ASAE 273, 729–732.

Parsons, A.J., Abrahams, A.D., 1992. Overland Flow: hydraulics and erosion mechanics, University College London Press, London. ISBN: 9781857280067.

Parsons, A.J., Wainwright, J., 2006. Depth distribution of interrill overland flow and the formation of rills. Hydrological Processes 20, 1511-1523.

Peñuela, A., Javaux, M., Bielders, C.L., 2013. Scale effect on overland flow connectivity at the plot scale. Hydrol Earth SystSci 17, 87–101. doi:10.5194/hess-17-87-2013

Peñuela, A., Javaux, M., Bielders, C.L., 2015. How do slope and surface roughness affect plot scale overland flow connectivity?. Journal of Hydrology 528,192-205.

Planchon, O., Fritsch, E., Valentin, C., 1987.Rill development in a wet savannah environment. In: Bryan, R.B. (ed.): Rill Erosion − Processes and Significance; Catena Supplement 8, Catena Verlag, Cremlingen-Destedt, 55−70.

Puigdefabregas, J., Sanchez, G., 1996. Geomorphological implications of vegetation patchiness in semi-arid slopes. In: Anderson, M., Brooks, S. Eds. , Advances in Hillslope Processes.Wiley, London, pp. 1027–1060.

Reaney, S.M., Bracken, L.J., Kirkby, M.J., 2007. Use of the connectivity of runoff model (CRUM) to investigate the influence of storm characteristics on runoff generation and connectivity in semi-arid areas.Hydrological Processes 21(7): 894-906.

Reaney, S.M., Bracken, L.J., Kirkby, M.J., 2014. The importance of surface controls on overland flow connectivity in semi-arid environments: results from a numerical experimental approach. Hydrol.Process. 28, 2116–2128. doi:10.1002/hyp.9769.

Rieke-Zapp D., Nearing M.A., 2005. Digital close range photogrammetryfor measurement of soil erosion. The Photogrammetric Record 20:69–87. DOI: 10.1111/j.1477-9730.2005.00305.x

Römkens, M.J.M., Helming, K., Prasad, S.N., 2001. Soil erosion under different rainfall intensities, surface roughness, and soil water regimes. Catena 46,103-123.

Savat, J., 1979. Laboratory experiments on erosion and deposition of löss by laminar sheetflow and turbulent rillflow. In: Vogt, H. & Vogt, Th. (eds.): Colloque sur l'érosion agricole des sols en milieu tempéré non Mediterranéen; Université Louis Pasteur, Strasbourg-Colmar, 139−143.

Savat, J., De Ploey, J., 1982. Sheetwash and rill development by surface flow. Chapter 6 in: Bryan, R.B. &Yair, A. (eds.): Badland Geomorphology and Piping; GeoBooks, Norwich, 408 pp.

Shaw, D.A., van der Kamp, G., Conly, F.M., Pietroniro, A.,Martz, L., 2012. The fill-spill hydrology of prairie wetland complexes during drought and deluge. Hydrological Processes, 26: 3147–3156.

Slattery, M.C., Bryan, R.B., 1992. Hydraulic conditions for rill incision under simulated rainfall: A laboratory experiment, Earth Surf. Processes Landforms, 17, 127-146.

Singh, V.P., 1995. Computer models of watershed hydrology. Water Resources Publications, LLC.

Singh, V.P., Frevert, D. 2002. Mathematical models of small watershed hydrology and applications, WaterResourcesPublications, LLC pages xxi + 950 pp.

Smith, M.W., Cox, N.J., Bracken, L.J., 2007.Applying flow resistance equations to overland flows. Progress in Physical Geography, 31, 363–387.

Smith, M.W., Bracken, L.J., Cox, N.J., 2010. Toward a dynamic representation of hydrological connectivity at the hillslope scale in semiarid areas. Water Resources Research 46, W12540

Smith, M.W., Cox, N.J., Bracken, L.J., 2011. Terrestrial laser scanning soil surfaces: a field methodology to examine soil surface roughness and overland flow hydraulics. Hydrological Processes 25, 842–860.

Smith, M.W., 2014. Roughness in the Earth Sciences, Earth-Science Reviews, vol. 136, pp. 202-225.

Spence C., 2007. On the Relation Between Dynamic Storage and Runoff: a Discussion on Thresholds, Efficiency, and Function. Water Resources Research 43: W12416, DOI: 10.1029/2006WR005645.

Spence C., 2010. A Paradigm Shift in Hydrology: Storage ThresholdsAcross Scales Influence Catchment Runoff Generation. GeographyCompass 4: 819–833, DOI: 10.1111/j.1749–8198.2010.00341.x.

Stomph,T.J., de Ridder, N., Steenhuis, T.S., van de Giesen, N., 2002. Scale effects of Hortonian overland flow and rainfall-runoff dynamics: Laboratory validation of a process based model. Earth Surface Processes and Landforms, 2002, Vol 27(8), 847-855.

Strickler, A., 1923. Beiträge zur frage der geschwindigkeitsformel und der rauhigkeitszahlen fur strome kanaele und geschlossene leitungen. Mitteilungen des eidgenossischen. Amtesfuer Wasserwirtschaft 16. Bern, Switzerland. (in German) (Translated as “Contributions to the question of a velocity formula and roughness data for streams, channels and closed pipelines” by Roesgan, T. and Brownlie, W.R).

Takken, I., Govers, G., Steegen, A., Nachtergaele, J., and Guerif, J., 2001a. The prediction of runoff flow directions on tilled fields. Journal of Hydrology, 248(1-4):1–13.

Takken, I., Jetten, V., Govers, G., Nachtergaele, J., and Steegen, A. 2001b. The effect of tillage-induced roughness on runoff and erosion patterns. Geomorphology, 37(1-2):1–14.

Taylor, P. D., Fahrig, L., Henein, K., Merriam, G., 1993. Connectivity Is A Vital Element Of Landscape Structure. Oikos, 68(3):571–573.

Tischendorf, L. and Fahring, L., 2000.On the usage and measurement of landscape connectivity.Oikos, 90(1):7–19.

Torri, D., Sfalanga, M., Chisci, G., 1987. Threshold conditions for incipient rilling. In: Bryan, R.B. (ed.): Rill erosion − Processes

and Significance; Catena Supplement 8, Catena Verlag, Cremlingen-Destedt, 97−105.

Toschi, I., Rivola, R., Bertacchini, E., Castagnetti, C., Dubbini, M., and Capra, A., 2013.Validation Tests of Open-Source Procedures for Digital Camera Calibration and 3d Image-Based Modelling, Int. Arch. Photogramm. Remote Sens. Spatial Inf. Sci., XL-5/W2, 647-652, doi:10.5194/isprsarchives-XL-5-W2-647-2013.

Tromp-van Meerveld H.J., McDonnell J.J., 2006a. Threshold relations in subsurface storm flow: 1. A 147-storm analysis of the Panola hillslope. Water Resources Research 42.

Tromp-van Meerveld H.J., McDonnell J.J., 2006b. Threshold relations in subsurface storm flow: 2. The fill and spill hypothesis. Water Resources Research, 42.

Tromp-van Meerveld, I., Weiler, M., 2008. Hillslope dynamics modeled with increasing complexity, Journal of Hydrology; 361 (1-2) : 24-40.

Turnbull, L., Wainwright, J., Brazier, R. E., 2008. A conceptual framework for understanding semi-arid land degredation: ecohydrological interactions across multiple-space and time scales, Ecohydrology, 1, 23-34.

Van de Giesen, N., Stomph, T.J., de Ridder, N. 2000.Scale Effects on Hortonian Overland Flow and Rainfall-Runoff Dynamics in a West African Catena Landscape. Hydrological Processes, 14 (1): 165-175.

Van Nieuwenhuyse, B.H.J., Antoine, M., Wyseure, G., Govers, G., 2011. Pattern-process relationships in surface hydrology: hydrological connectivity expressed in landscape metrics. HydrologicalProcesses, 25(24): 3760-3773.

Vázquez, E.V., Miranda, J. G.V., González., A.P., 2005. Characterizing anisotropy and heterogeneity of soil surface microtopography using fractal models. Ecol. Modeling 182(3-4): 337-353.

Verstraeten, G., Poesen, J., Demaree, G., Salles, C., 2006. Long-term (105 years) variability in rain erosivity as derived from 10-min rainfall depth data for Ukkel (Brussels, Belgium): Implications for assessing soil erosion rates, J. Geophys. Res.-Atmos., 111, D2210910, doi:10.1029/2006jd007169.

Vidal Vazquez, E., Vivas Miranda, J.G., Paz Gonzalez, A. 2005. Characterizing anisotropy and heterogeneity of soil surface

micro-topography using fractal models. Ecological Modelling, 182(3-4):337–353.

Western, A.W., Bloschl, G., Grayson, R.B., 1998. How well do indicator variograms capture the spatial connectivity of soil moisture? Hydrological Processes, 12(12):1851–1868.

Western, A.W., Grayson, R.B., Blöschl, G., Willgoose, G.R., McMahon, T.A., 1999. Observed spatial organisation of soil moisture and its relation to terrain indices. Water Resources Research 35, 797–810.

Western, A.W., Bloschl, G., Grayson, R.B., 2001.Toward capturing hydrologically significant connectivity in spatial patterns. Water Resources Research, 37(1):83–97.

Wood, E.F., Sivapalan, M., Beven, K., Band, L., 1988. Effects of spatial variability and scale with implications to hydrologic modeling. Journal of Hydrology, 102: 29-47.

Yair, A., Lavee H., 1985. Runoff Generation in arid and semi-arid zones. Hydrological Forecasting (1985): 183-220.

Yang, J., Chu, X., 2013. Quantification of the spatio-temporal variations in hydrologic connectivity of small-scale topographic surfaces under various rainfall conditions, J. Hydrol, 505, 65–77

Yang, J., Chu, X., 2015.A new modelling approach for simulating microtopography-dominated, discontinuous overland flow on infiltrating surfaces.Adv. Water Resour. 78, 80-93.

Yen, B.C., 1992. Hydraulic resistance in open channels, in Yen, B.C., ed., Channel flow: centennial of Manning's formula: Water Resources Publications, Littleton, Colo. p. 1–135.

Zhang, W., Cundy, T.W., 1989.Modeling of two-dimensional overland flow.Water Resource Research, 25(9), 2019–35.

Zehe E, Bloschl G., 2004. Predictability of hydrologic response at the plot and catchment scales: role of initial conditions. Water Resources Research 40, 21.

Zinn, B. and Harvey, C.F., 2003.When good statistical models of aquifer heterogeneity go bad: A comparison of flow, dispersion, and mass transfer in connected and multivariate Gaussian hydraulic conductivity fields. WaterResources Research, 39(3):1051.

Zobeck, T.M., Onstad, C.A., 1987. Tillage and rainfall effects on random roughness: A review. Soil Tillage Res. 9, 1–20. doi:10.1016/0167-1987(87)90047-X